

***THIOLATO SCHIFF BASE COMPLEXES OF NICKEL AND
PALLADIUM AS MESOGENS AND MOLECULAR WIRES.***

RICHARD MOTLHALETSI MOUTLOALI

**A Thesis Submitted In Partial Fulfillment Of The
Requirements For The Degree Of Doctor Philosophiae In The
Department Of Chemistry, University Of The Western Cape.**



DATE: May 2003

SUPERVISOR: PROFESSOR JAMES DARKWA

ABSTRACT

THIOLATO SCHIFF BASE COMPLEXES OF NICKEL AND PALLADIUM AS MESOGENS AND MOLECULAR WIRES.

R. M. Moutloali

PhD Thesis, Department of Chemistry, University of the Western Cape

Schiff base thiol compounds were prepared by the condensation of 4-aminothiophenol and 4-arylbenzaldehyde or 4-alkyloxybenzaldehyde ($\text{OHCC}_6\text{H}_4\text{OR}$, $\text{R} = \text{C}_6\text{H}_5$, $\text{CH}_2\text{C}_6\text{H}_5$, $\text{C}_n\text{H}_{2n+1}$, $n = 4, 6, 8, 10, 12, 14, 16, 20$) and 1,4-aryldialdehyde. Monoaldehydes formed $\text{HSC}_6\text{H}_4\text{NC}(\text{H})\text{C}_6\text{H}_4\text{OR}$ (**A**) whilst dialdehydes formed $\text{HSC}_6\text{H}_4\text{NC}(\text{H})\text{ArC}(\text{H})\text{NC}_6\text{H}_4\text{SH}$ ($\text{Ar} = 2,5$ -thiophene, 1,3-benzene, 1,4-benzene and 4,4'-biphenyl) (**B**). Compounds **A** and **B** reacted with $\text{NiX}(\text{PR}_3)(\eta^5\text{-C}_5\text{H}_5)$ ($\text{X} = \text{Cl}$ or Br , $\text{R} = \text{Ph}$ or Bu) to give mononickel complexes, $\text{Ni}(\text{SC}_6\text{H}_4\text{NC}(\text{H})\text{C}_6\text{H}_4\text{OR})(\text{PR}_3)(\eta^5\text{-C}_5\text{H}_5)$ (**C**) and dinickel complexes, $(\eta^5\text{-C}_5\text{H}_5)(\text{PR}_3)\text{Ni}(\text{SC}_6\text{H}_4\text{NC}(\text{H})\text{ArC}(\text{H})\text{NC}_6\text{H}_4\text{S})\text{Ni}(\text{PR}_3)(\eta^5\text{-C}_5\text{H}_5)$, (**D**) in high yields.

Compounds **A** reacted with nickelocene and diethyldithiocarbamatonicel(II) bromide to form $[\text{Ni}(\mu_2\text{-SC}_6\text{H}_4\text{NC}(\text{H})\text{C}_6\text{H}_4\text{OR})(\eta^5\text{-C}_5\text{H}_5)]_2$ (**E**) and $[\text{Ni}(\mu_2\text{-SC}_6\text{H}_4\text{NC}(\text{H})\text{C}_6\text{H}_4\text{OR})(\text{S}_2\text{CN}(\text{C}_2\text{H}_5)_2)]_2$ (**F**) respectively in low to moderate yields. Complexes **E** were also prepared from the reaction of $[\text{Ni}(\mu_2\text{-SC}_6\text{H}_4\text{NH}_2)(\eta^5\text{-C}_5\text{H}_5)]_2$ and $\text{OHCC}_6\text{H}_4\text{OR}$ ($\text{R} = \text{OC}_n\text{H}_{2n+1}$, $n = 4, 6, 14, 16$) in low to moderate yields. The complexes, bearing terdentate ligands, $(\text{C}_6\text{H}_3(\text{CH}_2\text{NEt}_2)_2)\text{PdSC}_6\text{H}_4\text{NC}(\text{H})\text{C}_6\text{H}_4\text{OC}_n\text{H}_{2n+1}$ ($n = 6, 12$) (**G**), $(\text{C}_6\text{H}_3(\text{CH}_2\text{S}^i\text{Pr}_2)_2)\text{PdSC}_6\text{H}_4\text{NC}(\text{H})\text{C}_6\text{H}_4\text{OC}_6\text{H}_{13}$ (**H**) and $(1,2\text{-SC}_6\text{H}_4\text{NC}(\text{H})\text{-}2\text{-C}_5\text{H}_4\text{N})\text{NiSC}_6\text{H}_4\text{NC}(\text{H})\text{C}_6\text{H}_4\text{OC}_n\text{H}_{2n+1}$ ($n = 14$ and 16) (**I**), were produced from the reactions of **A** with $\text{C}_6\text{H}_3(\text{CH}_2\text{NEt}_2)_2\text{PdBr}$, $\text{C}_6\text{H}_3(\text{CH}_2\text{S}^i\text{Pr}_2)_2\text{PdBr}$ and $(1,2\text{-SC}_6\text{H}_4\text{NC}(\text{H})\text{-}2\text{-C}_5\text{H}_4\text{N})\text{NiCl}$.

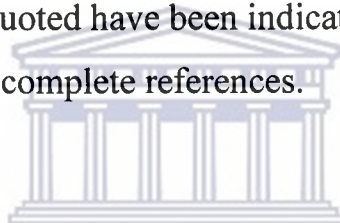
Thermal analysis data of compounds **A**, **C**, **F** and **I** established that they were non-mesogenic while **E** and **G** were found to be mesogenic. The lack of mesogenic behaviour of **A** could be attributed to hydrogen bonding. The non-mesogenic behaviour of **C** and **F** is due to reduced molecular anisotropy as a result of large lateral substituents. Complexes **I** decomposed at high temperatures and before melting and hence no liquid crystalline behaviour was found. It is likely that the high decomposition temperature is the result of increased molecular interactions. We found that removing the phosphine ligands and increasing molecular length induced liquid crystalline behaviour in complexes **E**. The more planar complexes **G** were also found to be liquid crystalline.

Cyclic voltammetry was used to probe the electrochemistry of compounds **D**, **E** and **F**. For the α,ω -dithiolato Schiff base complexes of nickel (**D**), we found that the dithiolato bridge allow electronic interaction between the two nickel centres. This was established from ΔE values between the two redox couples found in such complexes. These ranged from 296 mV to 300 mV, which are higher than the minimum value required for electronic interaction between two metal centres. Therefore the α,ω -dithiolato Schiff base compounds behave as molecular wires. Complexes **E** on the other hand, undergo two simultaneous one-electron redox processes with no electronic interaction between the two nickel centres. Compounds **F** undergo irreversible electrochemical processes, implying that the electron transfer processes are followed by chemical reactions.

Date: May 2003

DECLARATION

I declare that “*Thiolato Schiff base complexes of nickel and palladium as mesogens and molecular wires*” is my own work, that it has not been submitted for any degree or examination in any other university, and that all the sources I have used or quoted have been indicated and acknowledged by complete references.



RICHARD MOTLHALETSI MOUTLOALI.

UNIVERSITY of the
WESTERN CAPE

MAY 2003

.....

Date

Moutloali R.M.

.....

Signature

ACKNOWLEDGEMENTS

I would like to express my sincere gratitude to the following:

Professor James Darkwa, under whose guidance the research was conducted, for his invaluable advice and courage. The commitment and endurance he showed during the rough times in our research process.

Professor Folahan O. Ayorinde at Howard University (Washington DC, United States of America) for having allowed me the use of the MALDI-TOF mass spectrometer. His willingness and help in teaching and advising me on its use and interpretations of results obtained.

Professor Emmanuel I. Iwuoha for his advice and help in obtaining and interpreting electrochemical data of the complexes studied in this research. I would also like to thank Miss Aoife Morrin, an exchange student from Dublin City University, Ireland, working with him for obtaining some of the data in Chapter 3.

The Organometallics Research Groups of Professors Darkwa and Mapolie, University of the Western Cape, for everything. Those weekly meetings and “seminars” were a real eye opener and good experience.

Finally the Department of Chemistry, its staff and students, for having been a good host.

CONTENTS

Title page	i
Abstract	ii
Declaration	iv
Acknowledgements	v
Contents page	vi
List of figures	vii
List of tables	ix
Chapter 1: Introduction to metal thiolate chemistry.	1
Rationale and objectives	12
References	13
Chapter 2: Schiff base cyclopentadienylnickel(II) complexes as potential mesogens: Synthesis and Characterisation.	16
Introduction	17
Experimental Section	36
Results and discussion	46
References	90
Chapter 3: Synthesis of nickel(II) μ_2 -thiolato Schiff base complexes and pincer nickel and palladium thiolato Schiff base complexes. Spectroscopic and thermal analytical studies.	95
Introduction	96
Experimental Section	102
Results and discussion	111
References	150
Chapter 4: Bimetallic nickel complexes with bridging dithiolato ligands: Synthesis, mass spectral characterisation and electrochemistry.	154
General introduction	154
Experimental Section	175
Results and discussion	179
References	203
Chapter 5: Summary and outlook.	209

List of figures

1. Figure 1.1: Typical dithiolato liquid crystalline complexes. 9
2. Figure 1.2: Dithiolato mesogens with four-membered metallo-sulfur ring. 10
3. Figure 2.1: Possible melting sequence for a liquid crystalline material. 20
4. Figure 2.2: Plan view of smectic mesophase structures. 20
5. Figure 2.3: Commonly observed discotic mesophases: (a) nematic discotic, (b) nematic columnar and (c) nematic hexagonally ordered. 21
6. Figure 2.4: Typical thermograms of a liquid crystal on heating and cooling. 23
7. Figure 2.5: A schematic diagram of a hotstage polarising optical microscope with a sample. 24
8. Figure 2.6: Typical textures observed for nematic (a) and smectic (b) liquid crystalline material. 24
9. Figure 2.7: X-ray diffraction pattern for an ordered solid (a) and (b), liquid. 26
10. Figure 2.8: Examples of Schiff base compounds with mesogenic properties. 29
11. Figure 2.9: ^1H NMR spectrum of compound **5**. 52
12. Figure 2.10: Melting point variation with chain length for Schiff base compounds. 55
13. Figure 2.11: Thermograms for compound **6**. 59
14. Figure 2.12: Thermograms for compound **9**. 60
15. Figure 2.13: Thermograms for compound **10**. 61
16. Figure 2.14: Thermograms for compound **11**. 62
17. Figure 2.15: Optical micrograph for compound **10** showing focal conic texture. 63
18. Figure 2.16: ^1H NMR spectrum of complex **1a**. Inset: The aromatic region of spectrum of complex **1a**. 67
19. Figure 2.17: ^1H NMR spectrum of complex **3a**. Inset: Aromatic region of spectrum of complex **3b**. 67
20. Figure 2.18: X-ray crystal structure of complex **1a**. 73

21. Figure 2.19: Molecular packing diagram of complex 1a .	74
22. Figure 2.20: X-ray crystal structure of complex 3a .	75
23. Figure 2.21; Molecular packing diagram of complex 3a .	76
24. Figure 2.22: Melting point dependence of tributylphosphine complexes on chain length.	81
25. Figure 2.23: Thermograms for complex 6a .	86
26. Figure 2.24: Thermograms for complex 6b .	87
27. Figure 3.1: X-ray crystal structure of complex II .	113
28. Figure 3.2: ¹ H NMR spectrum of complex 1 .	117
29. Figure 3.3: ¹ H NMR spectrum of complex 12 .	124
30. Figure 3.4: ¹³ C NMR spectrum of complex 15 .	125
31. Figure 3.5: MALDI-TOF mass spectrum of complex 1 .	129
32. Figure 3.6: Cyclic Voltammogram of complex 2 .	133
33. Figure 3.7: Tafel plots of linear region of complexes 1 – 4 .	133
34. Figure 3.8: Cyclic voltammogram for complex 6 .	135
35. Figure 3.9: Thermograms for complex 2 (a) DSC on first heating, (b) DSC on first cooling and (c) DSC on second heating.	139
36. Figure 3.10: Photomicrograph of the texture for 2 , showing liquid crystalline texture with some homeotropic regions.	142
37. Figure 3.11: Thermograms of complex 12 before the onset of decomposition. (a) First heating, (b) first cooling and (c) second heating.	146
38. Figure 3.12: Thermograms of complex 16 with the DSC showing multiple endotherms and the TGA showing the decomposition.	147
39. Figure 3.13: Optical micrographs of complex 2 on cooling at 120 °C at different magnifications. (a) at 30 μm and (b) at 50 μm.	148
40. Figure 4.1: Orbital diagrams showing the situations necessary for delocalisation of metal based mixed valence states by (a) hole transfer through the HOMO of the bridging ligand and (b) electron transfer through LUMO of the bridging ligand.	159

41. Figure 4.2: (A) is an electron switch that works by changing the chemical state of a molecule. (B) is a schematic illustration of a nanoscopic electronic switch in A. 161
42. Figure 4.3: Schematics of the device fabrication. (A) Cross section of a silicon wafer with a nanopore etched through a suspended silicon nitride membrane. (B) Au-SAM-Au junction in the pore area. (C) Blowup of (B) with **IIc** sandwiched in the junction membrane. 162
43. Figure 4.4: Potential mechanism for the NDR effect. As voltage is applied, the molecule in the SAM (A) undergo a one-electron reduction to form the radical anion (B) that provides a conductive state. Further increase of the voltage causes another one electron reduction to form the dianion insulating state (C). Q is the charge. 164
44. Figure 4.5: A schematic of the MCB junction with (a) the bending beam, (b) the counter support, (c) the notched gold wire, (d) the glue contacts, (e) the pizeo element, and (f) the glass containing the solution. 165
45. Figure 4.6: Schematic of benzene-1,4-dithiolate SAM with one molecule bridging the electronic circuit. 165
46. Figure 4.7: (a) Experimental I-V characteristics of the benzene-1,4-dithiolate molecule. (b) Theoretical I-V characteristics of the benzene-1,4-dithiolate molecule. 166
47. Figure 4.8: Examples of complexes that have been studied for their molecular wire ability. 171
48. Figure 4.9: Binuclear ferrocenyl complexes with large NLO properties. 172
49. Figure 4.10: ^1H NMR spectrum of compound **1**. 181
50. Figure 4.11: ^1H NMR spectrum of complex **9**. Inset: ^{31}P NMR spectrum of complex **9**. 184
51. Figure 4.12: FAB mass spectrum of complex **6**. 188
52. Figure 4.13: Electrospray mass spectrum of complex **9**. 191
53. Figure 4.14: MALDI-TOF mass spectrum of **8** showing fragments in Table 4.3. 195

54. Figure 4.15: (a) Molecular ion peak observed at $m/z = 999$ and (b) the theoretical isotropic distribution of **7** and **8**. 195
55. Figure 4.16: Cyclic voltammograms for compounds **2**, **6**, **8** and **9**. 198



List of Tables

1. Table 2.1: Typical terminal and linker groups in mesogens.	28
2. Table 2.2: Selected ¹ H NMR and Infrared data and molecular ion peaks (relative intensity in brackets) for compounds iii – viii .	48
3. Table 2.3: Mass spectral data (relative intensity in brackets) for compounds 1 – 9 .	53
4. Table 2.4: DSC and melting point data for compounds 4 – 9 .	54
5. Table 2.5: Crystallographic and refinement data for complexes 1a and 3a .	70
6. Table 2.6: Selected bond distances (Å) and bond angles (°) for 1a .	71
7. Table 2.7: Selected bond distances (Å) and bond angles (°) for 3a .	71
8. Table 2.8: Melting point of selected complexes showing that melting point decreases with chain length.	80
9. Table 2.9: Percentage mass losses and the corresponding fragment.	83
10. Table 3.1: Mesogenic properties of some Pd, Ni and Cu complexes.	98
11. Table 3.2; Crystallographic data for complex II .	114
12. Table 3.3: Selected bond distances (Å) and bond angles (°) for II .	115
13. Table 3.4: Table of phenyl signals (H _a and H _b) for cyclopentadienyl complexes versus diethyldithiocarbamate complexes, with peak separation.	122
14. Table 3.5: Molecular ion and base peak values abundances obtained for different matrices.	128
15. Table 3.6: Electrochemical parameters for complexes 1 , 2 and 4 .	131
16. Table 3.7: Electrochemical parameters for complexes 5 – 10 .	135
17. Table 4.1: Common fragments in the PBU ₃ series.	189
18. Table 4.2: Some of the common fragment ion observed in the MALDI-TOF spectra.	194
19. Table 4.3: Cyclic voltammetry data of complexes NiBr(PBU ₃)(η ⁵ -C ₅ H ₅), 6 , 8 and 9 .	199

Part of the work contained in this thesis has been published. A list of the publications with the title and authors follows.

1. *Synthesis and thermal behaviour of cyclopentadienylnickel(II) thiolato complexes. Crystal structures of $Ni(\eta^5-C_5H_5)PBu_3(SC_6H_4NC(H)C_6H_4C_6H_5)$ and $Ni(\eta^5-C_5H_5)PBu_3(SC_6H_4NC(H)C_6H_4OC_4H_9)$.*

R.M. Moutloali, J. Bacsá, D.A. Ddamba and J. Darkwa; *J. Organomet. Chem.* 2001, 629, 171

2. *[2,6-Bis(isopropylthiomethyl)phenyl- K^3S,C^3S']bromopalladium(II)*

R.M. Moutloali, J. Bacsá, and J. Darkwa; *Acta Cryst. Sec C.*, 2002, C58, M109

3. *Bimetallic nickel complexes with bridging dithiolato Schiff base ligands: synthesis, mass spectral characterisation and electrochemistry*

R.M. Moutloali, F.A. Nevondo, J. Darkwa, E. Iwuoha, and W. Henderson; *J. Organomet. Chem.* 2002, 656, 262

Dedication

To my family: my mother, my brothers: Selepe, Matsie, Nyadiwa and my beloved sister: Ntsoaki, and my late grandmother, who passed away during my PhD studies. To Maite, my friend and companion, and to Mathabo.



Chapter 1

Introduction to metal thiolate chemistry.

1.1 General areas of transition metal thiolate research.	1
1.2 Metal thiolates as models for hydrodesulfurisation (HDS) catalysis.	3
1.3 Metal thiolates as sulfur dioxide absorbers.	6
1.4 Metal thiolates as electronic conductors.	7
1.5 Metal thiolates as liquid crystals.	8
1.6 Rationale and objectives.	12
1.7 References.	13

1.1 General areas of transition metal thiolate research.

The chemistry of metal complexes containing thiolate ligands (L_nM-SR) has developed extensively over the last several decades.¹ They are an enormously rich class of compounds and are presently a subject of great interest in chemistry. As typical soft ligands the electron-rich thiolate groups (RS^-) and their multifunctional homologues $^-SRS^-$ have a great affinity for a large number of metals. The electronic and steric capabilities offered by the monodentate and bidentate chelates have been used to stabilize a broad spectrum of mononuclear, oligomeric and polymeric metal complexes with new and remarkable structures and properties. The thiolate ligands (RS^- and $^-SRS^-$) are capable of extreme variations in their coordination and bonding to metals. The monofunctional ligand, RS^- , can bond in a monodentate² (A), μ_2 -bridging³ (B) or μ_3 -bridging manner⁴ (Chart 1.1). The coordination possibilities offered by the bifunctional thiolate anion, $^-SRS^-$, are even greater.⁵

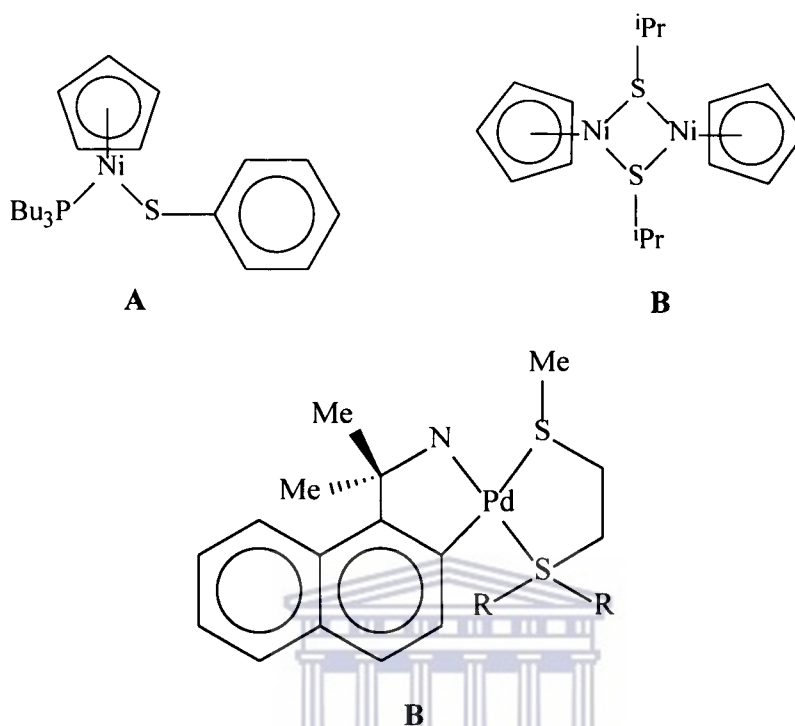


Chart 1.1: Typical binding modes of sulfur.

Metal thiolates are important for several applications; these are highlighted in the next two paragraphs. Metal centres with complete or partial sulfur coordination play an important part in the chemistry of life processes. Examples of this are provided by electron transferases such as the redox metalloprotein of iron, the ferredoxins, and oxidoreductases such as nitrogenases like plastocyanin, azurin and ceruloplasmin.⁶ Thus metal thiolates are extremely useful as models for metalloproteins⁷ and metalloenzymes⁸. Gold thiolates are also of importance as drugs, especially for the treatment of arthritis.⁹

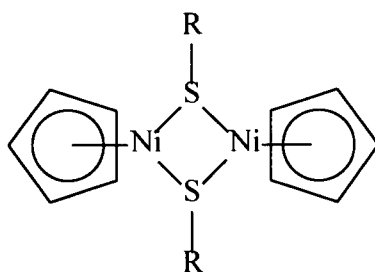
A new and interesting development is the use of volatile molecular metal thiolates as starting materials for chemical vapour deposition (CVD) of metallic or sulfidic surface layers.¹⁰ Metal thiolates also feature as models for hydrodesulfurisation (HDS) and in other catalytic systems.¹¹ In addition to the above, metal thiolates have potential applications in such diverse fields of material science from electronic (molecular) conductors¹² to liquid crystals¹³ and nonlinear optical (NLO)¹⁴ materials and as SO₂ absorbers or scrubbers¹⁵. Since the chemistry of metal-sulfur complexes is so wide, this

section will only deal with the following areas of interest: (i) metal thiolates as models for hydrodesulfurisation catalysis, (ii) metal thiolates as SO₂ absorbers and as catalysts, (iii) molecular or electronic conductors and (iv) as liquid crystals and nonlinear optical materials; since the metal thiolate reported in this thesis resemble complexes that have the above properties.

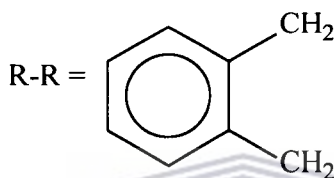
1.2 Metal thiolates as models for hydrodesulfurisation (HDS) catalysis.

Metal thiolates have been extensively studied as HDS catalysts.¹⁶ The mechanism of the HDS process¹⁷ is of interest to many inorganic chemists, because the catalytic action is poorly understood. Thus it provides an opportunity to prepare model compounds that can be used to mimic the heterogeneous process in homogenous reactions, metals such as Co, Ni and Nb are predominantly used in such studies.¹¹

Mechanistic investigation of the carbon-sulfur bond reduction with organometallic reagents under homogeneous conditions may provide useful information on the actual mode of heterogeneous desulfurisation reactions. Reactions of metal thiolates give molecular-level insights into these HDS processes by providing the structures and behaviour of molecular analogues.¹⁸ The ligation between the sulfur moiety and certain metals, such as Ni, Ti, Ru and Rh, activate the carbon-sulfur bond. The C-S bond cleavage is initiated thermally, photolytically or upon hydrogenation.¹⁹ Ho *et al.* studied the reductive cleavage of the C-S bond using LiAlH₄ in a series of complexes with a μ₂-sulfur bridge that have the general structure I.



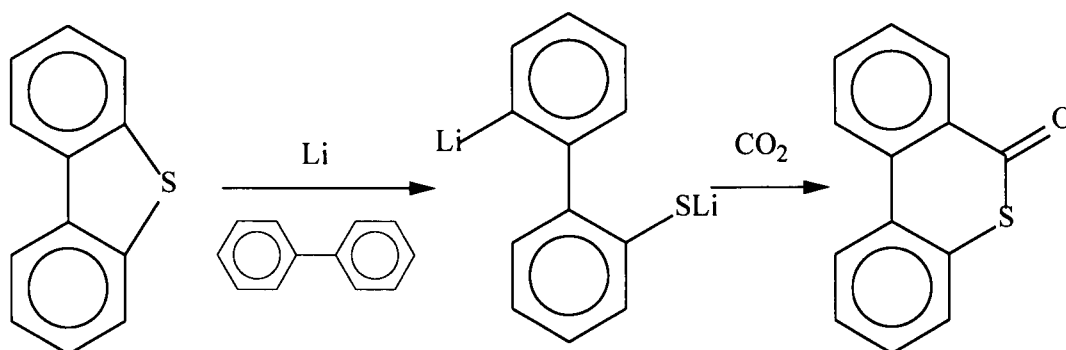
R = Ph, PhCH₂, 2-naphthyl, n-C₈H₁₇, R-R.



I

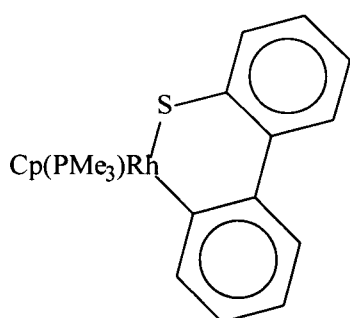
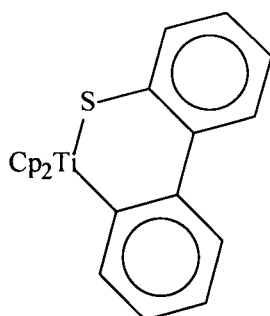
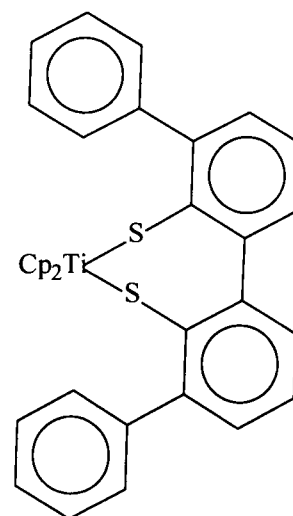
The Ho model suggests that the carbon-sulfur bond is activated by complexation with nickel and subsequent hydride transfer afford the corresponding reduced hydrocarbon. This result points to the role the hydridic species plays in the reduction. Yamamoto *et al.* on the other hand report that C-S bond reduction occurs upon thermolysis of the hydridothiolatonickel phosphine complexes²⁰ that indeed supports the involvement of the metal hydride in the C-S bond cleavage. The products from the reduction of the μ_2 -sulfur complexes with LiAlH₄ were benzene, toluene, decane, naphthalene and o-xylene, which all lack sulfur atoms.

Another good example of C-S bond activation is the reduction of dibenzothiophene (DBT) first reported in 1957 by Gilman and Dietrich.²¹ This reduction was later improved on by Eisch.²² DBT is one of the major sulfur-containing contaminants in fossil fuels and is amongst the most difficult compounds to desulfurise.²³



Scheme 1.1

Industrially these sulfur heterocycles are hydrogenolysed in HDS process by the action of metal catalysts to give hydrocarbons and hydrogen sulfide.²⁴ Thus the syntheses of metal complexes from sulfur-containing heterocycles is viewed as a way to study the mechanistic reactions of the HDS process by scientists.²⁵ Access to dibenzothiophene (BDT) metal complexes is generally *via* preactivation of the BDT (Scheme 1.1), followed by reaction with various organometallic fragments.² Some of the examples of HDS catalysts are **II**, **III** and **IV** shown below.²

**II****III****IV**

In using the compounds **II**, **III** and **IV** above as HDS catalysts, it was found that the sulfur to metal ratio was crucial. Only low sulfur-to-metal ratios led to desulfurisation,

whereas high sulfur to metal ratios actually formed organosulfur compounds such as thiophene.² Nevertheless the above study is a demonstration of how metal-thiolates can be used as models for HDS catalysis.

1.3 Metal thiolates as sulfur dioxide absorbers.

The ability of metal thiolates to absorb sulfur dioxide is another potential application for these complexes. Researchers are interested in the ability of metal thiolates to absorb sulfur dioxide, both reversibly and irreversibly, and its kinetics.² The research is driven by the need to remove the hazardous SO₂ from the environment. The combustion of fossil fuels and the roasting of metal sulfide ores is the primary cause of atmospheric sulfur dioxide pollution. One possible solution to this problem is to trap SO₂ before it is released into the atmosphere and research directed at solving the problem has led to reactions of metal thiolates with sulfur dioxide. In these complexes the sulfur dioxide can either bind to the metal¹⁶ or to the sulfur atom of the thiolate ligand. The former interaction seldom leads to reversible absorption of SO₂, whereas the latter invariably gives products that easily release sulfur dioxide gas; presumably because the ligand-sulfur dioxide interaction is generally weak.

Nickel thiolato complexes are some of the complexes that reversibly bind SO₂ molecules.³ In these complexes the Ni-SR functionality provides an excellent example of the nucleophilicity of the metal thiolates.³ This behaviour of the Ni-SR functionality is exemplified by the reversibility of the binding of SO₂ by (bme-daco)Ni(II) (bme-daco = 1,5-bis(mercaptoethylpropyl)-1,5-diazacyclooctane). Even though the possibility of SO₂ binding to the metal centre exists, it has been shown by X-ray crystallography that SO₂ exclusively binds to the sulfur atom of the thiolato ligand.^e The ability of these complexes to effectively reversibly absorb SO₂ gas effectively and reversibly, is influenced by the substituents on the thiolato ligand. Aryl substituents are found to enhance the reversibility whereas alkyl substituents do not. For example, reversibility of SO₂ absorption was observed for complexes (dppe)Ni(TDT) and (dppe)Ni(1,2-BDT)

(dppe = diphenylphosphinoethane; TDT = toluenedithiol, BDT = 1,2-benzenedithiol) but it was found that SO₂ does not bind to the metal when alkyl analogues are used.³

An alternative solution to the removing of SO₂ as a pollutant can be the activation of S=O bonds in SO₂ by transition metal thiolates, especially when reduced by hydrides and hydrogen.³ For example it has been shown that the complexes [(Me_nCp)Mo(μ-S)(μ-SH)]₂ (Cp = C₅H_{5-n}; n = 0, 1 or 5) and their chromium analogue (Cp^{*}Cr₂S₅; Cp^{*} = C₅Me₅) effectively catalyse the homogeneous hydrogenation of SO₂ to S₈ and H₂O.³

1.4 Metal thiolates as conductors.

The rapid developments in the field of telecommunication and computing devices are pressing the need for improved electronic components. The technology needed will mainly depend on the interplay between electrons and photons. Molecular chemistry offers a unique opportunity to design materials combining several properties (e.g. magnetism, conductivity and nonlinear optics or a combination of the three) that could be coupled in an actual interplay.³

Self assembled monolayer (SAM) structures composed of n-alkanethiol derivatives chemisorbed onto gold surfaces and bearing varying amounts of pendant electroactive species or groups have been shown to be excellent systems in which factors that govern the rate of electron transfer across interfacial barriers could be investigated for conduction.³ Various systems have been studied in order to obtain structure-property relationships that can be used to get a clearer picture of how structural effects could mediate the electron transfer processes.³ In most of the SAMs used, conjugated oligomers are α, ω-dithiol. The thiol functionality is necessitated by the need for binding between proximate gold probes in electronic conduction experiments.³

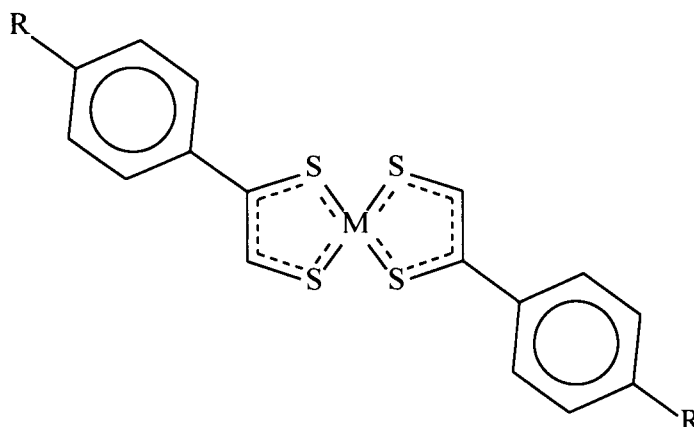
Several ways of introducing the terminal thiol functionality have been described and include; (i) the *in-situ* NH₄OH-promoted deprotection of acetyl protected thiol, (ii) the non-base promoted adsorption of thioacetyl terminated oligomers on gold, to finally form

surface-bound thiolates. When such systems are surface bound via an aromatic thiol unit there is no possibility of any insulation occurring, as there are no alkyl chains to do that.³

Such metal thiolate compounds effectively conduct, through electron movement along the thiolato ligands. When long alkyl or alkoxy chains are attached to thiolato ligands, the metal thiolates tend to behave as liquid crystalline materials and with shorter chains as nonlinear optical materials. Since this thesis deals mainly with metal thiolato complexes that may have potential mesogenic behaviour, a review of metal thiolato complexes with liquid crystalline properties will be given in subsequent sections of this chapter and a more detailed account of metallomesogens, as well as background information about the liquid crystalline state, in chapter 2.

1.5 Metal thiolates with liquid crystalline properties.

Ligands that have sulfur as the donor atom also form metal complexes with liquid crystalline properties. However, prior to the work that is reported in this thesis, all such complexes featured only bidentate thiolato ligands. Giroud and Muller-Westerhoff were the first to systematically study the d^8 (Ni(II), Pd(II) and Pt(II)) metal atoms with dithiolene ligands. The main types of complexes are exemplified by **V**, **VI** and **VII**. X-ray diffraction studies showed that the nickel complex had the expected M(II) square planar geometry, with substituents trans to each other,³ thus providing the platform for the desired packing in the liquid crystalline state.



M = Ni (V), Pd (VI) or Pt (VII), R = C_nH_{2n+1}, n = 4 - 12, .

Figure 1.1: A typical dithiolato liquid crystalline complexes.

The nickel and the platinum complexes form nematic and smectic mesophases. Complexes with n = 4 and 5 in 1.1 are nematic and those with n > 6 are smectic.⁴ The palladium complexes, however, have no mesogenic properties.⁴ It is surprising that the palladium analogues have no mesogenic behaviour, since the structural and electronic properties of these palladium complexes are similar to those of the nickel and platinum complexes.

Other types of thiolato complexes found to be mesogenic are the bis(4-alkoxydithiobenzoato) complexes of nickel(II) and palladium(II) (Fig. 1.2).⁴ These complexes are structurally similar to those synthesised by Giroud and Muller-Westerhoff in 1978 but have alkoxy chains instead of alkyl chains and a 4-membered metallo-ring instead of a 5-membered ring.⁴ Optical microscopy, combined with X-ray diffraction and differential scanning calorimetry (XD-DSC) study, confirmed the formation of smectic C, S_c, mesophases for the palladium complexes with longer chains (n ≥ 8) and of N phases for shorter chains (n = 4, 5).⁴ The nickel analogues showed similar results. Using the same ligand system as for groups V and VI metal complexes (Cu, Zn and Hg) with complex coordination geometries can be prepared. For example the zinc compound was found to be monomeric in solution, but binuclear in the solid state forming an eight

membered $Zn_2S_4C_2$ ring.⁴ The related mercury complexes $(Hg(S_2CC_6H_4OC_nH_{2n+1})_2$ ($n = 4, 8$) were found to possess intermolecular $Hg...S$ interactions in the solid state. They have two shorter trans $Hg-S$ bonds (2.41 Å) and two longer trans $Hg-S$ bonds (2.96 Å) in the same plane, but also had two additional axial intermolecular $Hg...S$ contacts (3.36 Å).^{3 b} Both the four membered metallo-sulfur ring and the five membered metallo-sulfur ring give rise to calamitic mesogens. However complexes with aromatic rings exhibit smectic mesophases as opposed to nematic phases produced by complexes with non-aromatic rings.

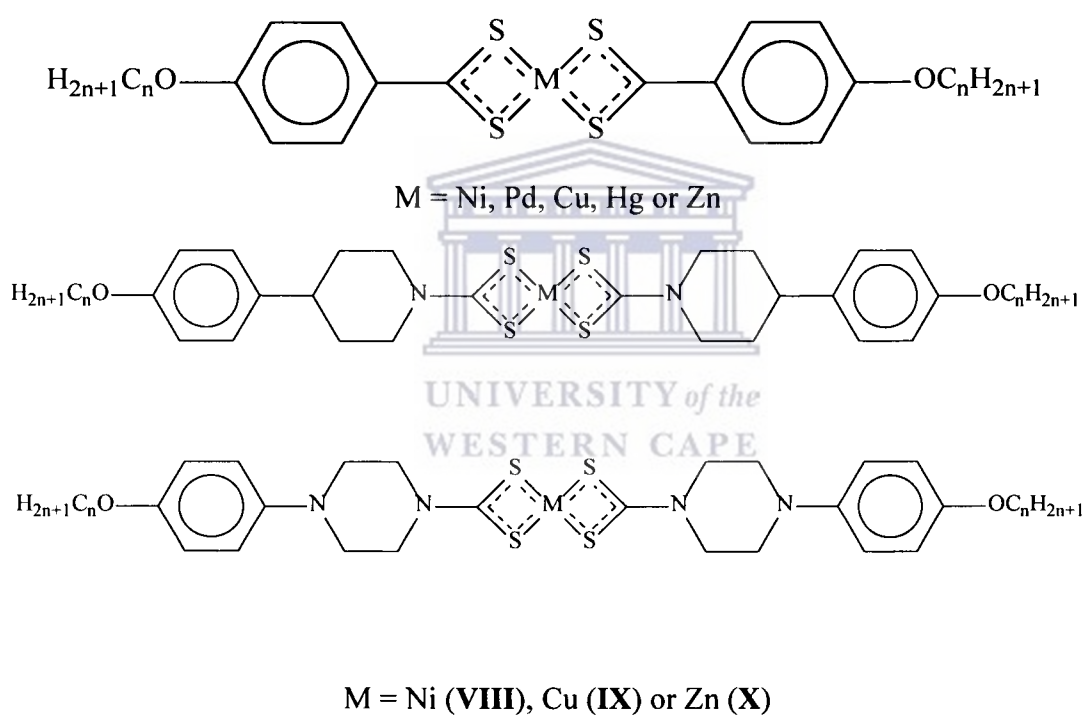
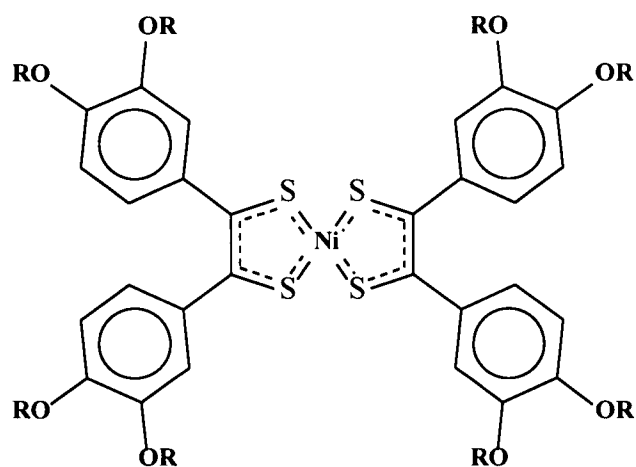


Figure 1.2: Dithiolato mesogens with a four-membered metallo-sulfur ring.

In addition to these calamitic mesogens, metal-sulfur complexes that form discotic mesogens are known.⁴ For example a nickel complex with four 3,4-bis(dodecyloxy)phenyl substituents, **XI**, characterised by X-ray diffraction, was found to form hexagonal disordered columnar mesophases (D_{hd}).⁴



XI

In spite of a fairly good number of bidentate dithiolato metallomesogens in the literature, there are no known examples of simple monothiolato metal complexes with mesogenic behaviour.

The research work reported in this thesis was undertaken to initially investigate the use of monothiols to prepare nickel thiolate mesogens. It later developed into the use of both mono- and dithiols in forming nickel and palladium thiolates. The section below thus outlines the final objectives of the research projects reported in the thesis.

1.6 Rationale and Objectives.

The literature that is devoted to dithiolates as ligands for metallomesogens chemistry is voluminous. On the other hand there is virtually no literature report on monothiols as ligands for metallomesogens. Therefore this thesis is an investigation on the use of monothiols as ligands for the preparation of metallomesogens. Secondly it deals with the study of the effects bulky ancillary ligands have on the thermal properties of compounds that are studied as liquid crystals. Most compounds that are studied for their liquid crystal behaviour have small lateral substituents and thus seek to retain the molecular shapes of their promesogenic ligands. Thirdly, this study compares the different shapes of molecules with respect to their mesogenic behaviour based on the size of the lateral substituents, the molecular lengths and the geometry around the metal atom.

Chapter 4 deals with the study of dithiol Schiff base compounds as bridging ligands for nickel compounds. This was done with the aim of probing the molecular wire ability of the dithiol Schiff base bridges. Most compounds that are studied for their molecular wire ability have purely carbon functional groups such as alkene and alkynes as linkers between aromatic rings. In such compounds the ligand is bound to the metal via a metal-carbon σ -bond. In the present study we have used the imine group as a linker and a metal-sulfur bond instead of the conventional metal-carbon bond. This was done with the view that most studies on electronic conduction in organic molecule-solid (usually gold) electrode nanojunctions, the binding sites are usually a sulfur atom. Rarely is a metal-sulfur bond used in solution state studies of molecular wires studies. Cyclic voltammetry was the technique of choice due to its simplicity and the fact that it does not depend on thermodynamic factors but only on the static spectroscopic parameters.

References

1. J. Arnold, *Prog. Inorg. Chem.* 1995, **43**, 353.
2. (a) Y.-P. Tian, W.-T. Yu, C.-Y. Zhao, M.-H. Jiang, Z. G. Cai, H. K. Fun, *Polyhedron* 2002, **21**, 1217, (b) J. Darkwa, F. Bothata, L. M. Koczon, *J. Organomet. Chem.* 1993, **455**, 235.
3. (a) Y. Mizobe, M. Hosomizu, Y. Kubota, M. Hidai, *J. Organomet. Chem.* 1996, **507**, 179; (b) T. E. Bitterwolf, W. B. Scallorn, B. Li, *Organometallics*, 2000, **19**, 3280; (c) F. Goldoni, L. Antolini, G. Pourtois, A. P. H. J. Schenning, R. A. J. Janssen, R. Lazzaroni, J.-L. Bredas, E. W. Meijer, *Eur. J. Inorg. Chem.* 2001, 821.
4. (a) S. Brooker, P. D. Croucher, T. C. Davidson, G. S. Dunbur, C. U. Beck, S. Subramanian, *Eur. J. Inorg. Chem.* 2000, 169; (b) R. Cao, X. Lei, Z. Huang, M. Hong, H. Liu, *J. Coord. Chem.* 1992, **25**, 165.
5. (a) R. M. Buonomo, I. Font, M. J. Maguire, J. H. Reibenspies, T. Tuntulani, M. Y. Darensbourg, *J. Am. Chem. Soc.* 1995, **117**, 963; (b) S. Y. M. Chooi, T. S. Andy Hor, P.-K. Leung, K. F. Mok, *Inorg. Chem.* 1992, **31**, 1494.
6. B. Krebs, G. Henkel, *Angew. Chem. Int. Ed. Engl.* 1991, **30**, 769.
7. B. S. Hammes, M. T. Kieber-Emmons, J. A. Letizia, Z. Shirin, C. J. Carrano, L. N. Zakharov, A. L. Rheingold, *Inorg. Chim. Acta*, 2003, **346**, 227
8. T. P. Smyth, J. G. Wall, Y. Nitanai, *Bioorg. Med. Chem.*, 2003, **6**, 991
9. B. P. Espósito, R. Najjar, *Coord. Chem. Rev.*, 2002, **232**, 137.
10. S. Kikkawa, *Ceram. Int.* 1996, **23**, 7.
11. (a) I. V. Babich and J. A. Moulijn, *Fuel*, 2003, **82**, 607; (b) S. J. Sawhill, D. C. Phillips, M. E. Bussell, *J. Cat.*, 2003, **215**, 208.
12. (a) N. Robertson, L. Cronin, *Coord. Chem. Rev.* 2002, **227**, 93; (b) K. Kubo, M. Nakano, S. Hamaguchi, G. Matsubayashi, *Inorg. Chim. Acta*, 2003, **346**, 43.
13. (a) T. V. Basova, A. G. Gürek and V. Ahsen, *Mat. Sci. Eng. C*, 2002, **22**, 99; (b) B. Bilgin Eran, D. Singer, J. Pickardt, K. Praefcke, *J. Organomet. Chem.* 2001, **620**, 249.
14. L. F. Veiros, *J. Organomet. Chem.*, 2001, **632**, 3.

15. (a) J. Darkwa, R. M. Moutloali, T. Nyokong *J. Organomet. Chem.*, 1998, **564**, 37;
(b) N. Rajendiran, J. Santhanalakshmi *Polyhedron* 2002, **21**, 951.
16. (a) H. Topsoe, B. S. Clause, *Catal. Rev.* 1984, **22**, 395; (b) B. Bodanovic, P. Gottsch, M. Rubach, *J. Mol. Catal.* 1981, **11**, 135; (c) D. Fenske, J. Ohmar, J. Hachgenei, K. Merzweiler, *Angew. Chem. Int. Ed. Engl.* 1988, **27**, 1277.
17. M. Rakowski-DuBois, *Chem. Rev.* 1989, **89**, 1.
18. K. E. Howard, J. R. Lockmeyer, M. A. Massa, T. B. Rauchfuss, S. R. Wilson, X. Yang, *Inorg. Chem.* 1990, **29**, 4385.
19. M. F. Ho, T. C. W. Mak, T.-Y. Luh, *J. Chem. Soc. Dalton Trans.* 1990, 3591.
20. K. Osakada, M. Hayashi, M. Maeda, T. Yamamoto, A. Yamamoto, *Chem. Lett.* 1986, 597.
21. H. Gilman, J. J. Dietrich, *J. Org. Chem.* 1957, **22**, 851.
22. J. J. Eisch, *J. Org. Chem.* 1963, **28**, 707.
23. P. R. Stafford, T. B. Rauchfuss, A. K. Verma, S. R. Wilson, *J. Organomet. Chem.* 1996, **526**, 203.
24. T. B. Rauchfuss, *Prog. Inorg. Chem.* 1991, **31**, 259.
25. W. D. Jones, R. M. Chin, *J. Am. Chem. Soc.* 1992, **114**, 9851.
26. S. Harris, *Polyhedron* 1997, **16**, 3219.
27. J. J. Garcia, B. E. Mann, H. Adams, N. A. Bailey, P. M. Maitlis, *J. Am. Chem. Soc.* 1995, **117**, 2179.
28. I. Kovacs, C. Pearson, A. Shaver, *J. Organomet. Chem.*, 2000, **596**, 193.
29. (a) K. A. Kubat-Martin, G. J. Kubas, R. R. Ryan, *Organometallics*, 1989, **8**, 1910;
(b) D. K. Mills, Y.-M. Hsiao, P. J. Farmer, E. V. Etnip, J. H. Reibenspies, M. Y. Darensbourg, *J. Am. Chem. Soc.* 1991, **113**, 142; (c) S. G. Davies, J. R. McNally, A. J. Smallbridge, *Adv. Organomet. Chem.* 1990, **30**, 1; (d) J. Amarasekera, T. B. Rauchfuss, A. L. Rheingold, *Inorg. Chem.* 1987, **26**, 201; (e) M. Y. Darensbourg, T. Tuntulani, J. H. Reibenspies, *Inorg. Chem.* 1994, **33**, 611.
30. (a) G. J. Kubas, R. R. Ryan, *J. Am. Chem. Soc.* 1985, **107**, 6138; (b) G. J. Kubas, R. R. Ryan, *Polyhedron* 1986, **5**, 473.
31. J. Darkwa, *Inorg. Chim. Acta*, 1997, **257**, 137.

32. (a) A. Toupadakis, G. J. Kubas, C. J. Burns, *Inorg. Chem.* 1992, **31**, 3810; (b) G. J. Kubas, R. R. Ryan, *Inorg. Chem.* 1984, **23**, 3181.
33. (a) G. J. Kubas, R. R. Ryan, K. A. Kubat-Martin, *J. Am. Chem. Soc.* 1989, **111**, 7823; (b) A. Shaver, P.-Y. Plouffe, *Inorg. Chem.* 1992, **31**, 1832; (c) I. Malfant, R. Andreu, P. G. Lacroix, C. Faulmann, P. Cassoux, *Inorg. Chem.* 1998, **37**, 3361.
34. (a) C. E. D. Chidsey, C. R. Bertozzi, T. M. Putvinski, A. M. Mujsce, *J. Am. Chem. Soc.* 1990, **112**, 4301; (b) C. E. D. Chidsey, *Science* 1991, **251**, 919.
35. R. P. Hsung, C. E. D. Chidsey, L. R. Sita, *Organometallics*, 1995, **14**, 4808.
36. J. M. Tour, L. Jones II, D. L. Pearson, J. J. S. Lamba, T. P. Burgins, G. M. Whitesides, D. Allara, A. N. Parith, S. V. Atre, *J. Am. Chem. Soc.* 1995, **117**, 9529.
37. (a) L. Brossard, M. Ribault, L. Valade, P. Cassoux, *J. Phys. B* 1986, **143**, 378; (b) P. Cassoux, L. Valade, H. Kobayashi, A. Kobayashi, R. A. Clark, A. Underhill, *Coord. Chem. Rev.* 1991, **110**, 115.
38. (a) P. Espinet, *Gold Bullet.* 1999, **32**, 127; (b) A. M. Giroud-Godquin, P. M. Maitlis, *Angew. Chem. Int. Ed. Engl.* 1991, **30**, 375.
39. A. M. Giroud, *Ann. Phys. (Paris)* 1998, **3**, 147.
40. A. M. Giroud-Godquin, *Chem. Rev.* 1998, **178-180**, 1485.
41. (a) A.-M. Giroud, A. Nazzal, U. T. Muller-Westerhof, *Mol. Cryst. Liq. Cryst.* 1980, **56**, 225; (b) U. T. Muller-Westerhof, A. Nazzal, R. J. Cox, A.-M. Giroud, *Mol. Cryst. Liq. Cryst.* 1980, **56**, 249.
42. A. M. Giroud, U. T. Muller-Westerhof, *Mol. Cryst. Liq. Cryst.* 1977, **41**, 11.
43. (a) M. Bonamico, G. Dessy, V. Fares, L. Scaramuzza, *J. Chem. Soc. Dalton Trans.* 1972, 2515.
44. H. Adams, N. A. Bailey, D. W. Bruce, R. Dhillon, D. A. Dunmur, S. E. Hunt, E. Lalinde, A. A. Maggs, R. Orr, P. Styring, M. S. Wragg, P. M. Maitlis, *Polyhedron* 1988, **7**, 1861.
45. K. Ohta, H. Hasebe, H. Ema, T. Fujimoto, *J. Chem. Soc. Chem. Commun.* 1989, 1610.

Chapter 2

Schiff base Cyclopentadienylnickel(II) complexes as potential mesogens: Synthesis and Characterisation.

2.1 Introduction to liquid crystals.	17
2.2 Characterisation of liquid crystalline materials.	21
2.2.1 Differential Scanning Calorimetry, DSC.	21
2.2.2 Hotstage Polarising Microscope.	22
2.2.3 X-ray diffraction spectrometry.	24
2.3 Designing liquid crystals.	25
2.4 Schiff base organic liquid crystals.	27
2.5 Metallomesogens: metal containing liquid crystals.	30
2.5.1 What are metallomesogens.	30
2.5.2 Advantages of the inclusion of a metal atom.	31
2.5.3 Metallomesogens with monodentate ligands.	31
2.6 Experimental section.	36
2.6.1 Materials and instrumentation.	36
2.6.2 Synthesis of Schiff base compounds.	37
2.6.3 Synthesis of cyclopentadienylnickel(II) Schiff base complexes.	41
2.7 Results and discussion.	46
2.7.1 Synthesis and characterisation of alkoxybenzaldehyde and Schiff base thiols.	46
2.7.2 Thermal behaviour of Schiff base compounds.	54
2.7.3 Synthesis and characterisation of cyclopentadienylnickel(II) Schiff base complexes.	64
2.7.4 Molecular structures of $\text{Ni}(\text{SC}_6\text{H}_4\text{NC}(\text{H})\text{C}_6\text{H}_4\text{C}_6\text{H}_5)(\text{PBu}_3)$ ($\eta^5\text{-C}_5\text{H}_5$) and $\text{Ni}(\text{SC}_6\text{H}_4\text{NC}(\text{H})\text{C}_6\text{H}_4\text{OC}_4\text{H}_9)(\text{PBu}_3)(\eta^5\text{-C}_5\text{H}_5)$.	69
2.7.5 Thermal studies of cyclopentadienylnickel(II) Schiff base complexes.	78
2.8 Summary	88

2.1 Introduction to liquid crystals.

Most solid materials produce isotropic liquids directly upon heating however when certain solids are heated they do not pass directly into a liquid state but adopt a structure which has properties intermediate between those of a true crystalline solid and those of a true liquid. These intermediate phases are called liquid crystalline phases or mesophases. On reaching a specific temperature when a liquid crystalline material is heated, the solid undergoes transformation into a turbid condition that is both birefringent and fluid. The consistency of the material in the turbid condition varies with different compounds from that of a paste to that of a freely flowing liquid. At a higher temperature, this turbid state changes into a true liquid. As the liquid cools from the isotropic state to the solid state the changes may take place in the reverse order.¹ Materials that have the above properties are known as thermotropic liquid crystals (or thermotropic mesogens) as the transformation that they undergo is brought about by changes in temperature. When the transformation occurs both on heating and on cooling the material is termed enantiotropic, while it is termed monotropic if the transformation either occurs only on heating or only on cooling.^{1, 2 a - c}

A similar behaviour can occur upon the destruction of the crystalline network by addition of solvent. Such mesogens are called lyotropic liquid crystals and show temperature and concentration dependent mesophases.^{2a} Thermotropic mesogens can display several transition temperatures between phases, e.g. crystal-crystal transitions (i.e. as normal solids), melting points (solid-mesophase transition), mesophase-mesophase (when several mesophases could be involved) and lastly the clearing point (mesophase-isotropic liquid).³ The transition from the crystalline solid to the mesophase is often termed the melting point, while that from the highest mesophase to the isotropic liquid is called the clearing point.^{2b} This reflects the fact that mesophases often appear turbid while isotropic liquids are clear. Thermotropic mesophases are subdivided into two main classes: calamitic (rod-like)⁴ and discotic (disc-like).⁵ These two classes are further divided into smectic and nematic mesophases with respect to their molecular arrangements. These distinctions are outlined below.

In a mesophase some, but not all, of the long-range order is maintained. As such these phases are distinguished by the extent of their long-range ordering. Brown and Shaw have outlined the transformations that occur from completely ordered solids through smectic and nematic structures to the true liquid as follows:¹

- (i) *Three-dimensional crystal.* In a truly 3-dimensional crystal, apart from vibration, the centres of gravity of all lattice units are fixed, and rotations are not possible.
- (ii) *Crystal with rotating molecules.* The centres of gravity of all the lattice units are fixed and rotation about one or more axes is possible. Examples of this type are butyl halides.
- (iii) *Smectic structure.* The centres of gravity of the units (molecules) that have smectic structures are mobile in two directions and rotation about one axis is permitted.
- (iv) *Nematic structure.* The centres of gravity of the units (molecules) are mobile in three directions and rotation about one axis is permitted.
- (v) *True liquid.* The centres of gravity of the molecules (units) are mobile in three directions and rotations about three axes that are mutually perpendicular to one another are possible.

Because the smectic phase arises if the lateral intermolecular forces are stronger than the terminal forces, on heating the terminal forces break down first. The result is the loss of in-plane translational order. The net result is that the molecules are arranged in a lamellar fashion in which molecular layers are not well defined. Due to possible correlation in the layers and between layers, there are several smectic modifications that can be formed. Hence the smectic phase is subdivided into several classes that portray the lamellar molecular layer arrangement. Figure 2.1 shows possible melting sequences for a liquid crystal material and Figure 2.2 shows the classes of smectic mesophases that are possible for smectic liquid crystals. The above fundamental differences in smectic and nematic mesophases can therefore be used to differentiate between the two liquid crystalline states and also further show the divisions in each type of mesophase.

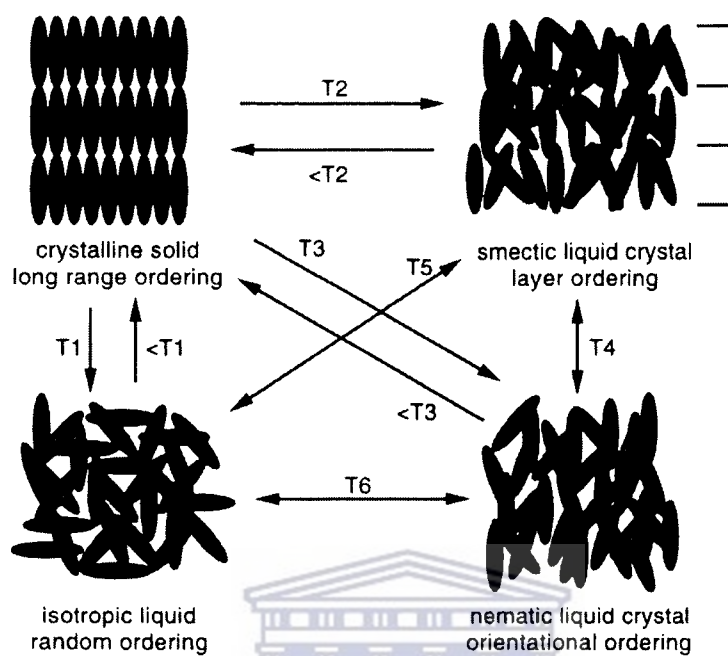


Figure 2.1: Possible melting sequence for a liquid crystalline material.⁶

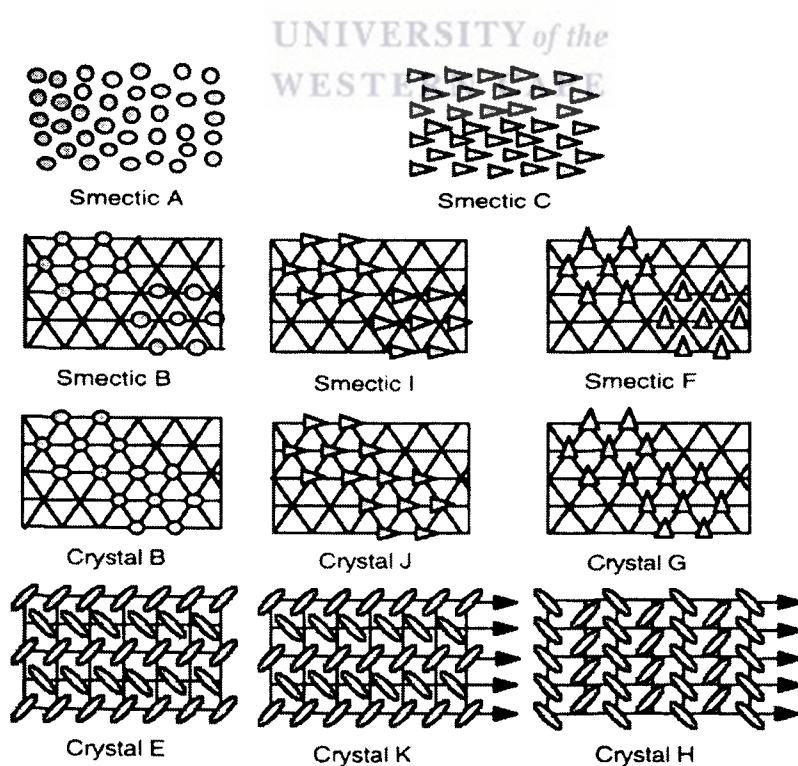


Figure 2.2 Plan view of smectic mesophase structures.⁶

Nematic mesophases are however generally found in discotic liquid crystals. Discotic phases have two types of packing, the columnar discotic and the nematic discotic, which are represented in Figure 2.3. The simplest type is the nematic phase in which the short axis of the molecules preferentially orient along a single direction. This phase is depicted in Figure 2.3a, where it is clear that there is no positional order in the phase. Positional order in discotic liquid crystals displays itself by the tendency of the molecules to arrange themselves in columns. This means that in the plane perpendicular to the columns, the molecules tend to arrange themselves in a two-dimensional lattice. In the more ordered arrangement the molecules will either arrange themselves in a rectangular or hexagonal fashion as they diffuse throughout the sample. The columnar arrangement of molecules is shown in Figures 2.3b and 2.3c.

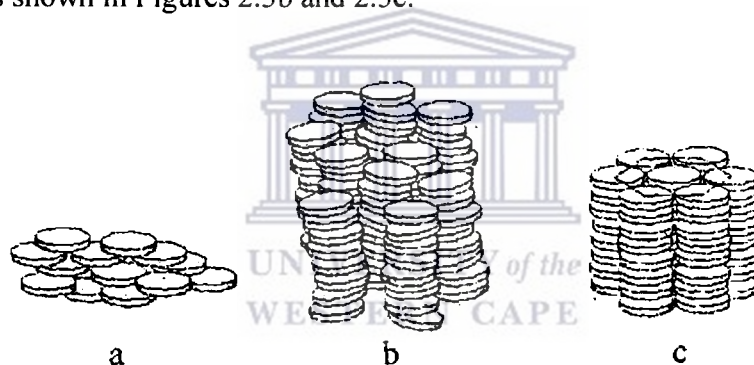


Figure 2.3: Commonly observed discotic mesophases: (a) nematic discotic; (b) nematic columnar; (c) discotic hexagonally ordered.⁷

Another modification of discotic mesophase is the cholesteric phase. The term cholesteric was coined because historically the phase was observed for derivatives of cholesterol. The phase is mobile like the nematic phase, but it is characterised by bright colours in reflected light and by a very high optical rotatory power. This phase, though predominantly associated with derivatives of cholesterol, can be obtained from other substances. To form a cholesteric phase the molecule must have a plate like structure as, for example, cholesterol and must be optically active, *i.e.* it must be chiral.^{3b} In addition to the orientational ordering, the smectic phases also possess varying degrees of spatial ordering and molecular tilt such that several smectic phases may exist.⁸

2.2 Characterisation of liquid crystal materials.

Three techniques are generally used to characterise liquid crystals. These are differential scanning calorimetry (DSC), polarised optical microscopy and X-ray diffraction studies.

2.2.1 Differential Scanning Calorimetry.^{1a, 5}

DSC reveals the presence of phase transitions in a material by detecting the enthalpy change associated with each phase transition. When a material melts, a change of state occurs from a solid to a liquid and this melting process requires energy (endothermic) from the surroundings. On the other hand, crystallisation of a liquid is an exothermic process and energy is released to the surroundings. The melting transition from a solid to a liquid is a relatively drastic phase transition in terms of the structural change. This is reflected by the high energy of transition. DSC can detect the subtle phase transitions that are involved in liquid crystalline materials. Thus when a DSC experiment is performed on a material that is a liquid crystal, the thermogram will consist of multiple endothermic events when the sample is heated. On cooling the sample there will be the reverse of phase changes that occurred on heating and hence the cooling will give rise to multiple exothermic events, although this is not always the case as in the case of monotropic liquid crystals alluded to in section 2.1. Figure 2.4 shows typical thermograms produced by a liquid crystalline material. The enthalpy changes involved in liquid crystalline phase transitions are however usually relatively small. Although the enthalpy changes at a transition cannot identify the types of phases associated with transitions, the magnitude of the enthalpy change is proportional to the changes in structural ordering of the phases involved. Typically, a melting transition from crystalline solid to a liquid crystal phase or the isotropic liquid phase generates an enthalpy change around 30 to 50 KJ.mol^{-1} , which indicates that considerable structural change is occurring. For example, the enthalpy changes for transitions from smectic phases to isotropic phases are larger than those of a nematic phase to isotropic phase, typically 4 to 6 kJ.mol^{-1} and 1 to 2 kJ.mol^{-1} respectively.

Therefore DSC measurement is the first and simplest of analytical data that can be used to detect liquid crystalline behaviour.

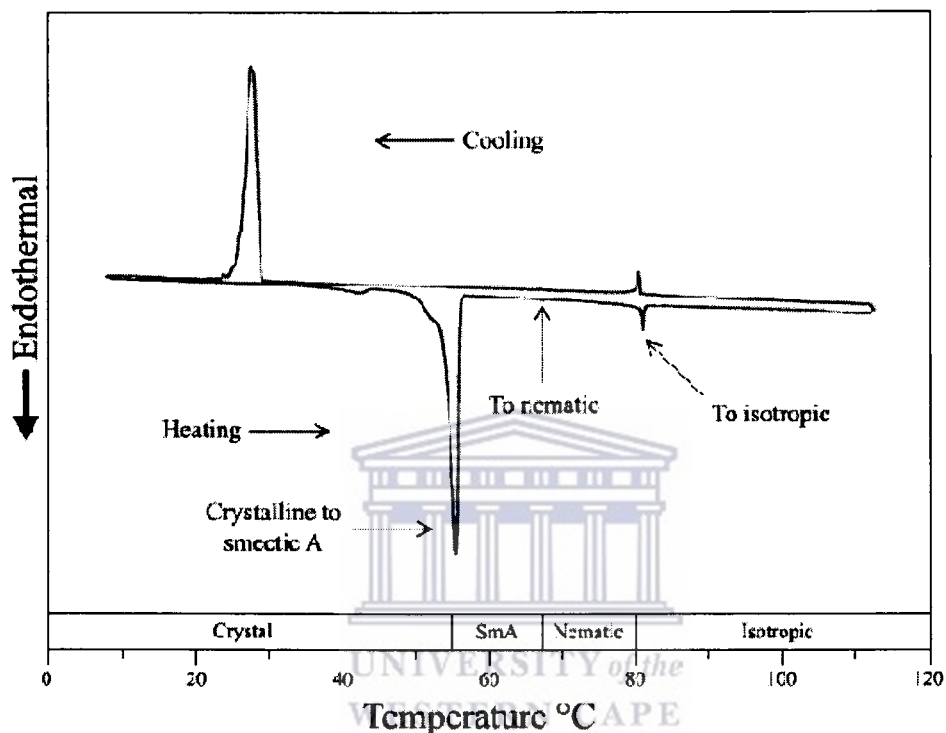


Figure 2.4: Typical thermograms of a liquid crystal on heating and on cooling.

2.2.2 Hotstage Polarising Optical Microscopy.

The use of polarised optical microscope to identify and characterise liquid crystals is not trivial and requires an expert who knows how to do this. The identification of mesophase through optical polarising microscopy involves the magnified view of a thin sample of a mesogenic material sandwiched between a glass microscope slide and a glass cover slip. Figure 2.5 is a schematic representation of the setup required for such an experiment. Since the polarisers in the microscope are crossed at 90° to each other, then with no sample in place light is extinguished and so blackness is seen. Similarly, if an isotropic liquid is analysed, the polarised light remains unaffected by the isotropic sample and so no light passes through the analyzer. However, when an anisotropic, birefringent medium is present light is not extinguished and an optical texture appears.

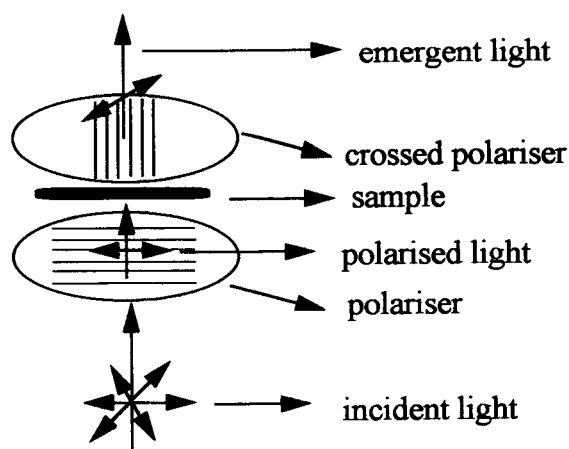


Figure 2.5: A schematic diagram of a hotstage polarizing optical microscope with a sample.

The texture that is observed gives information relating to the molecular arrangement within the medium that is analysed. Figure 2.6 shows typical textures that are found for nematic and smectic liquid crystals when the liquid crystalline state is viewed with a microscope between crossed polarisers. Optical microscopy is the main technique for identification of the type of mesophase, but unequivocal identification sometimes requires low angle X-ray diffraction studies on the mesophase.

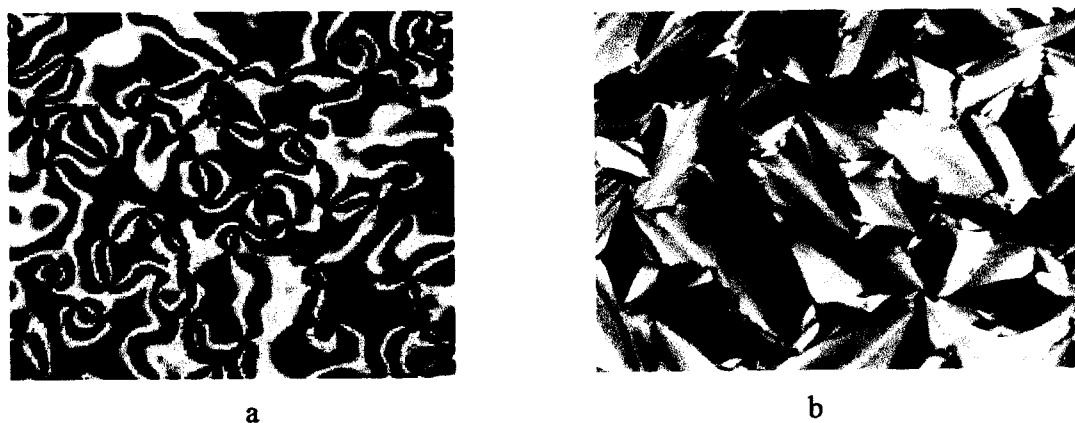


Figure 2.6: Typical textures observed for nematic (a) and smectic (b) liquid crystalline materials.

2.2.3 X-ray Diffraction

The structure of an ordered crystal is simply described using three positional (and appropriate thermal) parameters per atom. These parameters are obtained from a detailed X-ray or neutron diffraction study. The aim is to obtain up to ten independent Bragg intensities per structural parameter. For isotropic liquid, on the other hand, only diffuse diffraction peaks are observed and the structure can only be described in terms of a radial distribution function, which, for a molecular liquid, contains no atomic details. The diffraction pattern of all the phases (mesophases), because of the large amount of disorder always present, at most gives a very small number of independent Bragg reflections, plus considerable structured diffuse scattering. For true long-range order (a true crystal) the diffraction pattern consists of infinitely sharp peaks. For an isotropic phase only a diffuse peak is observed. For a liquid crystalline phase, which has a quasi-long range ordering, the diffraction pattern shows generally one peak that is sometimes broadened at the base. Thus the liquid crystalline phase shows X-ray characteristics that are intermediate between those of a true crystal and those of a true isotropic fluid. Figure 2.7 shows typical X-ray diffraction patterns associated with different phases of matter, including that of a liquid crystalline phase.

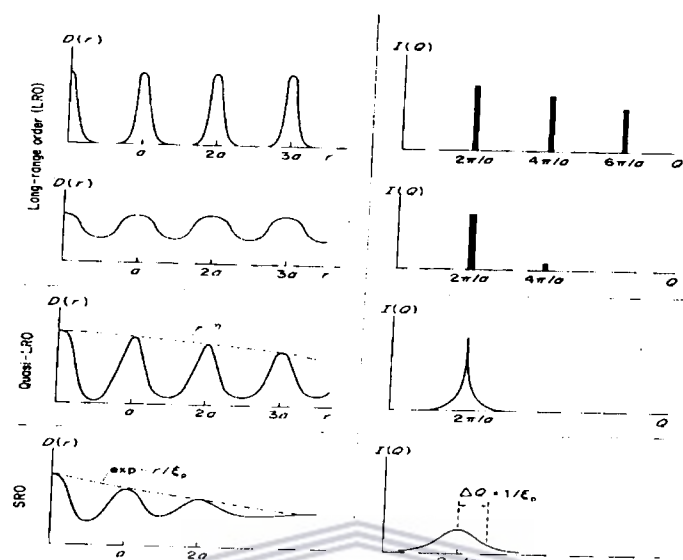


Figure 2.7: X-ray diffraction pattern for an ordered solid, a liquid crystalline material and an isotropic liquid.

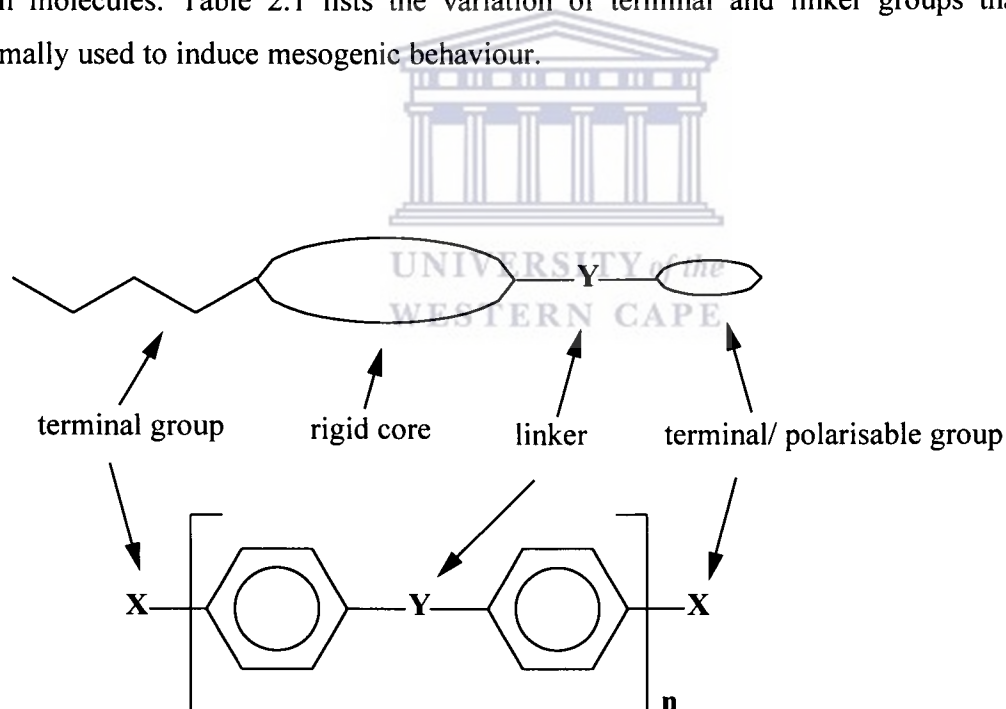
Generally for a full characterization of liquid crystal material, all three techniques are needed. However in most cases only DSC and optical microscopy are used.

2.3 Designing Liquid Crystals.

Mesogenic behaviour is a genuine supramolecular phenomenon based on the existence of extended weak interactions (e.g. dipole-dipole, dispersion forces, etc.) between molecules. A characteristic feature of a molecule that will show the mesomorphic state cannot be easily defined. Usually, for these forces to be important enough, it is necessary for the molecules to have anisotropic shapes to be able to pack efficiently; so that these weak interactions can be high in number, cooperate and become strong enough to keep the molecules associated in a preferred orientation, but free to move as they are not connected by rigid bonds. As a result mesomorphic behaviour is found in aromatic, aliphatic and multi-ring compounds. These compounds should have the ability to lose the long-range translational order of the molecular centres but still be able to maintain long-

range orientational order. Thus the material should have molecules with strong rotational anisotropy. Molecules that fulfill these requirements are plate-like or rod-like.^{3c}

In 1933 Bernal and Crowfoot⁹ proposed that for an aromatic molecule to show mesomorphic behaviour it must possess the following characteristics: (i) the molecules must be geometrically anisotropic and either rod-shaped or flat-shaped, (ii) there must not be more than one group in the molecule with a high dipole, and (iii) the molecule should contain moderately active groups such as $-CCl$, $-COC-$, $-CH=N$ and $-OCO_2-$ towards the extremities of the molecule.⁹ All these characteristics are combined in the design of liquid crystals and the schematic diagram below (Scheme 2.1) serves as a guide in designing such molecules. Table 2.1 lists the variation of terminal and linker groups that are normally used to induce mesogenic behaviour.



Scheme 2.1: Schematic and a generic structure for liquid crystal compound.

Thus rod-like liquid crystalline molecules must have a rigid core (two or more conjugated rings), associated with alkyl- or alkoxy- chains (contributing to the molecular polarisability and lowering of the transitional temperatures) as well as polarisable group X to introduce a dipole moment.^{3a}

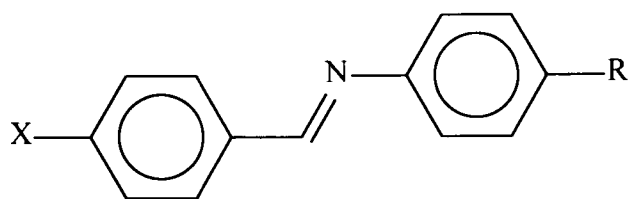
Table 2.1 Typical terminal and linker groups in mesogens.

X	Y
$C\equiv N$	$-C=N-$
Halogens (Br, Cl, F)	$-C\equiv C-$
$C_nH_{2n+1}-$	$-N=N-$
$C_nH_{2n+1}O-$	$-CH=N$
$-NO_2$	$-CO_2-$
$-NH_2$	$-CH=N-N=CH-$
$C_nH_{2n+1}OCO-$	$-CH=CH-CH=CH-$

2.4 Schiff base organic liquid crystals.

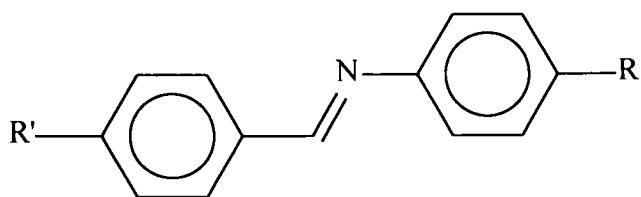
Schiff base compounds are very popular ligands in coordination chemistry and have been used to form complexes with most transition metals. However their use as liquid crystals only started in 1970.¹⁰ This began with the work of Kelker on methylbenzylidenebutylaniline (MBBA), which has since become one of the frequently studied organic liquid crystal compounds.¹¹ Even though Schiff base compounds have a rich polymorphism and have low transition temperatures between phases, they suffer from high sensitivity to moisture.

Most of the Schiff base compounds that have been studied for liquid crystalline behaviour have groups that induce strong dipole moments such as F, Cl, Br, NO_2 or CN at one end (Figure 2.8 A). This is partly due to the need for compounds to have high dielectric anisotropy in technological applications and also to limit the number of mesophases.¹² However, an increase in the dipole moment tends to increase the transition temperatures. To circumvent this problem Schiff base compounds having alkyl or alkoxy chains at both ends of the molecule have been used (Figure 2.8 B). A combination of alkyl and alkoxy chains at opposite ends of the molecule has also been used.^{13a, b, c} To achieve a low transition temperature El Guermai *et al.* replaced the polar groups or chains with a phenyl ring (Figure 2.8 C).¹⁴



X = F, Cl, Br, I, NO₂ or CN; R = alkyl or alkoxy chain

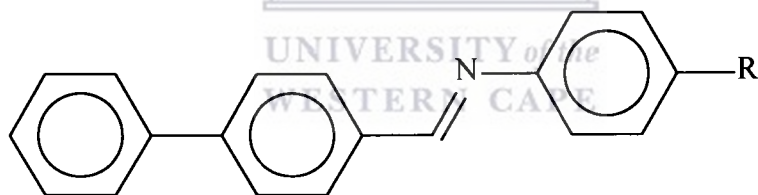
A



R' = R = alkyl or alkoxy chain

R' = alkyl chain; R = alkoxy chain

B



R = alkyl chain

C

Figure 2.8: Examples of Schiff base compounds with mesogenic properties.

Notwithstanding their high thermal transition temperatures, compounds with polar end groups are more widespread and a lot of research has centred on them. In one such work Galewski has compared the behaviour of Schiff bases with respect to the type of polar end groups and the effect of the conformation/positional order of the imine group relative to the polar end groups.¹² The study shows the following trends: (i) The melting point transitions are weakly dependent on the type of end group (*i.e.* X) used. (ii) The inversion of the conformation of the central imine group does not change the mesophase transition sequence, but only changes the melting temperatures. (iii) Increase in dipole moment of

molecules causes an increased stability of lattice packing, leading to higher melting points. (iv) When X is a nitro group the phase transitions are more dependent on the length of the alkyl or alkoxy chain than for the other X-groups. (v) The enthalpy change between mesophase transitions is weakly dependent on the central group inversion and the type of substituents at the end of the molecule. (vi) In a homologous series there is additivity of the enthalpies of phase transition between mesophases.

One of the main observations in terms of studies done on Schiff base compounds is that mesomorphic behaviour is only realised once the alkyl or alkoxy chain length is greater than three carbon atoms in the chain, i.e. butyl or propoxy chains or longer.¹² When both terminal groups of the molecule are flexible chains, compounds with alkyl chains always have lower clearing temperatures than the corresponding alkoxy analogues; in some cases the difference is 40-50 °C.^{13a} This means that compounds with alkoxy chains form more stable mesophases than those with alkyl chains. Literature reports for the homologous series of alkyl or alkoxy *para*-substituted benzoic acids and of 4'-substituted-4-cyanobiphenyl compounds show that the compounds with alkoxy chains always form more stable mesophases.¹⁵ It is believed that the non-bonded electron pair on the oxygen atom of the alkoxy group readily couples to the π -electrons of the phenyl rings leading to an increase in the polarisability of the molecule. This in turn leads to higher transition temperatures, as in higher K \rightarrow S or higher S \rightarrow clearing, of the mesophase¹⁶ and hence increased stability. It is therefore more desirable to use alkoxy chains in Schiff base mesogens.

The rich polymorphism inherent in the Schiff base compounds, together with the fact that compounds with alkoxy chains lead to more stable mesophases prompted us to synthesise Schiff base compounds bearing alkoxy chains of different lengths as ligands for our metal complexes. In designing our compounds the benzylidene alkoxy configuration of the imine functionality was maintained, as this does not affect the stability of the mesophase to any great extent. The terminal thiol group was chosen for the present study so that it could be used as an entry point into the synthesis of metal-thiolate complexes with potential mesogenic properties.

2.5 Metallomesogens: metal containing liquid crystals.

2.5.1 What are metallomesogens?

Metallomesogens is a term coined for metal complexes of organic ligands that exhibit liquid crystalline behaviour.^{3b} They combine the range of metal-based coordination chemistry with the extraordinary physical properties exhibited by liquid crystals. Many different types of metallomesogens have been made and include s-, p-, d- and even f-block elements.^{17a-d} Metal containing compounds which exhibit mesomorphism can be either organometallic or coordination complexes.¹⁸ Organometallic metallomesogens reported include mainly mercury, palladium or platinum compounds^{18, 19} while the coordination complexes are more widespread and include several transition metals.^{3b, 19a, 20} A variety of ligands have also been used. These include monodentate (4-substituted pyridines), bidentate (β -ketonates, dithiolenes, carboxylates, cyclometalated aromatic amines) and polydentate (phthalocyanines and porphyrines).^{3b} Key requirements for metallomesogens are the same as for organic liquid crystals. These are a rigid core, usually unsaturated and either rod- or disk-like in shape, and a flexible end, usually long alkyl or alkoxy chain. In some cases the ligands are themselves mesogenic but this is not a prerequisite; in other instances the introduction of metal atoms could lead to the loss of mesogenic behaviour of the ligand.^{21a, b.}

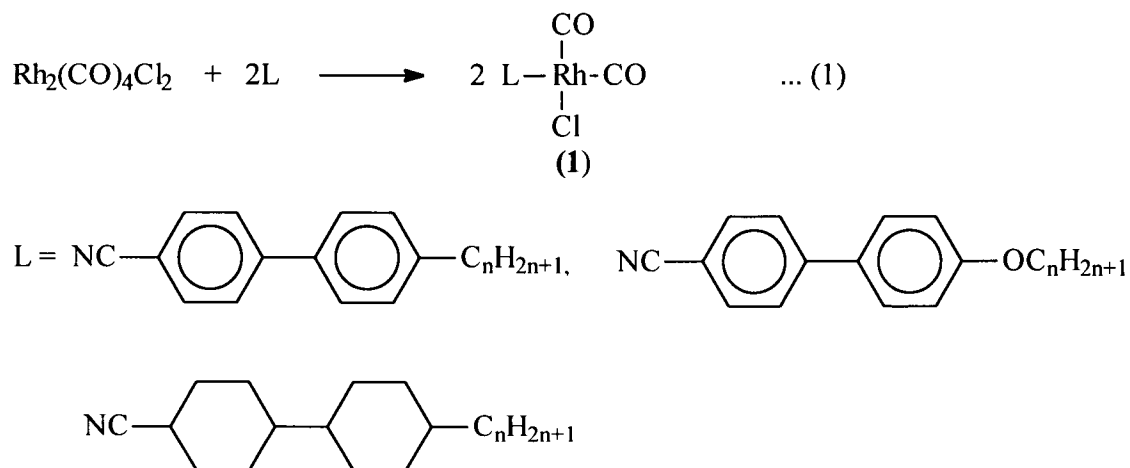
2.5.2 The advantages of the inclusion of metal atoms.

Many transition metal complexes give rise to interesting paramagnetic, nonlinear optical, photophysical, redox properties²² and colours^{3b} that can be controlled by the rational design of ligands. At times the high electron density on a metallic centre may lead to an increase in the polarisability and high birefringence, which, under the right conditions complexes may exhibit nonlinear optical (NLO) response.²³ The presence of the metal sometimes produce metallomesogens with unusual shapes that could not be expected from organic mesogens.^{3a} Some of these molecular geometries of liquid crystalline materials incorporating metals include linear mercury pyridine complexes,²⁴ open book

dinuclear palladium complexes,²⁵ H-shaped chloro-bridged dinuclear palladium complexes,²⁶ K-shaped benzylideneamine β -diketone palladium complexes²⁷ and square pyramidal geometry²⁸. A novel way of introducing chirality into liquid crystalline molecules²⁵ and fine tuning of chemical and physical properties could also be achieved by using the differences each metal centre brings about.²⁹ The main disadvantage of the introduction of a metal though is the increased transition temperatures, which sometimes affect their thermal stability.^{3a, 27a}

2.5.3. Metallomesogens with monodentate ligands.

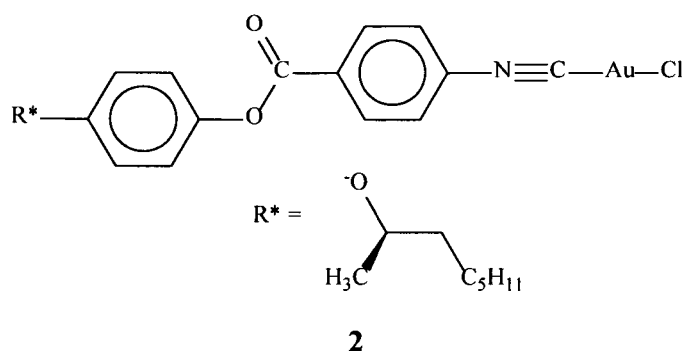
Monodentate metallomesogens are dominated by N-donor ligands and σ -bonded carbon ligands. Two types of monodentate complexes are known: (i) complexes with only one ligand and (ii) complexes with two monodentate ligands. First examples of monodentate metallomesogens were prepared by the Sheffield Liquid Crystal group, led by Maitlis, and which made use of nitrile ligands having a linear geometry.^{30a, b} These monoligated complexes synthesised by Maitlis *et al.* are exemplified by the complex **1** which was synthesised by the reaction of $[\text{Rh}_2(\text{CO})_4\text{Cl}_2]$ with two moles of the ligand, thus breaking the CO bridges between the two Rh centres (Scheme 2.2).^{30b}



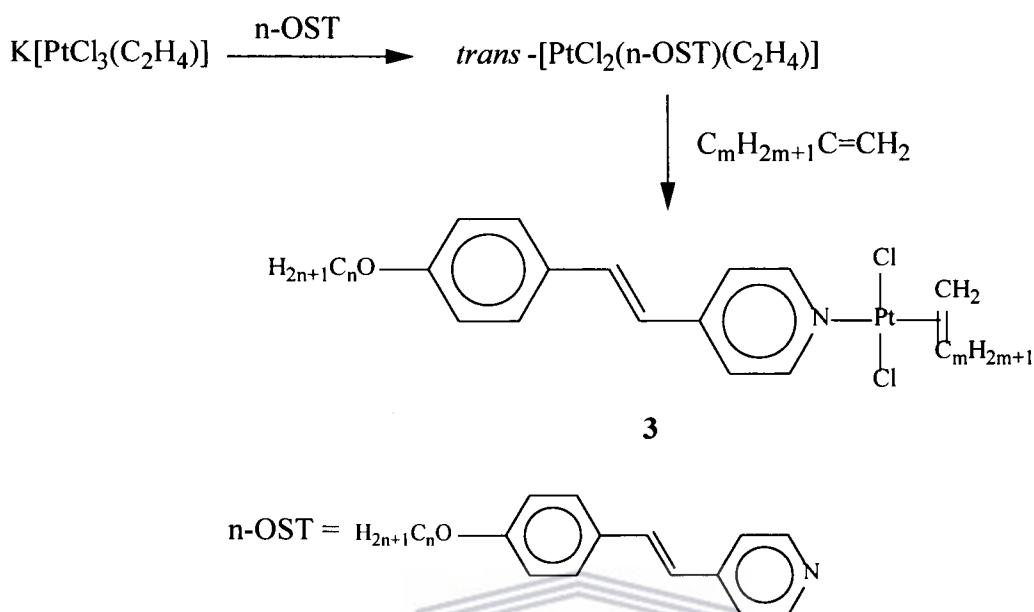
Scheme 2.2: Synthetic scheme for complex **1** synthesised by Maitlis *et al.*^{30b}

The rhodium complexes showed very short nematic ranges and decompose close to their clearing temperatures.³¹ Other examples of monodentate metallomesogens include work by Espinet and coworkers on gold complexes of the general formula X-Au-CNC₆H₄OC_nH_{2n+1} and X-Au-CNC₆H₄C₆H₄OC_nH_{2n+1} (X = Cl; n = 4, 6, 8, 10) in which isonitriles instead of nitriles are used as ligands. A general observation for the complexes described above is that mesogenic behaviour could be found even for complexes that have ligands with only one-ring, while the free ligands are not mesogenic.^{3a} This shows the importance of inclusion of the metal atom in promoting mesogenic properties. The electron-rich metal centre imparts significant polarisability to the molecule and does it better than nonmetallic atoms because of the presence of d-electrons.

Gold complexes similar to those prepared by Espinet have been studied by Omenat,³² by introducing a chiral centre on the chain and increasing the molecular length. These complexes showed helical smectic C* and smectic H mesophases. The significance of the introduction of chiral centres is that the resulting liquid crystals have ferroelectric properties, which increase the response time to applied electric field.³³ This is important in electronic display devices.

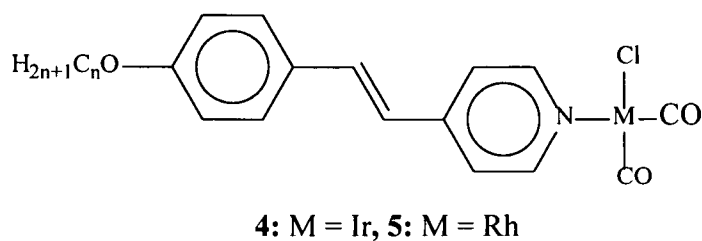


By far the best known monodentate metallomesogens are pyridine-coordinated complexes, which have been studied by several groups. One of the first mesogenic pyridine complex (complex **3**, Scheme 2.3) was prepared by Maitlis *et al.*, who found that mesogenic behaviour occurred for complexes with longer chains, i.e. $m + n \geq 8$, while those with $m + n < 8$ were non-mesogenic.³⁴



Scheme 2.3 Synthetic route to platinum mesogens prepared by Maitlis.

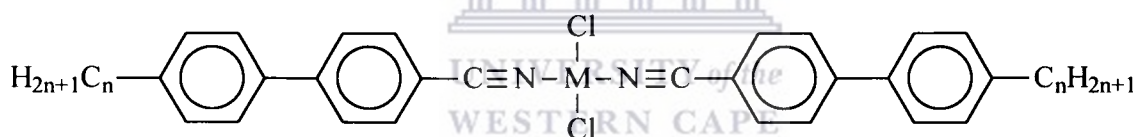
Serrano *et al.* have used other substituted pyridines as ligands to prepare metallomesogens.³⁵ The introduction of imino or aniline groups into the pyridine ligands appear to drastically change the mesogenic properties of their complexes. Thus the *cis*-iridium complex (**4**) containing short the chain, non-mesomorphic iminopyridine ligand (n-OIP, 4-alkoxy-N-(4-methylpyridine)aniline) formed mostly monotropic nematic phases, while those with longer chains ($n \geq 9$) formed smectic A (S_A) phases, with low transition temperatures. The rhodium complexes (**5**) also show a similar behaviour.^{36a}



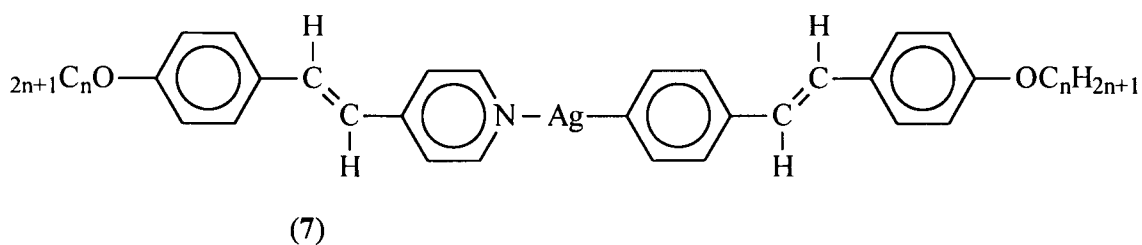
Complexes with two monodentate promesogenic ligands have also been studied extensively. The ligands are mainly the same as the ones used for the one monodentate complexes. Maitlis *et al.*³⁵ studied complexes of the types **6** and **7** while Serrano *et al.*³⁷

studied types **8**, **9** and **10**.³⁷ In these complexes the increased molecular lengths invariably led to more ordered mesophases, *e.g.* smectic A and C. Other complexes are cationic and the use of different counterions was shown to lead to different behaviour.

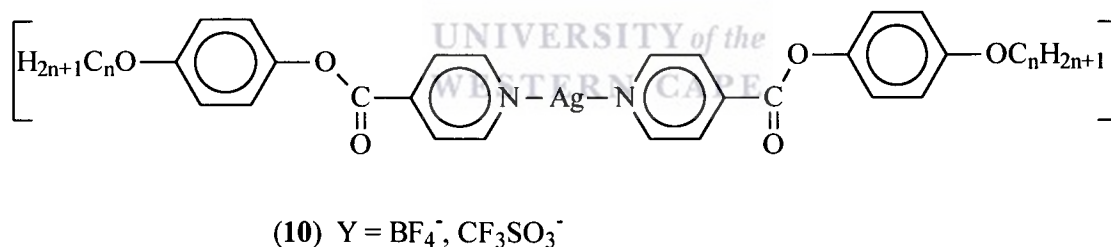
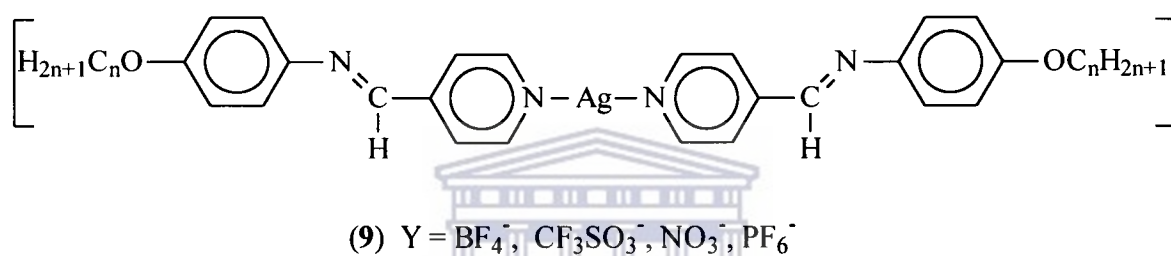
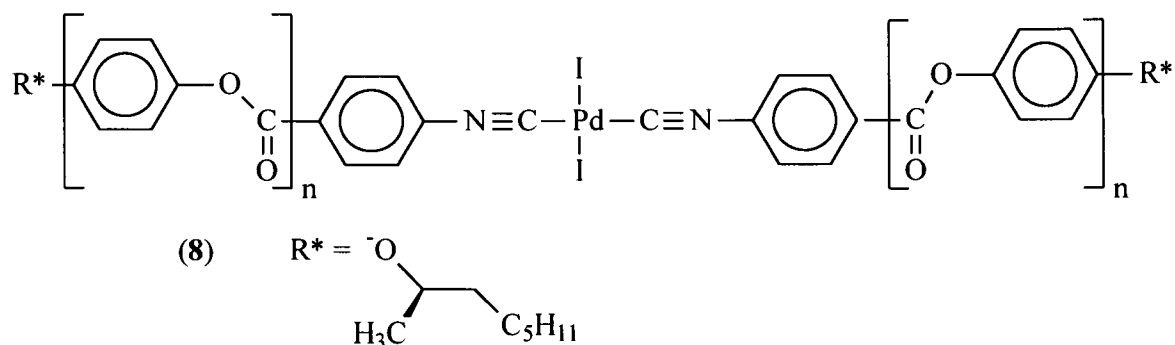
Generally metallomesogens with two monodentate ligands are dominated by *trans*-square planar geometry.³⁵ Bis(4-alkoxy-4'-cyanobiphenyl)platinum(II) complexes, **6** and **7**, give rise to smectic A and nematic mesophases. In contrast, the analogous palladium(II) complexes do not show nematic phases, but a smectic C appears, which was not present in the uncomplexed ligand. The transition temperatures of palladium(II) complexes are significantly lower than those of the corresponding platinum(II) complexes, and both kinds have significantly higher transition temperatures than those of the corresponding ligands. Even though the palladium and platinum complexes are isomorphous and isostructural they give different thermal behaviour.



(6) M = Pd and Pt



(7)



The prevailing reasoning for this is that the platinum ion being more electron-rich, is more polarisable and thus leads to stronger intermolecular interactions that lead to higher melting points and more stable mesophases. Replacement of alkoxy chains with alkyl chains leads to nematic mesomorphism.

The stilbazole or pyridine mesogens of silver (9 and 10) have also been extensively studied. This is partly because of the more stable metal-pyridine bonds as compared to the more labile metal-nitrile linkages. Non-mesogenic ($Y^- = \text{BF}_4^-$) and mesogenic ($Y^- = \text{C}_{12}\text{H}_{25}\text{OSO}_3^-$) anions were first used as counter ions for the silver complexes. The tetrafluoroborate derivatives with long alkoxy tails show smectic A and smectic C phases at higher temperatures, where decomposition occurs. However, lower transition

temperatures and richer liquid crystalline polymorphism were found for the lauryl sulfate derivatives.^{37a} Besides smectic A and C phases, complexes with shorter terminal chains show nematic behaviour. The role of the counter ion in determining the mesophase structure is strongly dependent on the ligand being used. For example, in complexes with the same anion, the ester derivatives exhibit better liquid crystalline properties than the analogous imine derivatives.^{37b}

2.6 Experimental Section

2.6.1 Materials and instrumentation

All commercially available chemicals were used as received. The following speciality chemicals were purchased from the specified vendors: 4-aminothiophenol (Fluka), 4-hydroxybenzaldehyde, 4-biphenylcarboxyaldehyde, 4-benzyloxybenzaldehyde, 4-butoxybenzaldehyde and triethylamine (Aldrich), 1-bromooctane, 1-bromodecane, 1-bromotetradecane, 1-bromododecane, 1-bromohexadecane and 1-bromoeicosane (Saarchem). The compounds $p\text{-OHCC}_6\text{H}_4\text{OC}_n\text{H}_{2n+1}$ ($n = 8, 10, 12, 14, 16$ and 20) were prepared by modified literature procedures.³⁸⁻⁴² The nickel compounds $\text{NiBr}(\text{PPh}_3)(\eta^5\text{-C}_5\text{H}_5)$ and $\text{NiBr}(\text{PBU}_3)(\eta^5\text{-C}_5\text{H}_5)$ were prepared by literature methods.^{43a,b} Reagent grade absolute ethanol and acetone were dried over activated molecular sieves. Hexane and CH_2Cl_2 were distilled over sodium and P_2O_5 respectively and then stored over activated molecular sieves, while toluene was distilled from sodium. All reactions were performed using standard Schlenk techniques under dinitrogen atmosphere. All alkoxybenzaldehydes and Schiff base compounds were characterised by a combination of $^1\text{H-NMR}$, IR, GC-MS and elemental analysis. Organometallic complexes were characterised by $^1\text{H-NMR}$, IR and elemental analysis and in some cases by single-crystal X-ray diffraction.

The ^1H and ^{31}P NMR spectra were acquired on a Varian Gemini 2000 spectrometer at 200 MHz and 80.961 MHz and referenced to residual CHCl_3 (δ 7.26) and externally to PPh_3 (δ -5.00) respectively. Mass spectra of the Schiff base compounds were run in

electron impact mode on a Finnigan MAT GCQ GC-MS spectrometer and elemental analyses were performed in-house in the Department of Chemistry at the University of the Western Cape on a CARLO ERBA NA analyser. Thermal analyses (TGA, DTA and DSC) were performed on a Universal V2.3H TA instrument connected to a nitrogen line. A clean aluminium crucible was weighed on an analytical balance and then 3-5 mg of dry sample was placed thereon. The crucible was then mounted in the instrument's furnace using forceps. The sample was heated at a rate of 10 °C/min.

X-ray diffraction data were collected at low temperatures (150(2) K and 173(2) K for **1a** and **3a** respectively) on a Nonius Kappa CCD diffractometer with 1.5 kW graphite-monochromated Mo radiation. A selection of crystal and refinement data is given in Table 3.3. The strategy for the data collection was evaluated using the *COLLECT* Software.⁴⁴ The data were scaled and reduced using *DENZO-SMN*.⁴⁵ Unit cell dimensions were refined on all data. The data were treated for absorption using the program *SORTAV*.⁴⁶ The structures were solved and refined using *SHELX97*.⁴⁷ Hydrogen atoms were placed in calculated positions and refined as riding atoms. Molecular graphics and additional material for publication were obtained using the program *PLATON*.⁴⁸

2.5.2 Synthesis of Schiff base compounds (1 – 9.)

All compounds were synthesised in a similar manner. A typical procedure is described for compound **1**.

HSC₆H₄NC(H)C₆H₄C₆H₅ (**1**)

A mixture of 4-aminothiophenol (0.41 g, 3.26 mmol) and 4-biphenylcarboxyaldehyde (0.59 g, 3.26 mmol) was dissolved in ethanol (60 mL) and then stirred at room temperature for 18 h. A cream-yellow precipitate started forming within one hour. After filtration the solid was washed with ethanol and dried by suction. The product was isolated in quantitative yield. Anal. Calcd for C₁₉H₁₅NS: C, 78.86; H, 5.22; N, 4.84. Found: C, 74.68; H, 5.56; N, 4.32%. ¹H NMR (CDCl₃): δ 8.48 (s, 1H, C(H)N), 7.96 (d, 2H, *J*_{HH} = 8.0 Hz, C(H)C₆H₄), 7.75 (d, 2H, *J*_{HH} = 8.6 Hz, NC₆H₄), 7.64 (d, 2H, *J*_{HH} = 8.6

Hz, C₆H₅), 7.45 (m, 5H, C₆H₄, C₆H₅), 7.14 (d, 2H, $J_{HH} = 8.6$ Hz, SC₆H₄). IR (Nujol mull, cm⁻¹) $\nu(\text{CH}=\text{N})$: 1608. EIMS (intensity): 289 (25%), 256 (13%), 165 (12%), 136 (100%).

HSC₆H₄NC(H)C₆H₄OCH₂C₆H₅ (2)

A yellow solid was isolated in 91% yield. Anal. Calcd for C₂₀H₁₇NOS: C, 75.21; H, 5.36; N, 4.38. Found: C, 74.92; H, 5.85; N, 4.45%. ¹H NMR (CDCl₃): δ 8.37 (s, 1H, C(H)N), 7.83 (d, 2H, $J_{HH} = 8.4$ Hz, C(H)C₆H₄), 7.40 (m, 7H, OCH₂C₆H₅, NC₆H₄), 7.08 (dd, 4H, OC₆H₄, SC₆H₄), 5.14 (s, 2H, OCH₂), 3.47 (s, 1H, SH). IR (Nujol mull, cm⁻¹) $\nu(\text{CH}=\text{N})$: 1604. EIMS (intensity): (319 (33%), 228 (12%), 136 (100%)

HSC₆H₄NC(H)C₆H₄OC₄H₉ (3)

A yellow solid was isolated in a yield of 83%. Anal. Calcd for C₁₇H₁₉NOS: C, 71.55; H, 6.71; N, 4.91. Found: C, 71.72; H, 6.43; N, 5.04%. ¹H NMR (CDCl₃): δ 8.36 (s, 1H, C(H)N), 7.82 (d, 2H, $J_{HH} = 8.8$ Hz, C(H)C₆H₄), 7.30 (d, 2H, $J_{HH} = 8.4$ Hz, NC₆H₄), 7.10 (d, 2H, $J_{HH} = 8.8$ Hz OC₆H₄), 6.97 (d, 2H, $J_{HH} = 8.8$ Hz, SC₆H₄), 4.03 (t, 2H, OCH₂), 3.47 (s, 1H, SH), 1.81 (q, 2H, OCH₂CH₂), 1.51 (q, 2H, OCH₂CH₂CH₂), 0.99 (t, 3H, CH₃) IR (Nujol mull, cm⁻¹) $\nu(\text{CH}=\text{N})$: 1615. EIMS (intensity): 285 (60%), 228 (14%), 136 (100%).

HSC₆H₄NC(H)C₆H₄OC₆H₁₃ (4)

A yellow solid was isolated in 86% yield. Anal. Calcd for C₁₉H₂₃NOS: C, 72.81; H, 7.39; N, 4.47. Found: C, 73.01; H, 7.41; N, 4.38%. ¹H NMR (CDCl₃): δ 8.36 (s, 1H, C(H)N), 7.82 (d, 2H, $J_{HH} = 8.4$ Hz, C(H)C₆H₄), 7.52 (d, 2H, $J_{HH} = 8.4$ Hz, NC₆H₄), 7.14 (d, 2H, $J_{HH} = 8.6$ Hz OC₆H₄), 6.96 (d, 2H, $J_{HH} = 8.6$ Hz, SC₆H₄), 4.02 (t, 2H, OCH₂), 1.79 (q, 2H, OCH₂CH₂), 1.63-1.30 (m, 6H, alkyl), 0.92 (t, 3H, CH₃). IR (Nujol mull, cm⁻¹) $\nu(\text{CH}=\text{N})$: 1617. EIMS (intensity): 313 (75%), 228 (12%), 136 (100%).

HSC₆H₄NC(H)C₆H₄OC₈H₁₇ (5)

A cream solid was obtained in a yield of 90%. Anal. Calcd for C₂₁H₂₇NOS: C, 73.86; H, 7.97; N, 4.10. Found: C, 74.11; H, 7.49; N, 4.23%. ¹H NMR (CDCl₃): δ 8.35 (s, 1H, C(H)N), 7.84 (d, 2H, $J_{HH} = 8.6$ Hz, C(H)C₆H₄), 7.52 (d, 2H, $J_{HH} = 8.6$ Hz, NC₆H₄), 7.16

(d, 2H, $J_{HH} = 8.4$ Hz OC₆H₄), 6.97 (d, 2H, $J_{HH} = 8.8$ Hz, SC₆H₄), 4.02 (t, 2H, OCH₂), 1.81 (m, 12H, alkyl), 0.89 (t, 3H, CH₃). IR (Nujol mull, cm⁻¹) ν (CH=N): 1615. EIMS (intensity): 341 (77%), 228 (13%), 136 (100%).

HSC₆H₄NC(H)C₆H₄OC₁₀H₂₁ (6)

A cream powder was obtained in 60% yield. Anal. Calcd for C₂₃H₃₁NOS: C, 74.75; H, 8.45; N, 3.79. Found: C, 73.73; H, 10.08; N, 3.67%. ¹H NMR (CDCl₃): δ 8.35 (s, 1H, C(H)N), 7.82 (d, 2H, $J_{HH} = 8.6$ Hz, C(H)C₆H₄), 7.52 (d, 2H, $J_{HH} = 8.4$ Hz, NC₆H₄), 7.15 (d, 2H, $J_{HH} = 8.6$ Hz OC₆H₄), 6.96 (d, 2H, $J_{HH} = 8.8$ Hz, SC₆H₄), 4.02 (t, 2H, OCH₂), 1.81-1.28 (m, 16H, alkyl), 0.90 (t, 3H, CH₃). IR (Nujol mull, cm⁻¹) ν (CH=N): 1613. EIMS (intensity): 371 (73%), 228 (8%), 136 (100%).

HSC₆H₄NC(H)C₆H₄OC₁₄H₂₉ (7)

A cream powder was obtained in quantitative yield. Anal. Calcd for C₂₇H₃₉NOS: C, 76.18; H, 9.23; N, 3.29. Found: C, 76.55; H, 8.95; N, 3.75%. ¹H-NMR (CDCl₃) δ : 8.35 (s, 1H, C(H)N), 7.81 (d, 2H, $J_{HH} = 8.8$ Hz, C(H)C₆H₄), 7.51 (d, 2H, $J_{HH} = 8.4$ Hz, NC₆H₄), 7.14 (d, 2H, $J_{HH} = 8.8$ Hz OC₆H₄), 6.96 (d, 2H, $J_{HH} = 8.8$ Hz, SC₆H₄), 4.01 (t, 2H, OCH₂), 1.78 (q, 2H, OCH₂CH₂), 1.26 (m, 22H, alkyl), 0.87 (t, 3H, CH₃). IR (Nujol mull, cm⁻¹) ν (CH=N): 1614. EIMS (intensity): 426 (70%), 228 (8%), 136 (100%).

HSC₆H₄NC(H)C₆H₄OC₁₆H₃₃ (8)

A white powder was obtained in 85% yield. Anal. Calcd for C₂₉H₄₃NOS: C, 76.77; H, 9.55; N, 3.09. Found: C, 76.61; H, 10.77; N, 2.78%. ¹H NMR (CDCl₃) δ : 8.36 (s, 1H, C(H)N), 7.82 (d, 2H, $J_{HH} = 8.8$ Hz, C(H)C₆H₄), 7.30 (d, 2H, $J_{HH} = 8.4$ Hz, NC₆H₄), 7.10 (d, 2H, $J_{HH} = 8.4$ Hz OC₆H₄), 6.96 (d, 2H, $J_{HH} = 8.8$ Hz, SC₆H₄), 4.02 (t, 2H, OCH₂), 3.47 (s, 1H, SH), 1.79 (q, 2H, OCH₂CH₂), 1.45-1.23 (m, 26H, alkyl), 0.88 (t, 3H, CH₃). IR (Nujol mull, cm⁻¹) ν (CH=N): 1616. EIMS (intensity): 454 (83%), 228 (6%), 136 (100%).

HSC₆H₄NC(H)C₆H₄OC₂₀H₄₁ (9)

A white solid was obtained in 90% yield. Anal. Calcd for C₃₃H₅₁NOS: C, 77.74; H, 10.08; N, 2.75. Found: C, 77.74; H, 9.75; N, 3.33%. ¹H NMR (CDCl₃) δ: 8.35 (s, 1H, C(H)N), 7.81 (d, 2H, *J*_{HH} = 8.8 Hz, C(H)C₆H₄), 7.51 (d, 2H, *J*_{HH} = 8.4 Hz, NC₆H₄), 7.14 (d, 2H, *J*_{HH} = 8.4 Hz OC₆H₄), 6.96 (d, 2H, *J*_{HH} = 8.8 Hz, SC₆H₄), 4.01 (t, 2H, OCH₂), 3.47 (s, 1H, SH), 1.78 (q, 2H, OCH₂CH₂), 1.45-1.26 (m, 34H, alkyl), 0.88 (t, 3H, CH₃). IR (Nujol mull, cm⁻¹) ν(CH=N): 1617. EIMS (intensity): 510 (66%), 228 (12%), 136 (100%).

BrC₆H₄NC(H)C₆H₄OC₆H₁₃ (10)

A white solid was obtained in 76% yield. Anal. Calcd for C₁₉H₂₂NOBr: C, 63.33; H, 6.15; N, 3.89. Found: C, 63.58; H, 6.25; N, 3.33%. ¹H NMR (CDCl₃) δ: 8.34 (s, 1H, C(H)N), 7.82 (d, 2H, *J*_{HH} = 8.4Hz, C(H)C₆H₄), 7.49 (d, 2H, *J*_{HH} = 8.8Hz, NC₆H₄), 7.06 (d, 2H, *J*_{HH} = 8.6Hz, OC₆H₄), 6.96 (d, 2H, *J*_{HH} = 8.8Hz, SC₆H₄), 4.02 (t, 2H, OCH₂), 1.80 (q, 2H, OCH₂CH₂), 1.56 – 1.32 (m, 6H, OC₆H₁₃), 0.92 (t, 3H, CH₃). IR (Nujol mull, cm⁻¹) ν(CH=N): 1605.

HSC₆H₄NC(H)C₆H₃(OC₁₀H₂₁)₂ (11)

A yellow solid was obtained in 82% yield. Anal. Calcd for C₃₃H₅₁NO₂S: C, 75.38; H, 9.77; N, 2.66. Found: C, 75.74; H, 9.75; N, 3.33%. ¹H NMR (CDCl₃) δ: 8.31 (s, 1H, C(H)N), 7.55 (m, 3H, NC₆H₄, C(H)C₆H₃), 7.13 (d, 2H, *J*_{HH} = 8.4Hz, C(H)C₆H₃), 6.90 (d, 2H, *J*_{HH} = 8.6Hz, SC₆H₄), 4.05 (q, 4H, OCH₂), 3.47 (s, 1H, SH), 1.83 (q, 4H, OCH₂CH₂), 1.55 – 1.20 (m, 28H, OC₁₀H₂₁), 0.88 (t, 6H, CH₃). IR (Nujol mull, cm⁻¹) ν(CH=N): 1625.

2.5.3 Synthesis of Ni(SC₆H₄NC(H)C₆H₄R')(PR₃)(η⁵-C₅H₅) (R = Ph or Bu; R' = Ph, OCH₂Ph, OC_nH_{2n+1} (n = 2, 4, 6, 8, 10, 12, 14 and 16)).

The preparation of cyclopentadienylnickel thiolato Schiff base complexes followed essentially the same procedure and hence only the preparation of compound **1a** is described.

Ni(SC₆H₄NC(H)C₆H₄C₆H₅)(PBu₃)(η⁵-C₅H₅) (1a)

To a degassed solution of HSC₆H₄NC(H)C₆H₄C₆H₅ (0.20 g, 0.63 mmol) and Ni(η⁵-C₅H₅)(PBu₃)Br (0.28 g, 0.68 mmol) in toluene (50 mL) was added excess Et₃N (1.5 mL). The maroon solution immediately turned dark green and was stirred at room temperature for 15 h to ensure complete reaction. The mixture was filtered to remove the white Et₃NHBr by-product and the filtrate evaporated. The residue obtained on evaporation was recrystallised from hexane at -15°C to give a green crystalline product in a yield of 0.12 g (38%). Anal. Calcd for C₃₆H₄₆NPSNi: C, 70.37; H, 7.53; N, 2.27. Found: C, 68.78; H, 7.89; N, 2.14%. ¹H NMR (CDCl₃): δ 8.52 (s, 1H, N=C(H)), 7.94 (d, 2H, *J*_{HH} = 8.4 Hz, C(H)C₆H₄), 7.67 (m, 5H, NC₆H₄, C₆H₅), 7.43 (m, 4H, C(H)C₆H₄, C₆H₅), 6.99 (d, 2H, *J*_{HH} = 8.6 Hz, SC₆H₄), 5.28 (s, 5H, η⁵-C₅H₅), 1.52-1.35 (m, 18H, butyl), 0.92 (t, 9H, CH₃). ³¹P{¹H} NMR (CDCl₃): δ 25.36.

The synthetic route for the remaining complexes is similar to that described for **1a**.

Ni(SC₆H₄NC(H)C₆H₄OCH₂C₆H₅)(PBu₃)(η⁵-C₅H₅) (2a)

A green solid was obtained in a yield of 0.34 g (33%). Anal. Calcd for C₃₇H₄₈NOPSNi: C, 68.95; H, 7.51; N, 2.18. Found: C, 69.22; H, 7.62; N, 2.08%. ¹H NMR (CDCl₃): δ 8.40 (s, 1H, N=C(H)), 7.82 (d, 2H, *J*_{HH} = 8.4 Hz, C(H)C₆H₄), 7.62 (d, 2H, *J*_{HH} = 8.0 Hz, NC₆H₄), 7.40 (m, 5H, OCH₂C₆H₅), 7.04 (d, 2H, *J*_{HH} = 8.4 Hz, OC₆H₄), 6.93 (d, 2H, *J*_{HH} = 8.4 Hz, SC₆H₄), 5.27 (s, 5H, η⁵-C₅H₅), 5.13 (s, 2H, OCH₂), 1.43-1.27 (m, 18H, butyl), 0.92 (t, 9H, CH₃). ³¹P{¹H} NMR δ: 27.33.

Ni(SC₆H₄NC(H)C₆H₄OC₄H₉)(PBu₃)(η⁵-C₅H₅) (3a)

Green crystals were obtained in a yield of 0.94 g (88%). Anal. Calcd for C₃₄H₅₀NOPSNi: C, 66.89; H, 8.25; N, 2.29. Found: C, 66.82; H, 8.33; N, 2.77%. ¹H NMR (CDCl₃): δ 8.39 (s, 1H, N=C(H)), 7.80 (d, 2H, *J*_{HH} = 8.8 Hz, C(H)C₆H₄), 7.61 (d, 2H, *J*_{HH} = 8.4 Hz, NC₆H₄), 6.94 (d, 2H, *J*_{HH} = 8.8 Hz, OC₆H₄), 6.93 (d, 2H, *J*_{HH} = 8.6 Hz, SC₆H₄), 5.26 (s,

5H, η^5 -C₅H₅), 4.02 (t, 2H, OCH₂), 1.80 (q, 2H, OCH₂CH₂), 1.41 (m, 20H, alkoxy, butyl), 0.98 (t, 12H, alkoxy, butyl). ³¹P{¹H} NMR (CDCl₃): δ 25.29.

Ni(SC₆H₄NC(H)C₆H₄OC₆H₁₃)(PBU₃)(η^5 -C₅H₅) (4a)

A green solid was obtained in 76% (0.58 g) yield. Anal. Calcd for C₃₆H₅₄NOPSNi: C, 67.93; H, 8.55; N, 2.20. Found: C, 68.04; H, 8.62; N, 2.40%. ¹H NMR (CDCl₃): δ 8.39 (s, 1H, C(H)N), 7.80 (d, 2H, J_{HH} = 8.2 Hz, C(H)C₆H₄), 7.60 (d, 2H, J_{HH} = 8.2 Hz, NC₆H₄), 6.94 (d, 2H, J_{HH} = 8.4 Hz, OC₆H₄), 6.93 (d, 2H, J_{HH} = 8.6 Hz, SC₆H₄), 5.26 (s, 5H, η^5 -C₅H₅), 4.02 (t, 2H, OCH₂), 1.80-1.25 (m, 26H, alkyl), 0.92 (t, 12H, alkoxy, butyl). ³¹P{¹H} NMR (CDCl₃): δ 25.26.

Ni(SC₆H₄NC(H)C₆H₄OC₈H₁₇)(PBU₃)(η^5 -C₅H₅) (5a)

A green solid was obtained in yield of 0.43 g (75%). Anal. Calcd for C₃₈H₅₈NOPSNi: C, 68.47; H, 8.77; N, 2.10. Found: C, 68.65; H, 8.52; N, 1.69%. ¹H NMR (CDCl₃): δ 8.39 (s, 1H, N=C(H)), 7.80 (d, 2H, J_{HH} = 8.4 Hz, C(H)C₆H₄), 7.60 (d, 2H, J_{HH} = 8.4 Hz, NC₆H₄), 6.94 (d, 2H, J_{HH} = 8.8 Hz, OC₆H₄), 6.93 (d, 2H, J_{HH} = 8.6 Hz, SC₆H₄), 5.26 (s, 5H, η^5 -C₅H₅), 4.01 (t, 2H, OCH₂), 1.80-1.23 (m, 30H, alkoxy, butyl), 0.92 (t, 12H, alkoxy, butyl). ³¹P{¹H} NMR (CDCl₃): δ 25.26.

Ni(SC₆H₄NC(H)C₆H₄OC₁₀H₂₁)(PBU₃)(η^5 -C₅H₅) (6a)

A green solid was obtained in a yield of 0.26 g (46%) was obtained. Anal. Calcd for C₄₀H₆₂NOPSNi: C, 69.16; H, 9.00; N, 2.02. Found: C, 70.15; H, 9.04; N, 2.11%. ¹H NMR (CDCl₃): δ 8.39 (s, 1H, N=C(H)), 7.80 (d, 2H, J_{HH} = 8.8 Hz, C(H)C₆H₄), 7.61 (d, 2H, J_{HH} = 8.4 Hz, NC₆H₄), 6.95 (d, 2H, J_{HH} = 8.8 Hz, OC₆H₄), 6.92 (d, 2H, J_{HH} = 8.6 Hz, SC₆H₄), 5.26 (s, 5H, η^5 -C₅H₅), 4.01 (t, 2H, OCH₂), 1.78 (q, 2H, OCH₂CH₂), 1.57-1.27 (m, 28H, alkoxy, butyl), 0.92 (m, 12H, butyl, alkoxy). ³¹P{¹H} NMR (CDCl₃): δ 25.29.

Ni(SC₆H₄NC(H)C₆H₄OC₁₄H₂₉)(PBu₃)(η⁵-C₅H₅) (7a)

A green solid was obtained in a yield of 0.48 g (49%) was obtained. Anal. Calcd for C₄₄H₇₀NOPSNi: C, 70.40; H, 9.40; N, 1.85. Found: C, 70.87; H, 9.33; N, 1.62%. ¹H NMR (CDCl₃): δ 8.40 (s, 1H, N=C(H)), 7.81 (d, 2H, *J*_{HH} = 8.8 Hz, C(H)C₆H₄), 7.62 (d, 2H, *J*_{HH} = 8.4 Hz, NC₆H₅), 6.95 (d, 2H, *J*_{HH} = 8.4 Hz, OC₆H₄), 6.94 (d, 2H, *J*_{HH} = 8.4 Hz, SC₆H₄) 5.27 (s, 5H, η⁵-C₅H₅), 4.02 (t, 2H, OCH₂), 1.81 (q, 2H, OCH₂CH₂), 1.59-1.27 (m, 28H, alkoxy, butyl), 0.93 (t, 12H, alkoxy, butyl). ³¹P{¹H} NMR (CDCl₃): δ 25.30.

Ni(SC₆H₄NC(H)C₆H₄OC₁₆H₃₃)(PBu₃)(η⁵-C₅H₅) (8a)

Green crystals were isolated in a yield of 0.14 g (87%) were isolated. Anal. Calcd for C₄₆H₇₄NOPSNi: C, 70.94; H, 9.57; N, 1.80. Found: C, 70.22; H, 10.52; N, 1.67%. ¹H NMR (CDCl₃): δ 8.39 (s, 1H, N=C(H)), 7.80 (d, 2H, *J*_{HH} = 8.6 Hz, C(H)C₆H₄), 7.60 (d, 2H, *J*_{HH} = 8.4 Hz, NC₆H₄), 6.94 (d, 2H, *J*_{HH} = 8.6 Hz, OC₆H₄), 6.93 (d, 2H, *J*_{HH} = 8.4 Hz, SC₆H₄), 5.26 (s, 5H, η⁵-C₅H₅), 4.01 (t, 2H, OCH₂), 1.80-1.30 (m, 46H, alkoxy, butyl), 0.92 (t, 12H, alkoxy, butyl). ³¹P{¹H} NMR (CDCl₃): δ 25.27.

Ni(SC₆H₄NC(H)C₆H₄OC₂₀H₄₁)(PBu₃)(η⁵-C₅H₅) (9a)

A green solid was isolated in a yield of 0.21 g (19%). Anal. Calcd for C₅₀H₈₂NOPSNi: C, 71.93; H, 9.90; N, 1.68. Found: C, 71.21; H, 10.26; N, 1.92%. ¹H NMR (CDCl₃): δ 8.40 (s, 1H, N=C(H)), 7.81 (d, 2H, *J*_{HH} = 8.8 Hz, C(H)C₆H₄), 7.62 (d, 2H, *J*_{HH} = 8.4 Hz, NC₆H₄), 6.95 (d, 2H, *J*_{HH} = 8.8 Hz, OC₆H₄), 6.94 (d, 2H, *J*_{HH} = 8.4 Hz, SC₆H₄), 5.27 (s, 5H, η⁵-C₅H₅), 4.01 (t, 2H, OCH₂), 1.81 (q, 2H, OCH₂CH₂), 1.52-1.27 (m, 40H, alkoxy, butyl), 0.93 (t, 12H, alkoxy, butyl). ³¹P{¹H} NMR (CDCl₃): δ 25.45.

Ni(SC₆H₄NC(H)C₆H₄C₆H₅)(PPh₃)(η⁵-C₅H₅) (1b)

A brown solid was obtained in a yield of 0.55 g (64%). Anal. Calcd for C₄₂H₃₄NPSNi: C, 74.80; H, 5.08; N, 2.08. Found: C, 74.14; H, 5.42; N, 3.27%. ¹H NMR (CDCl₃): δ 8.36 (s, 1H, N=C(H)), 7.83 (d, 2H, *J*_{HH} = 8.8 Hz, C(H)C₆H₄), 7.68 (t, 6H, PPh₃), 7.49 (m, 16H,

PPh_3 , NC_6H_4 , C_6H_5), 7.13 (d, 2H, $J_{\text{HH}} = 8.4$ Hz, $\text{C}(\text{H})\text{C}_6\text{H}_4\text{C}_6\text{H}_5$), 7.05 (d, 2H, $J_{\text{HH}} = 8.8$ Hz, SC_6H_4), 5.14 (s, 5H, $\eta^5\text{-C}_5\text{H}_5$). $^{31}\text{P}\{\text{H}\}$ NMR (CDCl_3): δ : 35.40.

Ni(SC₆H₄NC(H)C₆H₄OCH₂C₆H₅)(PPh₃)($\eta^5\text{-C}_5\text{H}_5$) (2b)

A green solid was obtained in a yield of 0.34 g (54%) was obtained. Anal. Calcd for $\text{C}_{43}\text{H}_{36}\text{NOPSNi}$: C, 73.31; H, 5.15; N, 1.97. Found: C, 72.19; H, 5.20; N, 1.83%. ^1H NMR (CDCl_3): δ 8.51 (s, 1H, $\text{N}=\text{C}(\text{H})$), 7.97 (d, 2H, $J_{\text{HH}} = 8.4$ Hz, $\text{C}(\text{H})\text{C}_6\text{H}_4$), 7.71 (m, 6H, PPh_3), 7.44 (m, 16H, PPh_3 , $\text{OCH}_2\text{C}_6\text{H}_5$, NC_6H_4), 7.19 (d, 2H, $J_{\text{HH}} = 8.4$ Hz, OC_6H_4), 6.90 (d, 2H, $J_{\text{HH}} = 8.4$ Hz, SC_6H_4), 5.30 (s, 2H, OCH_2), 5.15 (s, 5H, $\eta^5\text{-C}_5\text{H}_5$). $^{31}\text{P}\{\text{H}\}$ NMR (CDCl_3): δ 35.77. $^{31}\text{P}\{\text{H}\}$ NMR (CDCl_3): δ : 35.44.

Ni(SC₆H₄NC(H)C₆H₄OC₄H₉)(PPh₃)($\eta^5\text{-C}_5\text{H}_5$) (3b)

A brown solid was obtained in a yield of 0.38 g (74%). Anal. Calcd for $\text{C}_{40}\text{H}_{38}\text{NOPSNi}$: C, 71.66; H, 5.71; N, 2.09. Found: C, 71.89; H, 6.39; N, 2.11%. ^1H NMR (CDCl_3): δ 8.38 (s, 1H, $\text{N}=\text{C}(\text{H})$), 7.80 (d, 2H, $J_{\text{HH}} = 8.8$ Hz, $\text{C}(\text{H})\text{C}_6\text{H}_4$), 7.70 (t, 6H, PPh_3), 7.38 (s, 11H, PPh_3 , NC_6H_4), 6.95 (d, 2H, $J_{\text{HH}} = 8.4$ Hz, OC_6H_4), 6.85 (d, 2H, $J_{\text{HH}} = 6.4$ Hz, SC_6H_4), 5.13 (s, 5H, $\eta^5\text{-C}_5\text{H}_5$), 4.02 (t, 2H, OCH_2), 1.78 (q, 2H, OCH_2H_2), 1.49 (q, 2H, $\text{OCH}_2\text{CH}_2\text{CH}_2$), 0.99 (t, 3H, CH_3). $^{31}\text{P}\{\text{H}\}$ NMR (CDCl_3): δ : 35.40.

Ni(SC₆H₄NC(H)C₆H₄OC₈H₁₇)(PPh₃)($\eta^5\text{-C}_5\text{H}_5$) (5b)

A brown solid was obtained in a yield of 0.33 g (87%). Anal. Calcd for $\text{C}_{44}\text{H}_{46}\text{NOPSNi}$: C, 72.41; H, 6.38; N, 1.93. Found: C, 72.54; H, 6.44; N, 2.17%. ^1H NMR (CDCl_3): δ 8.38 (s, 1H, $\text{N}=\text{C}(\text{H})$), 7.80 (d, 2H, $J_{\text{HH}} = 8.8$ Hz, $\text{C}(\text{H})\text{C}_6\text{H}_4$), 7.71 (t, 8H, PPh_3 , NC_6H_4), 7.39 (m, 9H, PPh_3), 6.95 (d, 2H, $J_{\text{HH}} = 8.80$ Hz, OC_6H_4), 6.85 (d, 2H, $J_{\text{HH}} = 8.6$ Hz, SC_6H_4), 5.13 (s, 5H, $\eta^5\text{-C}_5\text{H}_5$), 4.02 (t, 2H, OCH_2), 1.78 (q, 2H, OCH_2CH_2), 1.6-1.16 (m, 10H, alkoxy), 0.88 (t, 3H, CH_3) $^{31}\text{P}\{\text{H}\}$ NMR (CDCl_3): δ 35.40.

Ni(SC₆H₄NC(H)C₆H₄OC₁₀H₂₁)(PPh₃)(η⁵-C₅H₅) (6b)

A brown solid was obtained in a yield of 0.36 g (82%). Anal. Calcd for C₄₆H₅₀NOPSNi: C, 73.22; H, 6.68; N, 1.86. Found: C, 73.19; H, 6.79; N, 1.45%. ¹H NMR (CDCl₃): δ 8.38 (s, 1H, N=C(H)), 7.80 (d, 2H, *J*_{HH} = 8.8 Hz, C(H)C₆H₄), 7.72 (t, 8H, PPh₃, NC₆H₄), 7.39 (m, 9H, PPh₃), 6.95 (d, 2H, *J*_{HH} = 8.8 Hz, OC₆H₄), 6.85 (d, 2H, *J*_{HH} = 8.8 Hz, SC₆H₄), 5.13 (s, 5H, η⁵-C₅H₅), 4.01 (t, 2H, OCH₂), 1.78 (q, 2H, OCH₂CH₂), 1.58-1.28 (m, 14H, alkoxy), 0.89 (t, 3H, CH₃). ³¹P{¹H}NMR (CDCl₃): δ 35.38.

Ni(SC₆H₄NC(H)C₆H₄OC₁₄H₂₉)(PPh₃)(η⁵-C₅H₅) (7b)

A brick red solid was obtained in a yield of 0.72 g (68%). Anal. Calcd for C₅₀H₅₈NOPSNi: C, 74.08, H, 7.21, N, 1.73. Found: C, 73.82, H, 7.22, N, 1.32%. ¹H NMR (CDCl₃): δ 8.38 (s, 1H, N=C(H)), 7.80 (d, 2H, *J*_{HH} = 8.4 Hz, C(H)C₆H₄), 7.70 (t, 6H, PPh₃), 7.38 (br s, 11H, PPh₃, NC₆H₄), 6.95 (d, 2H, *J*_{HH} = 8.8 Hz, OC₆H₄), 6.85 (d, 2H, *J*_{HH} = 8.4 Hz, SC₆H₄), 5.13 (s, 5H, η⁵-C₅H₅), 4.01 (t, 2H, OCH₂), 1.80 (q, 2H, OCH₂CH₂), 1.26 (br s, 22H, alkoxy), 0.88 (t, 3H, CH₃). ³¹P{¹H} NMR (CDCl₃): δ 35.41.

Ni(SC₆H₄NC(H)C₆H₄OC₁₆H₃₃)(PPh₃)(η⁵-C₅H₅) (8b)

A brick red solid was obtained in a yield of 0.49 g (77%). Anal. Calcd for C₅₂H₆₂NOPSNi: C, 74.46; H, 7.45; N, 1.67. Found: C, 74.22; H, 7.79; N, 1.53%. ¹H NMR (CDCl₃): δ 8.38 (s, 1H, N=C(H)), 7.80 (d, 2H, *J*_{HH} = 8.4 Hz, C(H)C₆H₄), 7.70 (m, 6H, PPh₃), 7.38 (m, 11H, PPh₃, NC₆H₄), 6.95 (d, 2H, *J*_{HH} = 8.40 Hz, OC₆H₄), 6.85 (d, 2H, *J*_{HH} = 8.6 Hz, SC₆H₄), 5.13 (s, 5H, η⁵-C₅H₅), 4.01 (t, 2H, OCH₂), 1.80-1.25 (m, 28H, alkoxy), 0.88 (t, 3H, CH₃). ³¹P{¹H} NMR (CDCl₃): δ 35.41.

Ni(SC₆H₄NC(H)C₆H₄OC₂₀H₄₁)(PPh₃)(η⁵-C₅H₅) (9b)

A brick red solid was isolated in a yield of 0.75 g (65.0%). Anal. Calcd for C₅₆H₇₀NOPSNi: C, 75.16; H, 7.88; N, 1.56. Found: C, 74.74; H, 7.15; N, 1.45%. ¹H NMR (CDCl₃): δ 8.31 (s, 1H, N=C(H)), 7.80 (d, 2H, *J*_{HH} = 8.8 Hz, C(H)C₆H₄), 7.70 (t, 6H, PPh₃), 7.38 (s, 11H, PPh₃, NC₆H₄), 6.95 (d, 2H, *J*_{HH} = 8.8 Hz, OC₆H₄), 6.85 (d, 2H,

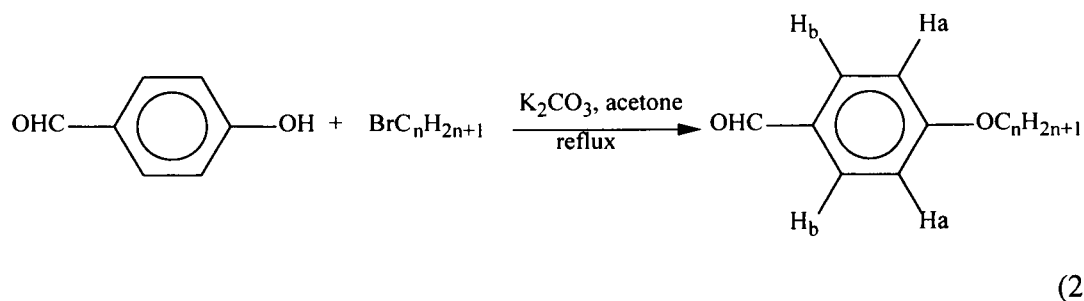
$J_{HH} = \text{Hz}$, SC_6H_4), 5.13 (s, 5H, $\eta^5\text{-C}_5\text{H}_5$), 4.01 (t, 2H, OCH_2), 1.78 (q, 2H, OCH_2CH_2), 1.27 (s, 34H, alkoxy), 0.88 (t, 3H, CH_3). $^{31}\text{P}\{^1\text{H}\}$ NMR (CDCl_3): δ 35.40.

2.7 Results and discussion

2.7.1 Synthesis and characterisation of alkoxybenzaldehydes and Schiff base compounds.

2.7.1.1 Synthesis of 4-alkoxybenzaldehydes, $\text{OHCC}_6\text{H}_4\text{OC}_n\text{H}_{2n+1}$ ($n = 8$ (iii), 10 (iv), 12 (v), 14 (vi), 16 (vii) and 20 (viii))

The *para*-alkoxybenzaldehydes needed for the preparation of the Schiff base compounds were prepared by the Williamson reaction. This was done by the reaction of the appropriate 1-bromoalkane and 4-hydroxybenzaldehyde in refluxing acetone. It was necessary to use three equivalents of finely grounded potassium carbonate; otherwise the yields of the alkoxybenzaldehydes were low. Trace amounts of a by-product formed from the deprotonation of the carboxylic group was formed in some cases. This was evident from the ^1H NMR of the crude product, but the by-product was easily separated from the product by column chromatography, using a silica gel stationary phase and CH_2Cl_2 :hexane solvent mixture in a 1:1 ratio as eluent to give an analytically pure product. The reaction is represented by equation 2.1. The difference between this synthetic protocol and those reported in the literature, where K_2CO_3 was used is in the choice of solvents. For example Binnemans *et al.* used butanone^{38a, b} while Scamporrino *et al* used a mixture of toluene and water³⁹. Other reaction conditions reported to effect the same reaction use potassium hydroxide in DMF⁴⁰ or ArSO_2Cl and phenol in ethanol: water (1:1) mixture.⁴¹ In all these literature procedures the yields of the alkoxyaldehydes were in the range from 75 - 95%. The products from our reaction were isolated in moderate to high yields, implying that we can use a cheaper solvent to obtain similar yield of product.



All compounds prepared as per eq. 2.1 had similar ^1H NMR and showed a peak due to the carbonyl hydrogen of the CHO group at 9.98 ppm. This peak is typical of benzaldehyde derivatives reported elsewhere.^{38a, b} In addition, there were two sets of doublets at 6.97 ppm and 7.82 ppm due to the H_a and H_b protons respectively. The signal of the H_b is expected to be upfield because of the shielding effect of the alkoxy chain while H_a is expected to be downfield because of the electron withdrawing nature of the carbonyl group. The simplicity of assigning the H_a and H_b is helpful in assigning the peaks of the Schiff base compounds produced when the alkoxybenzaldehydes above were reacted with 4-aminothiophenol. The alkyl chains in the compounds isolated in eq. 2.1 gave triplets, quartets, multiplets and triplets for protons (indicated in bold print in the alkoxy chain) $-\text{OCH}_2-$, $-\text{OCH}_2\text{CH}_2-$, $-\text{OCH}_2\text{CH}_2(\text{CH}_2)_n\text{CH}_3-$ and $-\text{O}(\text{CH}_2)_{n+2}\text{CH}_3-$ respectively. There was no obvious influence of the chain length on the chemical shifts of the phenyl protons (Table 2.2). Further characterisation of the alkoxybenzaldehydes was by electron impact mass spectrometry (EIMS). When the EIMS of the compounds were run they gave the appropriate molecular ion as well as a base peak at $m/z = 123$. The base peak is the fragment $\text{OHCC}_6\text{H}_4\text{O}-$ and shows that the alkyl chain in the alkoxy compounds is readily lost during the mass spectrometry experiments. Table 2.2 shows ^1H NMR and IR data and the relative intensity of the molecular ion peak for the compounds. Compounds **i** and **ii** with $n = 4$ and 6 respectively were obtained commercially.

Table 2.2: Selected ^1H NMR and Infrared data and the molecular ion peak (relative intensity in brackets) for compounds **iii** – **viii**.

compound	^1H NMR				IR	EIMS
	N	-CHO	H _b	H _a	-HC=O	(%)*
iii	8	9.98	7.82	6.97	1730 (s)	234 (5)
iv	10	9.97	7.82	6.98	1729 (s)	261 (13)
v	12	9.98	7.82	6.98	1730 (s)	290 (15)
vi	14	9.99	7.83	6.98	1730 (s)	321 (22)
vii	16	9.99	7.83	6.98	1729 (s)	347 (18)
viii	20	9.99	7.83	6.97	1730 (s)	403 (17)

* relative intensity of molecular ion in brackets.

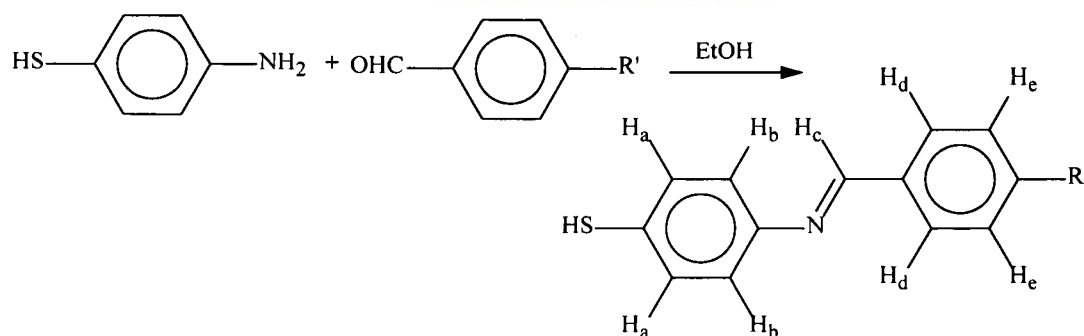
2.7.1.2 Synthesis of 4-alkoxybenzylidene-4-thioaniline or 4-alkoxybenzylidene-4-mercaptoaniline, 4-HSC₆H₄NC(H)C₆H₄-4'-OC_nH_{2n+1} (n = 4, 6, 8, 10, 14, 16, 20).

All the Schiff base ligands, HSC₆H₄NC(H)C₆H₄R'' (R'' = C₆H₅ (**1**), OCH₂C₆H₅ (**2**)), HSC₆H₄NC(H)C₆H₄OC_nH_{2n+1} (n = 4 (**3**), 6 (**4**), 8 (**5**), 10 (**6**), 14 (**7**), 16 (**8**), 20 (**9**)), HSC₆H₄NC(H)C₆H₃(OC₁₀H₂₁)_{2-3,4} (**10**) and BrC₆H₄NC(H)C₆H₄OC₁₆H₃₃ (**11**)) were prepared by condensation of equimolar amounts of 4-aminothiophenol and the appropriate aldehydes in ethanol (eq. 2.2). This condensation reaction is the common route for the formation of imine bonds.^{42a, b} The products precipitated as either yellow solids or thick yellow oils within 30 minutes. Generally products with short alkoxy chains (n = 4 and 6) separated from the reaction mixture as oils. However, analytically pure solids of compounds **3** and **4** could be isolated by slow diffusion of hexane into CH₂Cl₂ solutions of the compounds at -15°C. The remaining compounds were purified by recrystallisation from a mixture of CH₂Cl₂: hexane (1:2). Yields of the compounds **1** - **11** ranged from 60-100%.

Infrared and ^1H NMR spectroscopy and mass spectrometry were used to characterise the Schiff base compounds isolated. Infrared spectroscopy was a simple, but effective way to establish formation of the Schiff base. This is typically shown by the absence of the

carbonyl peak in the aldehyde (1730 cm^{-1}) and the appearance of an imine peak ($1604 - 1617\text{ cm}^{-1}$). For example the compounds N,N-bis(4-chlorobenzelidene)-2,2-diiminodiphenyl and 2-(2-Ph₂C₆H₄N=C(H))C₆H₄OH have peaks at 1597 cm^{-1} and 1614 cm^{-1} respectively.^{43b} Hence the imine peaks of compounds prepared in this project are typical of literature reports for similar compounds.

The presence of the imine group was confirmed by ¹H NMR spectroscopy. The imine proton resonance for **1** – **11** which occurs in the range 8.34 – 8.48 ppm is comparable to those of similar compounds synthesised by Nevondo *et al.* (HSC₆H₄NC(H)C₆H₄X-4, X = F, Cl, Br, SMe and Me).^{43a} In Schiff base compounds similar to ours (4-H_{2n+1}C_nOC₆H₄NC(H)C₆H₄OC_nH_{2n+1}-4') where alkyl chains replace the thiols **1** – **11**, proton signals are found at 8.50 ppm,¹⁴ again indicating that the effect of substituents on chemical shifts in these compounds are generally minimal. Figure 2.9 show the ¹H NMR spectrum of a compound with an alkoxy chain (**8**). The imine proton resonance in compounds with three rings is not different from those with two rings, for example compounds **2** and **8** have imine chemical shifts of 8.37 ppm and 8.36 ppm respectively.



(R' = C₆H₅ (**1**), OCH₂C₆H₅ (**2**), OC_nH_{2n+1}; n = 4 (**3**), 6 (**4**), 8 (**5**), 14 (**6**), 16 (**7**), 20 (**8**))

(2.2)

The rest of the ¹H NMR chemical shifts helped in identifying the products. All compounds with alkoxy chains had similar ¹H NMR spectra in the aromatic region, with the peak values being indifferent to the length of the alkyl chain. The only difference

between the spectra was the integration of the signals upfield for the alkyl chain, which helped in confirming the number of protons in the chain.

The general pattern of the ^1H NMR spectra of the compounds in the aromatic region consisted of four sets of doublets. They show typical AB type patterns for the four protons on the two phenyl rings. The most upfield doublet was due to H_a (6.96 ppm) with the next doublet at 7.10 ppm due to H_e . The H_a and H_c were assigned by making use of the assignment for the alkoxybenzaldehyde compounds (iii – viii) as well as compounds $\text{HSC}_6\text{H}_4\text{NC}(\text{H})\text{C}_6\text{H}_4\text{F}-4$ (7.32 ppm) and $\text{Me}_2\text{NC}_6\text{H}_4\text{C}(\text{H})\text{NC}_6\text{H}_4\text{F}-4$ (6.98 ppm).^{43a, b} The peak assignment of H_a and H_e protons in the ^1H NMR of $\text{Me}_2\text{NC}_6\text{H}_4\text{C}(\text{H})\text{NC}_6\text{H}_4\text{F}-4$ spectrum (6.98 ppm) and (7.89 ppm) was aided by further splitting of the resonance signals of these protons by the ^{19}F nucleus. Thus a direct comparison of chemical shifts in compounds 3 – 9 with those of the fluorinated compounds makes it easy to identify peaks of H_a and H_e and the rest of the aromatic protons. The most downfield doublet is assigned to H_a while the next doublet upfield was due to H_d (compare with those of the alkoxybenzaldehydes). All the other signals were typical of thiol and alkyl functional groups. The resonance signal for the SH protons was at 3.47 ppm for some of the compounds are similar to literature values of 3.45-3.48 ppm for organic thiols^{43, 50}, but in most cases the peak either integrated for less than one proton or was absent. This observation may imply proton exchange with the deuterated NMR (CDCl_3) solvent.

The ^1H NMR chemical shifts for the compounds with three rings were difficult to assign as most of the peaks in the aromatic region overlapped. The only peak that could be assigned unequivocally was that for the protons on the ring closest to the sulfur atom that was upfield. This peak assignment could also be inferred from the spectra of the alkoxybenzaldehyde compounds and Schiff base compounds with long chains. In the aromatic region there were five sets of doublets and a multiplet indicative of three rings with *para*-substituents as well as a terminal ring. The OCH_2 resonance was at 5.34 ppm. This value is comparable to those of similar compounds, for example compound ($\text{H}_{13}\text{C}_6\text{OC}_6\text{H}_4-4-\text{CO}_2\text{C}_6\text{H}_4-4'-\text{CO}_2\text{C}_6\text{H}_4-4''-\text{C}(\text{O})\text{OCH}_2\text{C}_6\text{H}_5$) had a peak due to OCH_2 at 5.37 ppm.⁵¹

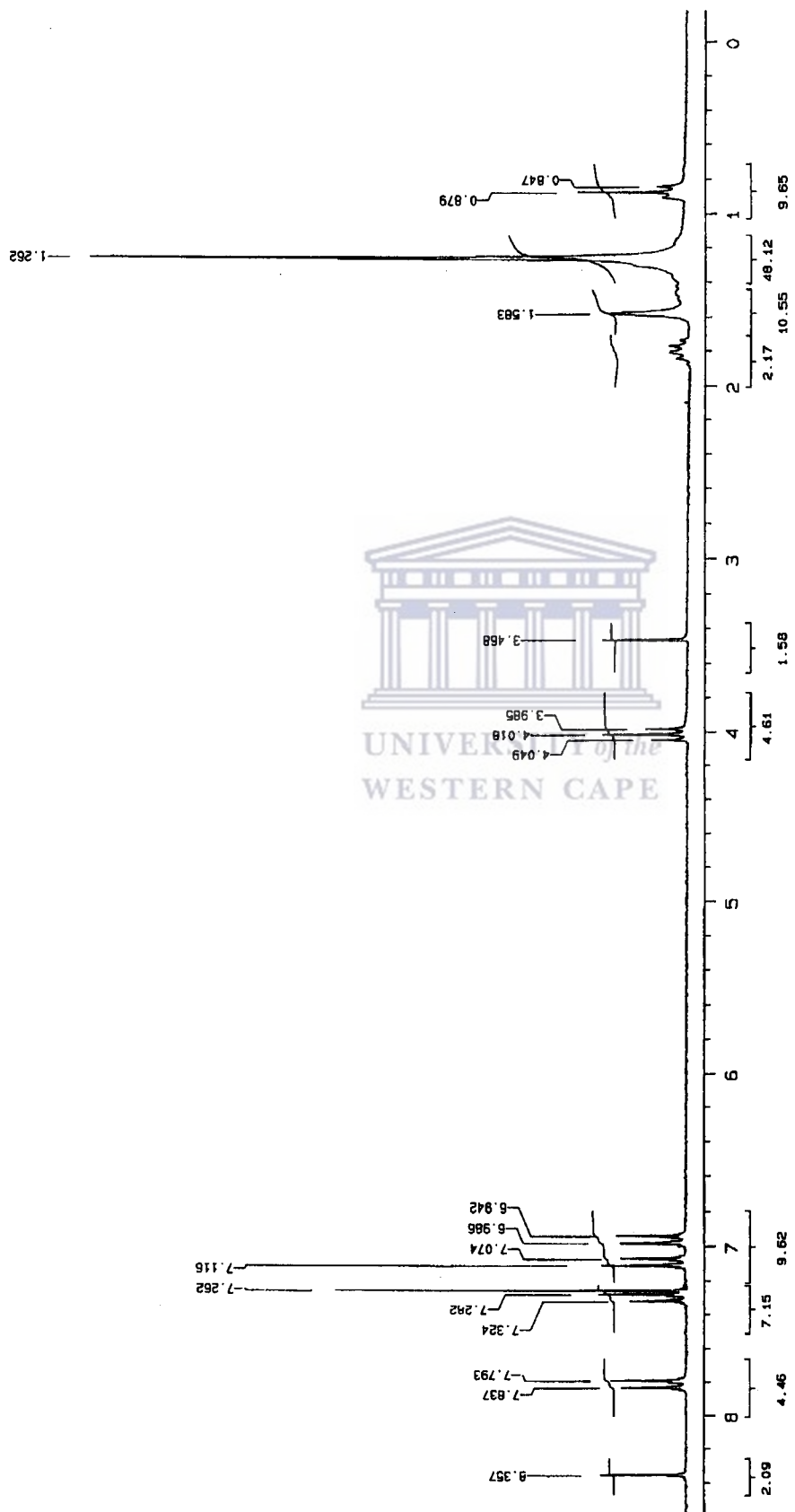


Figure 2.9: ^1H NMR for complex 5.

Mass spectrometry provided further characterisation of the Schiff base thiols (**1 – 9**). The mass spectra of compounds **1 - 9** had molecular ions of the specific compound (Table 2.3). Each compound had $m/z = 136$ as the base peak, which corresponds to the fragment $\text{HSC}_6\text{H}_4\text{NC(H)}$. A combination of all peaks enabled us to use mass spectrometry to characterise the ligands.

Table 2.3: Mass spectral data (relative intensity in brackets) for compounds **1 – 9**.

compound	Molecular ion	$\text{HSC}_6\text{H}_4\text{NC(H)}$	HSC_6H_4
1	305 (80)	136 (100)	109 (13)
2	319 (75)	136 (100)	109 (10)
3	285 (60)	136 (100)	109 (15)
4	313 (70)	136 (100)	109 (4)
5	341 (55)	136 (100)	109 (8)
6	369 (68)	136 (100)	109 (15)
7	425 (73)	136 (100)	109 (17)
8	453 (65)	136 (100)	109 (19)
9	509 (69)	136 (100)	109 (11)

2.7.2 Thermal behaviour of the Schiff base compounds.

Thermal Gravimetric Analysis (TGA) and Differential Scanning Calorimetry (DSC) were used to investigate the thermal behaviour of the Schiff base compounds. All compounds (**1-9**) were subjected to thermal analysis. The TGA showed that almost all the compounds decomposed at temperatures just above 200 °C. The exceptions to this were compounds **8** and **9**, which decomposed below 200 °C. Compounds with shorter chains ($n < 10$) showed three mass losses while those with longer chains ($n \geq 14$) showed only two mass fragment losses. In both cases the percentage of the mass lost of all the compounds did not correspond to any logical fragment of the molecule. Thus the decomposition of these compounds is believed to be more complex compared to those of the nickel complexes (**1a - 9b**) (See Section 2.3.3).⁵²

Compounds **1 - 9** were generally stable up to 180 °C before the onset of decomposition; however, from the DSC data compounds **1 - 8** did not show any multiple endotherms on heating or multiple exotherms on cooling. From the DSC data the endothermic peaks of compounds **1 - 8** were the melting points. This data was corroborated with normal melting point measurements (Table 2.4). Since multiple endotherms on heating or multiple exotherms on cooling in a DSC measurement are a sign of liquid crystalline behaviour, it can be concluded that compounds **1 - 8** are not liquid crystals. Interestingly the DSC of compound **9** had two endothermic peaks at 75.95 °C and 88.56 °C on heating. The endothermic event at 73.95 °C is the melting transition while the second 88.56 °C is the clearing point of the mesophase into an isotropic liquid.

Table 2.4: DSC and melting point data for compounds **4 - 9**.

Compound	m. p.*	DSC [#]
4	110 – 114	113
5	106 – 108	109
6	105 – 107	106
7	100 – 104	103
8	88 – 91	92
9	82 – 84	83

* melting point apparatus. [#] DSC measurement

The trend in the melting point temperatures is a steady decrease as the alkoxy chain length of compounds increased (Fig. 2.10). This is a trend that is usually observed for a homologous series of compounds that differ only in chain length.⁵³ We observed a trend from a high of 134 °C to a low of 74 °C for the shortest (n = 2) to the longest (n = 20) carbon chain compounds respectively. It is interesting to note that there is an almost linear decrease of melting points with increase in chain length. This observation will be compared to those of the nickel complexes in section 2.4.3.

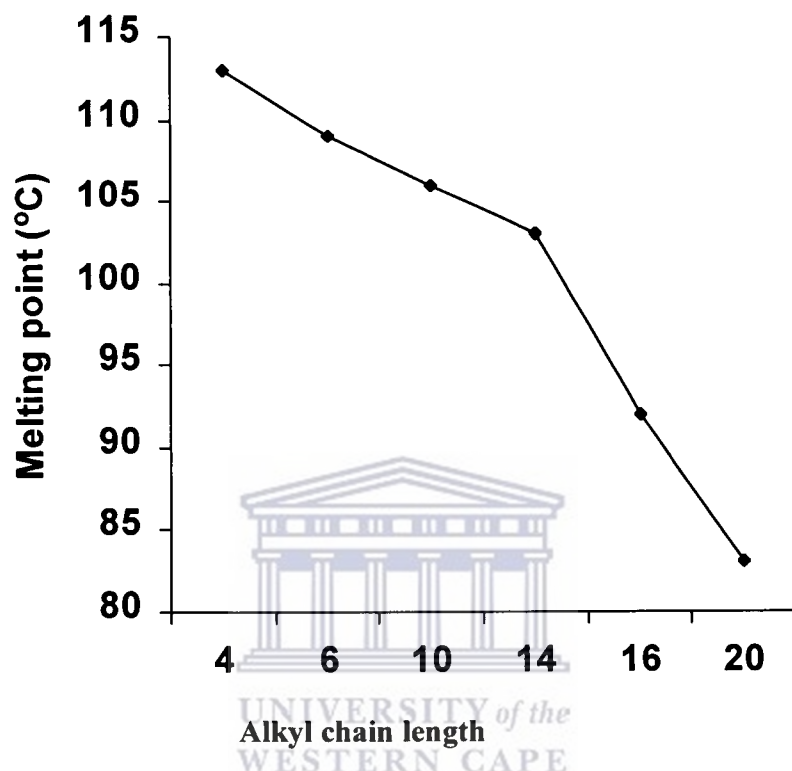
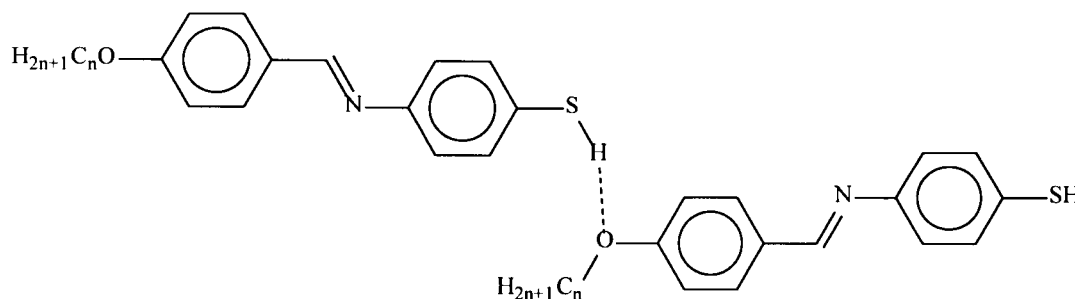


Figure 2.10: Melting point variation with chain length for Schiff base compounds.

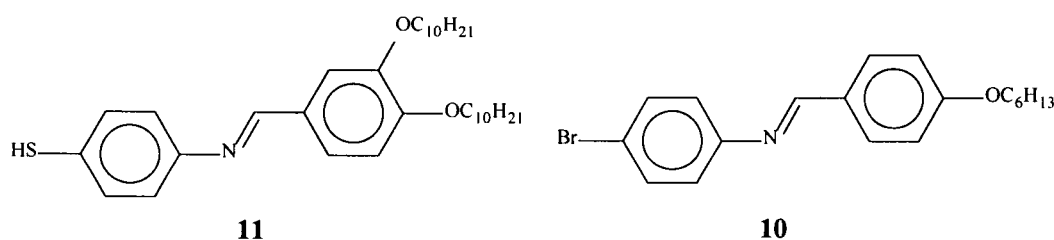
Comparing the melting points of compounds **10** and **11** with those of **1 - 8**, it was found that **11**, the compound with two alkoxy chains ($n = 10$), had the lowest melting point. This was even lower than for **9**, which has the longest chain ($n = 20$). This shows the disruptive effect the two chains have on the molecular packing, even though the chain length is moderate ($n = 10$). The additional chain that is laterally displaced will tend to disrupt lamellar packing of molecules leading to lower melting points. When one compares the melting point to those of similar Schiff base compounds with four alkoxy chains, $(\text{H}_{21}\text{C}_{10}\text{O})_2\text{C}_6\text{H}_3\text{NC}(\text{H})\text{C}_6\text{H}_3(\text{OC}_{10}\text{H}_{21})_2$, one observes a higher melting transition than that of the thiol Schiff base compound (**10**).⁵⁹ This is surprising since it would be expected that the compound with four chains will have a much lower melting point compared to the one with only two chains. But the reason for this behaviour can be rationalised in terms of the polarisability effect of the chains. Since the chains are

disposed *trans* to each other across the conjugated system, the resultant increase in the polarisability of the molecule will lead to an increase in the melting point transition temperatures. It is well known that an increase in the polarisability of a molecule results in an increase in its melting point.⁶⁰ On the other hand the bromo compound (**10**, $n = 6$) had a lower melting point than that of its thiol analogue. This observation alludes to the presence of hydrogen bonding between the molecules of the latter compound, which will lead to higher melting transitions. The hydrogen bonding, which was alluded to above, occurs between the H-atom of the thiol group and the O-atom of the alkoxy chain (Scheme 2.4). Hydrogen bonding is precluded in the bromo compound, hence a lower melting point.

We were surprised that compounds **1** - **8** have no mesogenic behaviour since they possess molecular structures that are known to lead to mesogenic behaviour (Fig. 2.11).³ It is likely that the lack of mesogenic behaviour is due to the presence of the thiol groups. Strong hydrogen bonding occurs between the thiol functional group and the oxygen atoms of the alkoxy group. This is illustrated in Scheme 2.4. To test this hypothesis, we replaced the thiol group in compound **4** by Br (**10**) and an alkoxy group (**11**) as shown in scheme 2.5.



Scheme 2.4: A representation of the possible hydrogen bonding between molecules.



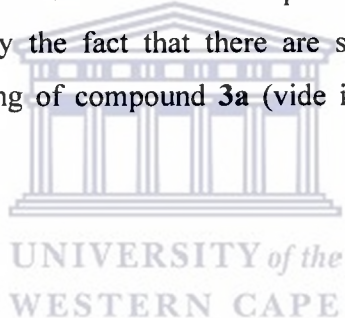
Scheme 2.5: Modifications that were performed on the Schiff base compounds.

Compounds **9**, **10** and **11** showed multiple endotherms in their DSC (Fig. 2.12, Fig. 2.13 and 2.14). In the DSC data for all three compounds, the heat involved in the melting was much higher than the heat for clearing point of the mesophase. Thus in contrast to compounds **1** – **8**, compounds **9**, **10** and **11** are liquid crystalline. For example compound **10** has two endothermic peaks on heating at 80.6 °C and 107.3 °C before the onset of decomposition (270 °C). Compound **11** had endothermic peaks at lower temperatures of 63.9 °C and 83.7 °C before decomposing at 300 °C. Multiple endotherms indicate mesogenic behaviour as alluded to in section 2.2.1. In order to confirm and identify the mesophases in compounds **9**, **10** and **11**, an optical microscopy study was done on compound **10**. The optical micrograph shows that **10** exhibited focal conic texture (Fig. 2.15). Focal conic texture are typically exhibited by smectic mesogens. For example Galveski observed focal conic textures for compounds $\text{ClC}_6\text{H}_4\text{C}(\text{H})\text{NC}_6\text{H}_4\text{-4-OC}_n\text{H}_{2n+1}$ ($n > 4$), the mesophases exhibited by these compounds were classified as smectic B.¹²

The observation of mesogenic behaviour in **9**, **10** and **11** supports the hypothesis that hydrogen bonding is the cause of nonmesomorphic behaviour in compounds **1** – **8**. In **9**, which is similar to **1** – **8**, but with a longer alkoxy chain, mesophases are induced by one of two influences: (i) Since the chain is long as compared to the rigid part of the molecule, it will reduce the interaction between the SH hydrogen and the alkoxy oxygen, by intercalating between molecules. Secondly (ii) the chain can induce mesophase formation in the same way polar chains form mesophases. For example silver compounds, $\text{AgSC}_n\text{H}_{2n+1}$ ($n = 4, 6, 8, 10, 12, 16$ and 18),^{34a} and copper alkanoates ($\text{Cu}_2(\text{CO}_2\text{R})_4$ where R is $\text{CH}_3(\text{CH}_2)_{n-2}$ with $n = 4 - 24$)^{34b} are known to form mesophase. In addition to hydrogen bonding compounds with shorter chains ($n < 6$) are usually nonmesogenic.³ The formation of mesophases in **11**, with SH functionality and two alkoxy chains, might be due to the lateral steric interactions caused by the two chains that weaken or destroy any hydrogen bonding that is formed. Also compounds with more than one alkoxy chain are also known to exhibit mesogenic behaviour. For example compound $3,4\text{-(H}_{21}\text{C}_{10}\text{O)}_2\text{C}_6\text{H}_3\text{NC}(\text{H})\text{C}_6\text{H}_3\text{-3',4'-(OC}_{10}\text{H}_{21})_2$ exhibits mesogenic behaviour.⁵⁹ There is no possibility of hydrogen bonding in compound **10** and thus the observation of

mesogenic behaviour in **10** supports the hypothesis that hydrogen bonding in **1 – 8** is the cause of the lack of mesomorphic behaviour. Compounds similar to **10** are known to show mesogenic behaviour.^{12, 55}

Most low molecular mass organic compounds with liquid crystal behaviour feature nitro, cyano, halo, alkoxy or alkyl end groups.⁵⁵ These groups are not involved in any hydrogen bond formation. For instance compounds with terminal –CN are mesogenic.⁵⁶ Hydrogen bonding is known to prevent formation of mesophases in compounds that are promesogenic.⁵⁷ Hydrogen bonding is also known to promote mesophase formation in otherwise nonmesogenic compounds. This is provided the hydrogen bonding leads to either rod-shaped or disc-shaped macromolecules.⁵⁸ The presence of hydrogen bonding in these compounds is supported by the fact that there are short S \cdots H and N \cdots H bond distances in the molecular packing of compound **3a** (vide infra) which are within the range of hydrogen bonding.⁵²



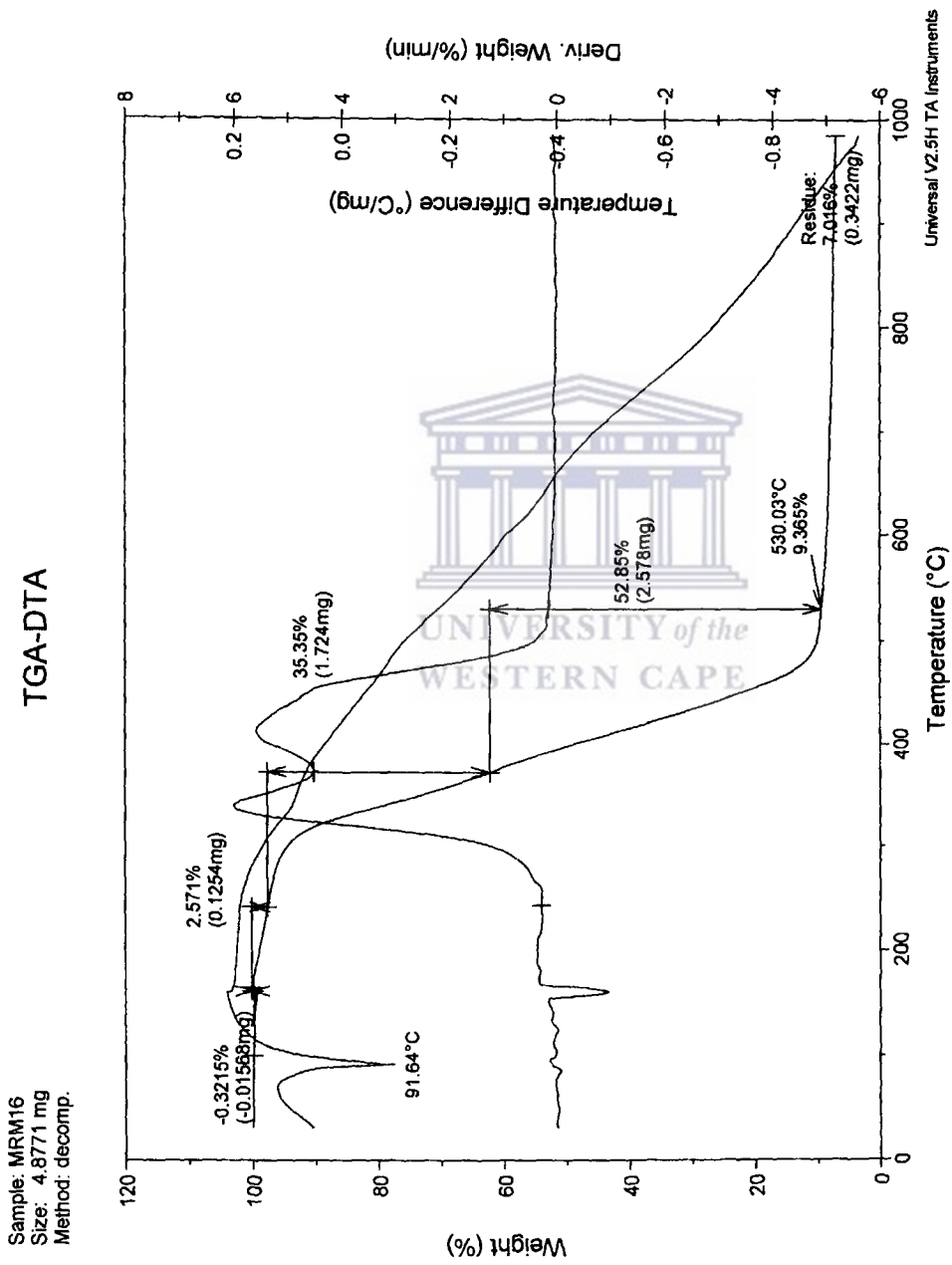


Figure 2.11: Thermograms for compound 6.

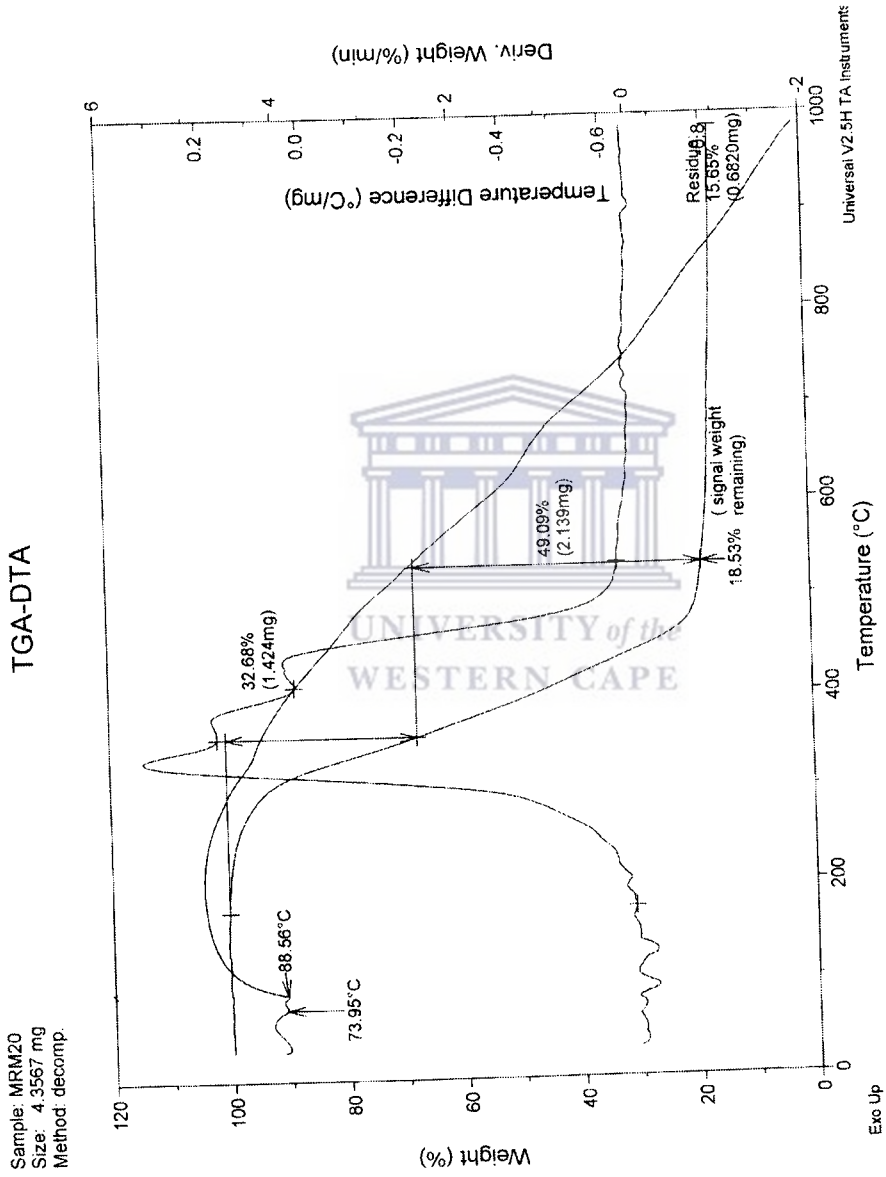


Figure 2.12: Thermograms for compound 9.

Sample: MIRM206
Size: 3.9237 mg
Method: decomp.

TGA-DTA

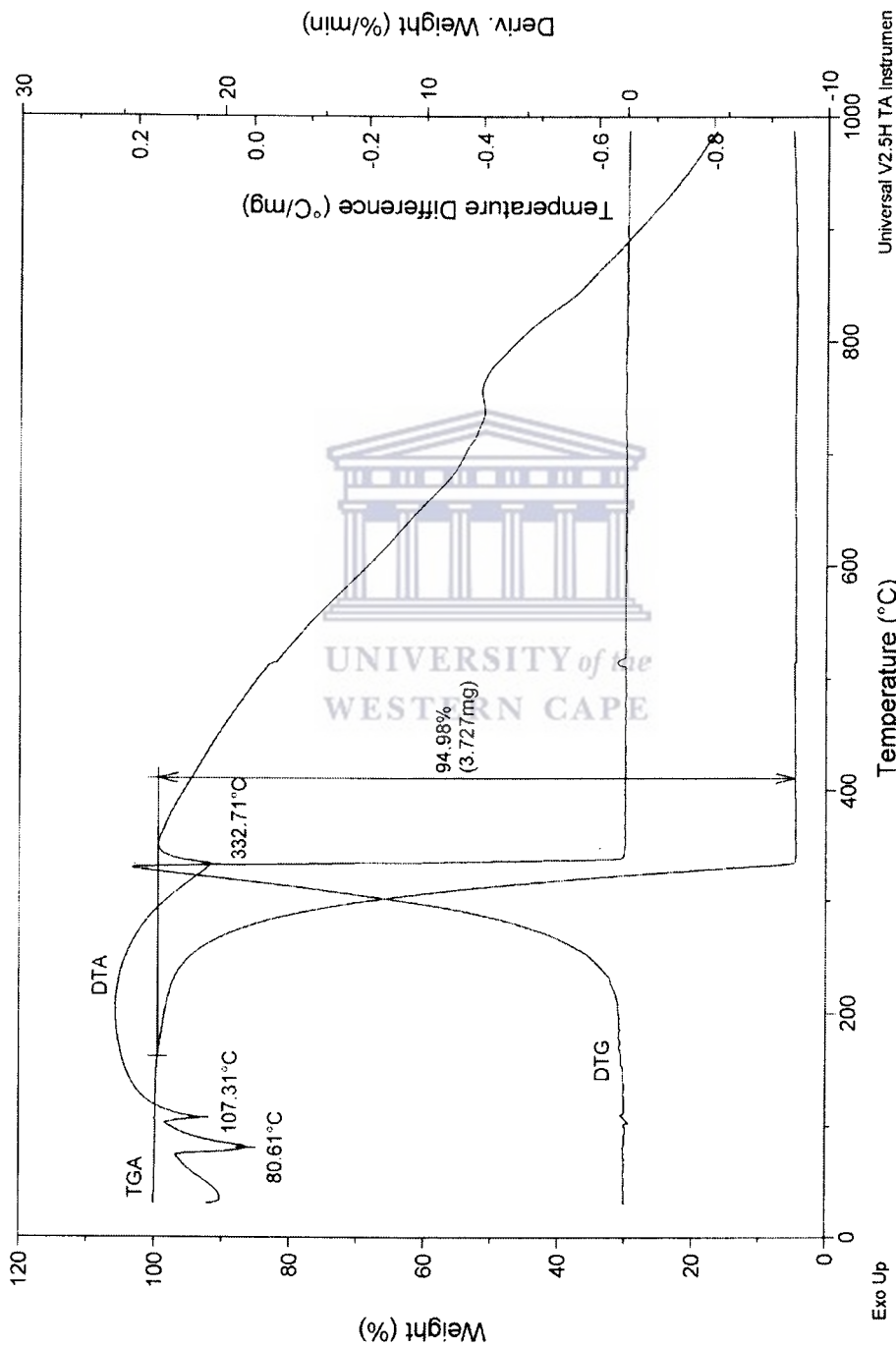


Figure 2.13: Thermograms for compound 10.

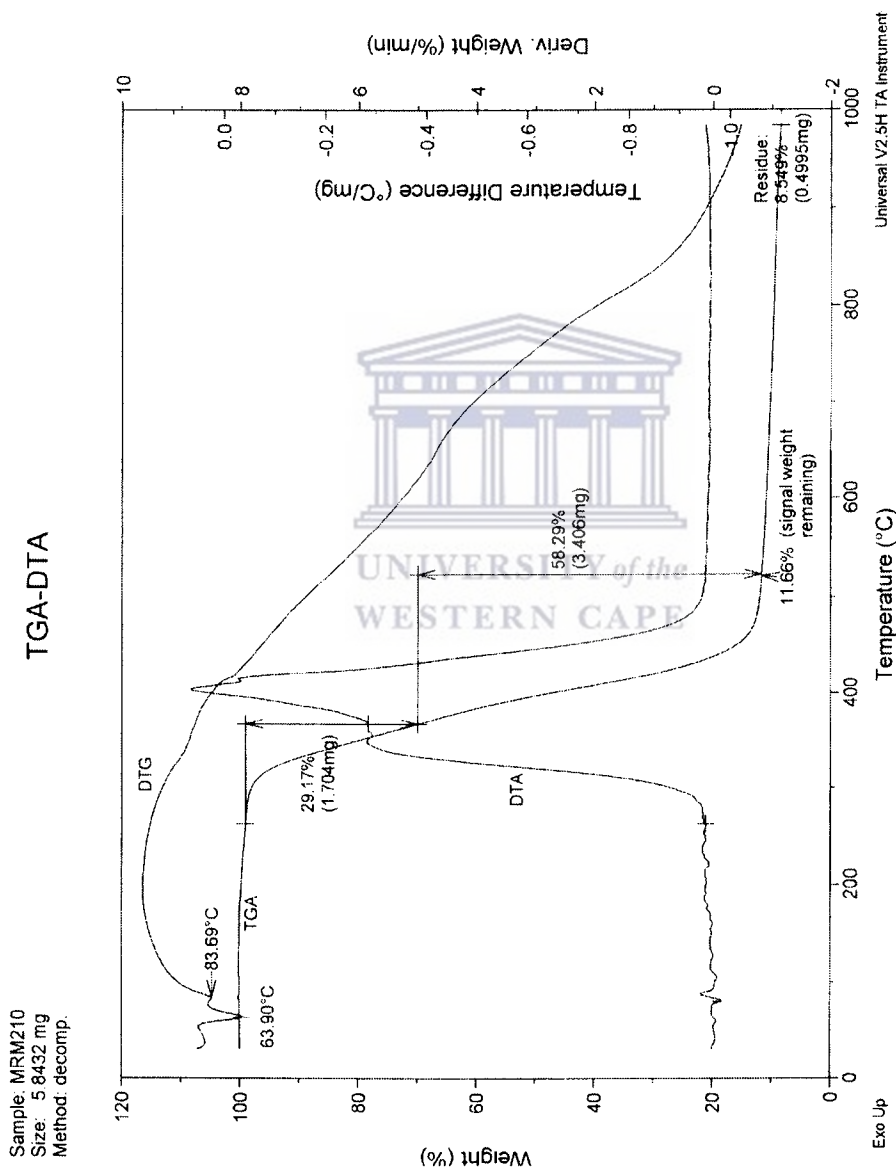


Figure 2.14: Thermograms for compound 11.

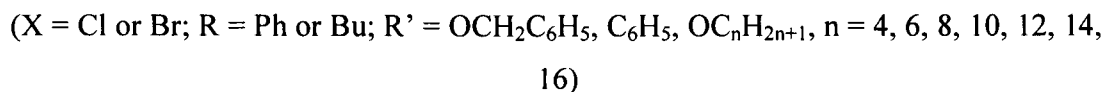
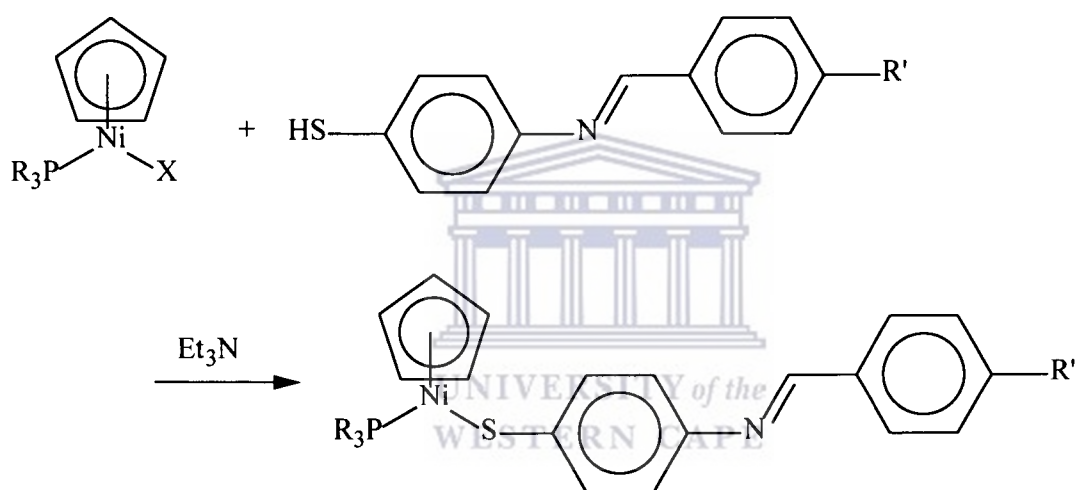


Figure 2.15: Optical micrograph showing the focal conic texture of compound 10.

2.7.2 Synthesis and characterisation of cyclopentadienylnickel(II) thiolato Schiff base complexes.

2.7.2.1 Synthesis and spectroscopic characterisation of the nickel complexes.

Complexes (**1a - 9a**, **1b - 9b**) were synthesised by reacting the thiol-imine ligands (**1 - 9**) with either $\text{NiBr}(\text{PBU}_3)(\eta^5\text{-C}_5\text{H}_5)$ or $\text{NiBr}(\text{PPh}_3)(\eta^5\text{-C}_5\text{H}_5)$ in the presence of a weak base, Et_3N , using 1:1 ratio of reactants (Eq. 2.3).



(2.3)

In all the reactions there was an immediate colour change from maroon to dark green on addition of the base, but the reaction mixtures were generally allowed to stir for 18 hours at room temperature to ensure complete reaction. The products were isolated from the salt by-product, $\text{Et}_3\text{NH}^+\text{Cl}^-$, by filtration as the salt was insoluble in toluene but the products were soluble. The complexes were recrystallised from $\text{CH}_2\text{Cl}_2/\text{hexane}$ at $-15\text{ }^\circ\text{C}$ to give analytically pure compounds. Generally the yields for the complexes were moderate to high ranging from 56% to 88% for the alkoxy chain complexes. The yields for the complexes with three-benzene ring were low to moderate (38% - 55%) compared to the alkoxy chain complexes. All products were air stable in the solid state under normal

laboratory conditions and could be stored in sample tubes under air for several weeks without decomposition.

The above synthetic protocol has been utilised extensively by Darkwa *et al.* in the preparation of complexes with the general formulae, $\text{Ni}(\text{SR})(\text{PPh}_3)(\eta^5\text{-C}_5\text{H}_5)$ (where $\text{R} = \text{C}_6\text{H}_5, \text{C}_6\text{H}_4\text{Me-4}$ or $\text{S}(\text{CH}_2)_4\text{SH}$),⁶¹ $\text{Ni}(\text{SR}'')(\text{PR}_3')(\eta^5\text{-C}_5\text{H}_5)$ (where $\text{R}' = \text{Ph, OPh, OEt, OMe}$ or Bu , and $\text{R}'' = \text{C}_6\text{H}_4\text{X-4}$, $\text{X} = \text{NH}_2, \text{Br}$ or Cl)⁵⁰ and $\text{Ni}(\text{SC}_6\text{H}_4\text{NC}(\text{H})\text{C}_6\text{H}_4\text{X-4}')(\text{PR}_3')(\eta^5\text{-C}_5\text{H}_5)$ (where $\text{R}' = \text{Ph}$ or Bu ; $\text{X} = \text{F, Cl, Br, CH}_3, \text{OH}$ and H)^{43a}. Similar complexes have been synthesised by Sato *et al.* who for example prepared the complex $\text{Ni}(\text{SC}_6\text{H}_4\text{Cl-4})(\text{PBU}_3)(\eta^5\text{-C}_5\text{H}_5)$ by the metathetical reaction between $[(\eta^5\text{-C}_5\text{H}_5)\text{Ni}(\text{PBU}_3)_2]^+\text{Cl}^-$ and $\text{NaSC}_6\text{H}_4\text{Cl-4}$ in 63% yield.⁶² The limitation of the Sato method is that it can only be carried out in aqueous or ethanolic media,⁶² whereas the synthetic method used here works in non-aqueous solvents and hence avoids having to remove water from the final product.

The complexes (**1a - 9a** and **1b - 9b**) are all green-brown in solution but have different colours in the solid state. Whereas the colour is dark green for PBU_3 complexes, the colour varied from dark brown to brick red for PPh_3 complexes. The colour difference in the solid and solution states could imply that the structures of the complexes in the solid and solution states are different, but from the spectroscopic data and X-ray structural data it seems that the structures in both the solid and solution states are the same. Full characterisation of all the compounds were by a combination of ^1H and ^{31}P NMR spectroscopy, elemental analysis and in two cases (**1a** and **3a**) by single crystal X-ray diffraction. The use of the analytical data to characterise the compounds are described in subsequent sections below.

^1H NMR spectral data show that the thiolato resonances of the complexes (**1a - 9a, 1b - 9b**) and those of the free ligands are very similar (Figure 2.16 and 2.17). Changes in the substituents of the thiolato ligands had no significant influence on the electronic environment of either the cyclopentadienyl ring or the phosphine ligands, as their proton NMR chemical shifts were not affected. For complexes with three benzene rings the

cyclopentadienyl shift is affected only by the change in phosphine and not by the nature of the three rings. For example the resonance signal of the cyclopentadienyl ring of all the tributylphosphine complexes (**1a** – **9a**) is between 5.26 and 5.28 ppm is insensitive to the change in the alkoxy chain length or whether the chain was replaced with a benzene ring. The same trend was found for **1b** – **9b**, with the cyclopentadienyl resonance peak between 5.13 – 5.15 ppm. When comparing the series **1a** – **9a** and **1b** – **9b**, the peak values change from 5.26 – 5.28 ppm to 5.13 – 5.15 ppm for tributylphosphino complexes to triphenylphosphino complexes respectively. The observed peak values are similar to those of similar complexes reported earlier by Darkwa *et al.* For instance, complexes $\text{Ni}(\text{SC}_6\text{H}_4\text{X-4})(\text{PBu}_3)(\eta^5\text{-C}_5\text{H}_5)$ ($\text{X} = \text{Cl}, \text{Br}$ or NH_2) have a cyclopentadienyl peak at 5.25 ppm, while for $\text{Ni}(\text{SC}_6\text{H}_4\text{X-4})(\text{PPh}_3)(\eta^5\text{-C}_5\text{H}_5)$ ($\text{X} = \text{Cl}, \text{Br}$ or NH_2) the cyclopentadienyl peak is at 5.13 ppm.⁵⁰ For complexes with Schiff base ligands, their cyclopentadienyl peak values are 5.27 ppm for $\text{Ni}(\text{SC}_6\text{H}_4\text{NC}(\text{H})\text{C}_6\text{H}_4\text{X-4})(\text{PBu}_3)(\eta^5\text{-C}_5\text{H}_5)$ ($\text{X} = \text{F}, \text{Cl}, \text{Br}, \text{H}, \text{OH}$ or Me) and 5.14 ppm for $\text{Ni}(\text{SC}_6\text{H}_4\text{NC}(\text{H})\text{C}_6\text{H}_4\text{X-4})(\text{PPh}_3)(\eta^5\text{-C}_5\text{H}_5)$ ($\text{X} = \text{F}, \text{Cl}, \text{Br}, \text{H}, \text{OH}$ or Me) respectively.^{43a} The thiolato ring protons were not affected by the substituents at the 4'-position of the Schiff base ligand. Peak values of 6.93 ppm and 6.85 ppm were observed for thiolato ring protons of **1a** – **9a** and **1b** – **9b** respectively. These observations show that the substituents on the *para*-position of the Schiff base ligand have no influence on the electronic environment around the nickel atom.

The $^{31}\text{P}\{^1\text{H}\}$ NMR chemical shift for **1a** – **9a** was 22.4 ppm while those for **1b** – **9b** were 35.5 ppm. The chemical shifts of the phosphorus atom are also insensitive to the substituent groups on the Schiff base ligands. These values compare well with those of $\text{Ni}(\text{SC}_6\text{H}_4\text{X-4})(\text{PBu}_3)(\eta^5\text{-C}_5\text{H}_5)$ ($\text{X} = \text{Cl}, \text{Br}$ or NH_2) (22.4 ppm) and $\text{Ni}(\text{SC}_6\text{H}_4\text{X-4})(\text{PPh}_3)(\eta^5\text{-C}_5\text{H}_5)$ ($\text{X} = \text{Cl}, \text{Br}$ or NH_2) (35.4 ppm) for the one ring complexes⁵⁰ and the values of 22.4 ppm and 35.4 ppm for the Schiff base complexes $\text{Ni}(\text{SC}_6\text{H}_4\text{NC}(\text{H})\text{C}_6\text{H}_4\text{X-4})(\text{PBu}_3)(\eta^5\text{-C}_5\text{H}_5)$ ($\text{X} = \text{F}, \text{Cl}, \text{Br}, \text{H}, \text{OH}$ or Me) and $\text{Ni}(\text{SC}_6\text{H}_4\text{NC}(\text{H})\text{C}_6\text{H}_4\text{X-4})(\text{PPh}_3)(\eta^5\text{-C}_5\text{H}_5)$ ($\text{X} = \text{F}, \text{Cl}, \text{Br}, \text{H}, \text{OH}$ or Me) respectively.^{43a}

The cyclopentadienyl ring ^1H NMR chemical shifts for the more basic phosphine, was more upfield than those for the less basic phosphine.

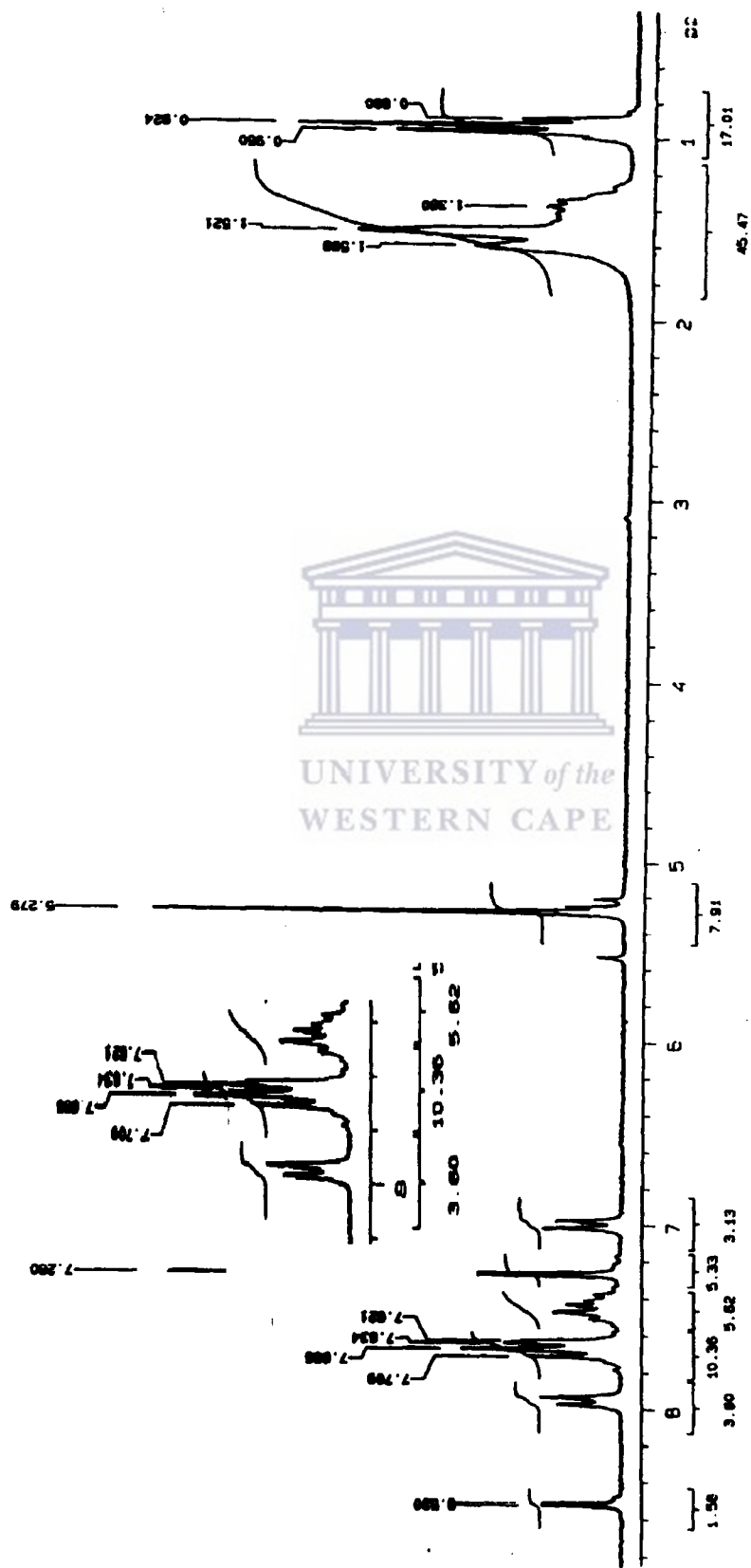


Figure 2.16. ¹H NMR spectrum of complex 1a. Inset: The aromatic region of spectrum of complex 1a.

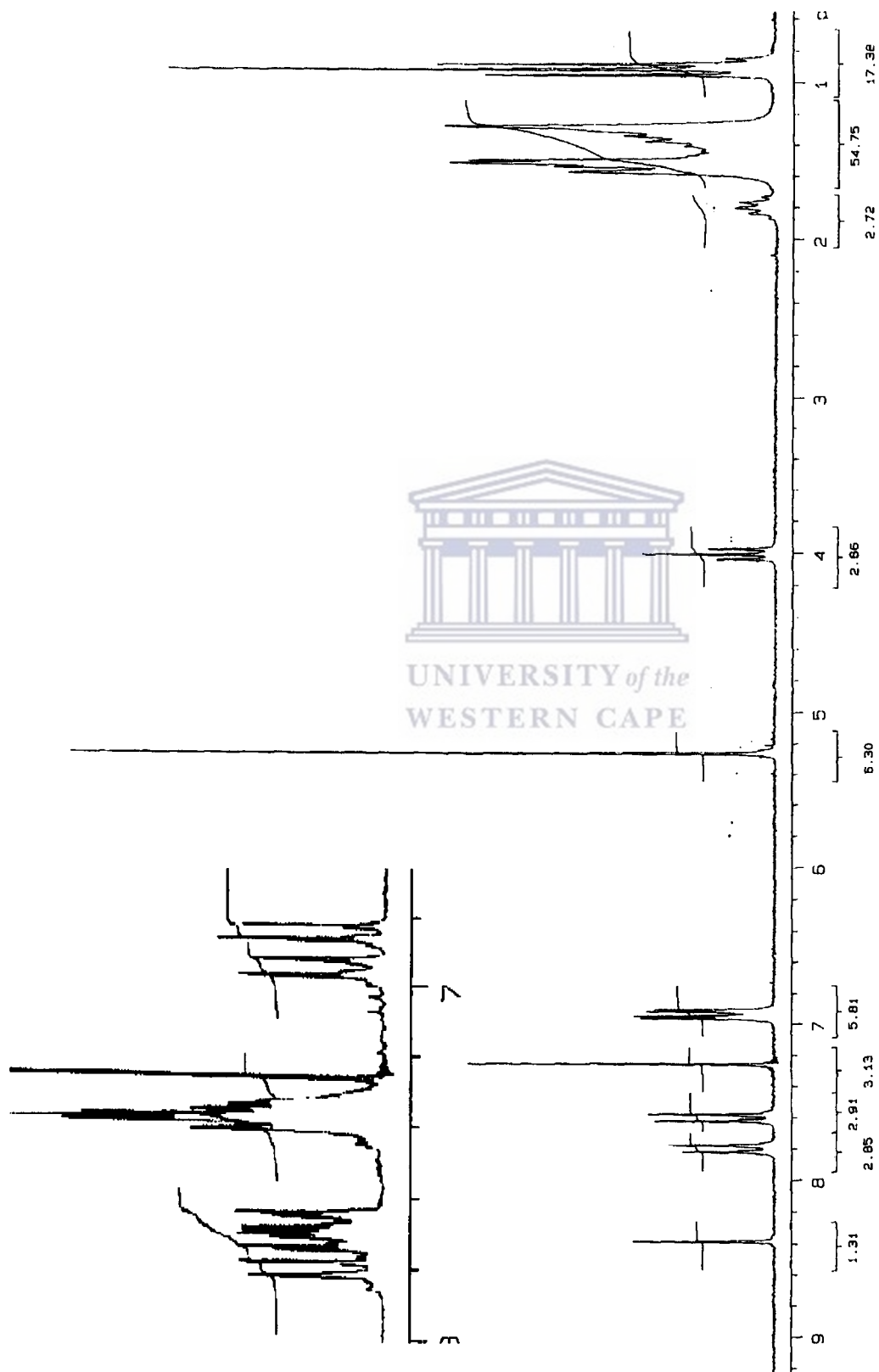


Figure 2.17. ^1H NMR spectrum of complex 3a. Inset: Aromatic region of spectrum of complex 3b.

The trend is reversed for the ^{31}P NMR chemical shifts with the more basic phosphine resonance being upfield and the less basic phosphine downfield. The basic phosphine, being electron rich, donates more electron density to the nickel centre, which in turn shields the cyclopentadienyl ring; hence a more upfield value for the cyclopentadienyl ring chemical shift. On the other hand more electron density on the nickel atom means that it will be able to effectively π -back donate to the phosphorus atom. This back donation will shield the phosphorus atom, and hence the upfield resonance for the more basic phosphine ligand in the ^{31}P NMR spectrum.

2.7.4 Molecular structures of **1a** and **3a**

The molecular structures of **1a** and **3a** were determined by X-ray crystallography. The solid state structures of **1a** and **3a** are shown in Figures 2.18 and 2.20 and confirm that the proposed structures from the analytical and spectral data are correct. A selection of crystal data and structural refinement for **1a** and **3a** are given in Table 2.5. Selected bond distances and angles are shown in Table 2.6 (**1a**) and Table 2.7 (**3a**). The structures are typical of monocyclopentadienylnickel complexes that have monophosphine ligands. If the centroid of the cyclopentadienyl ring is assumed to occupy one coordination site then the nickel atom has a distorted trigonal geometry. The cyclopentadienyl centroid-nickel bond distances in **1a** and **3a** are 1.750(3) Å and 1.752(3) Å respectively and lie within the range (1.743-1.764 Å) found for similar complexes $\text{Ni}(\text{SC}_6\text{H}_4\text{Cl})(\text{PPh}_3)(\eta^5\text{-C}_5\text{H}_5)$ (1.763 Å),⁶³ $\text{Ni}(\text{SC}_6\text{H}_4\text{X})(\text{PR}_3)(\eta^5\text{-C}_5\text{H}_5)$ (R =, Bu or Et; E = S, Se or Te; X = H, Cl or Me)⁶⁴ and $\text{Ni}(\text{SC}_6\text{H}_4\text{NC}(\text{H})\text{C}_6\text{H}_4\text{Br-4})(\text{PPh}_3)(\eta^5\text{-C}_5\text{H}_5)$ (1.743 Å) or $\text{Ni}(\text{SC}_6\text{H}_4\text{NC}(\text{H})\text{C}_6\text{H}_4\text{Me-4})(\text{PPh}_3)(\eta^5\text{-C}_5\text{H}_5)$ (1.764 Å)^{43a}. The Ni-S distances in **1a** (2.184(1) Å) and **3a** (2.192(1) Å) and the Ni-P distances in **1a** (2.145(1) Å) and **3a** (2.145(1) Å) are all similar to distances of Ni-S bonds and Ni-P bonds in cyclopentadienylnickel(II) complexes. For example the Ni-S bond length in $\text{Ni}(\text{SC}_6\text{H}_4\text{Cl-4})(\text{PPh}_3)(\eta^5\text{-C}_5\text{H}_5)$ and $\text{Ni}(\text{SC}_6\text{H}_5)(\text{PPh}_3)(\eta^5\text{-C}_5\text{H}_5)$ are (2.190 Å)⁶³ and (2.192(1) Å)⁶⁵ respectively. The Ni-P bond length is 2.144 Å for $\text{Ni}(\text{SC}_6\text{H}_4\text{Cl-4})(\text{PPh}_3)(\eta^5\text{-C}_5\text{H}_5)$, 2.139 Å for $\text{Ni}(\text{SC}_6\text{H}_5)(\text{PPh}_3)(\eta^5\text{-C}_5\text{H}_5)$ and 2.136(1) Å for $\text{Ni}(\text{SeC}_6\text{H}_4\text{Cl-4})(\text{PPh}_3)(\eta^5\text{-C}_5\text{H}_4\text{Me})$.

Table 2.5: Crystallographic and refinement data for compounds **1a** and **3a**

Compound	1a	3a
Empirical formula	C ₃₄ H ₅₀ N O P S Ni	C ₃₆ H ₄₆ N P S Ni
Formula weight	610.49	614.48
Temperature/ K	150(2)	173(2)
Wavelength /Å	0.71073	0.71073
Crystal system	Triclinic	Monoclinic
Space group	P $\bar{1}$	P 2 ₁ /c
a/Å	10.455(1)	13.164(2)
b Å	12.375(1)	20.277(2)
c/Å	13.567(1)	12.740(2)
α /°	104.25(1)	90.0
β /°	99.31(1)	106.46(1)
γ /°	92.47(1)	90.0
V/Å ³	1672.6(2)	3261.2(11)
Z, Calculated density/ Mg m ⁻³	2, 1.212	4, 1.252
Absorption coefficient/ mm ⁻¹	0.716	0.733
F(000)	656	1312
Crystal size/mm	0.35 x 0.35 x 0.25	0.41 x 0.37 x 0.25
No. reflections collected / unique	13454 / 7614	12387 / 6623
Completeness to theta = 25°	99.8%	97.9%
R(int.)	0.0191	0.0326
Data / restraints / parameters	7614 / 0 / 357	6623 / 0 / 463
Final R indices [$I > 2\sigma(I)$]	R ₁ = 0.0338, wR ₂ = 0.0717	R ₁ = 0.0409, wR ₂ = 0.0845
R indices (all data)	R ₁ = 0.0495, wR ₂ = 0.0774	R ₁ = 0.0693, wR ₂ = 0.0950
Largest peak and hole/ e ⁻ .Å ⁻³	0.332 and -0.353	0.445 and -0.418

Table 2.6: Selected bond distances (Å) and angles (°) for **1a**

Ni-S	2.193(1)	Ni-P	2.145(1)
Ni-Cp*	1.750(3)	C(18)-S	1.764(2)
C(24)-N	1.277(3)	C(6)-P	1.828(2)
C(10)-P	1.834(2)	C(14)-P	1.824(2)
S-Ni-Cp*	132.43(1)	P-Ni-Cp*	136.28(1)
C(18)-S-Ni	107.5(1)	C(14)-P-Ni	115.1(1)
P-Ni-S	91.7(1)	C(6)-P-Ni	113.6(1)
C(10)-P-Ni	114.6(1)	-	-

Table 2.7: Selected bond distances and (Å) and angles (°) for **3a**

Ni-S	2.184(1)	Ni-P	2.145(1)
Ni-Cp*	1.752(3)	C(18)-S	1.761(3)
C(24)-N	1.271(3)	C(14)-P	1.820(2)
C(6)-P	1.822(2)	C(10)-P	1.834(2)
S-Ni-Cp*	131.6(1)	Cp*-Ni-P	136.3 (1)
C(18)-S-Ni	109.7(1)	C(10)-P-Ni	113.7(1)
C(6)-P-Ni	113.4(1)	C(14)-P-Ni	115.2(1)
P-Ni-S	91.2(1)	-	-

*Cp is the cyclopentadienyl ring centroid.

The N=C double bond in **3a** is slightly long at 1.271(3)Å, compared to 1.261(5)Å and 1.258(5) Å.⁶⁶ The geometry around nickel atom is a distorted trigonal similar to those of related complexes. For example the P-Ni-S bond angles of 91.7(1)° and 91.2(1)° for **1a** and **3a** respectively are comparable to the P-Ni-S bond angles found in the complexes Ni(SC₆H₅)(PBU₃)(η⁵-C₅H₅)⁶⁵, Ni(SC₆H₄Cl-4)(PPh₃)(η⁵-C₅H₅)⁶³, Ni(SeC₆H₅)(PPh₃)(η⁵-C₅H₅)⁶⁷, Ni(SeC₆H₄Cl-4)(PPh₃)(η⁵-C₅H₄Me)⁵⁰ and Ni(SC₆H₄Cl-4)(PBU₃)(η⁵-C₅H₅)⁵⁰ with bond angles of 90.5°, 92.4(1)°, 91.48(4)°, 91.24(3)°, and 92.48(2)° respectively and those of the Schiff base complexes Ni(SC₆H₄NC(H)C₆H₄Br-4)(PPh₃)(η⁵-C₅H₅) (91.18(4)°)^{43a} or Ni(SC₆H₄NC(H)C₆H₄Me-4)(PPh₃)(η⁵-C₅H₅) (92.32(5)°)^{43a}. The Cp-Ni-S bond angles of 132.3(1)° (**1a**) and 131.6(1)° (**3a**) are close to those of Ni(SC₆H₄Cl-4)(PPh₃)(η⁵-C₅H₅) (132.3(1)°, Ni(SC₆H₅)(PPh₃)(η⁵-C₅H₅) (133.0°), Ni(SC₆H₄Cl-4)(PBU₃)(η⁵-C₅H₅) (132.0°) and Ni(SC₆H₄NC(H)C₆H₄Me-4)(PPh₃)(η⁵-C₅H₅) (134.8°) while the Cp-Ni-P bond angles are also in the same range at 136.28(1) (**1a**) and 136.3(1)° (**3a**) compared to those of Ni(SC₆H₄Cl-4)(PPh₃)(η⁵-C₅H₅) (135.3(5)°), Ni(SC₆H₅)(PPh₃)(η⁵-C₅H₅) (136.4°), Ni(SC₆H₄Cl-4)(PBU₃)(η⁵-C₅H₅) (134.9°) and Ni(SC₆H₄NC(H)C₆H₄Me-4)(PPh₃)(η⁵-C₅H₅) (132.8°).

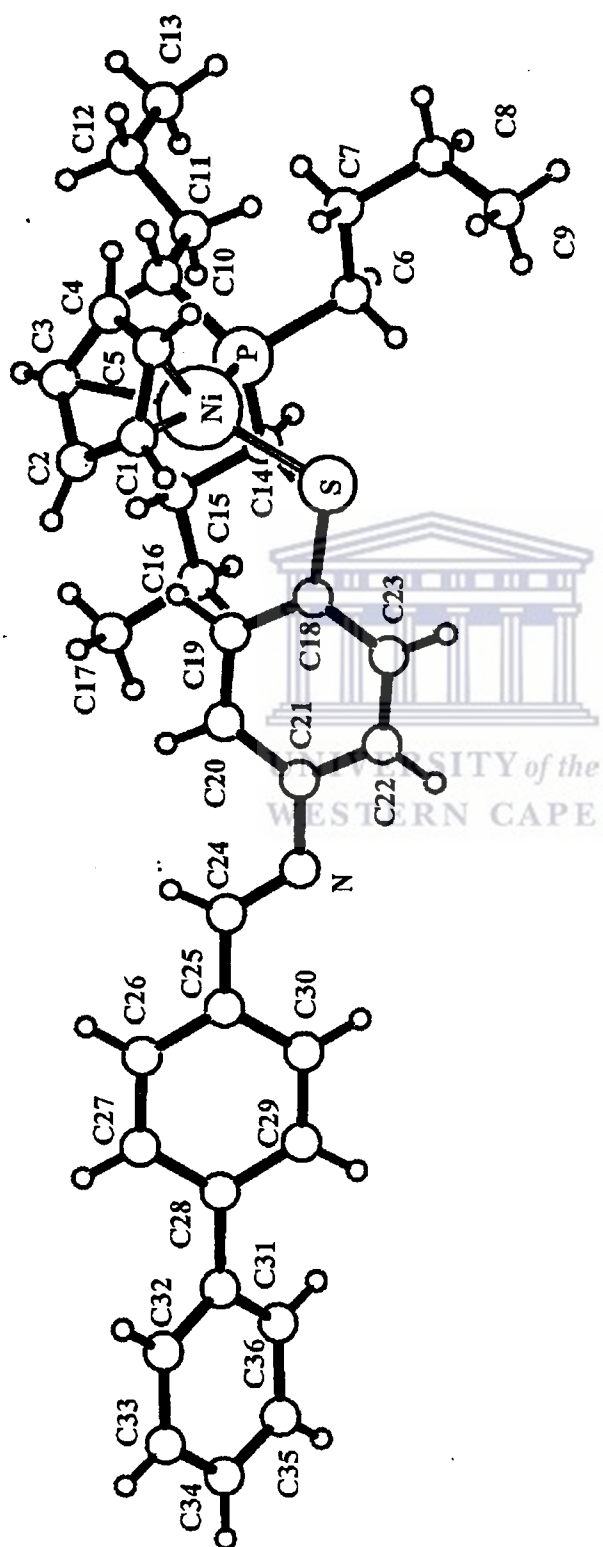


Figure 2.18: X-ray crystal structure of complex 1a.

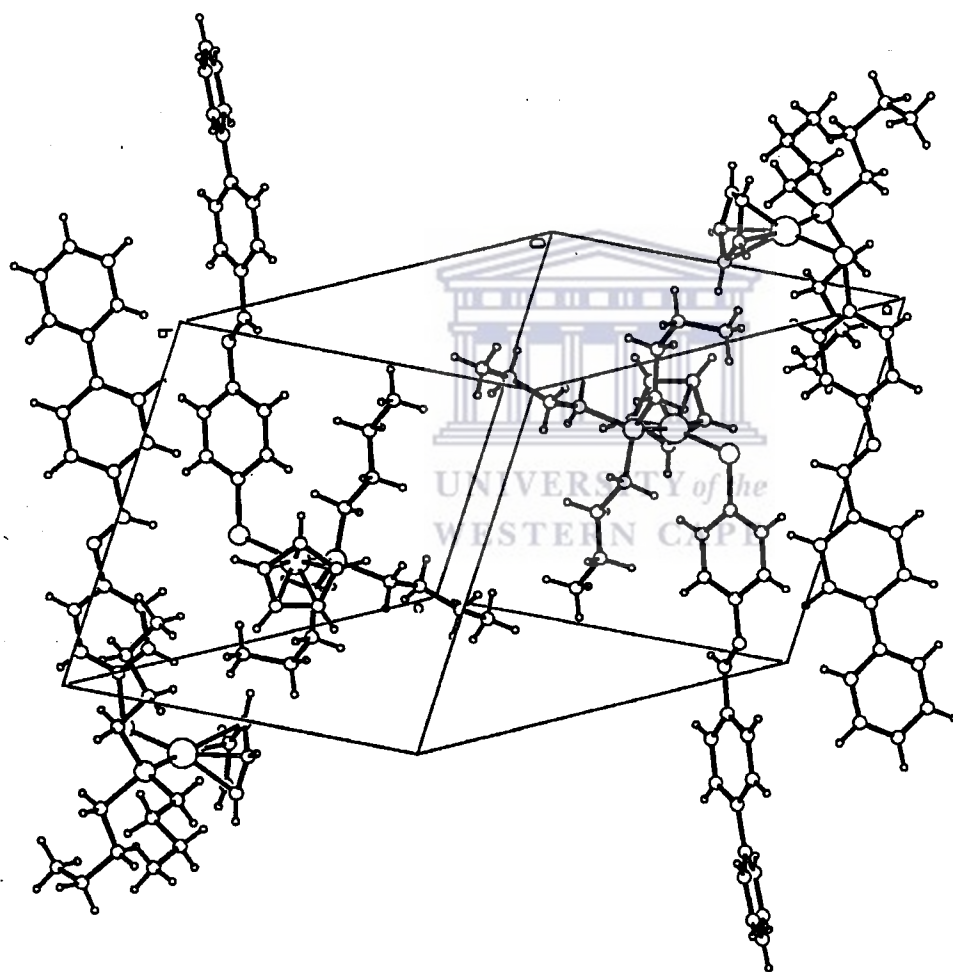


Figure 2.19: Molecular packing diagram of complex 1a.

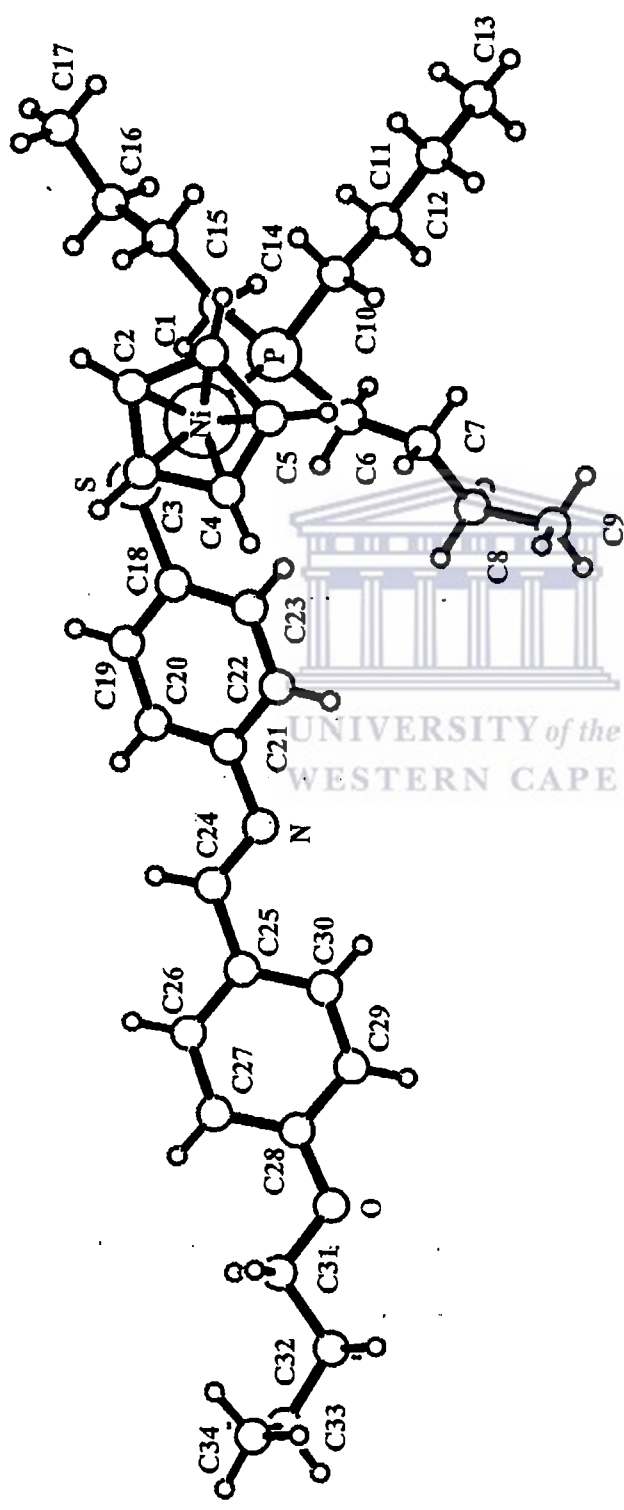


Figure 2.20 X-ray crystal structure of complex 3a.

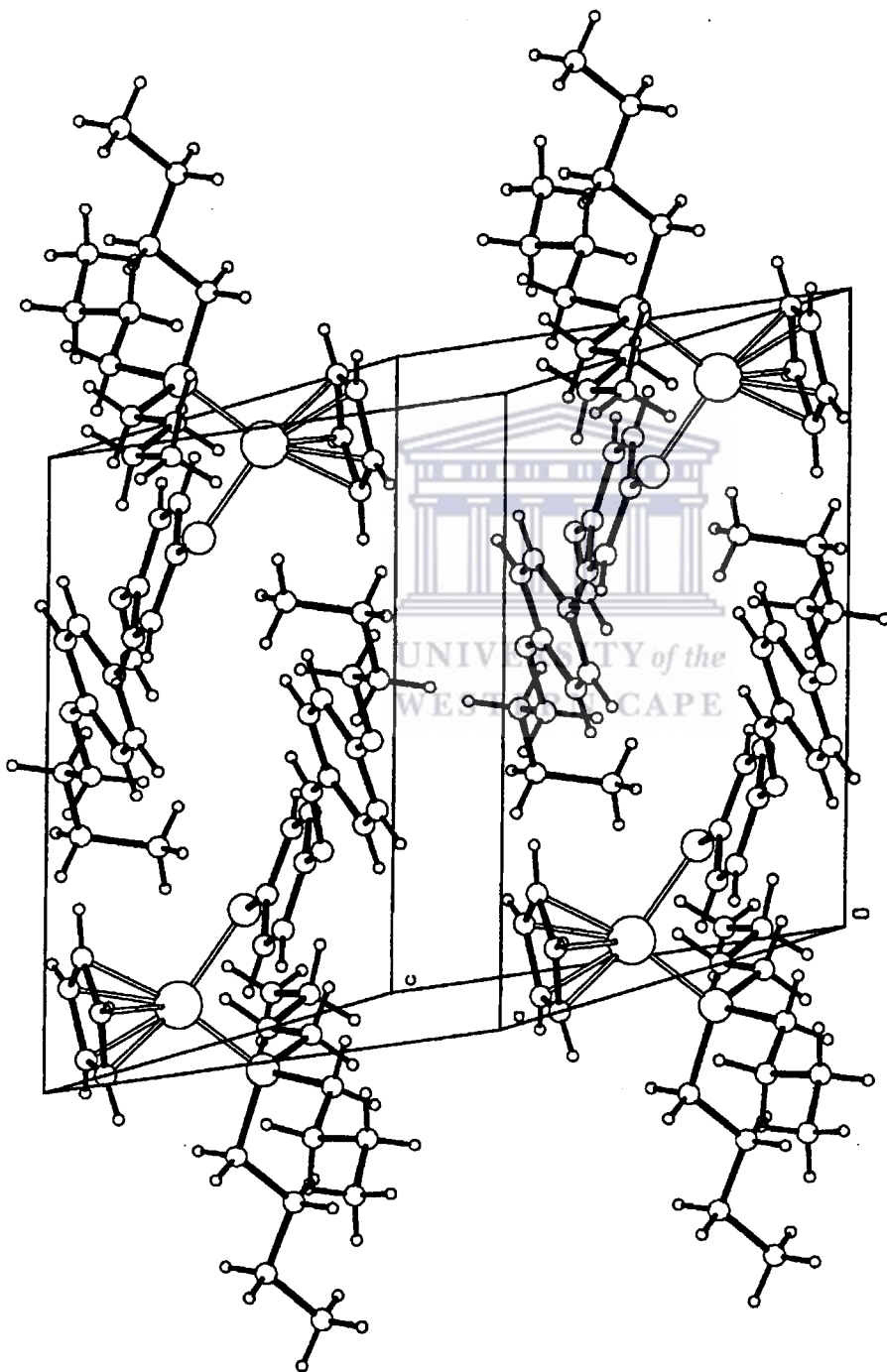


Figure 2.21: Molecular packing diagram of complex 3a.

Molecular packing in the unit cells of the two complexes is different. In both cases there is a pairwise association of molecules, with either two head-to-tail arrangements or head-to tail and tail-to-head arrangements if one considers the cyclopentadienylnickelphosphine moiety as the head. Thus **1a** has a head-to-tail pairwise association (Fig. 2.19) whereas **3a** has a head-to-tail, tail-to-head pairwise association (Fig. 2.21). The molecular packing in **3a** is similar to unit cell packing observed for Ni(SC₆H₄NC(H)C₆H₄Br-4)(PPh₃)(η⁵-C₅H₅) and Ni(SC₆H₄NC(H)C₆H₄Me-4)(PBU₃)(η⁵-C₅H₅)^{43a} in which each pair consists of head-to-tail, tail-to-head packing. Another striking feature in the X-ray structure of **1a** is that all three phenyl rings in the Schiff base ligand are not co-planar to each other, but are tilted with respect to each other. This suggests that there is a break in the π-conjugation between the rings. The ring closest to the sulfur atom is almost at right angles to the terminal ring. In both cases there is no π-interaction between the phenyl rings of the Schiff base ligands of neighbouring molecules as could be seen from the orientation of the rings and the inter-ring distances. In the ferrocenyl complex Fe(η⁵-C₅H₅)(η⁵-C₅H₄CH=NC₆H₄NO₂-4)⁶⁸ the phenyl rings from the two molecules were in a DAAD structural motif in which there were a C₆-ring π-π interactions with an inter-ring distance of 3.478 Å. Thus the latter compound had intermolecular π-interaction unlike the complexes in this chapter.

From the molecular packing diagrams of complexes **1a** and **3a**, it is evident that the molecules are associated pairwise. Thus the intramolecular interactions are largely localized in between pairs and there is no uniform, long range ordering among molecules. This is partly due to the bulky lateral groups (cyclopentadienyl ring and phosphine group) and the trigonal geometry around the nickel that causes the repulsions between pairs of molecules. This reduces the ability of all the molecules to have long-range association, which is a prerequisite for molecules to have liquid crystalline behaviour. It was therefore necessary to modify the design of complexes **1a** – **9a** and **1b** – **9b** in order to form complexes that are likely to produce mesogenic behaviour. The new complexes are discussed in chapter 3.

2.7.5 Thermal studies of cyclopentadienylnickel(II) complexes.

In order to test the complexes **1a - 9a** and **1b - 9b** for mesogenic behaviour thermal analysis experiments were performed on these complexes. All the nickel complexes were generally stable up to 180 °C before the onset of decomposition. The decomposition was indicated by the rapid mass loss in the TGA thermograms. The DSC of the complexes did not show multiple endothermic peaks and were therefore nonmesogenic. The premise that rigid rod shaped molecules with long alkoxy chains could lead to mesogenic behaviour is therefore not applicable to complexes **1a - 9a** and **1b - 9b**. The nonmesogenic behaviour is likely to be caused by the presence of bulky phosphine and the cyclopentadienyl ligands associated with the rigid core. In the known metallomesogens that have a cyclopentadienyl ring as ligand, mesogenic behaviour is only achieved when the number of benzene rings in the ligand is increased to at least three or four.^{69, 21b} Furthermore metal phosphine complexes with mesogenic behaviour are rare and in the known metal phosphine complexes, that have liquid crystalline properties, e.g. Pt(PMe₃)₂(C≡CC₆H₄-4-OC_nH_{2n+1})₂,⁷⁰ the phosphines used are less bulky and the geometry around the metal is square planar. Thus the lack of the mesogenic behaviour in the **1a - 9a** and **1b - 9b** is not surprising as the bulky phosphine ligands in these complexes prevent regular ordering on melting. One way of circumventing this problem is to increase the number of rings in the rigid ligand,^{69, 24b, 71} while avoiding the use of phosphines. This approach is used in chapter 3.

Nevertheless, the thermal data of the phosphine complexes are interesting in their own and is further discussed in subsequent paragraphs. Table 2.8 shows the melting points obtained from the DSC of the complexes. From these measurements it is obvious that melting points depended on two variables, namely the phosphine and the length of the alkoxy chain at the 4'-position in the Schiff base ligand. Firstly when the length of the alkoxy chain was increased there was a steady decrease in the melting points. This decrease leveled off as the number of the carbon atoms in the chain exceeded 12. Therefore the difference in the melting points of the complexes with longer ($n \geq 12$) chains was very small, almost negligible. Similar leveling off of the melting points with

an increase in the length of the chain in a homologous series of compounds had been observed before.⁷² Secondly the melting points were dependent on the type of phosphine used. For a given length of the alkoxy chain in a particular complex, the PBu₃ analogue had a lower melting point transition than its PPh₃ analogue. The difference in the melting points of complexes with different phosphines was in some cases as high as 60 °C. This observation could be explained in terms of the rigidity of the substituents on the phosphorus atom. When the substituents are rigid the melting points are high while for the more flexible substituents the melting points are lower.

The relationship between melting and chain length is not simple, but in general an increase in the chain length can have two opposite effects on the melting temperature. Firstly an increase in the length of the chain can cause an increase in the molecular polarisability thus leading to higher melting points.⁷³ Secondly an increase in the chain length can lead to an increase in the disorder of the chain, which will favour lower transition temperatures. Consequently the variation of the melting point as a function of chain length will depend on the dominant factor.⁷⁴ In complexes **1a** - **9b** it seems that both of these factors are operating. At longer chain length ($n \geq 12$) the first point is more dominant while at shorter chain lengths the second factor is more dominant.

Comparing the two-ring system with the three-ring systems it was found that the latter had invariably higher melting point. This observation was not at all surprising because an increase in the number of rings in the rigid fragment of the molecule will increase the molecular anisotropy. This favours lamella packing and an increase in intermolecular interactions leading to higher melting points.⁷⁵ The lack of flexible chains to cause any disruptions in the lamella packing leads to high melting points.

Table 2.8. Melting points of selected complexes showing that melting point decreases with chain length.

Complex	Melting point (°C)
3a	99.97
3b	138.83
6a	62.24
6b	120.11
7a	52.26
7b	90.21
8b	89.70
9a	49.70
9b	101.77

Heat changes (ΔH) associated with the DSC endothermic peaks for PPh_3 and PBu_3 complexes were different. Those of PBu_3 were 3-6 times higher than those of PPh_3 complexes. The difference in ΔH could be rationalised in terms of the nature and size of the phosphine groups. Since melting point of a compound is the temperature at which a three-dimensional ordered structure collapses into a disordered, isotropic liquid, the changes occurring are substantial.^{2c} Thus differences in the molecules could lead to large changes in the way the molecule pack in the crystal lattice and hence in the melting behaviour. Since the length of the alkoxy chain is the same for both series (**1a – 9a** and **1b – 9b**), the chain length cannot cause the difference in ΔH that was observed, which means this difference originates from the difference in the phosphines.

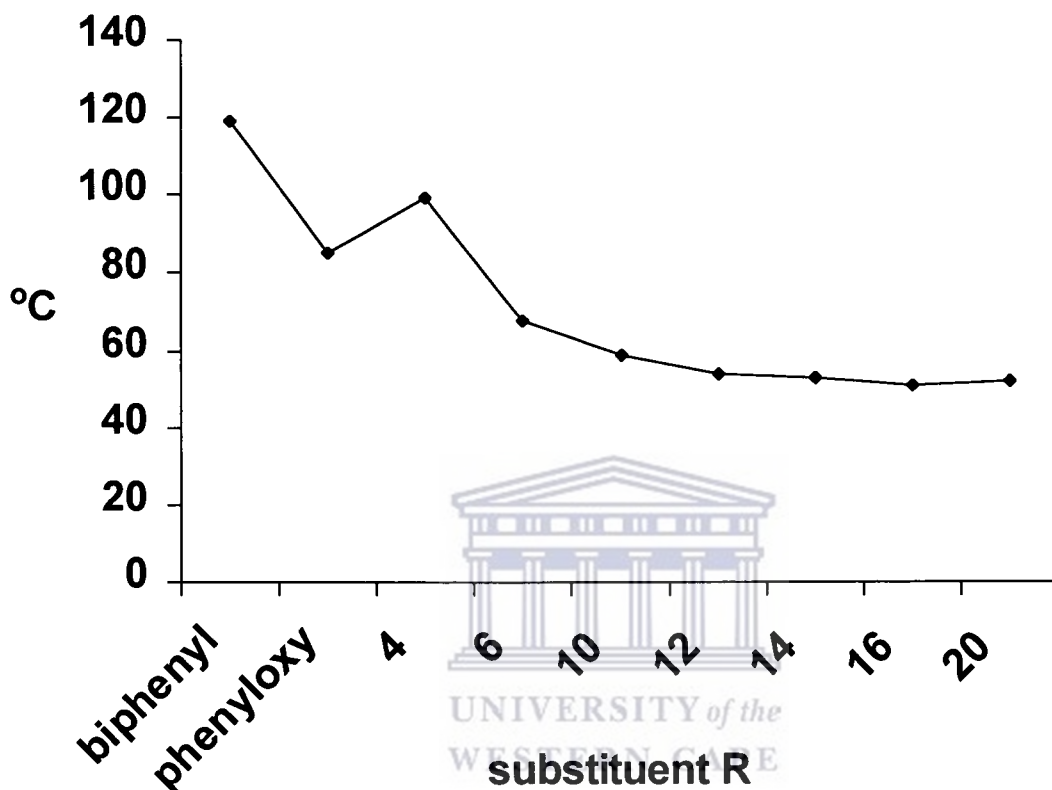


Figure 2.22: Melting points dependence of tributylphosphine complexes on chain length.

2.7.2.4. Thermal decomposition pathways of the complexes.

Two thermal decomposition pathways could be established from TGA data. These were dependent on the phosphine substituents. Complexes that had PPh_3 initially lost the cyclopentadienyl ligand followed by the loss of the phosphine and rupture of the Schiff base ligand (Scheme 2.6, Table 2.9). Figure 2.23 shows a representative thermogram for PPh_3 complex series, revealing three thermal events. The first step in the decomposition of PPh_3 complexes occurred at 180 °C and corresponds to the loss of a cyclopentadienyl ligand. The second step in the decomposition is the endothermic process in the temperature range 190-320 °C, corresponding to the loss of PPh_3 ligand. In comparison to the PBu_3 complexes, the PPh_3 ligand is lost at a relatively higher temperature suggesting

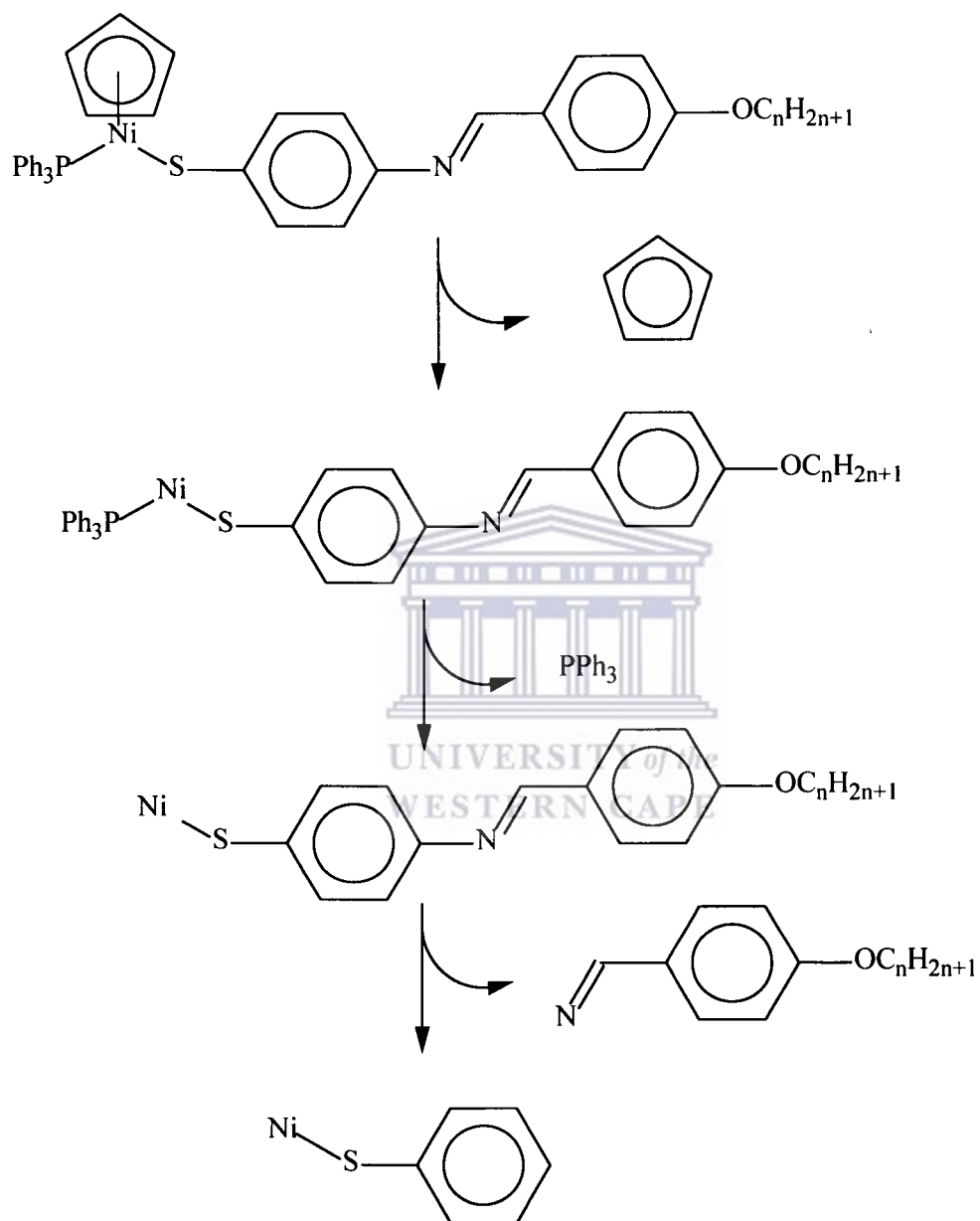
a stronger Ni-P bond. The third thermal event at about 400 °C was the exothermic rapture and subsequent loss of the Schiff base ligand, leaving a residual mass that corresponds to the Ni(SC₆H₅) moiety. The PBu₃ analogue on the other hand decomposed first by the simultaneous loss of cyclopentadienyl and phosphine ligand, followed by the rupturing of the Schiff base ligand (Scheme 2.7). Figure 2.24 shows representative TGA-DSC curves for PBu₃ complex series. The residual mass in all the cases correspond to a Ni(SC₆H₅) moiety. The above thermal decomposition pathways demonstrate the relative strengths of the three Ni-ligand (Ni-S, Ni-P, Ni-Cp) interactions. The strongest of these bonds appear to be the Ni-S bond in both types of complexes, which stays intact even at temperatures above 800 °C. The fact that there is a possibility of electronic conjugation from the nickel centre through the sulfur (using lone pairs on sulfur atom) to the Schiff base rings might explain why the Ni-S bond is the strongest bond around nickel. It is interesting to note that the Ni-P bonds of the more basic phosphine (PBu₃) only break around 200 °C, whilst those of the less basic phosphine (PPh₃) are only stable up to about 300 °C. This observation can be, at least, rationalised by the fact that phosphines are not good π -acceptors.⁷⁶ Thus the more basic, donating phosphine will increase the ability of the nickel atom to back-donate to the sulfur atom.

Table 2.9 Percentage mass losses and the corresponding fragment.

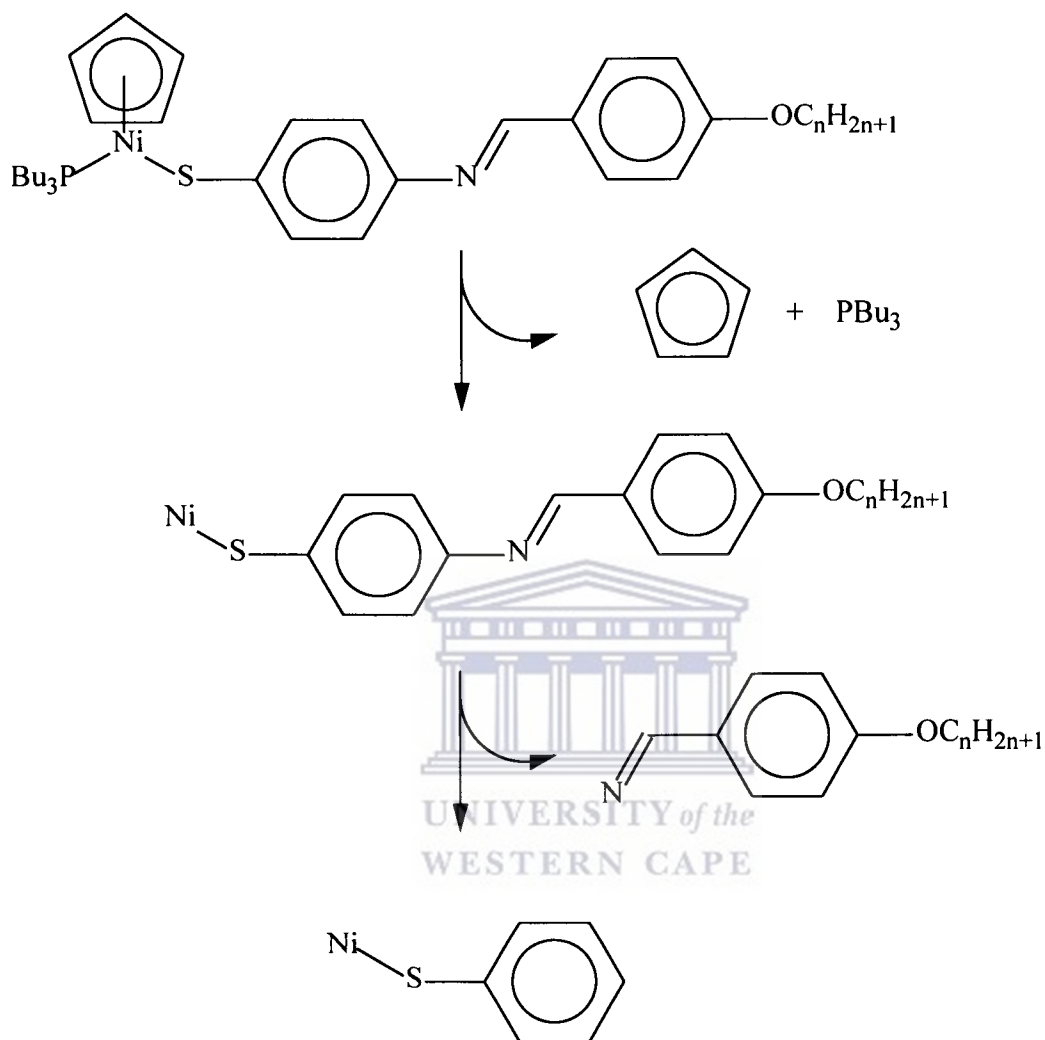
	C_5H_5	PBu_3	$NC(H)C_6H_4OC_nH_{2n+1}$	$Ni-SC_6H_4$	n
Calculated (%)	7.79	24.20	47.93		20
Found (%)	31.73*		31.24,	11.42	20.28
Temp. (°C)	213.18		389.22,	448.05	1000
Calculated (%)	8.67	26.95	42.16		14
Found (%)	34.01*		28.49,	13.23	20.00
Temp. (°C)			387.86,	449.37	1000
Calculated (%)	9.04	29.13	37.49		10
Found (%)	33.61		28.70		22.00
Temp. (°C)	208.90		355.96		1000
Calculated (%)	10.66	33.14	28.89		4
Found (%)	13.23	34.36	28.49		20.28
Temp. (°C)	449.37	211.75	387.86		1000

* denotes combined % mass loss for C_5H_5 and PBu_3 .

	C_5H_5	PPh_3	$NC(H)C_6H_4OC_nH_{2n+1}$	$Ni-SC_6H_4$	n
Calculated (%)	7.27	29.28	37.48		20
Found (%)	6.57		-		26.51
Temp. (°C)	180.45	256.11	-		1000
Calculated (%)	6.23	32.35	39.04		14
Found (%)	5.05	34.89	26.64	11.55	17.48
Temp. (°C)	177.79	253.17	389.02	442.38	1000
Calculated (%)	8.63	34.76	34.51		10
Found (%)	5.80	35.05	34.27		21.23
Temp. (°C)	177.99	247.45	387.61		100
Calculated (%)	9.71	39.12	26.29		4
Found (%)	8.31	40.11	29.40		20.89
Temp. (°C)	175.38	243.51	395.41		1000



Scheme 2.6: Thermal decomposition pathway of PPh_3 complexes.



Scheme 2.7 Thermal decomposition pathway of PBu_3 complexes.

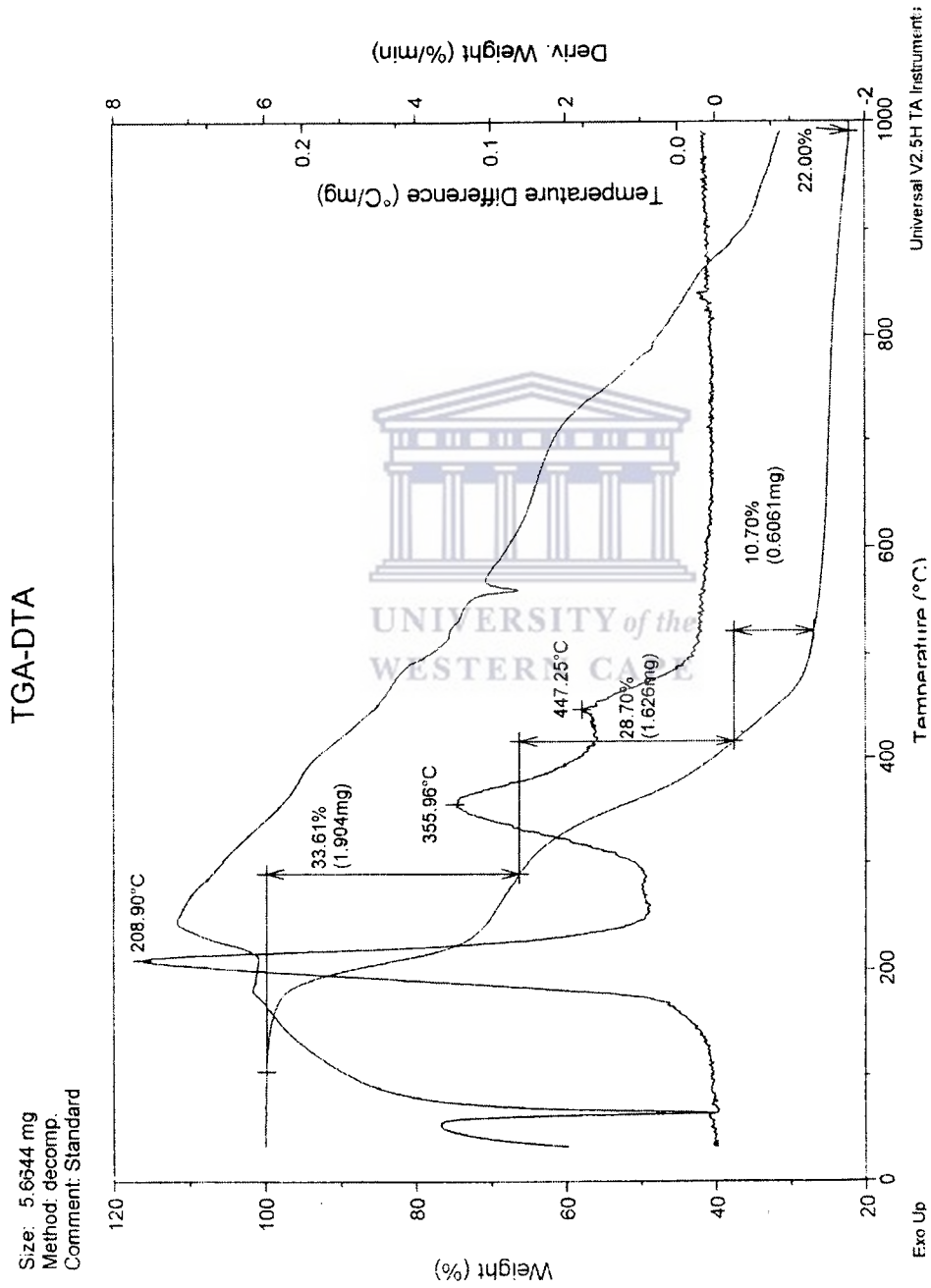


Figure 2.23: Thermograms for complex 6a.

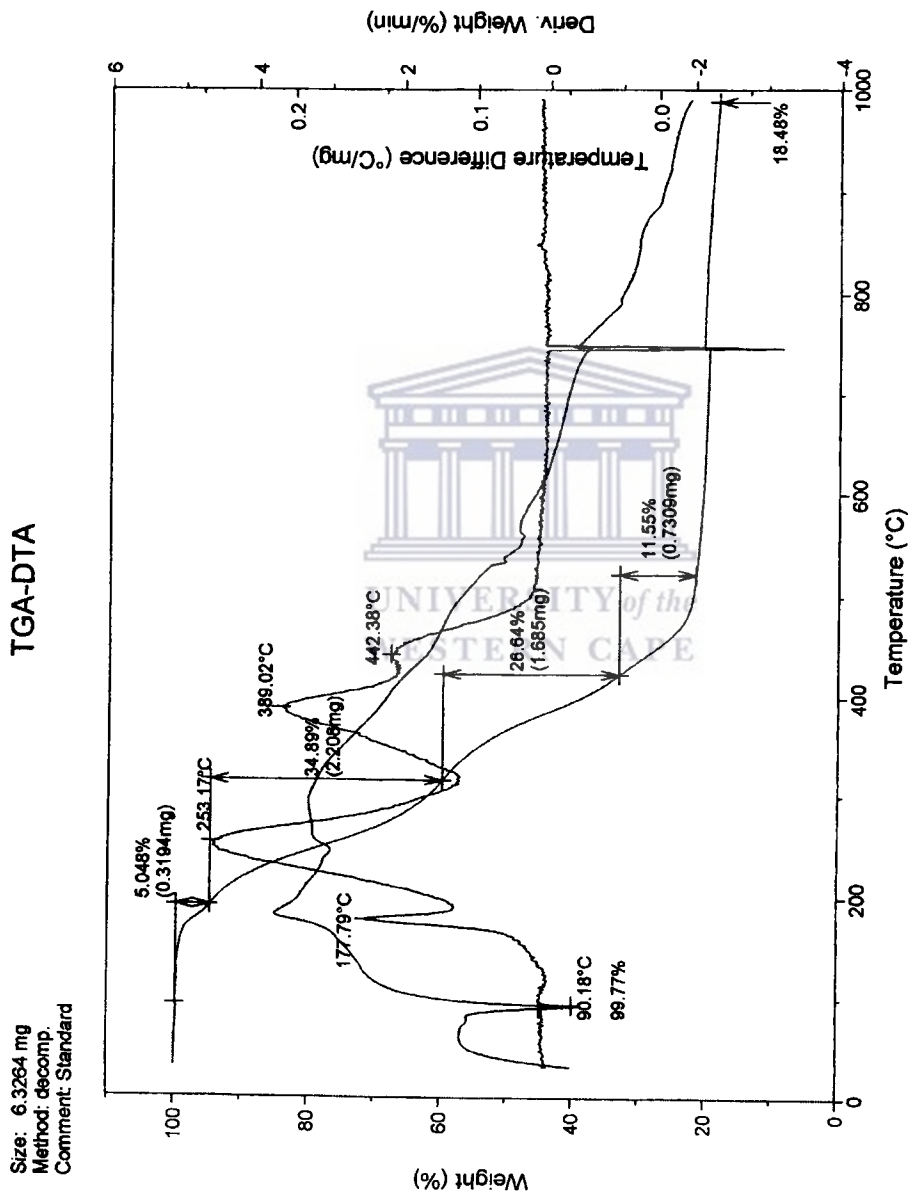


Figure 2.24: Thermograms for complex 6b.

2.7 Summary

All the compounds, both the thiol Schiff base ligands and the nickel complexes, were synthesised in moderate to high yields. Both the ligands and the nickel complexes are air stable for long periods under laboratory conditions. Their identity and purity were established by a combination of analytical techniques. In addition complexes **1a** and **3a** were analysed by single crystal X-ray diffraction studies. The two complexes, **1a** and **3a**, possessed a trigonal geometry around the nickel atom.

Liquid crystalline properties of the compounds were tested using thermal analysis and polarised optical microscopy. The thiol Schiff base compounds (**1** – **8**) and the nickel complexes did not show any multiple endotherms or exotherms on heating or cooling respectively and did not exhibit any birefringence under the polarised microscope, and are therefore not liquid crystalline. The modified Schiff base compounds, **10** and **11**, are mesogenic, with compound **11** exhibiting a smectic A mesophase. The lack of mesogenic behaviour in the thiol Schiff base compounds is attributed to hydrogen bond formation between the thiol hydrogen and the alkoxy oxygen. In the nickel complexes the lack of mesogenic behaviour is caused by the steric interactions caused by bulky lateral substituents, cyclopentadienyl ring and phosphines, which also reduce molecular anisotropy.

Thermal analysis shows that melting points of both the ligands and the nickel complexes depend on the length of the alkoxy chain. In the ligands there is a steady decrease with increasing chain length. The nickel complexes on the other hand show an initial decrease of melting point with increasing chain length, but this effect levels off when the chain length exceeds twelve carbons atoms.

Lastly complexes **1a** – **9a** and **1b** – **9b** followed different fragmentation pathways. This shows the effect of the donor ability of the phosphine on the bond strengths of atoms bound to the nickel centre, and hence the decomposition pathways.

The data reported in this chapter leads to the conclusion that for complexes of this nature to be mesogenic, it will require modifications in their design. One of these will be to remove the bulky phosphine groups and increase the overall length of the rigid core. The second one will be to replace the trigonal nickel centre geometry with a more planar square geometry. Both of these modifications have been attempted and are discussed in chapter 3.



References

1. G. H. Brown, W. G. Shaw, *Chem. Rev.* 1957, **57**, 1049;
2. (a) P. Espinet, *Gold Bull.* 1999, **32**, 127, (b) A. M. Giroud-Godquin, P. M. Maitlis, *Angew. Chem. Int. Ed. Engl.* 1991, **30**, 375; (c) J. N. Murrell, A. M. Boucher, *Properties of Liquids and Solutions*, Wiley and Sons, New York.
3. J. W. Goodby, G. W. Gray, *Handbook of Liquid Crystals*, VCH, Weinheim, 1999.
4. (a) D. Demus, *Mol. Cryst. Liq. Cryst.* 1988, **165**, 45; (b) D. Demus, *Mol. Cryst. Liq. Cryst.* 1989, **5**, 75.
5. (a) B. A. Gregg, M. A. Fox, A. J. Bard, *J. Chem. Soc. Chem. Commun.* 1987, 1134; (b) S. Kugimiya, M. Takemura, *Tetrahedron Lett.* 1990, **31**, 3157.
6. P. J. Collins, M. Hird, *Introduction to Liquid Crystals, Chemistry and Physics*, Taylor and Francis Publishers, Philadelphia, 1997.
7. P. H. J. Kowar, W. F. Jager, W. J. Mijs, S. J. Picken, *Macromolecules* 2000, **33**, 4336.
8. K. S. Goodman, R. P. Toake, *Pet. Rev.* 1984, **38**, 37.
9. J. D. Bernal, D. Crowfoot, *Trans. Faraday Soc.* 1933, **29**, 1032.
10. Z. Galweski, *Mol. Cryst. Liq. Cryst.* 1999, **79**, 77.
11. H. Kelker, B. Schuerler, R. Hatz, W. Bartsch, *Angew. Chem.* 1970, **82**, 99.
12. Z. Galweski, *Mol. Cryst. Liq. Cryst.* 1994, **249**, 43.
13. (a) D. Grasso, C. Gandolfo, S. Fasome, *Thermochim. Acta*, 1983, **70**, 99, (b) K. Murose, *Bull. Chem. Soc. Jpn.* 1972, 1772, J. van der Veen, W. H. de Jeu, A.-H. Grobber, J. Boven, *Mol. Cryst. Liq. Cryst.* 1972, **17**, 291.
14. K. El Guermai, M. Ayadi, K. Elboussiri, *Mater. Res. Bull.* 1999, **34**, 1243.
15. G. W. Gray, *Molecular Structures and Properties of Liquid Crystals*, Academic Press, New York, 1962.
16. J. van der Veen, W. H. de Jeu, M. W. M. Wanninkol, C. A. M. Tienhostein, *Mol. Cryst. Liq. Cryst.* 1976, **33**, 35.
17. (a) A. Skoulios, V. Luzzati, *Nature*, 1957, **183**, 11310; (b) C. Sirlin, L. Bosio, J. Simon, *J. Chem. Soc. Chem. Commun.* 1987, 393; (c) Z. Berarbi, C. Sirlin, J.

- Simon, J. Andre, *J. Phys. Chem.* 1989, **93**, 8105, (d) P. G. Schouten, J. M. Warman, M. P. de Hass, M. A. Fox, H.-L. Pan, *Nature* 1991, **353**, 736.
18. A. Omenat, M. Ghedini, *J. Chem. Soc. Chem. Commun.* 1994, 1309.
19. (a) S. A. Hudson, P. M. Maitlis, *Chem. Rev.* 1993, **93**, 861, (b) R. Deschenaux, J. W. Goodby (A. Togni, T. Hayashi (eds.)) in *Ferrocenes*, VCH, Weinheim, 1995, Chapter 9, p 491, (c) D. W. Bruce, X.-H. Liu, *J. Chem. Soc. Chem. Commun.* 1994, 729, (d) K. Praeckfe, B. Bilgin, N. Uslo'tseva, B. Heinrich, D. Gullion, *J. Mater. Chem.* 1995, **5**, 2257, (e) J. Buey, L. Diez, P. Espinet, H. S. Kitzerow, J. A. Miguel, *Chem. Mater.* 1996, **8**, 2375 (f) J. Ortega, C. L. Folcia, J. Extebarria, M. B. Ros, J. A. Miguel, *Liq. Cryst.* 1997, **23**, 285, (g) M. Ghedini, F. Neve, D. Pucci, *Eur. J. Inorg. Chem.* 1998, 501.
20. P. Espinet, M. A. Esteruellas, L. A. Oro, J. L. Serrano, E. Sola, *Coord. Chem. Rev.* 1992, **117**, 215.
21. (a) B. J. Coe, C. Jones, J. A. McCleverty, D. W. Bruce, *Polyhedron* 1993, **12**, 45.
22. C. Tschierske, *Angew. Chem. Int. Ed.* 2000, **39**, 2454.
23. M. Marcos, J. L. Serrano, T. Sierra, M. J. Giminez, *Angew. Chem. Int. Ed. Engl.* 1992, **31**, 4171.
24. B. Donnio, D. W. Bruce, *J. Mater. Chem.* 1998, **8**, 1993.
25. P. Espinet, J. Extebarria, M. Marcos, J. Perez, A. Remon, J. L. Serrano, *J. Am. Chem. Soc.* 1994, **116**, 1065.
26. M. J. Baena, J. Barbera, P. Espinet, A. Ezcurra, M. B. Ros, J. L. Serrano, *J. Am. Chem. Soc.* 1994, **116**, 1899.
27. (a) M. J. Baena, P. Espinet, M. B. Ros, J. L. Serrano, A. Ezcurra, *Angew. Chem. Int. Ed. Engl.* 1993, **32**, 1203, (b) N. Thompson, J. L. Serrano, M. J. Baena, P. Espinet, *Eur. J. Chem.* 1996, **2**, 116.
28. D. Bruins, D. L. Weaver, *Inorg. Chem.* 1970, **9**, 130.
29. M. Ghedini, D. Pucci, A. Crispini, G. Barberrio, *Organometallics*, 1998, **18**, 116.
30. (a) D. W. Bruce, E. Lalinde, P. Styring, D. A. Dunmur, P. M. Maitlis, *J. Chem. Soc. Chem. Commun.* 1986, 581; (b) P. M. Maitlis, D. W. Bruce, D. A. Dunmur, *Chem. Abstr.* 1987, **107**, 145375n.

31. H. Adams, N. A. Bailey, D. W. Bruce, D. A. Dunmur, E. Lalinde, M. Marcos, C. Ridgeway, A. J. Smith, P. Styring, P. M. Maitlis, *Liq. Cryst.* 1987, **2**, 381.
32. A. Omenat, J. L. Serrano, T. Sierra, D. B. Amabilino, M. Minguet, E. Ramos, J. Veciana, *J. Mater. Chem.* 1999, **9**, 2301.
33. I. Sage (G. W. Gray ed.) in *Thermotropic Liquid Crystals*, 1987, **22**, 64.
34. (a) J. P. Rourke, F. P. Fanazzi, N. J. S. Salt, D. W. Bruce, D. A. Dunmur, P. M. Maitlis, *J. Chem. Soc. Chem. Commun.* 1990, 229; (b) A. M. Giroud-Godquin, *Coord. Chem. Rev.* 1998, **178-180**, 1485.
35. (a) P. M. Maitlis, D. W. Bruce, R. Dhillon, D. A. Dunmur, F. P. Fanazzi, S. E. Hunt, R. le Legadec, E. Lalinde, R. Orr, J. P. Rourke, N. J. S. Salt, J. P. Atacey, P. Styring, *New J. Chem.* 1990, **14**, 549; (b) H. Adams, N. A. Bailey, D. W. Bruce, R. Dhillon, D. A. Dunmur, S. E. Hunt, E. Lalinde, A. A. Maggs, R. Orr, P. Styring, M. S. Wragg, P. M. Maitlis, *Polyhedron* 1988, **7**, 1861.
36. (a) M. A. Esteruelas, L. A. Oro, E. Sola, M. B. Ros, J. L. Serrano, *J. Chem. Soc. Chem. Commun.* 1989, 55; (b) M. A. Esteruelas, E. Sola, L. A. Oro, M. B. Ros, M. Marcos, J. L. Serrano, *J. Organomet. Chem.* 1990, **387**, 103.
37. (a) D. W. Bruce, D. A. Dunmur, P. M. Maitlis, P. Styring, M. A. Esteruelas, L. A. Oro, M. B. Ros, J. L. Serrano, E. Sola, *Chem. Mater.* 1989, **1**, 479; (b) D. W. Bruce, D. A. Dunmur, S. A. Hudson, P. M. Maitlis, P. Styring, *Adv. Mater. for Optics and Electronics*, 1992, **1**, 37.
38. (a) K. Binnemans, Y. G. Galyametdinov, S. R. Collinson, D. W. Bruce, *J. Mater. Chem.* 1998, **8**, 1551; (b) C. K. Lai, C.-H. Chang, C.-H. Tsai, *J. Mater. Chem.* 1998, **8**, 599.
39. E. Scamporrino, D. Vittalani, P. Mineo, *Macromolecules* 1999, **32**, 4247.
40. B. Bilgin-Eran, C. Yorur, S. Uzman, *J. Organomet. Chem.* 2002, **655**, 105.
41. Z. Li, C. Ning, S. Zhang, S. Cao, D. Zhang, Q.-F. Zhou, *Macromolecules* 1999, **32**, 7040.
42. (a) X. Yang, C. Stern, J. J. Marks, *J. Am. Chem. Soc.* 1994, **116**, 10015; (b) A. G. Lightenbarg, E. K. van den Beuken, A. Meetsma, N. Veldman, W. J. J. Smeets, A. L. Spek, B. Feringa, *J. Chem. Soc. Dalton Trans.* 1998, 268.

43. (a) F. A. Nevondo, A. M. Crouch, J. Darkwa, *J. Chem. Soc. Dalton Trans.* 2000, 43, (b) A. Houlton, J. Silver, D. Cunningham, *J. Chem. Soc. Dalton Trans.* 1992, 2235.
44. R. H. Blessing, *J. Appl. Crystallogr.* 1997, **30**, 421.
45. B. V. Nonius, *COLLECT Data Collection Software*, 1998.
46. Z. Otwenowski, W. Minor, (C. W. Carter, R. M. Sweet (eds.)) in: *Methods in Enzymology*, Academic Press, New York, 1997, **276**, 307.
47. G. M. Sheldrick, *SHELXL97*, Program for the refinement of crystal structures, University of Gottingen, Gottingen, Germany, 1997.
48. A. L. Spek, *PLATON: A program for Plotting Molecular and Crystal Structures*, University of Utrecht, The Netherlands, 1995.
49. B. Bilgin-Eran, *J. Organomet. Chem.* 2002, **655**, 105.
50. R. M. Moutloali, T. Nyokong, J. Darkwa, *J. Organomet. Chem.* 1998, **564**, 37.
51. C.-M. Leu, C.-F. Shu, C.-F. Teng, J. Shiea, *Polymer*, 2001, **42**, 2339.
52. R. M. Moutloali, J. Bacsá, W. A. Ddamba, J. Darkwa, *J. Organomet. Chem.* 2001, **629**, 17.
53. L. Jongen, K. Binnemanns, D. Hinz, G. Meyer, *Mat. Sci. and Eng.* 2001, **C18**, 199.
54. D. W. Bruce, D. A. Dunmur, E. Lalinde, P. M. Maitlis, P. Styring, *Nature* 1986, **323**, 791.
55. K. J. Toune, (G. W. Gray ed.) *Thermotropic Liquid Crystals*, Wiley, Chichester, 1987.
56. G. W. Gray, K. J. Harrison, J. A. Nash, *Electron Lett.* 1973, **9**, 130.
57. R. I. Nessim, *Thermochim. Acta*, 2002, **389**, 49.
58. (a) C. J. Lee, S. J. Lee, J. Y. Chang, *Tetrahedron Lett.* 2002, **43**, 3863, (b) C. Tschierske, *Curr. Opin. Colloid Interface Sci.* 2002, **7**, 355.
59. M. Lee, Y.-S. Yoo, M. G. Choi, H.-Y. Chang, *J. Mater. Chem.* 1998, **8**, 277.
60. P. Espinet, *Gold Bulletin* 1999, **32**, 127
61. J. Darkwa, F. Bothata, L. M. Koczón, *J. Organomet. Chem.* 1993, **455**, 235.
62. M. Sato, T. Yoshida, *J. Organomet. Chem.* 1973, **51**, 231.
63. J. Darkwa, W. Milius, *Acta Cryst.* 1996, **C52**, 2159.

64. (a) C. A. Tolman, *Chem. Rev.* 1977, **77**, 183; (b) R. Masson, D. W. Meek, *Angew. Chem. Int. Ed.* 1978, **17**, 183.
65. J. Darkwa, F. Bothata, *J. Organomet. Chem.* 1993, **455**, 235.
66. S. Ide, G. Oztaz, N. Ancin, M. Tuzun, *Acta. Cryst.* 1997, **C53**, 376.
67. J. Darkwa, *Organometallics* 1994, **13**, 4734.
68. D. J. Williams, *Angew. Chem. Int. Ed. Engl.* 1984, **23**, 690.
69. (a) R. Deschenaux, J. Santiago, *Tetrahedron Lett.* 1994, **35**, 2169, (b) R. Deschenaux, J.-I. Marende, J. Santiago, *Helvetica Chim. Acta*, 1993, **76**, 865, (c) Y. G. Galyametdinov, O. N. Kadkin, I. V. Ovchinnikov, *Izv. Akad. Nauk. Ser. Kim.* (Russia) 1992, **2**, 402.
70. S. Takahashi, Y. Takai, H. Morimoto, K. Sonogashira, *J. Chem. Soc. Chem. Commun.* 1994, 3.
71. M. Ghedini, D. Pucci, A. Crispini, G. Barberio, *Organometallics*, 1999, **18**, 2116.
72. R. Deschenaux, J. W. Goodby (A. Togni, T. Hayashi eds.) in *Ferrocenes*, VCH, Weinheim, Chapter 9, p 471.
73. S. Coco, P. Espinet, J. M. Martin-Alvarez, A. M. Levelut, *J. Mater. Chem.* 1997, **7**, 19.
74. S. Coco, P. Espinet, E. Marcos, *J. Mater. Chem.* 2000, **10**, 1297.
75. J. L. Serrano, *Metallomesogens, Synthesis, Properties and Applications*, VCH, Weinheim, 1996.
76. S. Song, E. C. Alyea, *Inorg. Chem.* 1986, **18**, 145.

Chapter 3

Synthesis of nickel(II) μ_2 -thiolato Schiff base complexes and pincer nickel and palladium thiolato Schiff base complexes. Spectroscopic and thermal analytical studies.

3.1 Introduction	96
3.2 Experimental section	102
3.2.1. Materials and instrumentation.	102
3.2.2. Synthesis of starting pincer metal precursors.	103
3.2.3. Synthesis of cyclopentadienylnickel(II) thiolato Schiff base complexes.	104
3.2.4. Synthesis of diethyldithiocarbamatonicel(II) thiolato Schiff base complexes.	106
3.2.5. Synthesis of metal pincer thiolato Schiff base complexes.	108
3.3 Results and discussion.	111
3.3.1. Synthesis of pincer metal complexes precursors.	111
3.3.2. X-ray structure of complex II.	112
3.3.3. Synthesis and spectroscopic characterisation of complexes 1 – 4.	115
3.3.4. Synthesis and spectroscopic characterisation of complexes 5 – 10.	120
3.3.5 Synthesis and spectroscopic characterisation of complexes 11 - 16.	122
3.4. MALDI-TOF mass spectrometry studies of selected complexes.	126
3.5 Electrochemistry of selected sulfur bridged nickel complexes.	130
3.5.1. Cyclic voltammetry studies of selected cyclopentadienylnickel(II) complexes.	130
3.5.2. Cyclic voltammetry study of diethyldithiocarbamatonicel(II) complexes.	134
3.6 Probing mesogenic properties of representative complexes.	136
3.6.1. Thermal studies of cyclopentadienylnickel(II) complexes.	136
3.6.2. Optical polarised microscopy studies of cyclopentadienyl-	

nickel(II) complexes.	140
3.6.3. Thermal analysis of complexes 12 , 15 , and 16 and optical microscope studies of 12 .	143
3.7 Summary.	149

3.1 Introduction

3.1.1 Metal thiolates in biochemistry

The chemistry of metal thiolates, specifically nickel thiolate complexes, has attracted attention partly due to the identification of nickel in the active site of the hydrogenase enzyme.¹ Hydrogenase is the metalloenzyme that catalyses the reversible two electron oxidation of dihydrogen. It contains iron, nickel and sulfur in the most common class² and iron, nickel and selenium in another class³. Considerable attention has been focused on the synthesis of model compounds of these metalloenzymes in an effort to understand the chemistry involved in the reaction of hydrogenases. This has resulted in the isolation of a number of nickel thiolato complexes. The isolated complexes range from simple monometallic thiolate complexes to high nuclearity complexes.

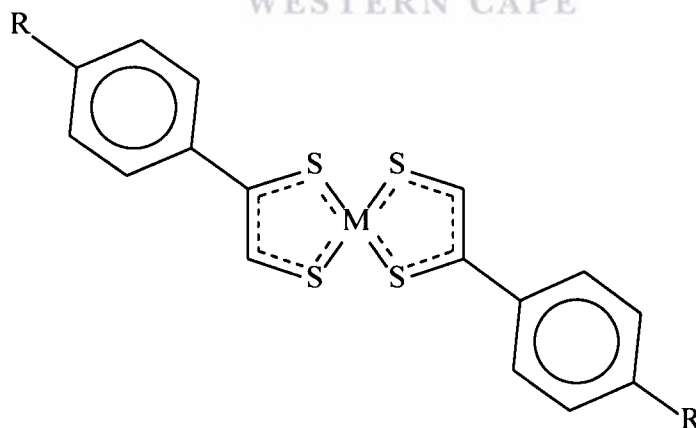
3.1.2 Electronic and steric influence of thiolates on their binding modes.

The nuclearity of nickel thiolate complexes appears to be highly dependent on the electron density at the nickel centre.⁴ The most common of these complexes are the mono- and the binuclear complexes. The presence of other ancillary ligands at the nickel centre that influence the electron density at the nickel atom have been found to affect the eventual structures of these sulfur complexes.⁴ Discrete thiolato complexes are predominant for thiolato ligands which contain electron withdrawing groups that decrease electron density on the sulfur atom.⁵ The role electron density plays in complex formation is amply illustrated by $[\text{Ni}(\text{dtc})(\mu_2\text{-SR})_2]$ (dtc = diethyldithiocarbamate; R = CH₂CH₃, C(CH₃)₃, C₆H₅, C₆H₄CH₃-4)⁶ and $[\text{Ni}(\text{S}_2\text{CSR}')(\mu_2\text{-SR}')_2]$ (R' = CH₂CH₃, CH₂C₆H₅).⁷ High electron density on the sulfur containing ligands leads to the formation of dative bonds with the second nickel atom resulting in dimer formation. This is further corroborated by the fact that by replacing sulfur with selenium results in the formation of

monomeric or dimeric complexes depending on the organic fragment attached to the selenium atom. For instance, aryl selenides form mononuclear complexes $\text{Ni}(\text{dtc})(\text{PPh}_3)(\text{SeR})$ ($\text{R} = \text{C}_6\text{H}_5, \text{C}_6\text{H}_4\text{Cl-4}$)⁵ whilst alkyl selenides form dimeric complexes $[\text{Ni}(\text{dtc})(\mu_2\text{-SeR}')_2]$ ($\text{R}' = \text{CH}_3, \text{CH}_2\text{C}_6\text{H}_5$).⁵ The steric bulkiness of the ligands also influence the formation of monomers. This is illustrated by the aggregation of nickel selenolates complexes, where the less bulky $\text{C}_6\text{H}_5\text{Se}$ forms $[\text{Ni}(\text{terpy})(\text{SeC}_6\text{H}_5)]_2$ ⁸ but the more bulky $2,4,6\text{-}(\text{Me})_3\text{C}_6\text{H}_2\text{Se}$ forms a mononuclear complex, $[\text{Ni}(\text{terpy})(2,4,6\text{-}(\text{Me})_3\text{C}_6\text{H}_3\text{Se})_2]$.⁸

3.1.3 Metal thiolates as liquid crystalline materials.

In addition to being studied as biological models, metal-thiolates are of interest in material science, specifically as liquid crystalline materials. The first report on covalent liquid crystalline coordination complexes appeared in 1977, when Giroud *et al.* described the mesomorphic properties of several nickel(II) and palladium(II) dithiolene derivatives A.⁹




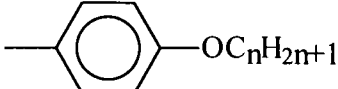
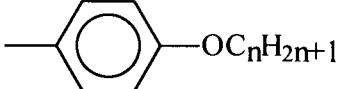
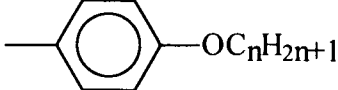
M = Ni, Pd and Pt

A

Subsequent studies of dithiolene complexes as liquid crystals centred on three metals, namely nickel, palladium and platinum. Ohta and co-workers employed alkoxythiocarboxylate (xanthate) as ligands to form nickel(II) complexes that exhibited

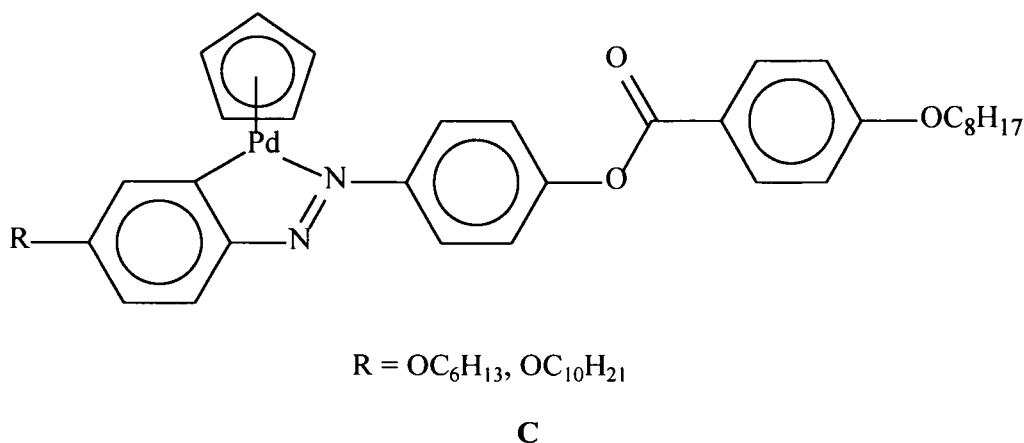
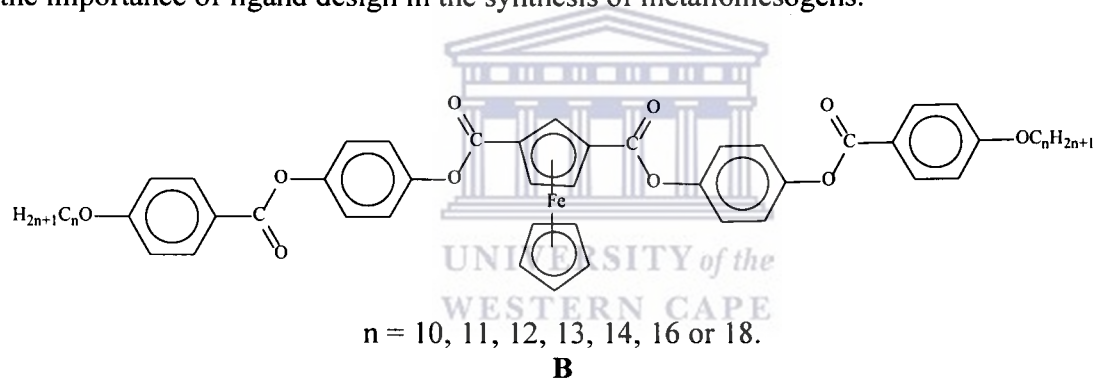
monotropic smectic phases.¹⁰ When a *para*-substituted thiobenzoate is used as a ligand, enantiotropic S_H and S_c mesophases are observed for $n = 8$.¹¹ Dithiocarbamate complexes derived from piperazines, when complexed with nickel, palladium and copper were shown to exhibit smectic and nematic mesophases (Table 3.1). Nematic mesophases are found when Y is an alkyl chain but for the more rigid alkoxyphenyl ligands the mesophase changes to smectic.¹² This observation alludes to the importance of rigid versus flexible groups in leading to more ordered mesophases for sulfur containing metallomesogens. The longer the rigid core, the more ordered the mesophases that are formed. For instance as the the rigid core is lengthened, the mesophases that is formed tend to be smectic as opposed to nematic for more flexible or shorter rigid core.

Table 3.1: Mesogenic properties of some Pd, Ni an Cu complexes.

			Mesomorphic properties			
Y	M	K	Sc	N	I	
-C ₆ H ₁₃	Pd	• 232		• 252	•	
-C ₈ H ₁₇	Pd	• 209		• 237	•	
	Pd	• 259	• 330		• (dec)	
	Ni	• 254	• 334		• (dec)	
	Cu	• 230	• 247		• (dec)	

3.1.4 Metallomesogens with cyclopentadienyl lateral groups.

Metallomesogens that have metal-ligands π -bonds are mostly dominated by ferrocene derivatives **B**.¹³ The other non-ferrocene cyclopentadienyl complex was reported by Ghedini *et. al.* and is derived from a cyclopalladated complex **C**.¹⁴ From these studies it was found that with the presence of the cyclopentadienyl ligand, mesogenic behaviour is only observed when the number of phenyl rings in the rigid part of the molecule is at least three. When the number of phenyl rings is two, the mesogenic behaviour of the ligands is lost in the metal complex. It could thus be concluded from this study that large lateral substituents could only be tolerated when the length of the promesogenic core is increased. Thus incorporation of metal fragments with large ancillary ligands have led to the loss of mesogenic properties of mesomorphic organic compounds.¹⁵ This underscores the importance of ligand design in the synthesis of metallomesogens.

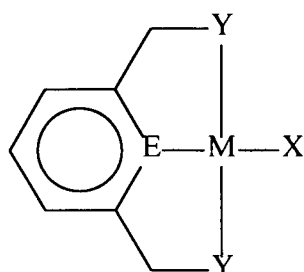


In the current study that is reported in the thesis, the knowledge that $(\eta^5\text{-C}_5\text{H}_5)\text{Ni}$ and $(\text{dtc})\text{Ni}$ fragments form stable μ_2 -sulfur bridged organometallic complexes was used to synthesise 1-thiolato Schiff base complexes incorporating these two nickel fragments.

These types of complexes feature a planar Ni_2S_2 ring with the thiol ligands *trans* to each other with a C_2 symmetry. Thus the metallocyclic core together with the *trans* ligands affords a bent rod-shaped geometry. It was envisaged that by increasing the number of phenyl rings in the thiol ligands and modifying them with long alkoxy chains, complexes with liquid crystalline behaviour would result. In this way the bulkiness associated with the cyclopentadienyl or dithiocarbamate ligands could be masked and thus would not have an adverse effect on the mesogenic properties of the complexes. With the above design features in mind, a series of complexes, with generic formulae $[(\eta^5\text{-C}_5\text{H}_5)\text{Ni}(\mu\text{-SC}_6\text{H}_4\text{NC}(\text{H})\text{C}_6\text{H}_4\text{OC}_n\text{H}_{2n+1})]_2$ ($n = 4, 6, 14, 16$) and $[(\text{dtc})\text{Ni}(\mu\text{-SC}_6\text{H}_4\text{NC}(\text{H})\text{C}_6\text{H}_4\text{OC}_n\text{H}_{2n+1})]_2$ ($n = 4, 6, 10, 14, 16, 20$), were synthesised and their mesogenic and electronic properties evaluated.

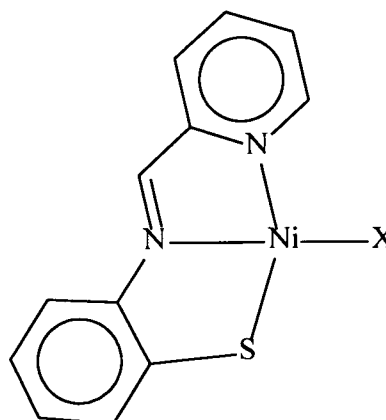
3.1.5 Pincer type complexes as potential mesogens.

In another modification of the geometry of the complexes we have introduced a more planar geometry around the metal centre, nickel and palladium. The geometry is based on the so-called pincer metal fragments. In pincer complexes the metal is constrained between three atoms imposing a *trans* disposition for the Y groups relative to the metal atom. Pincer metal fragments have been used mostly for catalytic purposes. For example, complexes of the type shown in **1** and **2**, which have a metal bound by a ligand in a tridentate fashion through the central carbon of the benzene (or the heteroatom of the heterocyclic ring) and the two donor atoms of group Y, have been extensively studied¹ as catalysts for catalytic dehydrogenation of alkanes¹⁶, ethers¹⁷, alkyarenes¹⁸, as Lewis acid catalysts and aldol reactions between benzaldehydes and methyl isocyanoacetate¹⁹.



M = Ni, Pd or Pt; E = C or N, X = halide
Y = NR₂, SR or PR₂ (R = alkyl or aryl)

1

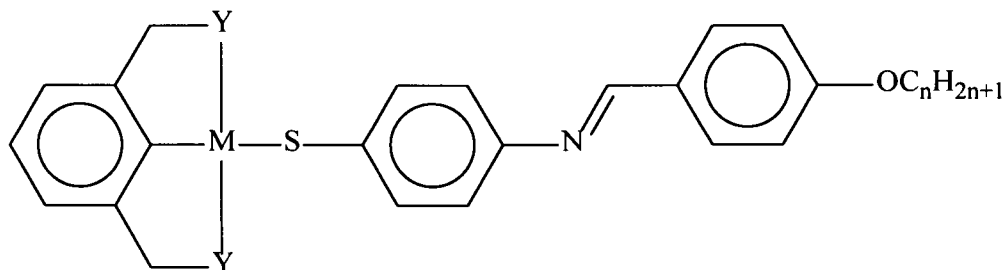


X = halide

2

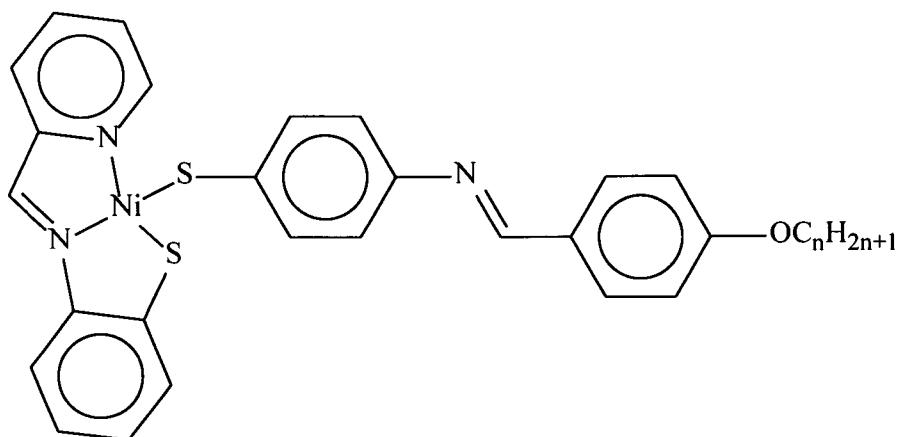
Moreover, the tridentate nature results in the rigid coordination that is planar, which when conveniently modified, it should eventually produce metal containing liquid crystals. These molecular designs could also be tuned for use, not only as liquid crystals, but also in the field of nonlinear optics. This is because a metal in such a square planar coordination should give rise to structures (1) which have a net dipolar moment in the direction of the E-M-X bonds.²⁰ This, plus the anisotropic shape of the structure could result in the induction of interesting and unusual electronic properties.

Our interest here was to use this planar rigid pincer complex as part of the rigid backbone that would result in the formation of calamitic liquid crystals. In pursuit of this idea a series of complexes with generic structural types **D** and **E** shown below were synthesised.



M = Pd, Y = NEt₂ or SⁱPr

D

**E**

Chapter 3 therefore deals with the modifications of complexes in Chapter 2 to include the pincer fragment described above. These are (i) increasing the effective molecular length of the complexes and thus the molecular anisotropy and (ii) replacing the trigonal geometry about the metal with a more planar geometry. These two molecular designs generally lead to the formation of mesophases.

UNIVERSITY of the
WESTERN CAPE

3.2 Experimental Section

3.2.1 Materials and Instrumentation

All reactions were performed using standard Schlenk techniques under dinitrogen atmosphere but their work-up was done in air. Reagent grade hexane and toluene were distilled from sodium and stored over activated molecular sieves. All commercially available chemicals were used as received. The starting materials were prepared by literature methods. Nickelocene²¹, Ni(dtc)(PR₃)Br²² (R = Ph or Bu) and [Ni(η⁵-C₅H₅)(SC₆H₄NH₂-4)]₂²³, the pincer complex precursors 1,3-bis(disubstituted aminomethyl)benzene²⁴ and 1,3-bis(disubstituted thiomethyl)benzene²⁵ were prepared by the method of van Koten *et al.* and Venanzi *et al.* Compound 2-(2-pyridyl)benzothiazoline was synthesised following the method of Lindoy *et al.*²⁶. The Schiff base compounds were synthesised by procedures described in chapter 2 and

elsewhere.²⁷ The nickel and palladium complexes were characterised by NMR spectroscopy on a Varian Gemini 2000 spectrometer at 200 MHz and referenced to residual CHCl_3 at δ 7.26, mass spectrometry was performed on a Perseptive Biosystems-Voyager-DE STR mass spectrometer equipped with a nitrogen laser (337 nm) and operating in reflector mode with accelerating voltage of 20 kV per sample, thermal analysis were obtained on a Universal V2.3H TA instrument and elemental analysis was done on a CARLO ERBA NA instrument. Electrochemical measurements were recorded on a Bioanalytical systems BAS 50W using a three electrode cell configuration.

3.2.2 Synthesis of starting pincer metal precursor materials.

Synthesis of 1,3- $\text{C}_6\text{H}_3(\text{CH}_2\text{NEt}_2)_2\text{PdBr}$ (I)

1,3- $\text{C}_6\text{H}_4(\text{CH}_2\text{NEt}_2)_2$ (2 g, 8.12 mmol) was suspended in hexane (60 mL) and charged with excess $^t\text{BuLi}$ (9 mL, 12.2 mmol) at room temperature. The milky solution turned pink and was stirred for 4 h. To this was added $\text{Pd}(\text{COD})\text{Br}_2$ (1.4 g, 4.9 mmol) suspended in toluene (30 mL). The solution was stirred overnight in which time it turned black. The solvent was removed and the residue extracted with CH_2Cl_2 and then passed through celite to give an orange filtrate. The filtrate was concentrated and hexane added and cooled at -15°C to give an orange solid. Yield = 0.43 g, 21%. Anal. Calcd for $\text{C}_{16}\text{H}_{28}\text{N}_2\text{PdBr}$: C, 44.20; H, 6.49. Found: C, 44.30; H, 6.44%. ^1H NMR (CDCl_3): δ 6.92 (t, 1H, $J_{\text{HH}} = 7.8$ Hz, C_6H_3), 6.68 (d, 2H, $J_{\text{HH}} = 7.8$ Hz, C_6H_3), 4.03 (s, 4H, CH_2), 3.47 (m, 4H, $J_{\text{HH}} = 7.2$ Hz, CH), 2.68 (m, 4H, $J_{\text{HH}} = 7.0$ Hz, CH), 1.61 (t, 12H, $J_{\text{HH}} = 7.0$ Hz, CH_3).

Alternate route to I. 1,3- $(\text{Et}_2\text{NCH}_2)_2\text{C}_6\text{H}_4$ (1 mL, 3.06 mmol) was dissolved in ethanol (40 mL). To the ethanol solution was added $\text{Pd}(\text{OAc})_2$ (0.7 g, 3.10 mmol) and the reaction mixture stirred for 5 h at room temperature. The initial red colour turned black. Excess sodium bromide (1.0 g) was added and the mixture changed to a greenish colour immediately. The reaction was left for 18 h after which the solvent was removed *in vacuo* to leave a black residue. The residue was extracted with a 1:1 mixture of CH_2Cl_2 : H_2O (50 mL) and the organic layer was separated and filtered through celite and then dried

over MgSO_4 . The solvent was removed to leave an orange solid. Yield = 0.43 g, (35%). Anal. Calcd for $\text{C}_{16}\text{H}_{28}\text{N}_2\text{PdBr}$: C, 49.24; H, 7.23. Found: C, 49.69; H, 7.70%. ^1H NMR (CDCl_3): δ 6.92 (t, 1H, $J_{\text{HH}} = 7.8$ Hz, C_6H_3), 6.68 (d, 2H, $J_{\text{HH}} = 7.8$ Hz, C_6H_3), 4.03 (s, 4H, CH_2), 3.47 (m, 4H, $J_{\text{HH}} = 7.2$ Hz, CH), 2.68 (m, 4H, $J_{\text{HH}} = 7.0$ Hz, CH), 1.61 (t, 12H, $J_{\text{HH}} = 7.0$ Hz, CH_3).

Synthesis of 1,3- $\text{C}_6\text{H}_3(\text{CH}_2\text{S}^i\text{Pr})_2\text{PdBr}$ (II)

Palladium acetate (0.5 g, 2.23 mmol) was dissolved in glacial acetic (40 mL), charged with 1,3- $\text{C}_6\text{H}_4(\text{CH}_2\text{S}^i\text{Pr})_2$ (0.71 mL, 2.23 mmol) and the mixture refluxed for 0.5 h. To this was added LiBr (0.5 g, 12.2 mmol) and the reaction stirred at room temperature for 1 h. The solvent was removed and the residue extracted with CH_2Cl_2 and passed through a plug of silica gel (7 cm). The plug of silica was subsequently washed with copious amount of CH_2Cl_2 . Solvent was removed from the combined CH_2Cl_2 fractions to leave an orange solid with a yield of 0.83 g (94%). Anal. Calcd for $\text{C}_{14}\text{H}_{22}\text{S}_2\text{PdBr}$: C, 38.15; H, 5.03. Found C, 38.22; H, 5.12%. ^1H NMR (CDCl_3): δ 6.97 (s, 3H, C_6H_3), 4.20 (s, 4H, CH_2), 3.64 (q, 2H, $J_{\text{HH}} = 6.8$ Hz, ^iPr), 1.58 (d, 12H, $J_{\text{HH}} = 6.8$ Hz, ^iPr).

Synthesis of 1,6- $\text{C}_6\text{H}_4\text{S}(\text{N}=\text{CH})(\text{C}_5\text{H}_4\text{N})\text{NiCl}$ (III)

A solution of Nickel chloride hexahydrate (0.44 g, 1.85 mmol) in was slowly added via a pressure equalizing dropping funnel to a refluxing ethanol solution of 2-(2-pyridyl)benzothiazoline (0.4 g, 1.85 mmol). The yellowish-green solution turned brownish-red with a brown-red precipitate forming within 30 min. The reaction was left for 3 h. The mixture was cooled and then filtered to leave a brown-red insoluble solid. The yield was 0.47 g (83%). Anal. Calcd for $\text{C}_{10}\text{H}_9\text{N}_2\text{SNiCl}$: C, 42.38; H, 3.20; N, 9.88. Found C, 42.44; H, 3.08; N, 10.11%.

3.2.3 Synthesis of $[\eta^5\text{-C}_5\text{H}_5)\text{Ni}(\mu\text{-SC}_6\text{H}_4\text{-4-NC(H)C}_6\text{H}_4\text{-4-OC}_n\text{H}_{2n+1})]_2$. (n = 4, 6, 14, 16)

Synthesis of $[(\eta^5\text{-C}_5\text{H}_5)\text{Ni}(\mu\text{-SC}_6\text{H}_4\text{NC}(\text{H})\text{C}_6\text{H}_4\text{OC}_{16}\text{H}_{33})]_2$. (12)

In a typical reaction, which represents how this series of compounds were prepared, toluene (50 mL) was added to a mixture of nickelocene (0.11 g, 0.60 mmol) and $\text{HSC}_6\text{H}_4\text{NC}(\text{H})\text{C}_6\text{H}_4\text{OC}_{16}\text{H}_{33}$ (0.27 g, 0.60 mmol) to give a green solution which gradually changed to brown-black within 1h. The reaction mixture was allowed to stir for 18 h at room temperature. After filtration the solvent was removed *in vacuo* to leave a black residue that was recrystallised from CH_2Cl_2 /hexane solution at -15°C to yield the product in 35% (0.08g). Anal. Calcd for $\text{C}_{68}\text{H}_{94}\text{N}_2\text{S}_2\text{Ni}_2$: C, 72.84; H, 8.22; N, 2.43. Found: C, 72.01; H, 8.48; N, 2.48%. ^1H NMR (CDCl_3): δ 8.40 (s, 2H, C(H)N), 8.08 (d, 4H, $J_{\text{HH}} = 8.6$ Hz, C(H) C_6H_4), 7.83 (d, 4H, $J_{\text{HH}} = 8.4$ Hz, NC_6H_4), 7.05 (d, 4H, $J_{\text{HH}} = 8.4$ Hz, OC_6H_4), 6.97 (d, 4H, $J_{\text{HH}} = 8.8$ Hz, SC_6H_4), 4.63 (s, 10H, C_5H_5), 4.03 (t, 4H, $J_{\text{HH}} = 6.6$ Hz, OCH_2), 1.80 (q, 4H, $J_{\text{HH}} = 7.8$ Hz, OCH_2CH_2), 1.26 (br s, 26H, $\text{OC}_{16}\text{H}_{33}$), 0.88 (t, 6H, CH_3).

An alternate route for the syntheses of these complexes is as described for 2.

Synthesis of $[(\eta^5\text{-C}_5\text{H}_5)\text{Ni}(\mu\text{-SC}_6\text{H}_4\text{NC}(\text{H})\text{C}_6\text{H}_4\text{OC}_{14}\text{H}_{29})]_2$. (13)

A mixture of anhydrous MgSO_4 (2g), $[(\eta^5\text{-C}_5\text{H}_5)\text{Ni}((\mu\text{-SC}_6\text{H}_4\text{NH}_2\text{-4})]_2$ (0.50g, 1.01 mmol) and *p*- $\text{OHCC}_6\text{H}_4\text{OC}_{14}\text{H}_{29}$ (0.30g, 1.13 mmol) was charged with toluene and stirred for 18h. The brown mixture was filtered and the filtrate evaporated to dryness. The residue was recrystallised from CH_2Cl_2 and hexane at -15°C to afford a brown-greenish solid in a yield of 45%. Anal. Calcd for $\text{C}_{66}\text{H}_{90}\text{N}_2\text{S}_2\text{Ni}_2$: C, 72.08; H, 8.30; N, 2.56. Found: C, 72.15; H, 8.73; N, 2.61%. ^1H NMR (CDCl_3): δ 8.40 (s, 2H, C(H)N), 8.08 (d, 4H, $J_{\text{HH}} = 8.4$ Hz, C(H) C_6H_4), 7.84 (d, 4H, $J_{\text{HH}} = 8.8$ Hz, NC_6H_4), 7.06 (d, 4H, $J_{\text{HH}} = 8.4$ Hz, OC_6H_4), 6.98 (d, 4H, $J_{\text{HH}} = 8.8$ Hz, SC_6H_4), 4.62 (s, 10H, C_5H_5), 4.03 (t, 4H, $J_{\text{HH}} = 6.2$ Hz, OCH_2), 1.82 (q, 4H, $J_{\text{HH}} = 7.4$ Hz, OCH_2CH_2), 1.27 (br s, 22H, $\text{OC}_{14}\text{H}_{29}$), 0.89 (t, 6H, $J_{\text{HH}} = 5.4$ Hz, CH_3). $^{13}\text{C}\{^1\text{H}\}$ NMR (CDCl_3) δ : 161.98, 159.37, 150.52, 135.68, 134.30, 130.52, 130.04, 129.06, 121.66, 120.67, 114.75, 93.79, 68.27, 31.92, 29.65, 29.58, 29.35, 29.20, 26.02, 22.068, 14.09.

Synthesis of $[(\eta^5-C_5H_5)Ni(\mu-SC_6H_4NC(H)C_6H_4OC_6H_{13})]_2 \cdot CH_2Cl_2$ (14)

A brown solid with a yield of 50% was obtained. Anal. Calcd for $C_{48}H_{52}N_2S_2Ni_2 \cdot CH_2Cl_2$: C, 63.67; H, 6.06; N, 3.06. Found: C, 63.50; H, 5.98; N, 3.38%. 1H NMR ($CDCl_3$): δ 8.40 (s, 2H, C(H)N), 8.08 (d, 4H, $J_{HH} = 8.0$ Hz, C(H) C_6H_4), 7.86 (d, 4H, $J_{HH} = 8.2$ Hz, NC_6H_4), 7.05 (d, 4H, $J_{HH} = 8.0$ Hz, OC_6H_4), 6.98 (d, 4H, $J_{HH} = 8.4$ Hz, SC_6H_4), 4.63 (s, 10H, C_5H_5), 4.03 (t, 4H, $J_{HH} = 5.8$ Hz, OCH_2), 1.82 (q, 4H, $J_{HH} = 6.0$ Hz, OCH_2CH_2), 1.57-1.27 (m, 12H, OC_6H_{13}), 0.92 (t, 6H, CH_3).

Synthesis of $[\eta^5-C_5H_5)Ni(\mu-SC_6H_4NC(H)C_6H_4OC_4H_9)]_2$ (15)

A brown solid with a yield of 55% was obtained. Anal. Calcd for $C_{44}H_{46}N_2S_2Ni_2$: C, 67.38; H, 5.91; N, 3.57. Found: C, 67.05; H, 5.87; N, 3.44%. 1H NMR ($CDCl_3$): δ 8.40 (s, 2H, C(H)N), 8.08 (d, 4H, $J_{HH} = 8.8$ Hz, C(H) C_6H_4), 7.84 (d, 4H, $J_{HH} = 8.4$ Hz, NC_6H_4), 7.05 (d, 4H, $J_{HH} = 8.2$ Hz, OC_6H_4), 6.98 (d, 4H, $J_{HH} = 8.4$ Hz, SC_6H_4), 4.63 (s, 10H, C_5H_5), 4.04 (t, 4H, $J_{HH} = 6.4$ Hz, OCH_2), 1.82 (q, 4H, $J_{HH} = 6.0$ Hz, OCH_2CH_2), 1.54-1.27 (m, 4H, $OCH_2CH_2CH_2$), 0.92 (t, 6H, $J_{HH} = 7.2$ Hz, CH_3).

3.2.4 Synthesis of $[(dte)Ni(\mu_2-SC_6H_4NC(H)C_6H_4OC_nH_{2n+1})]_2$ (n = 4, 6, 10, 14, 16, 20)

$[(dte)Ni(\mu_2-SC_6H_4NC(H)C_6H_4OC_{20}H_{41})]_2$ (16)

In a typical reaction $Ni(dte)(PBU_3)Br$ or $Ni(dte)(PPh_3)Br$ (0.5 mmol) and $HSC_6H_4-4-NC(H)C_6H_4-4-OC_{20}H_{41}$ (0.5 mmol) were dissolved in toluene to give a maroon solution. When excess Et_3N (3 mL) was added the colour gradually turned dark green. The reaction was stirred at room temperature for 18 h. An off white solid was removed on filtration to give a green filtrate, from which the solvent was removed to leave a brownish green residue. This was recrystallised from CH_2Cl_2 and hexane at $-15^\circ C$ to give a green solid in a yield of 83%. Anal. Calcd for $C_{76}H_{120}N_4O_2S_6Ni_2$: C, 63.76; H, 8.45; N, 3.91. Found: C, 63.99; H, 8.10; N, 3.87%. 1H NMR ($CDCl_3$): δ 8.38 (s, 2H, C(H)N), 7.89 (m, 8H, NC_6H_4 , C(H) C_6H_4), 7.22 (d, 4H, $J_{HH} = 8.6$ Hz, OC_6H_4), 6.96 (d, 4H, $J_{HH} = 8.4$ Hz, SC_6H_4), 4.03 (t, 4H, OCH_2), 3.61 (q, 8H, dte), 1.80 – 1.09 (m, 84H, $OC_{20}H_{41}$, dte), 0.89 (t, 6H, $OC_{20}H_{41}$).

All the complexes were synthesized in a similar fashion.

[(dte)Ni(μ_2 -SC₆H₄NC(H)C₆H₄OC₁₆H₃₃)]₂ (17)

A green solid was obtained in a yield of 78%. Anal. Calcd for C₆₈H₁₀₄N₄S₆Ni₂: C, 63.35; H, 8.13; N, 4.34. Found: C, 64.01; H, 8.22; N, 4.65%. ¹H NMR (CDCl₃): δ 8.38 (s, 2H, C(H)N), 7.90 (m, 8H, NC₆H₄, C(H)C₆H₄), 7.20 (d, 4H, J_{HH} = 8.4 Hz, OC₆H₄), 6.96 (d, 4H, J_{HH} = 8.0 Hz, SC₆H₄), 4.02 (t, 4H, OCH₂), 3.60 (q, 8H, dtc), 1.80 – 1.09 (m, 68H, OC₁₆H₃₃, dtc), 0.88 (t, 6H, OC₁₆H₃₃).

[(dte)Ni(μ_2 -SC₆H₄NC(H)C₆H₄OC₁₄H₂₉)]₂ (18)

A green solid was obtained in a yield of 81%. Anal. Calcd for C₆₄H₉₈N₄S₆Ni₂: C, 62.33; H, 8.01; N, 4.54. Found: C, 63.00; H, 8.22; N, 4.96%. ¹H NMR (CDCl₃): δ 8.35 (s, 2H, C(H)N), 7.82 (d, 4H, J_{HH} = 8.8 Hz, C(H)C₆H₄), 7.52 (d, 4H, J_{HH} = 8.6 Hz, NC₆H₄), 7.14 (d, 4H, J_{HH} = 8.8 Hz, OC₆H₄), 6.96 (d, 4H, J_{HH} = 8.8 Hz, SC₆H₄), 4.02 (t, 4H, OCH₂), 3.60 (q, 8H, dtc), 1.80 (q, 4H, OCH₂CH₂), 1.60 – 1.19 (m, 56H, OC₁₄H₂₉, dtc) 0.88 (t, 6H, CH₃).

[(dte)Ni(μ_2 -SC₆H₄NC(H)C₆H₄OC₁₀H₂₁)]₂ (19)

A green solid was obtained in a yield of 75%. Anal. Calcd for C₅₆H₈₂N₄S₆Ni₂: C, 60.00; H, 7.37; N, 5.00. Found: C, 60.22; H, 7.62; N, 5.55%. ¹H NMR (CDCl₃): δ 8.36 (s, 2H, NC(H)); 7.82 (d, 4H, J_{HH} = 8.6 Hz, NC₆H₄); 7.20 (d, 4H, J_{HH} = 8.4 Hz, C(H)C₆H₄); 7.14 (d, 4H, J_{HH} = 8.4 Hz, OC₆H₄); 6.96 (d, 4H, J_{HH} = 8.8 Hz, SC₆H₄); 4.02 (t, 4H, J_{HH} = 6.2 Hz, OCH₂); 3.55 (q, 8H, dtc); 1.79 (q, 4H, OCH₂CH₂); 1.46 – 1.08 (m, 40H, dtc, OC₁₀H₂₁), 0.88 (t, 6H, OC₁₀H₂₁).

[(dte)Ni(μ_2 -SC₆H₄NC(H)C₆H₄OC₆H₁₃)]₂ (20a)

A green solid was obtained in a yield of 77%. Anal. Calcd for C₄₈H₆₆N₄S₆Ni₂: C, 57.15; H, 6.59; N, 5.55. Found: C, 57.88; H, 6.33; N, 6.09%. ¹H NMR (CDCl₃): δ 8.35 (s, 2H, NC(H)); 7.86 (d, 4H, J_{HH} = 8.8 Hz, NC₆H₄); 7.50 (d, 4H, J_{HH} = 8.4 Hz, C(H)C₆H₄); 7.13 (d, 4H, J_{HH} = 8.4 Hz, OC₆H₄), 6.96 (d, 4H, J_{HH} = 8.8 Hz, SC₆H₄), 4.02 (t, 4H, J_{HH} = 6.8

Hz, OCH₂), 3.47 (m, 8H, dtc); 1.80 (q, 4H, OCH₂CH₂); 1.46 – 1.09 (m, 24 H, dtc, OC₆H₁₃); 0.91 (t, 6H, OC₆H₁₃).

[(dtc)Ni(μ₂-SC₆H₄NC(H)C₆H₄OC₄H₉)]₂ (21)

A green solid was obtained in a yield of 72%. Anal. Calcd for C₄₄H₅₆N₄S₆Ni₂: C, 55.59; H, 5.94; N, 5.89. Found: C, 56.05; H, 6.52; N, 5.99%. ¹H NMR (CDCl₃): δ 8.38 (s, 2H, NC(H)); 7.89 (d, 8H, C(H)C₆H₄, NC₆H₄); 7.07 (d, 4H, *J*_{HH} = 8.4 Hz, OC₆H₄), 6.96 (d, 4H, *J*_{HH} = 8.8 Hz, SC₆H₄), 4.03 (t, 4H, *J*_{HH} = 6.8 Hz, OCH₂), 3.47 (m, 8H, dtc); 1.80 (q, 4H, OCH₂CH₂); 1.50 (m, 4H, OC₄H₉); 1.12 (t, 12H, dtc), 0.98 (t, 6H, OC₄H₉).

(dtc)Ni(μ₂-SC₆H₄NC(H)C₆H₄OC₆H₁₃)(PBU₃) (20b)

The complex was formed as a by-product from the second crop of recrystallisation of complex **9a**. The green solid was obtained in a yield of 26%. Anal. Calcd for C₂₅H₄₆N₂PS₃Ni: C, 53.57; H, 8.27; N, 5.00. Found: C, 53.68; H, 8.59; N, 5.09%. ¹H NMR (CDCl₃): δ 8.40 (s, 1H, NC(H)); 7.79 (d, 2H, *J*_{HH} = 8.8 Hz, NC₆H₄); 7.47 (d, 2H, *J*_{HH} = 8.4 Hz, C(H)C₆H₄); 6.95 (m, 4H, SC₆H₄, OC₆H₄); 4.00 (t, 2H, *J*_{HH} = 6.6 Hz, OCH₂); 3.55 (m, 4H, dtc); 1.80 – 0.90 (m, 44H, PBu₃, dtc, OC₆H₁₃).

3.2.5 Synthesis of Pincer Schiff base complexes 22-27.

Synthesis of 1,3-C₆H₃(CH₂NEt₂)₂PdSC₆H₄NC(H)C₆H₄OC₁₂H₂₅ (22)

Excess Et₃N (1.4 mL) was added into a pale orange toluene (30 mL) solution of **1a** (0.3 g, 0.78 mmol) and HSC₆H₄NC(H)C₆H₄OC₁₂H₂₅ (0.39 g, 0.78 mmol) and the reaction left overnight (18 h). A white precipitate was filtered off to give a bright red filtrate. The solvent was evaporated to leave analytically pure red solid (0.25 g, 43%). Anal. Calcd for C₄₁H₆₂N₃OSPd: C, 65.62; H, 8.19; N, 5.60. Found: C, 65.74; H, 8.23; N, 5.63%. ¹H NMR (CDCl₃): δ 8.42 (s, 1H, NC(H)); 7.81 (d, 2H, *J*_{HH} = 8.4 Hz, C₆H₄N); 7.58 (d, 2H, *J*_{HH} = 8.2 Hz, C(H)C₆H₄), 2.23 (d, 2H, *J*_{HH} = 8.4 Hz, OC₆H₄); 6.92 (d, 2H, *J*_{HH} = 8.2 Hz, SC₆H₄); 6.88 (t, 1H, C₆H₄(CH₂N)₂); 6.76 (d, 2H, *J*_{HH} = 7.8 Hz, C₆H₄(CH₂N)₂); 4.07 (s, 4H, CH₂N); 4.00 (t, 2H, OCH₂); 3.31 (m, 4H, NCH₂CH₃); 1.80 (q, 2H, OCH₂CH₂); 1.61 (t, 12H, NEt); 1.60-1.15 (m, 18H, OC₁₂H₂₅), 0.88 (t, 3H, OC₁₂H₂₅). ¹³C{H} NMR

(CDCl₃): δ 11.66, 13.84, 14.09, 22.09, 26.03, 29.33, 29.61, 31.89, 46.67, 57.45, 57.65, 58.37, 66.63, 68.12, 68.60, 114.58, 117.73, 118.32, 120.38, 123.96, 130.00, 130.48, 134.27, 147.67.

Synthesis of 1,3-C₆H₃(CH₂NEt₂)₂PdSC₆H₄NC(H)C₆H₄OC₆H₁₃ (23)

C₆H₃(CH₂NEt₂)₂PdCl (30 mg, 0.08 mmol), HSC₆H₄NC(H)C₆H₄OC₆H₁₃ (0.02 g, 0.08 mmol). Yield = 33 mg (62%). Anal. Calcd for C₃₅H₅₀N₃OSPd: C, 63.10; H, 7.41; N, 6.30. Found: C, 63.15; H, 7.43; N, 6.53%. ¹H NMR (CDCl₃): δ 8.28 (s, 1H, C(H)N), 7.74 (d, 2H, *J*_{HH} = 7.2 Hz, C₆H₄), 7.44 (d, 2H, *J*_{HH} = 8.4 Hz, C₆H₄), 7.06 (d, 2H, *J*_{HH} = 8.4 Hz, C₆H₄), 6.92 (m, 3H, C₆H₃), 6.61 (d, 2H, *J*_{HH} = 7.6 Hz, SC₆H₄), 3.95 (m, 4H, CH₂), 3.39 (m, 4H, CH₂CH₃), 2.60 (m, 2H, CH₂CH₃), 1.77 (q, 2H, CH₂), 1.53 (t, 12H, CH₂CH₃), 1.39 (m, 6H, OC₆H₁₃), 0.84 (t, 3H, CH₃). ¹³C{¹H} NMR (CDCl₃): δ 162.05, 159.95, 152.03, 147.55, 133.84, 130.59, 129.99, 128.83, 123.98, 121.64, 118.25, 114.72, 68.23, 66.65, 58.45, 57.68, 31.54, 29.68, 29.12, 25.67, 22.56, 14.00.

Synthesis of 1,3-C₆H₃(CH₂NEt₂)₂PdSC₆H₄NC(H)C₆H₄OC₄H₉ (24)

C₆H₃(CH₂NEt₂)₂PdCl (0.04 g, 0.11 mmol), HSC₆H₄NC(H)C₆H₄OC₄H₉ (0.03 g, 0.11 mmol), Yield = 0.01 g (33%). Anal. Calcd for C₃₃H₄₆N₃OSPd: C, 61.99; H, 7.25; N, 6.57. Found: C, 62.01; H, 7.29; N, 6.67%. ¹H NMR (CDCl₃): δ 8.35 (s, 1H, C(H)N), 7.81 (d, 2H, *J*_{HH} = 8.8 Hz, C₆H₄), 7.51 (d, 2H, *J*_{HH} = 6.6 Hz, C₆H₄), 7.12 (d, 2H, *J*_{HH} = 8.8 Hz, NC₆H₄), 6.96 (d, 2H, *J*_{HH} = 8.8 Hz, SC₆H₄), 6.88 (t, 1H, C₆H₃), 6.70 (d, 2H, C₆H₃), 4.03 (s, CH₂, 4H), 3.40 (m, 4H, Et), 2.70 (m, 4H, Et), 1.80 (q, 2H, OC₄H₉), 1.61 (t, 12 H, Et), 1.45 (q, 2H, OC₄H₉), 0.96 (t, 3H, OC₄H₉).

*Synthesis of 1,3-C₆H₄(CH₂^{*S*}Pr)₂PdSC₆H₄NC(H)C₆H₄OC₆H₁₃ (25)*

HSC₆H₄NC(H)C₆H₄OC₆H₁₃ (0.2 g, 0.64 mmol) was stirred with Na (0.15 g, 6.4 mmol) in CH₂Cl₂ overnight. The solution was transferred via canula through a frit into a suspension of C₆H₃(CH₂SiPr)₂PdBr (0.3 g, 0.68 mmol) in Et₃N (15 mL). The resultant solution stirred for 3 h and then filtered to give an orange red filtrate. The solvent was removed and the orange residue recrystallised from CH₂Cl₂ and hexane at -15°C to give an orange solid with a yield of 0.35 g (70.4%). Anal. Calcd for C₃₉H₄₄NOS₂Pd: C, 65.65; H, 6.22;

N, 1.91. Found: C, 65.63; H, 6.30; N, 1.88%. $^1\text{H NMR}$ (CDCl_3): δ 8.35 (s, 1H, C(H)N), 7.81 (d, 2H, $J_{\text{HH}} = 8.8$ Hz, C(H)C₆H₄), 7.51 (d, 2H, $J_{\text{HH}} = 8.4$ Hz, NC₆H₄), 7.14 (d, 2H, $J_{\text{HH}} = 8.0$ Hz, OC₆H₄), 6.96 (m, 5H, C₆H₃, SC₆H₄), 4.02 (s, 4H, CH₂), 4.02 (t, 2H, $J_{\text{HH}} = 6.6$ Hz, OCH₂), 1.79 (q, 2H, OCH₂CH₂), 1.44 (m, 6H, O(CH₂)CH₃, ⁱPr), 0.91 (t, 3H, CH₃).

Synthesis of (1,2-SC₆H₄NC(H)C₅NH₄)NiSC₆H₄NC(H)C₆H₄OC₁₂H₂₅ (26)

To a yellow toluene solution of HSC₆H₄NC(H)C₆H₄OC₁₂H₂₅ (0.1 g, 0.23 mmol) was added 1,2-(SC₆H₄)N=C(H)-2-C₅H₄NNiCl (0.06 g, 0.23 mmol). The colour changed from maroon to greenish on addition of excess Et₃N (2 mL) and the reaction was left for 24 h. The mixture was poured into a 1:1 ethanol: water solution (50 mL) and stirred for 15 minutes. The organic layer was dried over K₂CO₃/Na₂SO₄ and filtered. The solution was evaporated to dryness to leave a green residue, which was recrystallised from CH₂Cl₂: hexane mixture at -15°C. The green product was obtained in 86.4% (0.13 g) yield as a powder. Anal. Calcd for C₃₇H₄₃N₃S₂Ni: C, 68.10; H, 6.64; N, 6.44. Found: C, 69.01; H, 6.92; N, 6.81%. $^1\text{H NMR}$ (CDCl_3): δ 8.67 (d, 1H, $J_{\text{HH}} = 4.4$ Hz, C₅H₄N), 8.49 (s, 1H, C₅H₄C(H)), 8.43 (s, 1H, C(H)C₆H₄), 7.82 (d, 4H, C(H)C₆H₄), 7.68 (d, 1H, $J_{\text{HH}} = 8.0$ Hz, NC₆H₄), 7.53 (t, 1H, C₅H₄N), 7.43 (t, 1H, C₅H₄N), 7.20 (d, 2H, 1,2-SC₆H₄N), 7.00 (dd, 4H, OC₆H₄, SC₆H₄), 6.77 (m, 1H, C₅H₄N), 4.01 (t, 2H, OCH₂), 1.80 (q, 2H, OCH₂CH₂), 1.77 – 1.26 (m, 18H, OC₁₂H₂₅), 0.88 (t, 3H, CH₃).

Synthesis of (1,2-SC₆H₄NC(H)C₅NH₄)NiSC₆H₄NC(H)C₆H₄OC₁₄H₂₉ (27)

The green solid was obtained in 81.4% (0.22 g) yield. Anal. Calcd for C₃₉H₄₇N₃S₂Ni: C, 68.82; H, 6.96; N, 6.17. Found: C, 68.75; H, 6.74; N, 6.03. $^1\text{H NMR}$ (CDCl_3): δ 8.71 (d, 1H, $J_{\text{HH}} = 4.0$ Hz, C₅H₄N), 8.44 (s, 2H, C₅H₄C(H), C(H)C₆H₄), 7.82 (m, 4H, C(H)C₆H₄, 1,2-SC₆H₄N), 7.63 (d, 2H, $J_{\text{HH}} = 8.0$ Hz, NC₆H₄), 7.50 (m, 2H, C₅H₄N), 7.16 (d, 2H, 1,2-SC₆H₄N), 7.00 (d, 2H, OC₆H₄), 6.74 (t, 1H, NC₆H₄), 4.01 (t, 2H, OCH₂), 1.78 (q, 2H, OCH₂CH₂), 1.71 – 1.26 (m, 22H, OC₁₄H₂₉), 0.88 (t, 3H, CH₃).

3.3 Results and discussions

3.3.1 Synthesis of pincer metal complexes (I, II, and III).

Pincer ligand complexes (**I** and **II**) were prepared by the cyclometallation of 1,3-bis(di-aminomethyl)benzene or 1,3-bis(di-*isopropyl*thiomethyl)benzene. Complex **I** was prepared by the method of van Koten *et al.*²⁴ and Rimml *et al.*²⁵ respectively. The van Koten method involves the lithiation of the pincer ligand in position 2 followed by addition of Pd(COD)Cl₂. An orange solid was obtained in 25% yield. Complex **I** could also be prepared in an analogous manner to that of complex **II** as the second route to **I**. However in the second route to **I** ethanol was used and there was no heating. The second route to **I** gave a slightly higher yield than the former method, with yields of 34% compared to 24%. Complex **II** was prepared by refluxing the pincer ligand with palladium acetate in glacial acetic acid followed by addition of lithium bromide. The total reaction time was about two hours. The yield of complex **II** was 94%, much higher than yields obtained for complex **I**. The two complexes were orange solids. The latter method has been used to prepared similar complexes. For example Errington *et al.*²⁸ synthesised [PdCl{C₆H₃(CH₂S^tBu)₂-2,6}] in 1980 while complexes [PdCl{C₆H₃(CH₂SCH₂CH₃)₂-2,6}] and [PdCl{C₆H₃-(CH₂SC₆H₅)₂-2,6}] were prepared by Lucena *et al.*²⁹ in 1996. Complex **III** on the other hand was prepared by the method of Lindoy *et al.*²⁶ This entails refluxing 2-(2-pyridyl)benzothiazoline and nickel chloride to produce a maroon insoluble solid in 83%.

Complexes **I** and **II** were characterised by a combination of NMR spectroscopy and elemental analysis, and in one case, **II**, by single crystal X-ray diffraction. Complex **III** was only characterised by elemental analysis, as it was insoluble in common organic solvents. The proton NMR spectrum of complex **I** showed peaks due to the aryl ring as a triplet and a doublet as expected. The benzyl protons gave a singlet integrating for four protons. The resonance signals of the NCH₂CH₃ gave two multiplets due to NCH₂ and a singlet due to NCH₂CH₃. This was interesting in that it meant that the protons on the two ethyl groups on NCH₂ are magnetically inequivalent. In the free ligand the inversion

about the nitrogen in the CNEt_2 moiety is rapid on the NMR time scale, which renders the ethyl groups homotopic. This inversion at the nitrogen is blocked by coordination to the palladium metal resulting in a stable prochiral nitrogen centre. This means that the protons on the ethyl group will lack a plane of symmetry, and as a result the ethyl groups will become diastereotopic. This results in the inequivalent chemical shifts and the magnetic couplings between protons on the NCH_2 group. Compound **II** on the other hand gave the expected signals due the aryl and benzylic protons, similar to those of compound **I**. The peaks due to the isopropyl group were a quartet from the proton on the carbon bound to sulfur and a doublet for the CH_3 groups.

3.3.2 The X-ray characterisation of [2,6-Bis(isopropylthiomethyl)phenyl- κ^3 -S,C¹,S']bromopalladium(II), (**II**).

The molecular structure of **II** is shown in Figure 3.1, Table 3.2 gives crystallographic parameters and selected bond distances and angles are given in Table 3.3. The coordination number of the palladium atom in **II** is four and the donor atoms are arranged in a square planar geometry, with the sulfur atoms *trans* to each other. The two palladium-sulfur distances differ only slightly (2.2924(6) Å and 2.3110(6) Å). This is in contrast to complexes in which the S atoms are *cis* to each other. In the *cis* complexes, the Pd-S distances differ significantly. For example, the two Pd-S distances in $\text{Pd}(\text{C}_6\text{H}_{12}\text{S}_3)\text{Br}_2$ of 2.274(2) Å and 2.256(2) Å are noticeably different.³⁰ In complex **II**, the 1,3-bis(thiomethyl)benzene unit behaves as a tridentate ligand. The two S-atoms in **II** are separated by a distance of 4.587(8) Å and are therefore suitably disposed to form two Pd-S bonds oriented *trans* to each other. The two isopropyl substituents are in axial positions on the same side of the molecular plane, whereas the *tert*-butyl groups are on opposite sides in $\text{PdCl}(\text{C}_6\text{H}_4)(\text{CH}_2\text{S}^t\text{Bu})_2$.²⁸ The axial conformation is preferred as the isopropyl repulsions are minimised. Potential repulsion between the two-isopropyl substituents is also minimized when they are on opposite sides. However, in contrast with the tertiary butyl analogue, the two-isopropyl groups in **II** are *cis* to each other. In this conformation, the shortest distance between hydrogen atoms is 2.315(7) Å.

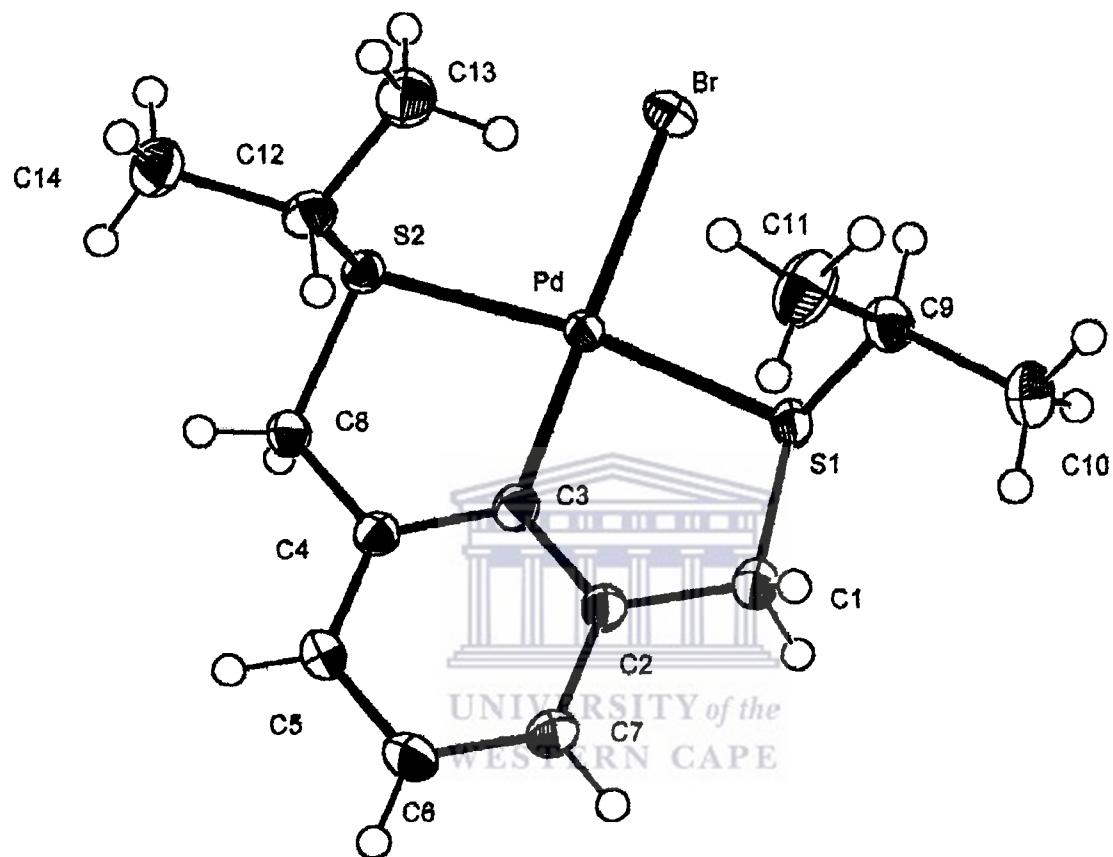


Figure 3.1: X-ray crystal structure of complex II.

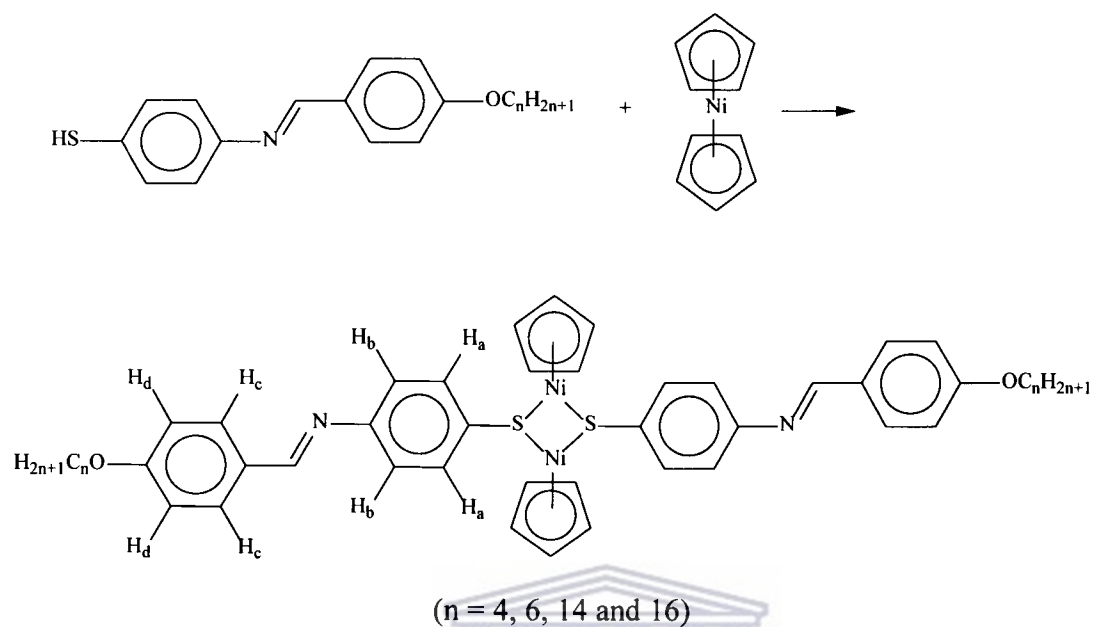
Table 3.3: Selected bond distances (Å) and selected bond angles (°) for complex II.

Pd-C(1)	1.984(2)	Pd-S(2)	2.3110(6)
Pd-S(1)	2.2924(6)	Pd-Br	2.5471(3)
C ¹ -Pd-S(1)	85.08(7)	C(1)-Pd-Br	178.91(7)
C ¹ -Pd-S(2)	85.17(7)	S(1)-Pd-Br	94.549(17)
S ¹ -Pd-S(2)	170.19(2)	S(2)-Pd-Br	95.180(16)

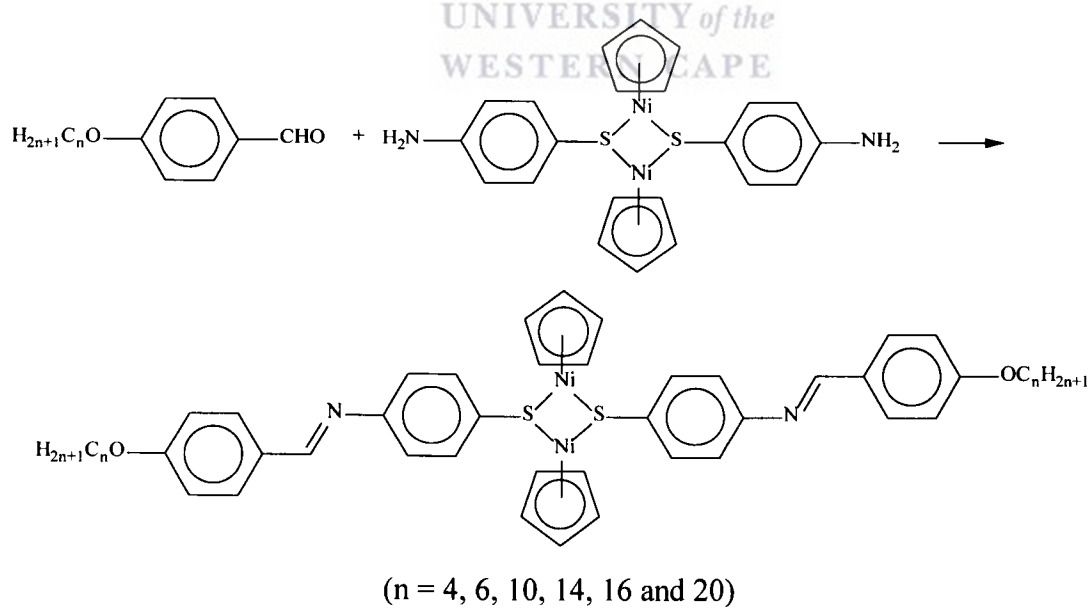
3.3.3 Synthesis and spectroscopic characterisation of Cyclopentadienylnickel(II) thiolato Schiff base complexes (12 – 15).

Two synthetic routes were used as an entry into the cyclopentadienyl complexes. The first route involved the reaction of nickelocene with the preformed thiolato Schiff base compounds to give the μ_2 -sulfur complexes (Scheme 3.1). The green toluene solution turned brown-black within the first thirty minutes and in all the cases the reaction was left to stir for 18 h before workup. The second route was by the condensation reaction between the known compound $[(\eta^5\text{-C}_5\text{H}_5)\text{Ni}(\mu_2\text{-SC}_6\text{H}_4\text{NH}_2)]_2^{23}$ with the appropriate 4-alkoxybenzaldehyde (Scheme 3.2). This reaction was also left to stir for 18 h before workup. In the latter case there was no colour change as both the product and one of the starting material are brown-black. Both of these routes gave complexes in moderate yields. All the complexes were air stable in solution as well as in the solid state. The identities and the integrity of the complexes were established by a combination of C, H, N analyses, NMR spectroscopy and in some cases by mass spectrometry. The elemental analyses showed that the complexes were of the expected formulation, while in one case, 14, a mole of CH_2Cl_2 was found in the analysis.

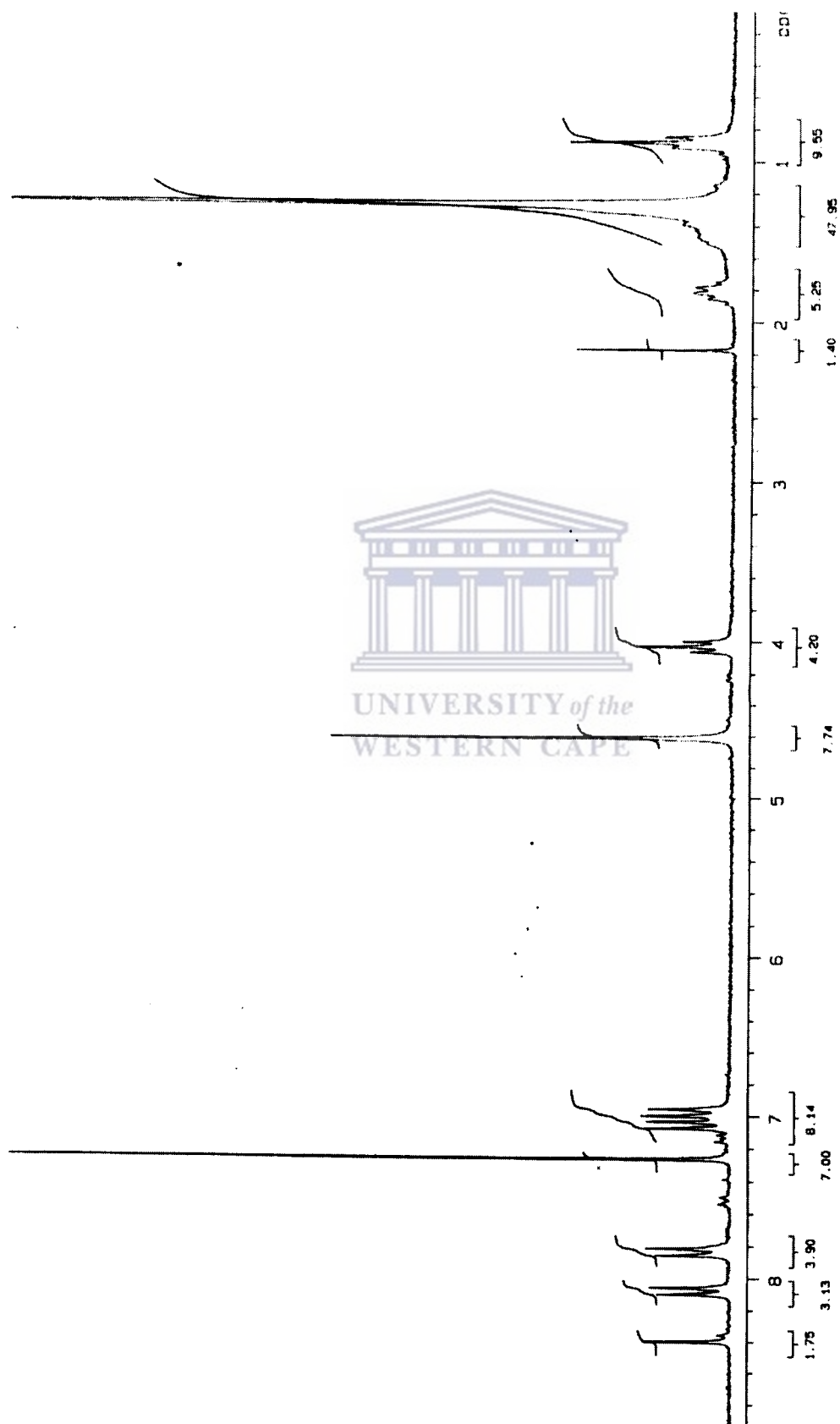
The $^1\text{H-NMR}$ spectra of the metal complexes were similar and in general did not differ much with those of the free thiol ligands (Figure 3.2). The difference between the complex and ligand spectra is that the complexes had an additional peak around 4.60 ppm due to the cyclopentadienyl ring. The similarities in the spectra are found in the four doublets of the two rings.



Scheme 3.1: Reaction of nickelocene with thiol Schiff base ligand to form cyclopentadienylnickel(II) thiolate complexes.



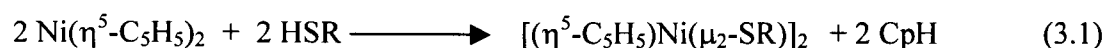
Scheme 3.2: Alternate synthetic route to cyclopentadienylnickel(II) complexes.

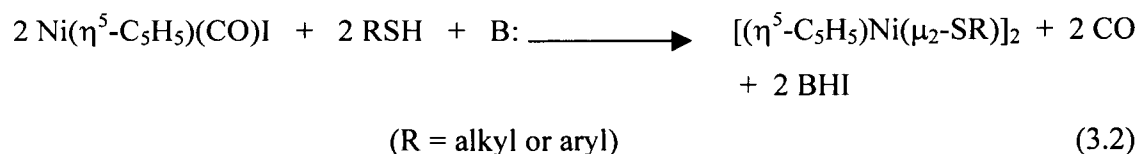
Figure 3.2: ^1H NMR spectrum of complex 12.

While in the free thiol ligands protons H_a and H_d were well separated, in the nickel complexes these peaks invariably overlap to give four spectral lines integrating for eight protons. This implies that the doublet due to H_a has shifted downfield and is therefore deshielded. This deshielding could only happen if the electron density of the sulfur atom in the complexes is less than in the free ligands. The coordination of the sulfur atom to a second nickel centre involves the σ -donation of the lone pair of electrons on the sulfur. This results in the decrease in electron density on the sulfur, which is then compensated by the donation of electrons on the ring thereby deshielding the protons on that ring; hence the downfield shift.

The cyclopentadienyl resonance peak at 4.60 ppm is slightly more downfield than those of similar complexes (with one aryl ring). For example the cyclopentadienyl ring resonance for $[(\eta^5\text{-C}_5\text{H}_5)\text{Ni}(\mu_2\text{-SC}_6\text{H}_5)]_2$, $[(\eta^5\text{-C}_5\text{H}_5)\text{Ni}(\mu_2\text{-SC}_6\text{H}_4\text{Br})]_2$, $[(\eta^5\text{-C}_5\text{H}_5)\text{Ni}(\mu_2\text{-SC}_6\text{H}_4\text{Cl})]_2$ and $[(\eta^5\text{-C}_5\text{H}_5)\text{Ni}(\mu_2\text{-SC}_6\text{H}_4\text{NH}_2)]_2$ are at 4.50,³¹ 4.15, 4.58 and 4.59 ppm²³ respectively. When one compares these chemical shifts it is apparent that there is no systematic variation of chemical shifts with electron withdrawing or donating ability or strength. This observation is puzzling in light of the fact that for a series of complexes, the variation of chemical shifts normally follows the electron withdrawing or donating abilities of the ligands or substituents.^{23b} The variation of the NMR signals amongst the Schiff base complexes was insensitive to the change in chain length.

The reaction of nickelocene with thiols has been widely used to prepare complexes with similar architecture to the ones reported here. For example Schropp reported μ_2 -sulfur bridged complexes in 1962, which used benzene as solvent. In these syntheses nickelocene and thiols were allowed to stir at room temperature for 12 h. The complexes reported by Schropp are of the general formula $[(\eta^5\text{-C}_5\text{H}_5)\text{Ni}(\mu_2\text{-SR})]_2$ (R = aryl or alkyl) (eq. 3.1).³² It was reported in the same publication that an alternate route to the complexes is the reaction between a thiol ligand and a nickel compound, in the presence of a weak base, as depicted in equation 3.2.

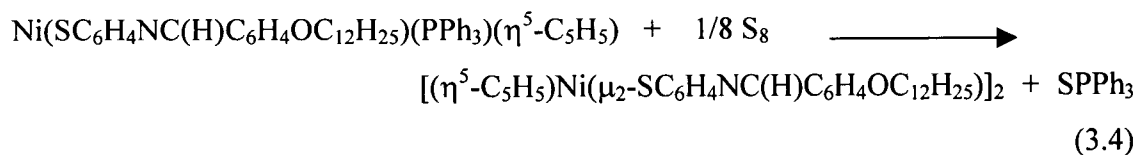




Photolysis of $[(\eta^5\text{-C}_5\text{H}_5)\text{Ni}(\text{CO})]_2$ in the presence of organic disulfides (RSSR) also gives μ_2 -sulfur bridged complexes with the same generic formula. The reaction is accompanied by the loss of carbon monoxide (equation 3.3).³³



However, we explored other routes to μ_2 -thiolato nickel complexes. One of them involved removal of phosphine. For example, when the complexes, $\text{Ni}(\text{SC}_6\text{H}_4\text{NC}(\text{H})\text{C}_6\text{H}_4\text{OC}_n\text{H}_{2n+1})(\text{PPh}_3)(\eta^5\text{-C}_5\text{H}_5)$ ($n = 12$ and 16) were reacted with elemental sulfur, μ_2 -sulfur complexes could be identified in their spectra (eq. 3.4). The problem with this method was that it was impossible to separate the products from SPPH_3 by-product. This is because the by-product co-precipitates with the desired product when the latter is crystallised from a mixture of either toluene or dichloromethane and hexane. Chromatography was not used as it was feared that the compound might not be able to elute from the column. From the proton NMR spectra of the isolated products there was no evidence of the starting material but peaks of the expected products and those from SPPH_3 were found. The expected signals are similar to those of the authentic sample prepared through other methods. Phosphine removal with elemental sulfur has been used previously to produce $[(\eta^5\text{-C}_5\text{H}_5)\text{Ni}(\mu_2\text{-SC}_6\text{H}_5)]_2$ (equation 3.4) but even here the SPPH_3 had to be physically separated from the desired product.³⁴ Hence it appears that this methodology works but no appropriate workup exist for isolation of the pure product. Some of our workup included chromatography but the nickel product adsorb to most of our stationary phases, such as silica, alumina and glass bead.

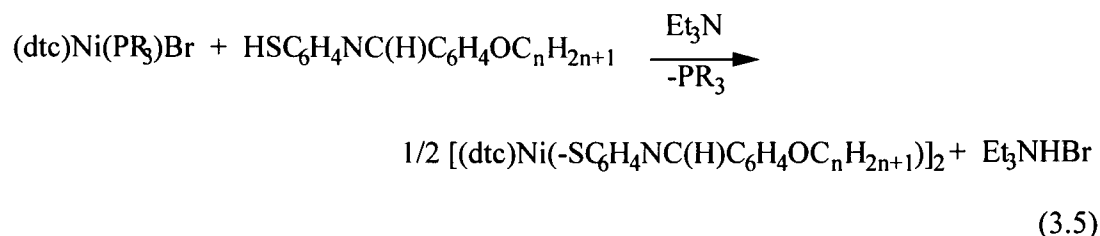


Taube and co-workers in 1985³⁵ found $[(\eta^5\text{-C}_5\text{H}_5)\text{Ni}(\mu_2\text{-SC}_6\text{H}_5)]_2$ as 1% impurity when they reacted nickelocene and $\text{C}_6\text{H}_5\text{SCH}_2\text{Li}$ in the presence of PPh_3 . In the absence of PPh_3 , the sulfur bridged complex was obtained with concomitant release of ethylene and cyclopropane, even at low temperatures, -20°C .³⁵

Of the three literature routes to μ_2 -thiolato complexes, we found the reaction using nickelocene the simplest and adopted this as our main synthetic entry into the μ_2 -thiolato nickel complexes in this thesis.

3.3.4. *Synthesis and spectroscopic characterisation of diethyldithiocarbamatonickel(II) thiolato Schiff base complexes. (16 – 21)*

The diethyldithiocarbamato (dtc) complexes were synthesised by reacting the Schiff base thiol ligands with either $\text{NiBr}(\text{PBU}_3)(\text{dtc})$ or $\text{NiBr}(\text{PPh}_3)(\text{dtc})$ in the presence of Et_3N (eq. 3.5). The dimeric product was the only product in all the cases, except in one isolated case where a monomer was obtained as a minor product of the reaction. This happened where the phosphine used was tributylphosphine.



The progress of the reaction could be followed by the gradual colour change from maroon to dark green within 30 minutes of adding the base. This synthetic route has been

extensively used by Darkwa *et al.* in synthesising mono- and dinuclear diethyldithiocarbamate nickel complexes.³⁶ The formation of the mono- or the dinuclear complexes is said to be dependent on the ability of the chalcogenide or specifically the thiolate sulfur to donate an electron pair to the second nickel atom, and secondly on the steric bulkiness of the phosphine group used, the latter playing a minor role in the monomer-dimer equilibrium. In the present complexes evidence of monomer formation was absent, except in only one case as previously mentioned. The absence of any monomer formation in the present study might arise from the length of the reaction times used in the two cases. Whereas Darkwa *et al.* did their reactions in 2 h, in the present synthetic route the reactions were left for more than 18 h. The former authors showed that indeed the monomer slowly converts to the dimer when it is left to stand in solution for more than 24 h. Hence reaction time appears to be a major factor in dimer formation.

The ¹H NMR spectra of the dithiocarbamate complexes consisted of two sets of doublets from the aryl protons of the two rings in the Schiff base ligand. These are similar to those of the cyclopentadienyl complexes in appearance. Additional peaks due to the ethyl groups of the dithiocarbamate group were upfield at 3.60 ppm and 1.80-1.09 ppm (overlap with alkoxy chain) for the CH₂ quartet and the CH₃ triplet respectively. The triplet usually appeared as a shoulder on the upfield-side of the broad signal of the long alkoxy chain, but more downfield compared to the triplet of the CH₃ group of the chain. In addition to the ¹H NMR spectral characterisation, the complexes were characterised by elemental analysis and in some cases by ¹³C NMR spectra and for two complexes (n = 6 and 10) by MALDI-TOF mass spectroscopy.

When ¹H NMR chemical shifts of the two types of complexes (cyclopentadienyl and diethyldithiocarbamate) are compared it is obvious that the cyclopentadienyl ring affected the resonance shifts differently from the diethyldithiocarbamate group (Table 3.4). Whereas for the cyclopentadienyl complexes the resonances due to H_a are always downfield, those of H_b are always upfield when they are compared with those of the diethyldithiocarbamate complexes. This is partly due to the shielding effect the dtc group has in comparison with cyclopentadienyl ring. The electronic difference induced by these

groups becomes more obvious when the electrochemical behaviour of the two types of complexes is compared (Section 3.5).

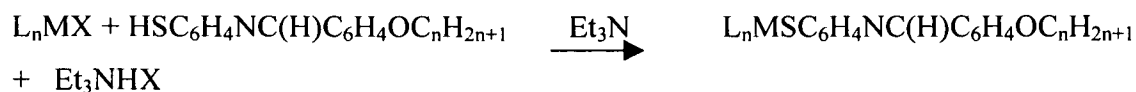
Table 3.4: Table of phenyl signals (H_a and H_b) for cyclopentadienyl complexes versus those of the diethyldithiocarbamate complexes, with the peak separation.

n	$\eta^5\text{-C}_5\text{H}_5$			$\text{S}_2\text{CN}(\text{CH}_2\text{CH}_3)_2$		
	H_a	H_b	Δ^*	H_a	H_b	Δ^*
4	6.98	7.84	0.86	6.96	7.89	0.91
6	6.98	7.86	0.88	6.96	7.89	0.91
14	6.98	7.84	0.86	6.96	7.92	0.96
16	6.97	7.83	0.86	6.96	7.90	0.94

* Δ = separation between the doublets of the first ring on the thiol Schiff base ligand.

3.3.5 Synthesis of pincer metal thiolato Schiff base complexes (22 - 27).

All pincer complexes were synthesised by reacting equimolar amounts of the metal starting materials with the thiol ligands in the presence of triethylamine. The reaction is represented by equation 3.6.



(M = Pd (**D**), n = 4, 6 and 12; Ni (**E**), n = 12 and 14)

(3.6)

In the case of types **D** (where M is palladium) complexes, no colour change was observed. This is due to the fact that both the starting material and the product are of similar colours. Low yields were obtained for the palladium complexes and high yields for the nickel complexes. The low yields for the palladium pincer complexes and the instability of the *isopropyl* analogue, which generally decomposed on recrystallisation to starting materials, means that the steric interactions caused by the groups at binding sites of the pincer ligand are great. For example it has been found that by substituting NMe_2 ³⁷

by NEt_2 in the pincer starting complexes, their ability to absorb SO_2 is reduced.³⁸ In fact the NEt_2 complexes does not absorb SO_2 gas.³⁸ The *isopropyl* groups impart more steric repulsion than the amine groups. For type **E** complexes the colour changed from maroon to dark green, with the final products being dark green soluble solids. The yields were high for **26** and **27**. In all the synthesis of **22** to **27** the reaction was left to stir for 18 h to ensure complete conversion. The products were characterised by a combination of ^1H and ^{13}C NMR spectroscopy and elemental analysis.

The NMR spectra of complexes **22** – **24** were similar (Fig. 3.3). On the downfield side, the spectra consisted of the imine proton resonance at 8.29 ppm and four sets of doublets from the two rings of the Schiff base ligand. In addition the resonance of the aryl ring from the terdentate ligand appeared as a triplet and a doublet at 6.88 and 6.70 ppm respectively. The peak at 4.03 ppm, integrating for six protons, was due to the benzylic protons of the terdentate ligand and the OCH_2 group from the alkoxy chain. The aminoethyl protons gave two sets of multiplets at 3.40 and 2.70 ppm and a triplet at 1.61 ppm. The multiplets integrated for four protons each while the triplet integrated for twelve protons. The remaining signals were due to the alkoxy chain protons of the Schiff base. Complex **25**, the *isopropyl* analogue of **22** – **24**, had a similar proton spectrum to those of **22** – **24**. The only difference is that complex **25** had a multiplet at 1.44 ppm due to the *isopropyl* group and the absence of resonance signals from the NEt_2 group. In addition the imine proton resonance is slightly more downfield for complex **25**. In all cases there was a slight shift in the resonance signals of the terdentate group. The two signals from the aryl protons coalesced as compared to those of the uncomplexed pincer palladium compound. The proton NMR spectra of **26** and **27** were more complicated than those of **22** – **25**. In addition to the obvious resonance signals from the Schiff base ligand, the presence of signals from two more aryl rings made the assignment very difficult. There were two imine resonance signals due to the Schiff base's imine functionality and the terdentate ligand's imine group. There was also a smaller peak next to the peaks due to the imine protons, probably due to the isomer of the product.

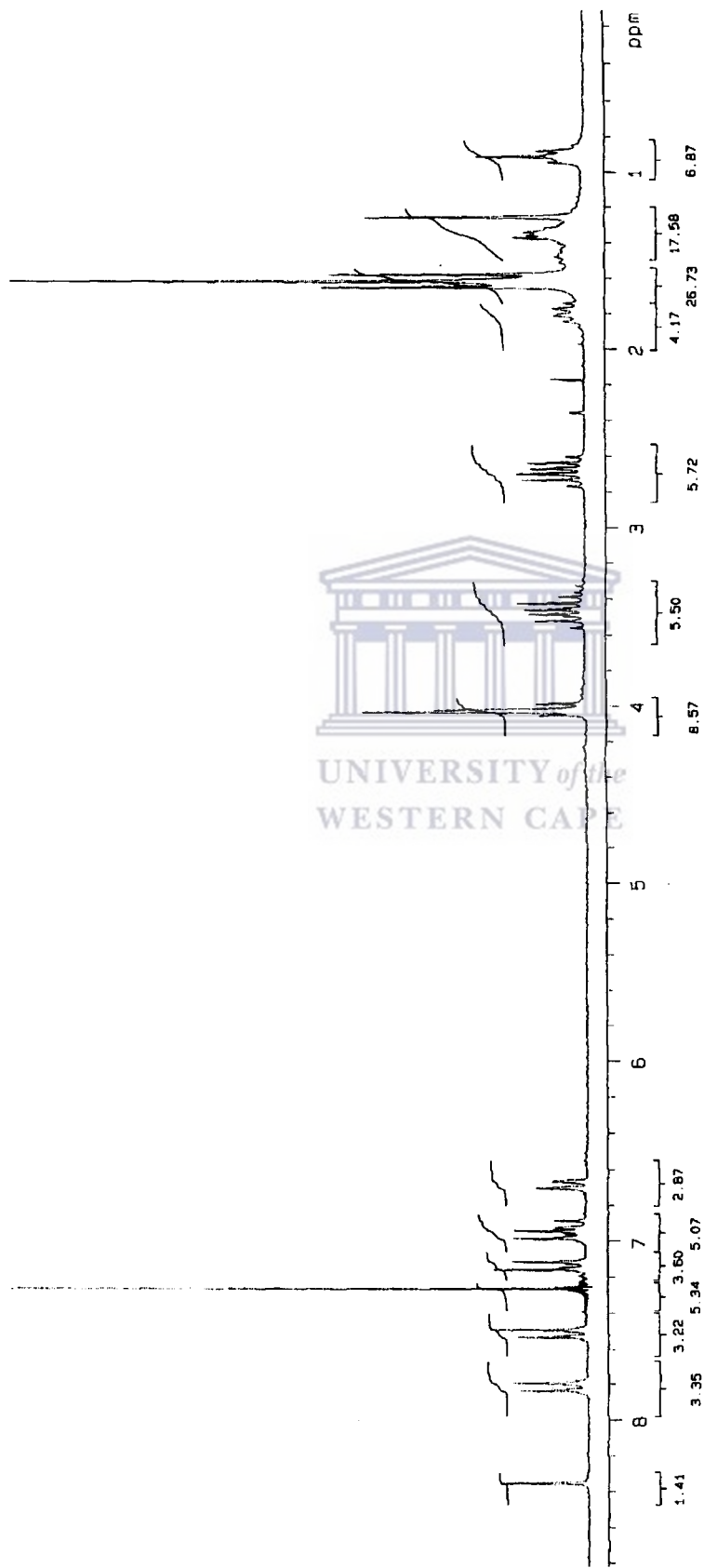


Figure 3.3: ¹H NMR spectrum of complex 23.

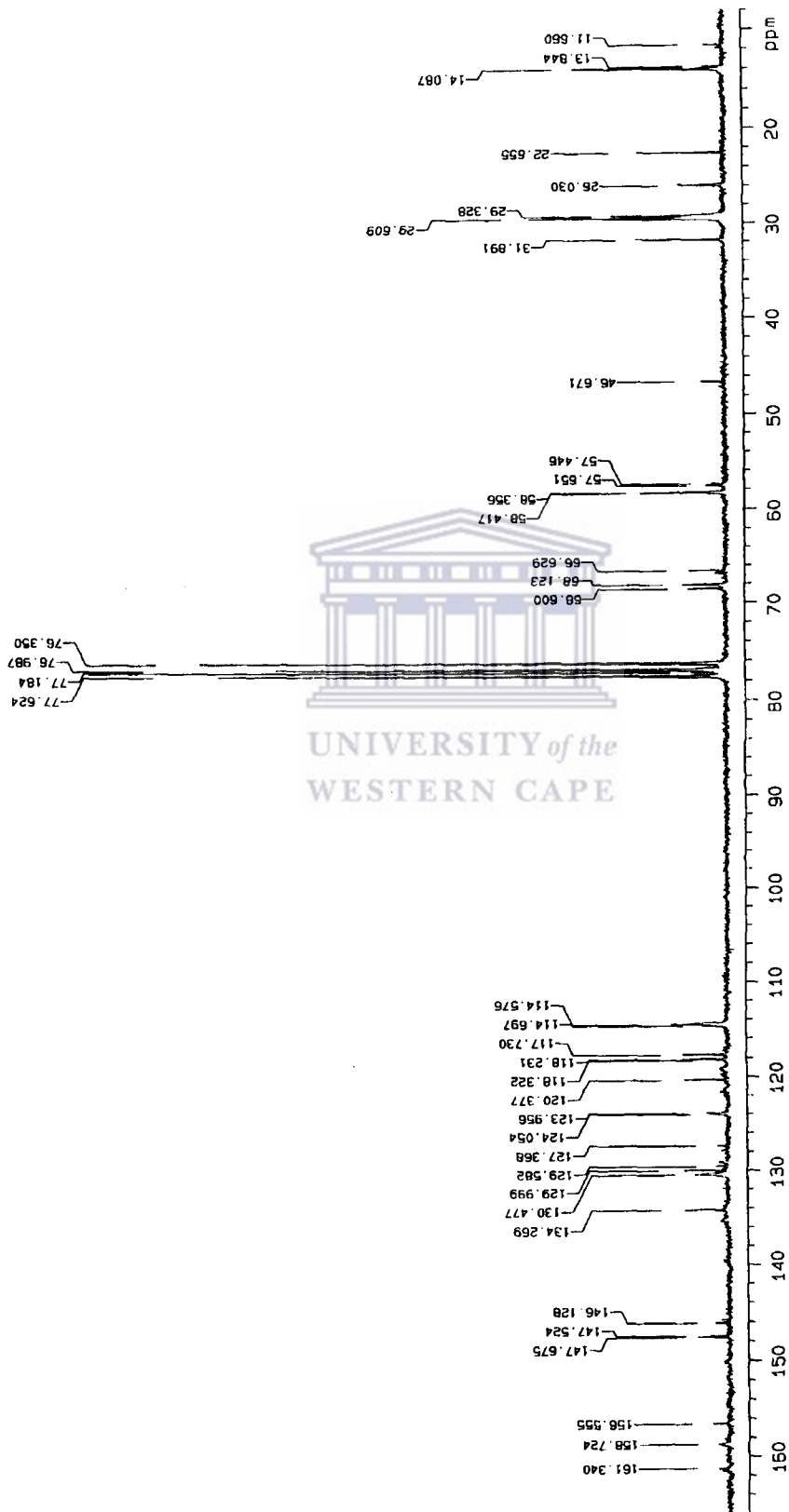


Figure 3.4: ¹³C NMR spectrum of complex 26.

The carbon-13 spectrum of complex **26** (Fig. 3.4) showed that there were resonance signals attributed to the pyridyl ring, which appeared at between 146 ppm and 161 ppm. These were more downfield as compared to those from the benzene rings. The aromatic region (115 ppm to 135 ppm) had peaks that could only be accounted for when the terdentate ligand is present. Notwithstanding the difficulty in assigning the peaks in the proton NMR spectra, the microanalysis data of these complexes confirmed their proposed structures. Further characterisation by MALDI-TOF mass spectroscopic analysis for **19** and **20** showed the molecular ions (Table 3.5). Thus the combination of NMR and elemental analysis (mass spectrometry for **19** and **20**) could be used to propose structures of complexes isolated in this study as shown in equations 3.4 and 3.5. Further discussions of the MALDI-TOF spectrometry is provided in the next section to show how this analytical technique was used in characterisation of the complexes isolated. It also shows some of the difficulties encountered and hence limitations that MALDI-TOF MS has in characterisation of coordination compounds.

3.4 MALDI-TOF mass spectrometry analysis of **12–15** and **19** and **20**.

Matrix Assisted Laser Desorption Ionisation Time of Flight (MALDI-TOF) mass spectrometry is a new technique that has been developed specifically for the analysis of biological and natural products. It is however increasingly being used for the analysis of organic and organometallic compounds as well as polymer samples.

MALDI-TOF mass spectrometry was used to study the complexes in this chapter because it is perceived as a soft ionisation technique. We have also found out in our study of bimetallic nickel thiolato complexes that FAB and ES mass spectrometry techniques did not give molecular ion peaks for all our complexes (Chapter 4). In running the experiments three types of matrices were used. These were tetrafluorophenylporphyrin (F₂₀-TPP), dithranol and dimethylhydroxycinnamic acid. In addition we used NaOH as a cationic source to assist in the ionisation process. These matrices have different laser absorption abilities and hence different abilities to transfer the laser energy to the sample. Mass spectral data of complexes **12 – 15**, **19** and **20** were collected using all three types

of matrices. The matrices have different properties in terms of molecular mass and acidity or basicity as well as their ability to absorb laser energy, and hence are expected to interact with the complexes in different ways.

These characteristics of matrices are normally used as a guide in selecting matrices; however our choice of matrices were limited by the range available. The three that we used satisfied most of the basic requirements for MALDI-TOF matrices. Different matrix: analyte ratios were used, while in some cases a cation source was added. When no matrix was used no signals were observed in all cases even though the complexes themselves were highly conjugated and thus were expected to absorb laser energy. The addition of a cation source did not improve the results in the selected experiments where they were added and therefore the cation was not added in most cases.

The best results were obtained when F₂₀-TPP (Flourine-20-tetraphenylporphyrin) matrix was used. This is based on the slightly higher abundance of the molecular ion peaks as compared to results from the other two matrices, even though the other two matrices also gave molecular ions for the complexes. Typically molecular ion abundance of a high of 12 to a low of 5 percent were observed (Figure 3.5 and Table 3.7). In all cases the most abundant peak (100 %) gave a molecular mass that is half the molar mass of the parent ion. This observation is true for both the cyclopentadienyl and diethyldithiocarbamate complexes. This clearly shows that the complexes were cleaving at the dative coordination Ni-S bond of the thiolato Schiff base ligand and the second nickel atom in the molecule. The Ni-S cleavage happened irrespective of which matrix was used. At very low laser intensities (1500, minimum for the instrument used) no ionization occurred. This contrasts with very high laser intensities (above 3000) that resulted in extensive fragmentations, with only molecular ions clusters of m/z less than 200 being observed.

The Ni-S bond cleavage was not observed in similar complexes when other ionisation sources were used, specifically fast atom bombardment (FAB) and electrospray (ES) ionisation. In these cases the parent/base peak observed corresponded to the fragment

(dte)₂Ni (m/z = 354).³⁶ The proposed mechanisms for this to occur do not include the Ni-S bond cleavage. This is quite surprising, as one would expect that the perceived weaker Ni-S dative bond to be the first bond to be broken.

Table 3.5: Molecular ion and base peak values abundances obtained for different matrices

Complex (n)	Molecular mass	F20-TPP* (abundance %)	DHC* (abundance %)	Dithranol (abundance %)
15 (4)	816	408 (100)	408 (100)	408 (100)
		816 (2)	816 (3)	
14 (6)	838	496 (10)	492 (100)	492 (100)
		417 (100)	984 (8)	984 (5)
13 (14)	1092	547 (100)	548 (100)	548 (100)
		1034 (12)	818 (50)	565 (60)
				817 (50)
12 (16)	1121	575 (100)	575 (100)	575 (100)
		1121 (5)	1121 (8)	
19 (10)	1121	566 (100)	566 (100)	566 (100)
		1120 (5)	1120 (3)	1120 (3)
20 (6)	1008	528 (100)	528 (100)	528 (100)
		1056 (4)	1056 (2)	1056 (3)

* F20-TPP = Florine20-tetraphenylporphine; DHC = 2,5-dimethoxy-4-hydroxy cinnamic acid.

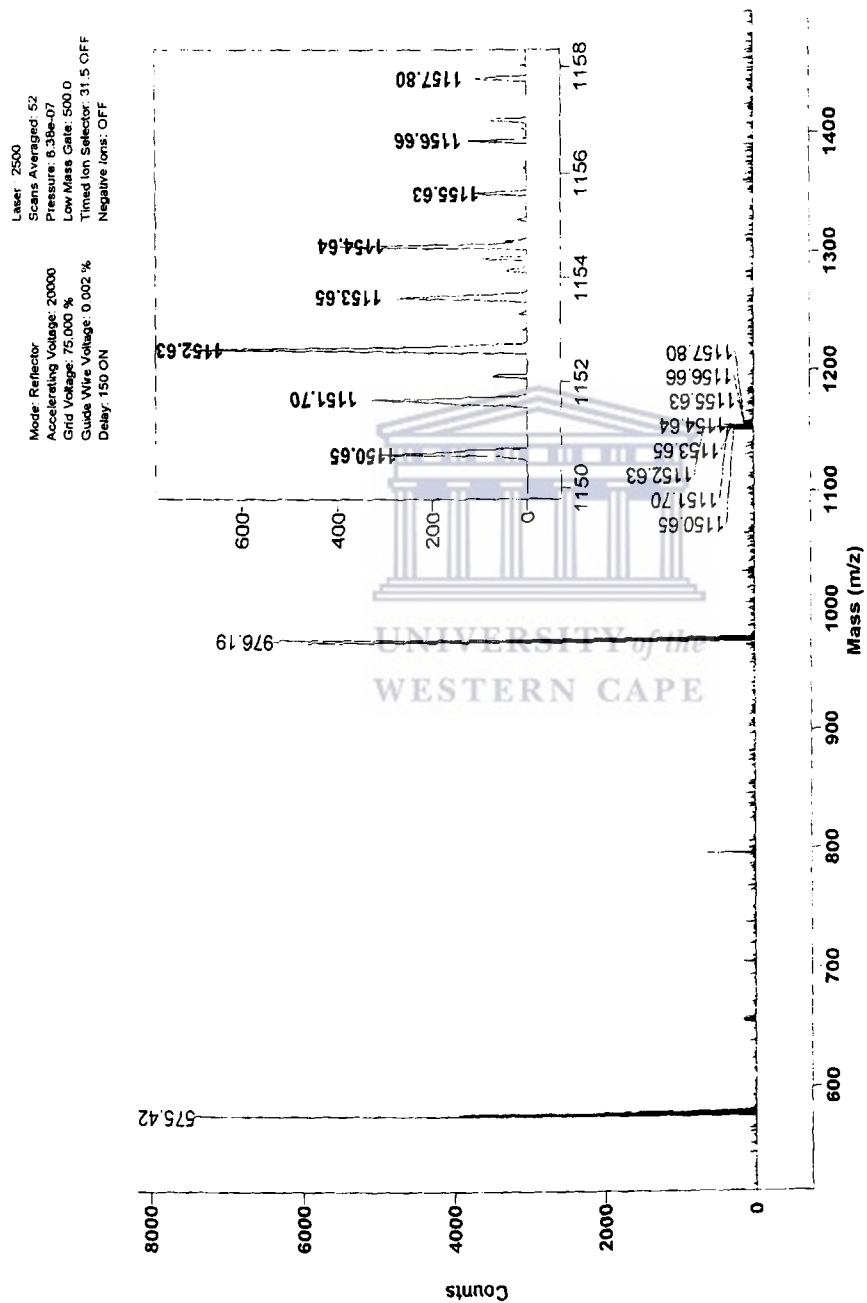


Figure 3.5: MALDI-TOF mass spectrum of complex 12.

3.5 Electrochemistry of selected nickel(II) μ_2 -thiolato Schiff base complexes.

To probe the electrochemical properties of the μ_2 -thiolato complexes prepared, the redox behaviour of selected complexes were studied by cyclic voltammetry. The electrochemical measurements were performed on a BAS 50W bioanalytical instrument. A standard three-electrode electroanalytical cell configuration equipped with a platinum disc-working electrode (1.5 mm diameter), a silver/silver chloride (Ag/AgCl) reference electrode and platinum wire counter electrode was used. Tetrabutylammonium tetrafluoroborate (TBA-TFB) was used as a supporting electrolyte in CH_2Cl_2 at 0.1 M concentrations. The concentration of the analyte was 0.03×10^{-3} M. In all cases measurements were referenced internally to the ferrocene/ferrocenium redox couple at 440 mV.



3.5.1 Cyclic voltammetric studies of $[(\eta^5\text{-C}_5\text{H}_5)\text{Ni}(\mu_2\text{-SC}_6\text{H}_4\text{NC}(\text{H})\text{C}_6\text{H}_4\text{OC}_n\text{H}_{2n+1})]_2$ ($n = 4, 14, 16$)

The cyclopentadienylnickel(II) complexes underwent two one electron oxidation reactions. The first oxidation occurred at *ca.* +200 mV and the second oxidation at *ca.* +900 mV. The $E_{1/2}$ values of the complexes studied were dependent on the length of the alkoxy chain. The $E_{1/2}$ values shifted to more positive oxidation values as the chain length was increased. For example complex **12** ($n = 16$) had an $E_{1/2}$ value of 220 mV, **13** ($n = 14$) of 212 mV while complex **15** ($n = 4$) had a value of 179 mV. The chain length similarly affected the potential of the second oxidation wave. The first oxidation peaks of complexes **12**, **13** and **15** had corresponding reduction peaks while the second oxidation peaks did not have corresponding reduction peaks. This observation implies the first electrochemical process is quasi-reversible, but the second electrochemical process is irreversible. One way of measuring reversibility of redox reactions is the determination of ΔE_p , ($= |E_{\text{ox}} - E_{\text{red}}|$). For a reversible process ΔE_p values of about 60 mV are expected for a one electron process; values of ΔE_p greater than 80 mV are usually associated with quasi-reversible redox behaviour. In addition to ΔE_p values, reversibility of redox reactions can also be determined by peak current ratios. A ratio of $i_{\text{ox}}/i_{\text{red}}$ equal to one is a

measure of reversibility; ratios lower than one however signify irreversible redox behaviour. Table 3.6 shows both ΔE_p and i_{ox}/i_{red} ratios for the complexes studied and confirm the quasi-reversibility of the first electrochemical events in all the compounds. The ΔE_p values were affected by chain length in a different manner. For example, for the complex with the longest chain the ΔE_p value was the smallest while that for the shortest chain complex was largest (Table 3.6). The values ranged from 154 through 128 to 86 mV for complexes **15** through **13** to **12** respectively.

Table 3.6: Electrochemical parameters for complexes of **12**, **13** and **15**.

Complex	ΔE_p (mV)*	$E_{1/2}$ (V)#	i_{ox}/i_{red}
15	154	179	0.97
13	128	212	0.778
12	86	220	0.73

* = $\Delta E_p = |E_{ox} - E_{red}|$, # = $E_{1/2} = (E_{ox} + E_{red})/2$

The current peak ratios of the first redox couple increased from 0.73 to 0.97 for the complex with the longest chain to the complex with the shortest chain respectively. The first oxidation (redox couple) is a one electron reversible process. The number of electrons involved in oxidation or reduction was estimated using Tafel analysis. The slope of the linear region of oxidation wave at different concentration gives the number of electrons. Figure 3.6 shows the estimated number of electrons for complex **12** and different concentration. The values from the Tafel plots of the linear region of the redox peak gave two electrons for the oxidation peak of complex **12**. This was not surprising given that the two nickel centres were being oxidized simultaneously. The reversibility of the redox couple was established by a combination of current ratios and ΔE_p values. For example the known one electron reversible redox peak of the ferrocene/ferrocenium couple has a ΔE_p value of 124 mV and peak ratios approaching unity. These values are not different from the values obtained in the present study. The second oxidation step was irreversible in all the complexes. This behaviour is similar to those of other μ_2 -sulfur

bridged complexes. In these μ_2 -sulfur complexes the first redox couple was always reversible while the second redox couple was irreversible.⁴⁰ The $E_{1/2}$ values for **12**, **13** and **15** for the first redox couple indicate that these complexes are more difficult to oxidize than other $[(\eta^5\text{-C}_5\text{H}_5)\text{Ni}(\mu_2\text{-SR})_2]$ (where R = C₆H₅, *p*-MeC₆H₄ and *p*-ClC₆H₄) complexes. For example when R was a phenyl group or a substituted phenyl the values of 90 mV, 80 mV and 70 mV for R = C₆H₅, *p*-MeC₆H₄ and *p*-ClC₆H₄ were found respectively. The oxidation potential for the second redox couple is however similar to literature values of 1040 mV, 930 mV and 800 mV for C₆H₅, *p*-MeC₆H₄ and *p*-ClC₆H₄ respectively.⁴⁰ The ΔE_p values are greater than 60 mV, the value for the peak separation of a non-equilibrium one electron transfer process³, in all the three complexes studied. A representative voltamogram is presented in Figure 3.6. As in similar μ_2 complexes studied by Frisch *et. al.*, the electrochemical activity is centred at the metal.⁴⁰



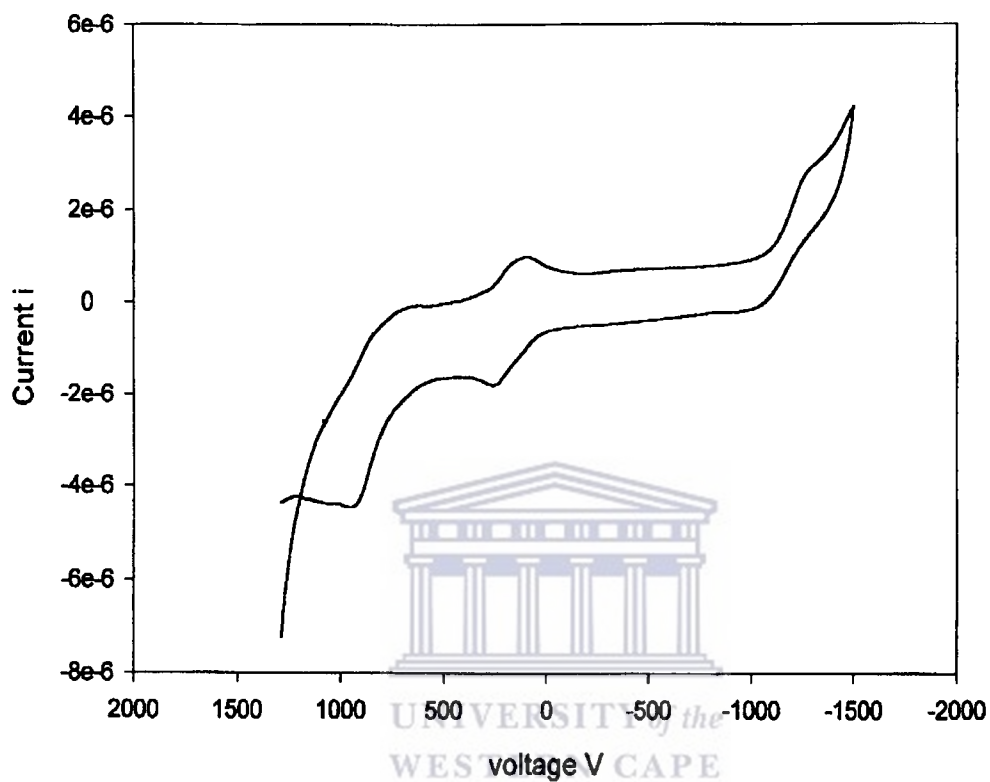


Figure 3.6: Cyclic voltammogram for complex 13

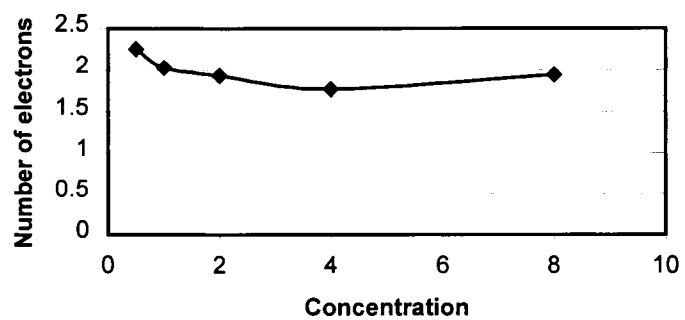


Figure 3.7: Tafel plot of the linear region of cyclic voltammogram of 13.

3.5.2 Cyclic voltammetric studies of $[(\text{dtc})\text{Ni}(\mu_2\text{-SC}_6\text{H}_4\text{NC}(\text{H})\text{C}_6\text{H}_4\text{OC}_n\text{H}_{2n+1})]_2$ (22 - 26)

Unlike the cyclopentadienylnickel(II) μ_2 -thiolato complexes, the diethyldithiocarbamate (dtc) complexes showed different electrochemical behaviour. The (dtc)Ni complexes showed only one well-defined oxidation peak when sweeping in the cathodic direction and had some ill-defined reduction peaks in the anodic direction. The cyclic voltammogram of complex 17 is shown in Figure 3.8. Here an oxidation peak was observed at *ca.* 1080 mV, with a shoulder at *ca.* 629 mV. The reduction peaks were at *ca.* 123 mV and -438 mV but the potentials of these peaks were depended on the scan rates. At higher scan rates (500 mV/s) the potentials shifted to lower values as compared to when the scan rates were low (100 mV/s). Table 3.7 list the electrochemical data for the (dtc)Ni complexes studied.

The irreversibility of the redox couples in the dtc complexes points to a possibility that a chemical step follows the electrochemical process, an EC mechanism. In fact, in a series of metal dtc complexes of Pd and Pt, it was shown that the oxidized species rapidly decomposed according to the process⁴¹: $\text{Pt}(\text{dtc})_3^+ \longrightarrow \text{Pt}(\text{dtc})_3^- \longrightarrow \text{Pt}(\text{dtc})_2 + \text{dtc}^-$.⁴¹ Bowmaker *et. al.* have studied a series of nickel(II) bis(dialkyldithiocarbamate) complexes, $\text{Ni}(\text{R}_2\text{NCS}_2)_2$, and found that at best the complexes exhibit a quasi-reversible one-electron redox behaviour.⁴² In the complexes studied by Bowmaker the peak current ratios of the reverse to the forward scans varies from 0.77 to 0.94 for scan rates in the range of 50 to 200 $\text{mV}\cdot\text{s}^{-1}$. Thus the reversibility increased on increasing the scan rate, a diagnostic feature of an irreversible process. They reasoned that the behaviour was due to the species that was initially formed in the electrochemical process changing to some other form or decomposing to products that are not reoxidised at the same potential as the original species. Analysis of the variation in current ratios to scan rates showed that the electrochemical process was followed by a first order chemical process or EC mechanism. We propose that the lack of reversibility in the dtc complexes was due to a chemical process that rapidly followed the electrochemical process. Other nickel

bidentate sulfur complexes like $\text{Ni}(\text{bdt})_2$ ($\text{bdt} = 1,2\text{-benzenedithiolate}$) also show quasi-reversible or irreversible redox behaviour.⁴³

668

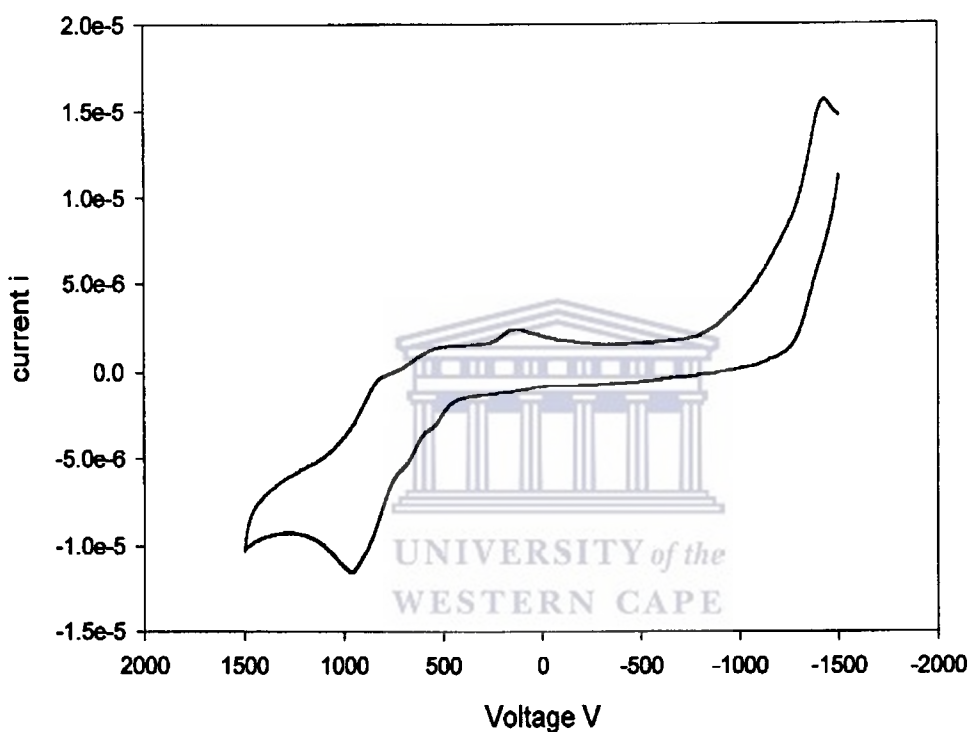


Figure 3.8: Cyclic voltammogram for complex 17.

Table 3.7: Electrochemical parameters for complexes 17 - 21.

Complex (n)	Oxidation (mV)	Reduction (mV)
$(\text{dtc})_2\text{Ni}$	+930	+150
21 (4)	+933	+123
20 (6)	+629, +1080	+123
19 (10)	+650, +1065	-
18 (14)	+1067	+154
17 (16)	+889	+155

3.6 Probing mesogenic behaviour of representative complexes.

Two techniques were used to probe liquid crystal properties of the complexes described in chapter 3. The techniques used were DSC and hotstage optical microscopy to obtain transition temperatures and mesophase textures respectively.

3.6.1 Thermal studies of cyclopentadienylnickel(II) complexes.

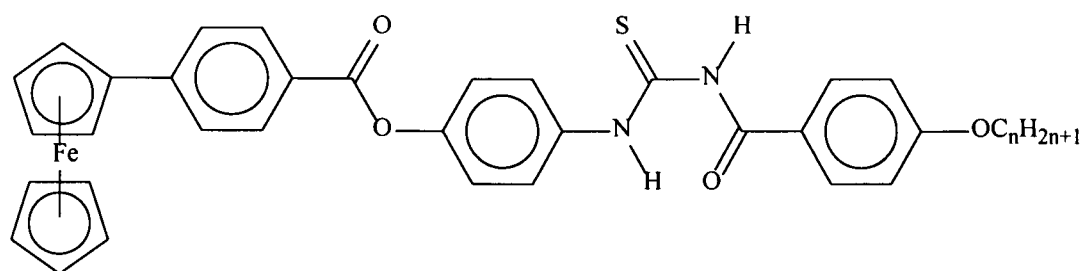
The thermal and liquid crystal properties of $[\text{CpNi}(\mu_2\text{-SC}_6\text{H}_4\text{NC(H)C}_6\text{H}_4\text{OC}_n\text{H}_{2n+1})]_2$ ($n = 4, 14$ and 16) were investigated by a combination of differential scanning calorimetry (DSC) and polarised optical microscope (POM).

Thermal gravimetric analysis (TGA) showed that the complexes decomposed at temperatures above $180\text{ }^\circ\text{C}$. This is indicated by mass losses in the thermograms of complexes **15**, **13** and **12**. The mass loss was accompanied by an exothermic peak, which was centred at $190\text{ }^\circ\text{C}$, which indicated the position of the decomposition event. DSC showed that complex **15** has only one endothermic peak corresponding to melting followed immediately by an exotherm indicative of decomposition of the complex. Thus complex **15** decomposed on melting and as such could not be expected to show any mesogenic behaviour. On the other hand complexes **12** and **13** showed multiple endothermic events before the onset of decomposition (indicated by mass loss and an exothermic peak). For example complex **13** showed two prominent endothermic peaks and two smaller ones (Fig. 3.9). Figure 3.9(a) represents the DSC on first heating of the sample, which gives four endothermic peaks. Figure 3.9(b) represents the thermogram on cooling the sample after first heating. There were no exotherms observed, though the reverse process was expected to release heat if the first heating cycle gave endothermic peaks. Figure 3.9(c) represents the thermogram when the sample was heated a second time. The thermogram of the second heating though does not have the same shape as (a); indicating that the mesomorphism in **13** might not be stable. The large peaks centered at $86.3\text{ }^\circ\text{C}$ and $116.1\text{ }^\circ\text{C}$ with smaller peaks at $91.0\text{ }^\circ\text{C}$ and $122.2\text{ }^\circ\text{C}$. Complex **12** on the

other hand had two endothermic peaks at 86.0 °C and 117.1 °C. The multiple endotherms in the two complexes are indicative of mesogenic behaviour.⁴⁴ The first endothermic peak corresponds to melting of the solid to a liquid crystalline phase, with a clearing point at 129 °C and 117 °C for **13** and **12** respectively into isotropic states. Since thermal analytical methods could not give the nature of the mesophases, optical experiments were performed in order to elucidate the type of mesophases that were formed.

The high melting point in complex **15** is attributed to its short flexible chain and longer rigid core. In fact the compound decomposed before any melting could be observed. In contrast complexes with longer chains melted well before the onset of decomposition. The behaviour shows how the length of the flexible chain affects thermal behaviour and stability of the nickel complexes.

Multiple endothermic events might represent transitions from one crystalline state to another crystalline state, a C to C₁ state, which occur when the substance exist in different molecular packing in the solid state at different temperatures.⁴⁵ Thus the solid will be polymorphic. This is true, especially for complex **12**, because complexes with longer chains tend to exhibit crystal-crystal transitions as opposed to those with shorter chains. For example, in the work reported by Seshadri and Haupt, the complex with n = 18 (Scheme 3.3) showed crystal-crystal transformation, while those with n = 8, 12 and 16 did not show any crystal-crystal transformation. This crystal-crystal transformation could



(n = 8, 12, 16, 18)

Scheme 3.3

be ruled out because liquid crystalline textures (Fig. 3.10) were observed after annealing as discussed below. Chiara-Aversa *et. al.*⁴⁶ have also come to the same conclusion when they observed two endothermic events in their DSC analysis and had difficulties in observing any optical textures. They could only observe some evidence of birefringent texture on cooling and as such could not identify the mesophase type.⁴⁶ On the basis of the molecular structures of their complexes and with comparison with similar molecules they concluded that their complexes gave columnar mesophases. Following the same line of reasoning, based on the molecular structures of complexes **12** and **13**, and comparing them with the 1,3-ferrocenomesogens of Imrie and Deschenaux,⁴⁷ coupled with the observation of textures on the melt after heating with the gas burner, it could be concluded the complexes exhibit liquid crystalline properties. Unequivocal characterisation of the mesophase requires the use of X-ray scattering techniques, which has not being used in our present study.

For both complexes (**12** and **13**) no endothermic peaks were observed on cooling (Figure 3.9). The observation could mean that the mesophase is captured in a glassy state.⁴⁵ On heating such a glassy state an exothermic peak is usually observed corresponding to cold crystallisation followed by an endothermic peak for mesophase-isotropic transition.⁴⁵ In complexes **12** and **13**, no endothermic peak was observed during the cooling, but on second cycle heating there was an exothermic peak at 56 °C followed by an endothermic peak at 110 °C. When this happens the 1st and 2nd thermograms are not the same, as the phase sequence is not the same. This scenario is similar to the one observed by Seshandri and Haupt.⁴⁵ Imrie *et. al.* also observed different phase sequence for their ferrocenomesogens.^{47a} To further confirm the presence of a glassy state on cooling, a glass transition was observed at *ca.* 30 °C. The glass transition was indicated by the change in baseline at about 30 °C. The behaviour is not unique as it was previously observed by Seshandri *et al.* for the ferrocenyl mesogens shown in Scheme 3.3.⁴⁵

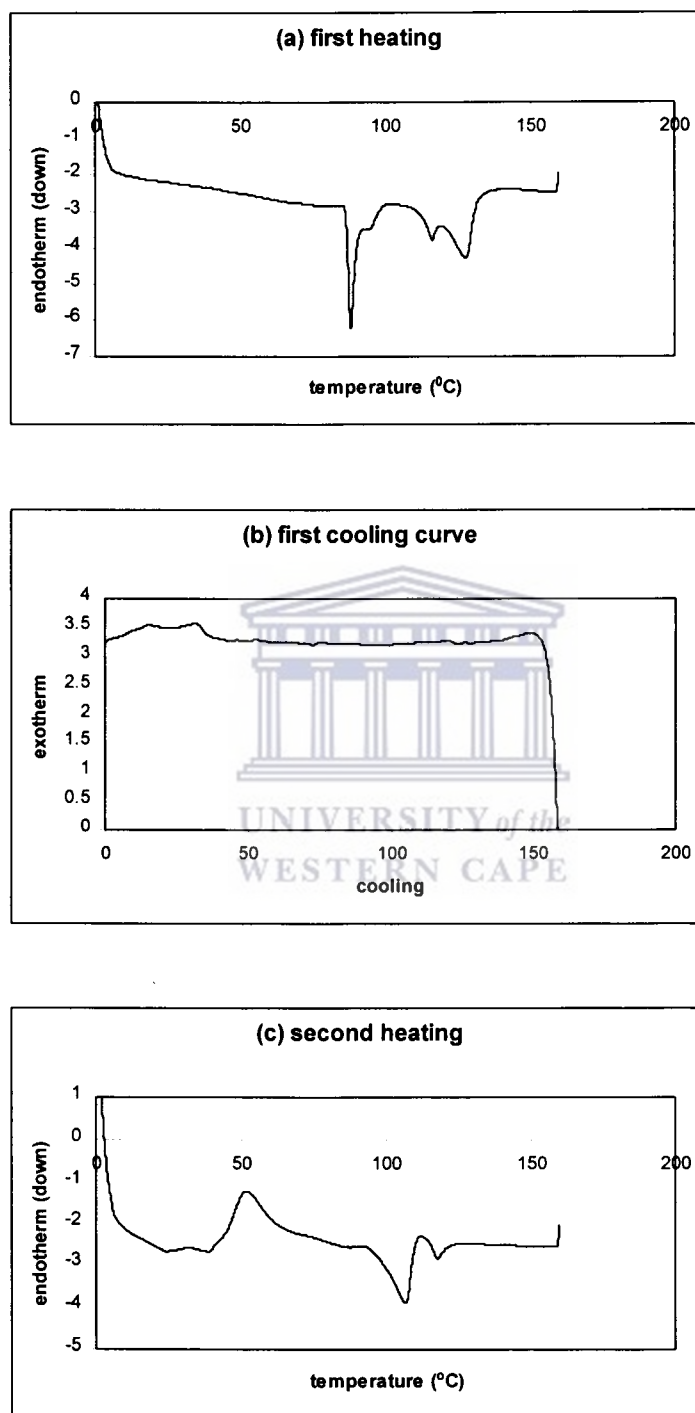


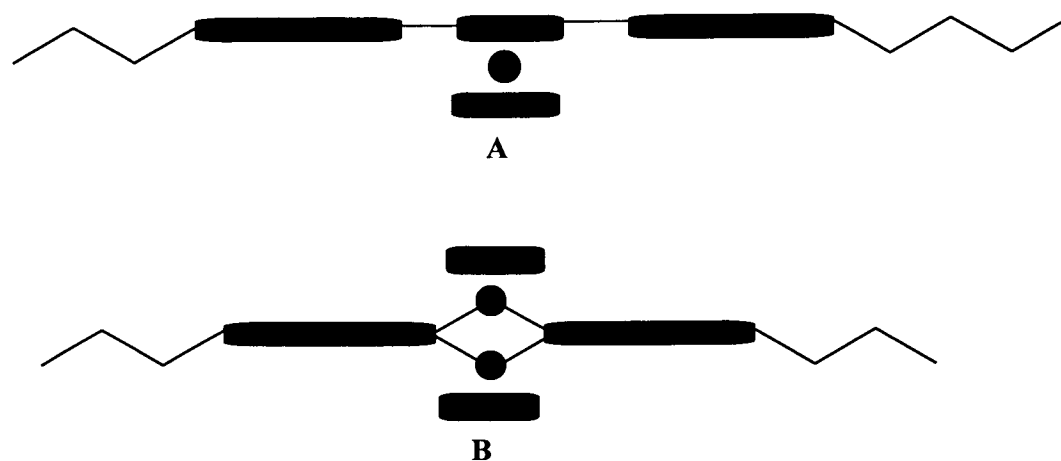
Figure 3.9: Thermograms for complex 13.

3.6.2 Optical microscopic studies of the cyclopentadienylnickel(II) complexes.

The observation of multiple endotherms for the complexes pointed to mesomorphic behaviour. Optical studies were undertaken to confirm that the complexes were mesogenic. When all the complexes were gradually heated on a Mettler hotstage and observed through a microscope, no visible textures were observed. Visible textures could however be observed after rapid heating of the sample followed by annealing (Figure 3.10). The complexes treated in this way showed columnar-like mesophase textures. It was difficult to identify which liquid crystalline phase the complexes exhibited. This was caused by the indistinctiveness of the textures.

The generation of characteristic textures is not always possible, sometimes transitions between the phases are accompanied by only slight changes, and the textures that often appear are those of the phase which resulted from cooling, the so-called paramorphosis.⁴⁸ It is generally encouraged to observe textures on cooling the sample rather than on heating.⁴⁹ This point is demonstrated here, even though the textures observed were not clear enough.

The incorporation of two cyclopentadienylnickel groups into the linear framework of the Schiff base thiolato ligand will cause steric repulsions with neighbouring molecules (Scheme 3.4). As a consequence of these steric repulsions, well-behaved mesogenic properties might be reduced. Generally it has been observed that by increasing the ratio of length (L) to width (W) better liquid crystalline behaviour is observed. For example, Deschenaux *et al.* have studied a series of 1,3-disubstituted ferrocene complexes and have found that the length to width ratios of 5 to 7 are needed for complexes to produce liquid crystalline properties.^{47b}



Scheme 3.4: Models for **A** 1,3-disubstituted ferrocene and **B** the nickel complex.

The lack of well-defined textures shows the lack of mesophase stability (Fig. 3.10). This lack of stability of the mesophases is attributed to a disruption of molecular interactions forced by the lateral substituents.

In this case the lateral group, a cyclopentadienyl ring, acts as a spacer separating the aromatic rings from each other. As a consequence, intermolecular attractions become weak and result in the loss of stable mesophases. In the case of ferrocene mesogens one of the rings forms part of the rigid core with only one lateral cyclopentadienyl ring. In the present case both cyclopentadienyl rings are laterally displaced relative to the rigid core.



Figure 3.10: Photo micrograph of texture for **13**, showing liquid crystalline texture with some homeotropic regions.

From a theoretical point of view, the complexes in Chapter 3 are expected to produce molecules with slightly bent morphology slightly resembling the 1,3-disubstituted ferrocene mesogens.

The 1,3-disubstituted ferrocene mesogens gave staggered molecular packing.⁵⁰ Due to the lateral width of the nickel complexes steric repulsion with neighbouring molecules will be increased. The high ratios of length-to-width in the nickel system as compared to that in the ferrocene system lead to more repulsive forces in the former. This repulsion leads to mesophase destabilisation; hence it was difficult to achieve stable mesophase for the nickel complexes.

In order to eliminate the undesired effects induced by the cyclopentadienyl-nickel core, intensification of the intermolecular attractions is necessary to restore stable liquid crystalline behaviour. This can be achieved by increasing the length (L) of the rigid core, i.e. by increasing the number of aromatic rings.^{47b} In order to obtain more stable mesophases in the nickel complexes two approaches could be taken: (1) increasing the number of rings in the Schiff base ligand and (2) by replacing the cyclopentadienyl ring with less bulky substituents.

In the next section 3.6.3 we have tried to address the shortcomings of the two approaches used in both chapters 2 and section 3.6.2 and 3.6.3. Thus we have replaced the trigonal geometry of complexes in chapter 2 with a more flat geometry, the square planar, and secondly we have replaced the lateral substituents with those that are in the same plane with the rigid framework of the Schiff base.

3.6.3. Thermal analysis of complexes 23, 26 and 27 and thermal optical studies of 23.

In order to assess the thermal and mesogenic properties of complexes **23**, **26** and **27**, TGA and DSC techniques were used. In addition to these techniques, thermo-optical measurements were performed on **23**, **26**, and **27**.

TGA study showed that complex **23** started to decompose at 190 °C. This was evidenced by the initial mass loss of 6-7%. This mass loss was followed by a gradual mass loss from 220 °C to 480 °C to leave a residual mass of 31%. The DSC thermogram showed that the complex had two endothermic events before the onset of decomposition. Decomposition was accompanied by an exotherm at 193 °C. The palladium pincer complex (**23**) showed two endothermic events on heating (Figure 3.11). The two endothermic events were centred at 105 °C and 131 °C. The transformations were attributed to the melting and clearing points respectively. The differences in the enthalpy changes points to the extent that the molecular packing changes during the thermal transformation. The higher the enthalpy change the higher the degree of change in molecular packing.⁵²

For the two nickel complexes, TGA showed that they decomposed above 240 °C. Complexes **26** and **27** lost 20% and 28% of their masses respectively. This was followed by a loss of 41% or 43% for **26** or **27**. The DSC of both complexes showed that they exhibited multiple endotherms. In complex **26** these were at 92 °C, 147 °C, 209 °C and 238 °C. Thermogram of complex **27** is shown in Figure 3.12. The transition at 238 °C corresponded to decomposition of the complex. The endothermic events in **27** were at slightly lower temperatures of 80 °C, 156 °C, 199 °C and 233 °C. The two complexes had three endothermic events each before the onset of decomposition. The lower transition temperatures in **27** show the disruptive effects of a longer chain. From the similarities of the thermal behaviour of **26** and **27** it follows that the two undergo similar thermal transformations.

The significance of the two or more endothermic events is that complex **23** exhibit polymorphism. In the case of **23** this could be attributed to mesophase formation, because the structure of the complex is lath-like. It was also suspected that these complexes will behave better than those in chapter 2. This is based on the premise that due to their more flat nature as compared to the trigonal geometry of complexes in chapter 2. Most metallomesogens are based on a planar or linear geometry at the metal centre.⁵¹ In order to show and unequivocally prove that the two endothermic events were due to melting and clearing points associated with mesophase formation, hotstage-optical studies were undertaken on the complex.

When complex **23** was gradually heated on a Mettler hotstage, equipped with an optical microscope, no visible textures was initially observed. Visible textures could however be observed on rapid heating of **23** followed by annealing of the sample. The observed texture is shown in Figure 3.13. The observation of the textures on cooling after rapid heating might be caused by super cooling of the sample, which captures the mesophase before the melting point is reached.⁵² In the case of bis(salicylideneaniline) copper(II), vanadium(II) and palladium(II) liquid crystalline complexes synthesized by Marcos *et al.*⁵³ once the complexes melt from the new crystals, no crystallization but solidification into a glassy state is observed. Multiple endotherms could only be observed in subsequent

heating and cooling cycles. The palladium complex (**23**) also undergoes cold crystallisation on reheating from the glassy state. This indicates that the mesophase that is formed is not very stable. The destabilisation might be due to the lateral interaction of the diethyl groups on the nitrogen atoms of the pincer ligand. The four short chain on the nitrogen atom cause steric interaction that prevents efficient molecular packing with adjacent molecules. This reduces the intermolecular attraction that is necessary for stable liquid crystalline phase formation. This effect was also observed in n-alkyl diketonate salicylaldehyde mesogens in which the short chains were said to be freely moving at the side of the rigid core disrupting both crystal packing and the lateral interactions that are necessary for the formation of mesophases.⁵⁴ The short chains have a similar effect as the cyclopentadienyl ring in analogous complexes; the effect is to make the molecule non-planar, disrupting the packing and thus bringing both melting and clearing points down.⁵⁵ Generally, though, it is said that rapid cooling of the sample from an isotropic state will induce formation of liquid crystalline phases.⁵⁶ This is essentially what was observed for complex **23**.

For the nickel complexes a different behaviour was found. Even though the complexes showed multiple endotherms on heating, closer examination of the micrographs showed that none of the complexes showed any fluid phase between the cover slips. It was observed that the samples were hard and black (probably due to decomposition) at 240 °C. This characterizes a behaviour that is usually observed for crystal-crystal transformation rather than crystal-liquid crystal transformation followed by decomposition. The difference in behaviour maybe attributed to the two rigid aromatic rings around the nickel atom. The two rings together with the rigid framework of the Schiff base ligand will tend to drastically increase the molecular anisotropy and intermolecular interactions. Because of the size of the rigid framework compared to only one flexible chain, the disruptive effect caused by the disorder in the flexible chain will be small on heating.

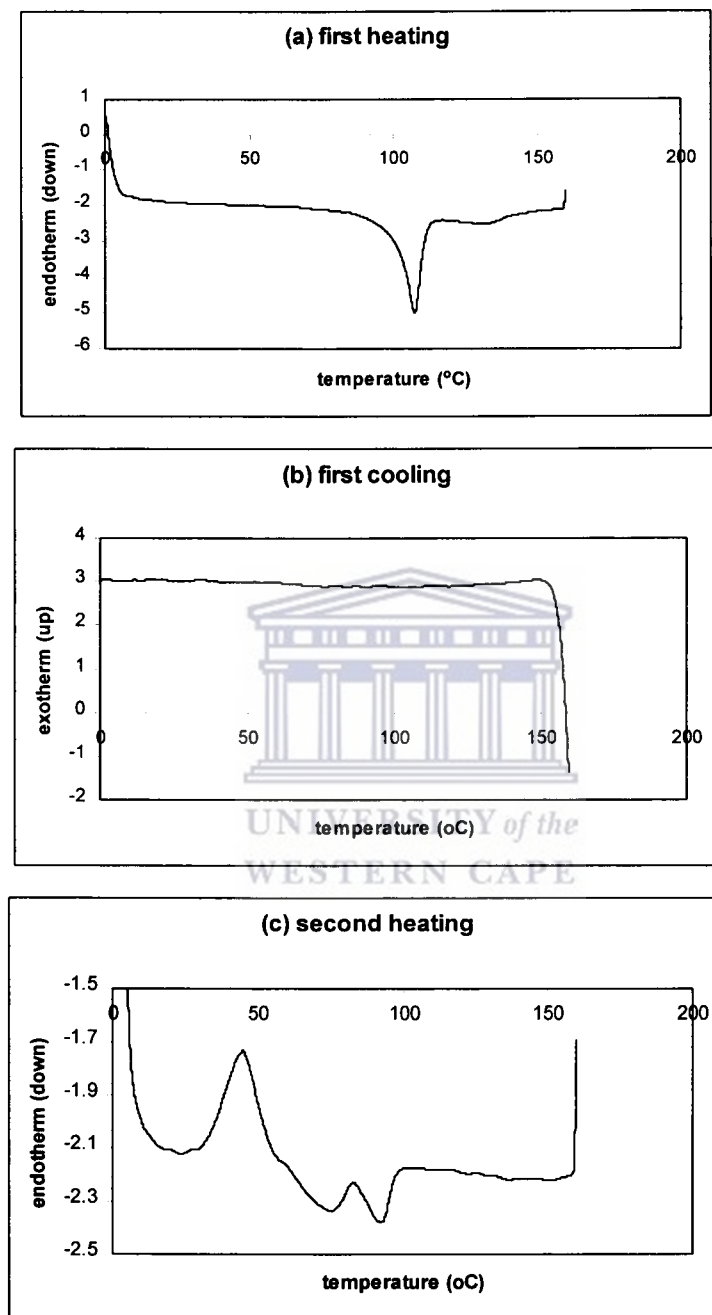


Figure 3.11: Thermograms of complex 23 before onset of decomposition.

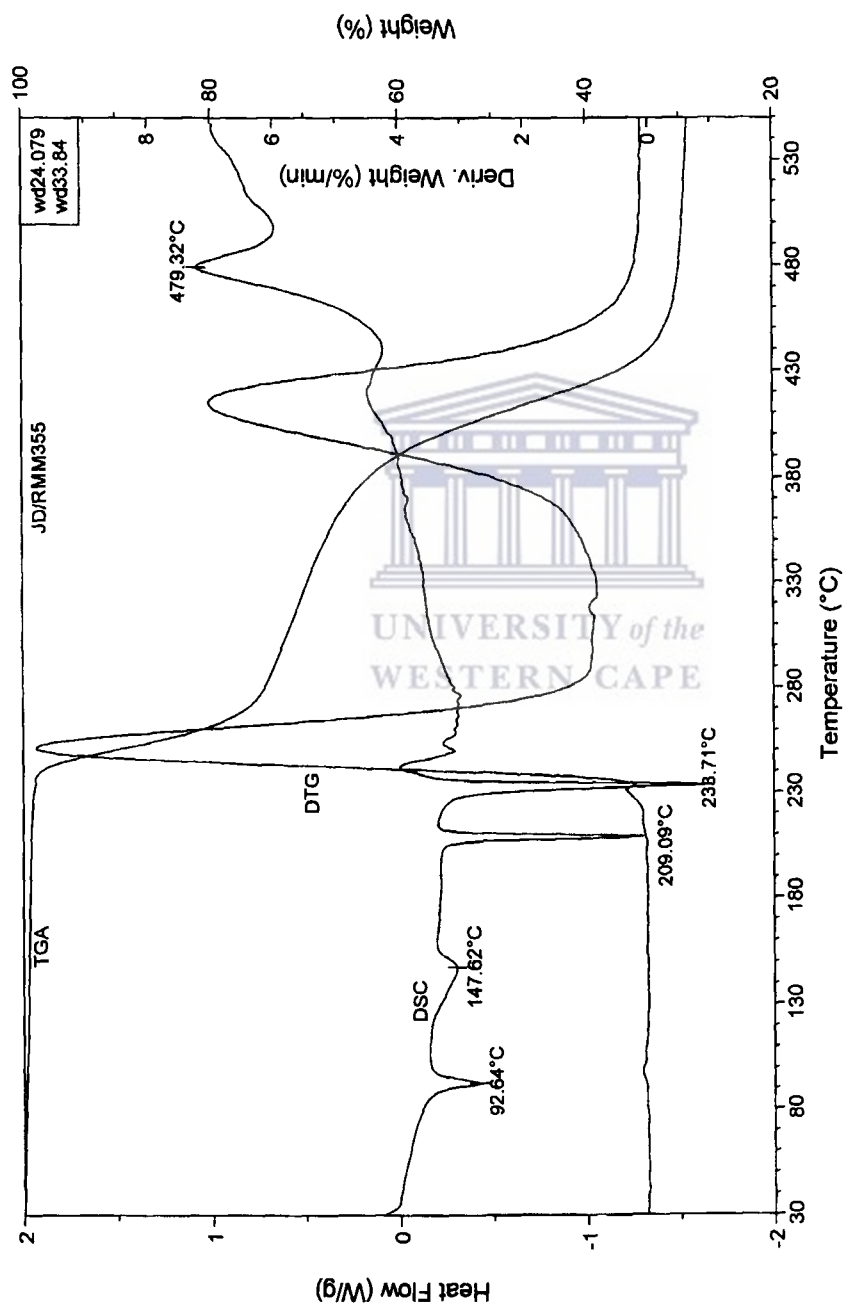
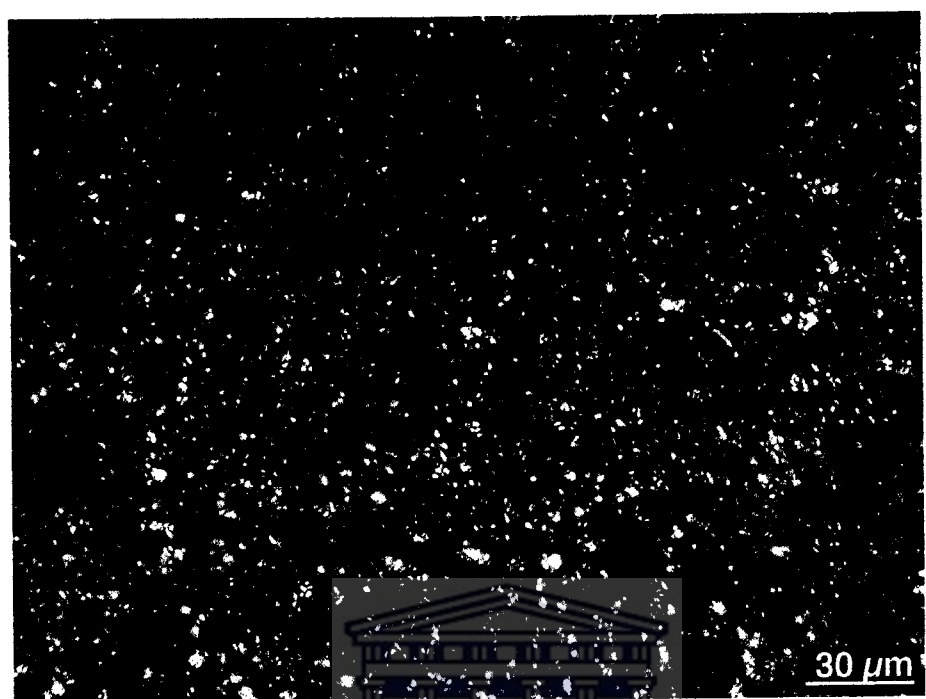
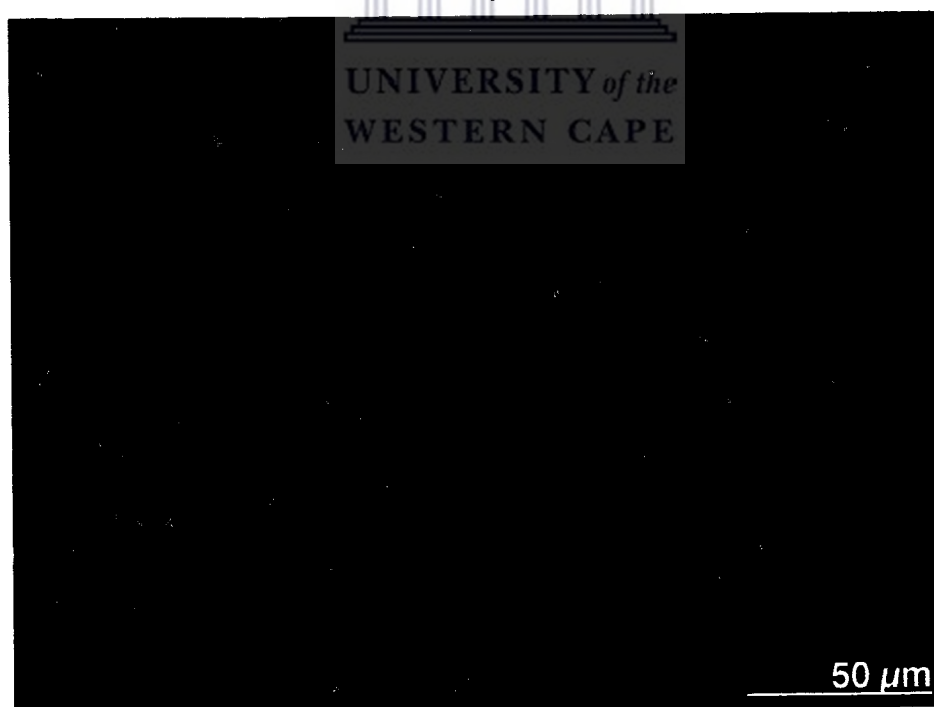


Figure 3.12: Thermograms of complex 27 with DSC showing multiple endotherms and TGA showing the decomposition.



(a)



(b)

Figure 3.13: Optical micrographs of complex **23** on cooling at 120 °C at different magnification, (a) at 30 μm and (b) 50 μm .

Mesogenic behaviour of the complexes might be induced if more than one chain is introduced into the molecule, probably at opposite ends of the molecule. Very strong intermolecular interactions are known to increase melting temperatures to above the clearing (or decomposition) temperatures.⁵⁷

3.7 Summary

The nickel(II) thiolato Schiff base complexes were synthesised in moderate yields. The two routes that were used gave comparable results, both in the yields as well as the purity of the complexes. MALDI-TOF mass spectroscopy analysis showed that the complexes were formed. The complexes all cleaved at the nickel-sulfur bond to yield molecular fragments containing one nickel atom with half the molar mass of the parent ion as the most abundant peak.

Electrochemistry showed that the cyclopentadienylnickel(II) complexes had quasi reversible one electron reactions. The diethyldithiocarbamatonickel(II) complexes had irreversible behaviour. This showed the different influences of the cyclopentadienyl ring compared to the diethyldithiocarbamato ligand in stabilising the ions formed.

Thermal studies of the complexes showed that the complexes were stable up to 180 °C. The cyclopentadienylnickel(II) complexes with longer chains showed multiple endothermic peaks indicative of mesogenic behaviour. Increasing molecular length and/or introducing planar metal cores led to formation of liquid crystalline phases. On the other hand when molecular anisotropy was drastically increased, molecular interactions resulted leading to crystal-crystal transformation and not liquid crystal phases before the complexes decomposed on melting. The textures of these phases could however not be observed when the samples were heated gradually. Visible textures could only be observed after rapid heating. The nature of the mesophases could not be assigned due to the indistinctiveness of the textures. The present study shows that there is a fine balance between anisotropic molecular design and liquid crystalline behaviour.

References

1. M. Teixeira, I. Moura, D.V. Der Vartanian, J. LeGall, H. D. Peck jr., B. H. Huynh, J. J. G. Moura, *Eurp. J. Biochem.* 1983, **130**, 481.
2. G. Fauque, H. D. Peck jr., J. J. Moura, B. H. Hugnh, Y. Berlier, D. V. Der Vartanian, M. Teixeira, A. E. Pryzybyla, P. A. Lespinat, I. Moura, J. LeGall, *FEMS Microbiol. Rev.* 1985, **55**, 299.
3. M. Teixeira, G. Fauque, I. Moura, P. A. Lespinat, Y. Berlier, B. Prickril, H. J. Peck, A. V. Xavier, J. LeGall, J. J. Moura, *J. Biochem.* 1987, **167**, 47.
4. J., Darkwa, E. Y. Osei-Twum, L. A. Litorja jr., *Polyhedron* 1999, **18**, 1115.
5. S. Babikanyisa, J. Darkwa, *Inorg. Chim. Acta* 1997, **256**, 15.
6. J. Darkwa, J. M. Frost, L. M. Koczon, *Synth. React. Inorg. Met-Org. Chem.* 1993, **23**, 509.
7. (a) A. C. Villa, A. G. Manfredotti, M. Nardelli, C. Pelizzi, *J. Chem. Soc. Chem. Commun.* 1970, 1322; (b) J. M. Andrews, D. Coucouvanis, J. P. Fackler jr., *Inorg. Chem.* 1972, **11**, 493, (c) J. P. Fackler jr., W. J. Zegarski, *J. Am. Chem. Soc.* 1973, **95**, 8566.
8. N. Baidya, B. C. Noll, M. M. Olmstead, P. K. Mascharak, *Inorg. Chem.* 1992, **31**, 2999.
9. A. M. Giroud, U. T. Muller-Westerhoff, *Mol. Cryst. Liq. Cryst.* 1977, **41**, 11.
10. K. Ohta, H. Ema, I. Yamamoto, K. Matsuzaki, *Liq. Cryst.* 1988, **3**, 1671.
11. K. Ohta, H. Ema, Y. Morizumi, T. Watanabe, T. Fujimoto, I. Yamamoto, *Liq. Cryst.* 1990, **8**, 311.
12. N. Hoshino-Miyajima, *J. Chem. Soc. Chem. Commun.* 1993, 1442.
13. R. Deschenaux, J. W. Goodby, in *Ferrocenes* (A. Togne, T. Hayashi (eds.), VCH, Weinheim 1995, ch. 9.
14. M. Ghedini, D. Pucci, F. Neve, *J. Chem. Soc. Chem. Commun.* 1996, 137.
15. B. J. Coe, C. J. Jones, J. A. McCleverty, D. W. Bruce, *Polyhedron* 1993, **12**, 45.
16. (a). D. Morales-Morales, D. W. Lee Z. Wang, C.M. Jensen, *Organometallics* 2001, **20**, 1144; (b). M. Gupta, C. Hagen, W. C. Kaska, R. Flesher, C. M. Jensen, *J. Am. Chem. Soc.* 1997, **119**, 840; (c). W.-W. Xu, G. Rossini, M. Gupta, C. M.

- Jensen, W. C. Kaska, K. Krough-Jespersen, A. S. Goldman, *J. Chem. Soc. Chem. Commun.*, 1997, 2273; (d). F. Liu, B. Pake, B. Singh, M. C. Jensen, A. S. Goldman, *J. Am. Chem. Soc.* 1999, **121**, 1.
17. M. Gupta, W. C. Kaska, C. M. Jensen. *J. Chem. Soc. Chem. Commun.*, 1997, 2083.
18. D. Morales-Morales, C. Grause, K. Kasaoka, R. Redón, R. E. Cramer, C. M. Jensen, *Inorg. Chim. Acta* 2000, **300**, 958.
19. (a) H. P. Dijkstra, M. Meijer, J. Patel, R. Kreiter, G. P. M. van Klink, M. Lutz, A. L. Spek, A. J. Canty, G. van Koten, *Organometallics* 2001, **20**, 3159; (b). F. Gorla, A. Togni, L. M. Venanzi, A. Albinati, F. Lianza, *Organometallics* 1994, **13**, 1607; (c). J. M. Langmire, X. Zhang, M. Shang, *Organometallics* 1998, **17**, 4374; (d). M. A. Stark, C. J. Richards, *Tetrahedron Lett.* 1997, **38**, 5881; (e). M. A. Stark, G. Jones, C. J. Richards, *Organometallics* 2000, **19**, 1282, (f) Y. Montoyama, H. Narusawa, h. Nishiyama, *Chem. Commun.* 1999, 131.
20. P. Espinet, C. Lorenzo, J. A. Minguel, *Inorg. Chem.* 1994, **33**, 2052.
21. (a) L. T. Reynolds, G. Wilkinson, *J. Inorg. Nucl. Chem.* 1959, **9**, 86; (b) P. C. Ellgen, C. D. Gregory, *Inorg. Chem.* 1971, **10**, 980.
22. P. L. Maxfield, *Inorg. Nucl. Chem. Lett.* 1970, **6**, 693.
23. (a) R. M. Moutloali, *M. Sc. thesis, University of the North* 1998; (b) J. Darkwa, R. M. Moutloali, T. Nyokong, *J. Organomet. Chem.* 1998, **564**, 37.
24. A. A. H. van der Zeijden, G. van Koten, R. Luijck, R. A. Nordemann, A. L. Spek, *Organometallics* 1988, **7**, 1549.
25. H. Rimml, L. M. Venanzi, *J. Organomet. Chem.* 1983, **259**, C3.
26. L. F. Lindoy, S. E. Livingstone, *Inorg. Chem.* 1968, **7**, 1149.
27. R. M. Moutloali, F. A. Nevondo, E. I. Iwouha, J. Darkwa, W. Henderson, *J. Organomet. Chem.* 2002, **656**, 262.
28. J. Errington, W. S. McDonald, B. L. Shaw, *J. Chem. Soc. Dalton Trans.* 1980, 2312.
29. N. Lucena, J. Casabó, L. Escriche, G. Sánchez-Castelló, F. Teixidor, R. Kivekäs, R. Sillanpää, *Polyhedron* 1996, **15**, 3009.

30. K. Wieghart, H. Kuppers, E. Raabe, C. Kruger, *Angew. Chem. Int. Ed. Engl.* 1986, **25**, 1101.
31. N. F. Ho, T. C. W. Mak, T. Y. Luh, *J. Chem. Soc. Dalton Trans.* 1990, 3591.
32. W. K. Schropp, *J. Inorg. Nucl. Chem.* 1962, **24**, 1688.
33. P. W. Jolly (G. Wilkinson, F. G. A. Stone, E. W. Abel eds.), *Comprehensive Organometallic Chemistry*, Pergamon Press, 1982, **6**, 189.
34. J. Darkwa, F. Bothata, *J. Organomet. Chem.* 1993, **455**, 235.
35. R. Taube, D. Steinborn, W. Hobold, *J. Organomet. Chem.* 1985, **284**, 385.
36. J. Darkwa, E. Y. Osei-Twum, L. A. Litorja jr., *Polyhedron* 1999, **18**, 1115.
37. M. Albrecht, R. A. Gossage, M. Lutz, A. L. Spek, G. van Koten, *Chem. Eur. J.* 2000, **6**, 1.
38. G. van Koten, M. Albrechts, *Angew. Chem. Int. Ed. Engl.* 2001, **40**, 3750.
39. R. Murray (A. J. Bard ed.) *Electroanalytical Chemistry*, Marcel Dekker, New York, 1984, 191.
40. D. Frisch, M. K. Lloyd, J. A. McCleverty, D. Seddon, *J. Chem. Soc. Dalton Trans.* 1973, 2268.
41. J. G. M. Van Der Linden, A. H. Dix, *Inorg. Chim. Acta* 1979, 65.
42. G. A. Bowmaker, P. D. W. Boyd, G. K. Campbell, J. M. Hope, R. L. Martin, *Inorg. Chem.* 1982, **21**, 1152.
43. J.-L. Xie, X.-M. Ren, C. He, Y. Song, C.-Y. Duan, S. Gao, Q.-J. Meng, *Polyhedron* 2003, **22**, 299.
44. J. M. G. Cowie, *Polymers: Chemistry and Physics of Modern Materials*, 2nd edition.
45. T. Seshadri, H.-J. Haupt, *J. Mater. Chem.* 1998, **8**, 1345.
46. M. Chiava Aversa, P. Bonaccorsi, D. W. Bruce, F. Caruso, P. Giannetto, S. Lanza, S. Morroni, *Inorg. Chim. Acta* 1997, 256, 235.
47. (a) C. Imrie, C. Loubster, P. Engelbrecht, C. W. McClelland, Y. Zheng, *J. Organomet. Chem.* 2003, **665**, 48, (b) R. Deschenaux, I. Kosztics, J.-L. Marendaz, *Chimia*, 1993, **47**, 206.
48. D. Demus. *Liquid Crystals*, Academic Press 1983, **6**, 1.
49. D. W. Bruce (J. D. Woolins ed.) in *Inorganic Experiments VCH*, p 271.

50. R. Deschenaux, J. W. Goodby (A. Togni, T. Hayashi eds.) in *Ferrocenes*, VCH, Weinheim, 1995.
51. J. M. Elliot, J. R. Chipperfield, S. Clark, E. Sinn, *Inorg. Chem. Commun.* 2002, **5**, 99.
52. P. J. Collings, M. Hird, *Introduction to Liquid Crystals, Physics and Chemistry*, 1997, p 43.
53. R. Iglesias, M. Marcos, J. L. Serrano, T. Sierra, M. A. Perez-Jubindo, *Chem. Mater.* 1996, **8**, 2611.
54. G. W. V. Cave, D. P. Lydon, J. P. Rourke, *J. Organomet. Chem.* 1998, **555**, 81.
55. D. P. Lydon, G. W. V. Cave, J. P. Rourke, *Mater. Chem.* 1997, **7**, 403.
56. D. P. Lydon, J. P. Rourke, *J. Chem. Soc. Chem. Commun.* 1997, 1741.



Chapter 4

Bimetallic nickel complexes with bridging dithiolato ligands: Synthesis, mass spectral characterisation and electrochemistry

4.1.	General introduction	154
4.2.	An overview on molecular wires	156
4.3.	How to gauge the ability of molecular wire to conduct	159
4.4.	Measuring electronic conducting properties of single molecule.	160
	4.4.1 The use of scanning tunneling microscope to probe conductance	160
	4.4.2 Conductance of a single molecule junction between two metal contacts	161
	4.4.3 The use of cyclic voltammetry (CV) to measure conductance of molecular wires	167
4.5.	Bimetallic complexes as nonlinear optical materials	171
4.6.	Background to the work reported in this chapter	173
4.7.	Experimental section	175
4.8.	Results and discussion	179
4.8.1.	Synthesis and characterisation of ligands	179
	4.8.2 Synthesis and characterisation of complexes	181
	4.8.3 Mass spectrometric studies of complexes	186
	4.8.3.1 Fast atom bombardment mass spectroscopic study	186
	4.8.3.2 The electrospray mass spectrometry study	190
	4.8.3.3 MALDI-TOF mass spectral analysis	193
	4.8.3.4 Electrochemical studies.	196
4.9	Summary	202
4.10.	References	203

4.1. General introduction

Complexes containing unsaturated ligand such as vinyl or an aromatic group constitute an important class of compounds; specifically as building blocks for the synthesis of di- or polynuclear complexes linked by π -conjugated system. This is because unsaturated systems can provide a facile pathway for electron delocalisation between metal centres.¹ Dinuclear complexes in which a strong electronic interaction between redox active metals that afford a stable mixed valence state are of interest because of: (i) the fundamental study of electron transfer under carefully controlled conditions and (ii) development of “molecular wires” in which electrons can be transported over long distances for possible use in molecular scale electronic devices.² Such dinuclear complexes could also help to rationalise the factors that affect conduction properties like: (i) the nature of the transition metal atom and its coordination, (ii) the conjugation of the π -electron system for the bridging ligand and (iii) the nature of the ligand field.³ Polynuclear organometallic complexes are of interest as catalyst precursors, models for metal surfaces with chemisorbed small molecules and biological models like large iron-sulfur proteins.⁴ In many cases the molecules that are probed for their conducting properties have a terminal sulfur group, which acts like an alligator clip to bind to electrodes which are usually gold surfaces. In such cases the molecules are α,ω -dithiol substituted oligomers.⁵

Mixed valence complexes were initially treated as models for intramolecular electron transfer but are now regarded as prototypes for molecular switches and wires.⁶ From the late 1970's, organometallic complexes have generated a series of new electrodes by modification of the electrode surfaces with monolayers⁷ or electroactive polymeric materials⁸, some of which have found applications in electroanalytical techniques and probes. Thus the use of electrochemical or electroanalytical techniques to screen bimetallic molecules is widespread. In fact, the use of electrochemical methods to study intramolecular electron transfer dates back to the work of Taube *et al.*⁹ and even further for the study of mechanisms of electron transfer.¹⁰ Electrochemical methods offer specific advantages over the more sophisticated methods based on flash photolysis in that the experiments are simple, and more importantly, the methods are essentially insensitive to intermolecular electron transfer. This is due to the small probability of having a reduced site of one molecule in close proximity to the oxidised site of a different

molecule.^{3b} The overall electrochemical oxidation and reduction of organic and organometallic molecules often consist of a complex sequence of electrochemical and chemical steps. The electrochemical step is defined as a step that involves the loss or gain of an electron at the electrode surface interface, whilst the chemical step is taken as surface chemical reactions involving adsorbed species or it takes place in solution among diffusing reactants.¹¹

The major goal of synthesising metal compounds that show electronic communication between metal centres is to assemble subunits containing transition metals by suitable molecular or supramolecular techniques in order to systematically tune their physical properties. These physical properties include optical or magnetical properties, redox behaviour or their use as catalytically active compounds.¹² In our contribution to this field, we have synthesised and studied the electrochemistry of cyclopentadienylnickel(II) bimetallic complexes. The complexes show electronic communication between the metal centres. The next section is devoted to the background of current research into the field of molecular wires, and the basic concepts and terminologies that are used.

4.2. An overview of molecular wires.

As the limit of silicon based electronics is rapidly approached, researchers are looking at other functional devices that are faster and cheaper than conventional electronics, because they will be built with molecules as electronic components rather than big pieces of doped silicon and metal wires. This is also driven by the need to miniaturise various electronic components. The current industrial approach is to develop new materials with great processability and to scale down the electronic circuitry using new technologies like nanolithography. However with the ultimate limit ever reachable for reduction being the molecular level, the field of molecular wires is to tackle the problem of miniaturisation by starting from the molecular building blocks. It is tempting to suggest that, as the resolution of surface patterning techniques such as electron beam lithography improves, conventional transistors could simply be made smaller. Unfortunately the electronic properties of solids and solid-solid interfaces are inherently different on the nanometer

scale or level.¹³ Thus it is evident that if electronic integrated circuitry is to reach its ultimate potential, radical changes in the way transistors are made and operated will be necessary, hence the approach from the molecular route. With the progress in synthetic organic methodology and the increasing availability of advanced analytical methods for the purification and characterisation of very large molecules, monodisperse (that is, with the same number of monomer units) linear π -conjugated oligomers have recently reached the 10 nm length mark, which is about the current resolution limit for microstructure manufacturing by the state of the art lithographic techniques.¹⁴ This so-called bottom-up fabrication methods aim to assemble and integrate molecular components exhibiting specific functions into electronic devices that are of the orders of magnitude smaller than anything that can be fabricated using state of the art lithographic techniques. This field is said to constitute the cradle of big innovations in the future.¹⁵

The concept of constructing a molecular computer based solely on organic or organometallic molecules as an ultimate system in terms of information storage density and speed still remains a vigorously discussed and controversial issue.¹⁶ It is generally accepted that future nanoelectronic and nanophotonic processes will likely require π -conjugated molecular rods of defined lengths as key components for ultra dense and ultra fast information transportation, processing and storage.¹⁷ Fundamental to this bottom up approach is the ability to control electron/hole transport across the molecular components. Organic molecules containing redox centres support resonant tunneling and display promising functional behaviour as molecular wires. Molecular wires are among the key components in the emerging field of molecular electronics. In their simplest form, molecular wires can be viewed as conjugated molecules that form one dimensional electronic conductors to interconnect such proposed molecular devices as single electron transistors, electron turnstiles, molecular switches and chemical sensors.¹⁸ A molecular wire is thus defined as a “one dimensional molecule allowing a through-bridge exchange of an electron or hole between its remote ends or terminal groups, themselves able to exchange electrons or holes with the outside world”.¹⁹ Thus such compounds must possess two redox active termini.^{2b} Even if very promising, the molecular approach also has its uncertainties and problems. First, it constitutes a tremendous synthetic challenge

to build molecular wires of increasing length, controlling the shape of the molecules at each stage of their synthesis and the chemical purity of the final material. Another point that is not yet clear is whether these molecular wires or conductors will behave in a similar manner as their bulk conductors or follow the same physical laws, or will they exhibit peculiarities related to their molecular nature. Current theoretical and experimental studies shed light on this point.²⁰

Many molecular wire candidates have been reported, including both organic and organometallic compounds by Tour in 1994.²¹ Organometallic or metal containing conductors are very appealing over organic ones owing to the possibility of fine tuning the electronic properties of the wire, e.g. by variation of the ancillary ligands present on the metal centres or by change in their oxidation state.²²

Organometallic binuclear or polynuclear metal complexes in which the metals are linked by unsaturated bridging ligands are of particular interest with regard to the study of electron transfer in mixed valence systems.²³ The archetypal example²³ is the Creutz-Taube ion, $[(\text{NH}_3)_5\text{Ru}(\text{NC}_4\text{H}_4\text{N})\text{Ru}(\text{NH}_3)_5]^{5+}$, whose theoretical study has received a great deal of attention and thereby contributed considerably to the understanding of electron transfer theory.²⁴ Studies on extended Creutz-Taube type complexes with up to five trans double bonds between the pyridyl groups have been done in order to gauge or determine the effects of the length of the molecular wire on electron transfer and metal-metal interactions. These studies showed that electronic interaction between the metal centres decreases exponentially with increasing distances between the metal centres.²⁵ Another variation to increasing the length of the molecular wires is changing the type of connecting groups between aromatic fragments or organometallic fragments. As such a variety of linkers such as alkenes, alkynes, imine and azo have been used.

Binuclear complexes, which can be viewed as representative for their polymeric analogues, in which strong electronic interaction between redox active metal centres affords a stable mixed valence state are gradually helping in understanding: (i) the fundamental study of electron transfer under carefully controlled conditions and (ii) the

development of the above mentioned molecular wires and (iii) as nonlinear optical materials.

To achieve a strong electronic interaction it has been found that it is necessary to match the energy of the metal based redox orbitals with an appropriate bridging ligand orbital, such that delocalisation in the mixed valence state can be optimised by super exchange process involving the bridging ligand by either a hole transfer through the HOMO of the bridging ligand (Figure 4.1a) or by electron transfer through the LUMO of the bridging ligand (Figure 4.1b).²⁶

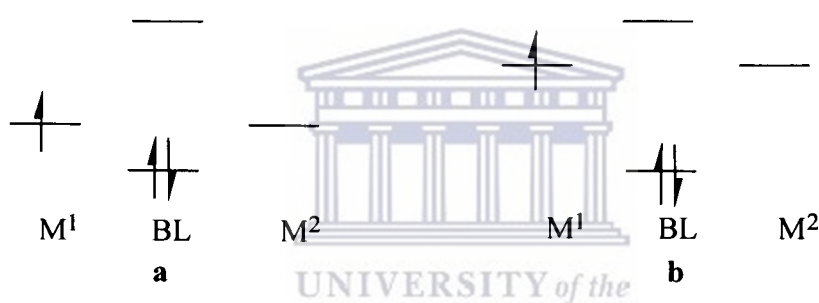


Figure 4.1: Orbital diagrams showing the situations necessary for delocalisation of metal based mixed-valence states by (a) hole transfer through the HOMO of the bridging ligand and (b) electron transfer through the LUMO of the bridging ligand.²⁶

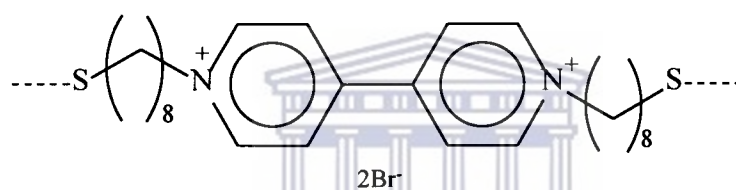
4.3. How to gauge the ability of a molecular wire to conduct.

Three ways are presently used to measure the ability of molecular wires to conduct. These are: (i) direct measurement of the bulk conductivity of a material in an amorphous state or in the crystalline state. This approach is usually used for polymers.^{27, 28} (ii) The second one uses cyclic voltammetry (CV) to look at the electronic interaction between the redox active termini. If odd-electron states are stable, near infrared (NIR) spectrometry and electroabsorption spectroscopy (Stark effect) are usually used to obtain additional information.²⁹ (iii) Finally a direct measurement of the conductivity of a single molecule or crystal is done. This is by positioning the single molecule or crystal in a nanojunction and then using conventional techniques to measure its conductivity.³⁰

4.4 Measuring electronic conducting properties of a single molecule.

4.4.1 The use of scanning tunneling microscope to probe conductance.

Schiffirin *et al.* has used scanning tunneling microscopy measurements to show that organic molecules containing redox centres can be used to attach metal nanoparticles to electrode surfaces and so control the electron transport between them. In this study the organic molecules consisted of a central, reversibly reducible bipyridium moiety with terminal polymethylene chains terminated by thiol groups.



An example of a molecule used as a redox gate.

UNIVERSITY of the
WESTERN CAPE

The redox group (“redox gate”) forms the backbone of a bifunctional ligand that attaches a gold nanoparticle to a gold substrate (usually a gold electrode). The electron or hole that is injected into the redox centre is controlled using the potential applied between the substrate and a counter electrode. The resulting change in barrier transparency can be used to control electron tunneling between the nanoparticle and the substrate. The tip of the scanning tunneling microscope (STM) is positioned above the nanoparticle, and used to monitor electron tunneling. A schematic representation of the operation of a nanoscopic electronic switch is illustrated in Figure 4.2. Figure 4.2 (B) shows the energy levels corresponding to the conduction bands of the substrate and the scanning tunneling microscope tip (S, gold substrate; T STM tip) and the lowest unoccupied molecular orbital and the highest occupied molecular orbital of the bipyridium moiety. Three redox states are: bipy^{2+} (a), bipy^{+} (b) and bipy^0 (c). When the redox gate molecule is in its bipy^{+} reduced state (centre) the device shows a high redox barrier transparency.³¹

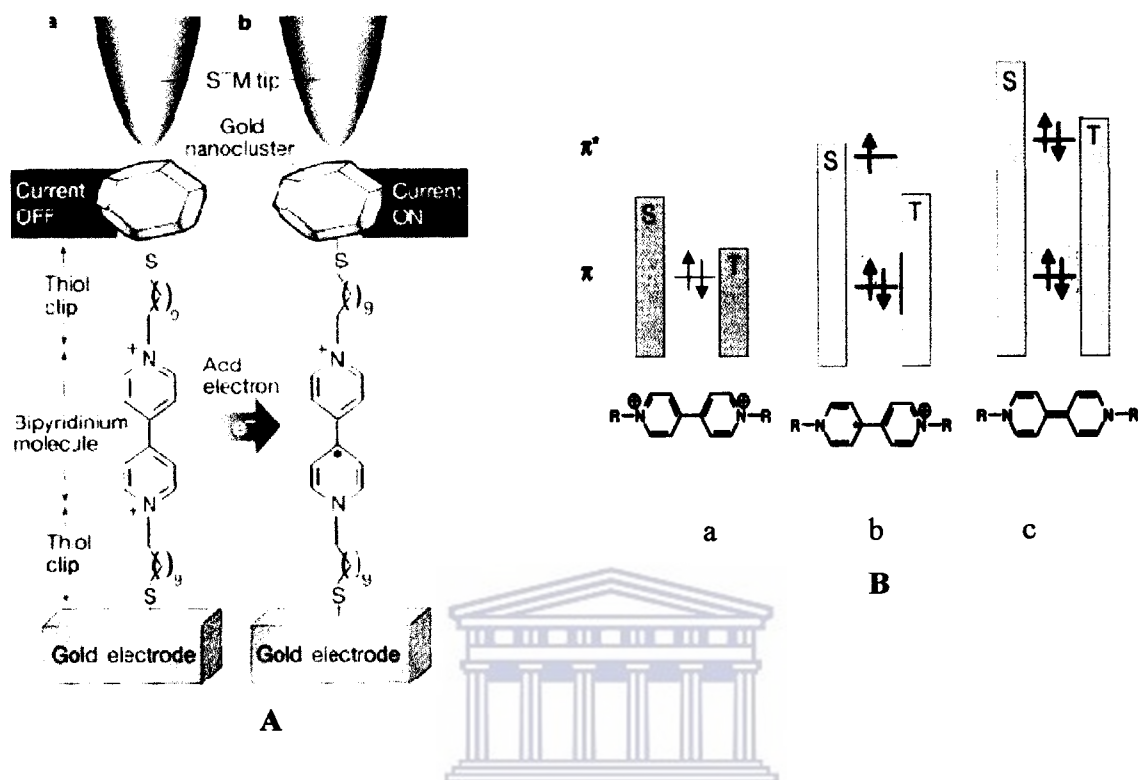


Figure 4.2: (A) is an electronic switch that works by changing the chemical state of a molecule. (B) is a schematic illustration of a nanoscopic electronic switch in A.³¹

4.4.2 Conductance of a single molecule junction between two metal contacts.

Tour *et al.* have used a molecule that contains a nitroamine redox centre (2'-amino-4-ethynylphenyl-4'-ethynyl-5'-nitro-1-benzenethiol) in the active self-assembled monolayer in an electronic device.³² Electronic measurements were performed in a nanostructure that had a metal tip contact, a self-assembled monolayer (SAM) active region, and a metal bottom contact. This configuration is shown Figure 4.3.

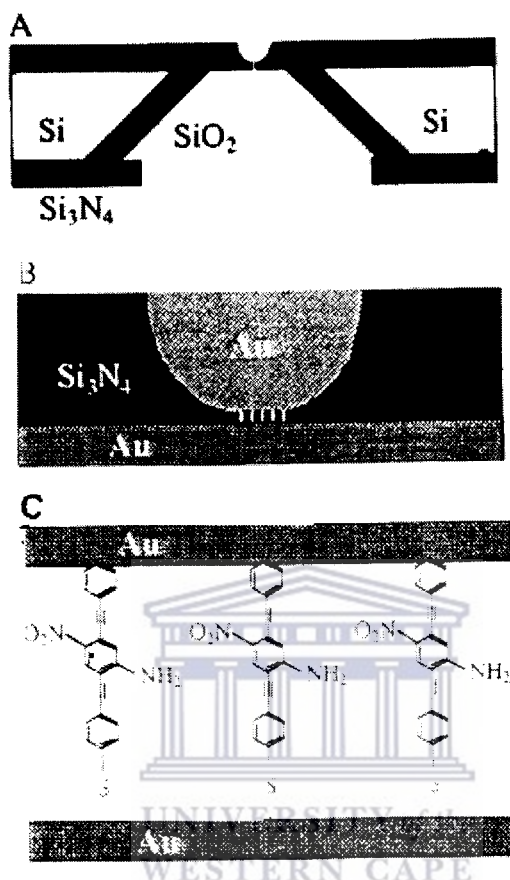
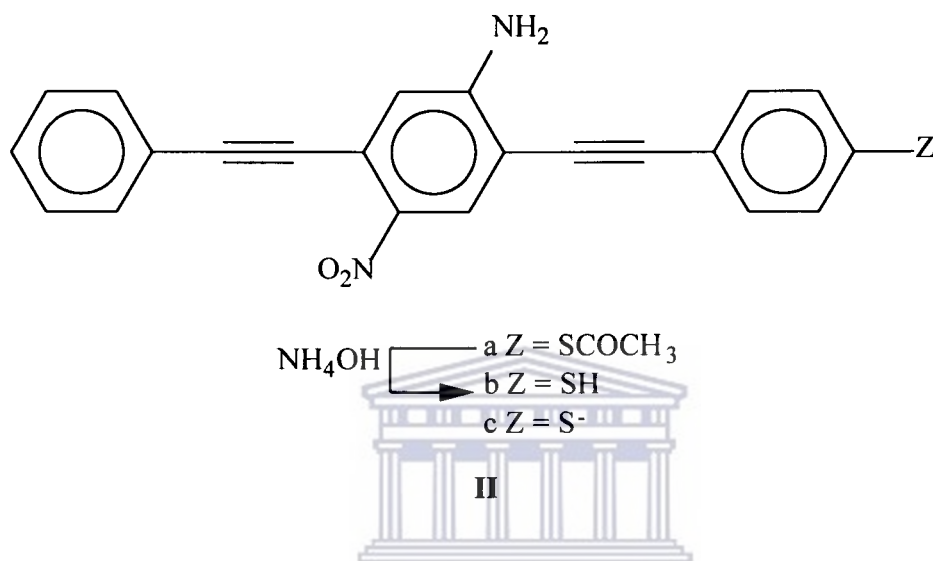


Figure 4.3: Schematics of the device fabrication. (A) Cross section of a silicon wafer with a nanopore etched through a suspended silicon nitride membrane. (B) Au-SAM-Au junction in the pore area. (C) Blowup of (B) with **IIc** sandwiched in the junction membrane.^{32a}

A series of controlled experiments were performed with alkanethiol-derived SAMs, silicon nitride membranes without pores, and membranes with pores but without 2'-amino-4-ethynylphenyl-4-ethynyl-5'-nitro-1-benzenethiol molecules. In both instances when Au-alkanethiol-Au junctions or Au-silicon nitride membranes-Au junctions were used, the experiment showed that the current levels observed were at the noise limit of the apparatus (< 1 pA) used for both bias polarities at room and lower temperatures. The result shows that there was no conduction through the junction. In another experiment, a device containing an SAM of conjugated molecules similar to **IIc** but not bearing the nitroamine functionalities was fabricated and measured in nearly identical conditions and did not exhibit any negative differential resistance behaviour (NDR). The Au-**IIc**-Au

device at 60K showed peak current density of 53 Acm^{-2} , NDR of $< -380 \mu\text{ohm.cm}^2$ and the peak-to-valley ratio (PVR) of 1030:1. This clearly shows that the nitroamine device exhibits a robust and large NDR, both in the positive and negative bias voltages.



A candidate mechanism for the NDR in a two-step reduction process that modifies charge transport through the molecule was proposed (Figure 4.4). In this mechanism as the voltage is increased, the molecule initially undergoes a one-electron reduction, thereby supplying a charge carrier for electron flow through the system. A further increase in voltage causes a second electron reduction with subsequent blocking of current. The width of current/voltage $2(\text{V})$ ($\sim 0.70\text{V}$) correlates well with the difference between the one electron and two electron peak reduction potentials ($E_{p2} - E_{p1} = \Delta E_p = 0.63\text{V}$ and 0.68V for compounds with end groups of SCH_3 and H respectively). The NDR response/behaviour was absent in the control systems.

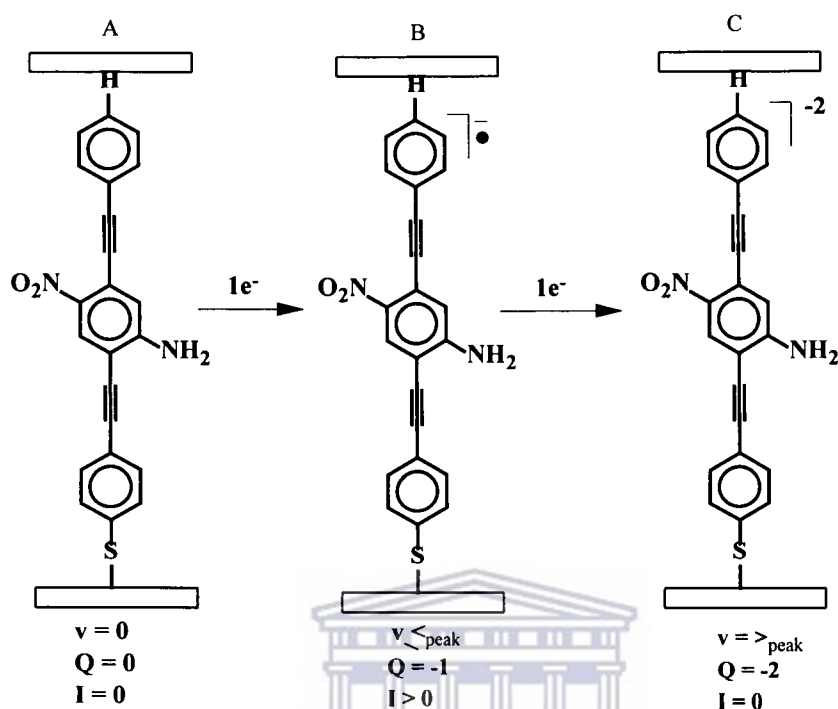


Figure 4.4: Potential mechanism for the NDR effect. As voltage is applied, the molecules in the SAM (A) undergo a one-electron reduction to form the radical anion (B) that provides a conductive state. Further increase of the voltage causes another one-electron reduction to form the dianion insulating state (C). Q is the charge.^{32a}

Tour *et al.* have also performed conductance measurements in the configuration of a single molecule between metallic contacts. Specifically they have used benzene-1,4-dithiolate connected between two stable, proximal, metallic gold contacts at room temperature. Experiments were conducted at room temperature with a mechanically controllable break junction (Figure 4.5).

In the experiment a notched metal wire was glued onto a flexible substrate and was fractured by bending the substrate. It was shown by the quantisation of current that the metal contacts were atomically sharp. The 1,4-benzenedithiol was adsorbed from a 1mM

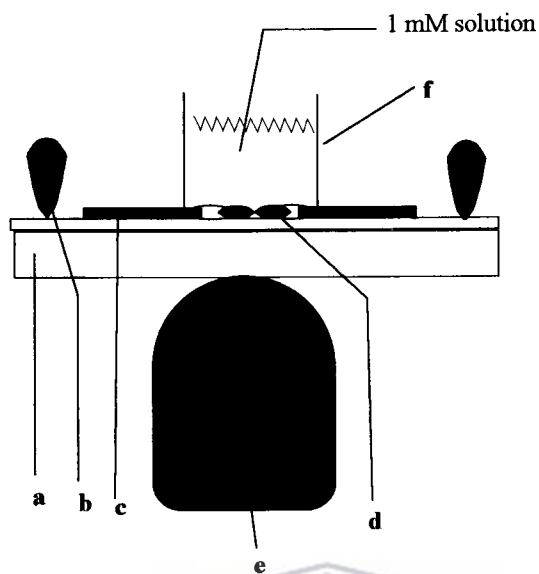


Figure 4.5: A schematic of the MCB junction with (a) the bending beam, (b) the counter support, (c) the notched gold wire, (d) the glue contacts, (e) the piezo element, and (f) the glass containing the solution.^{32b}

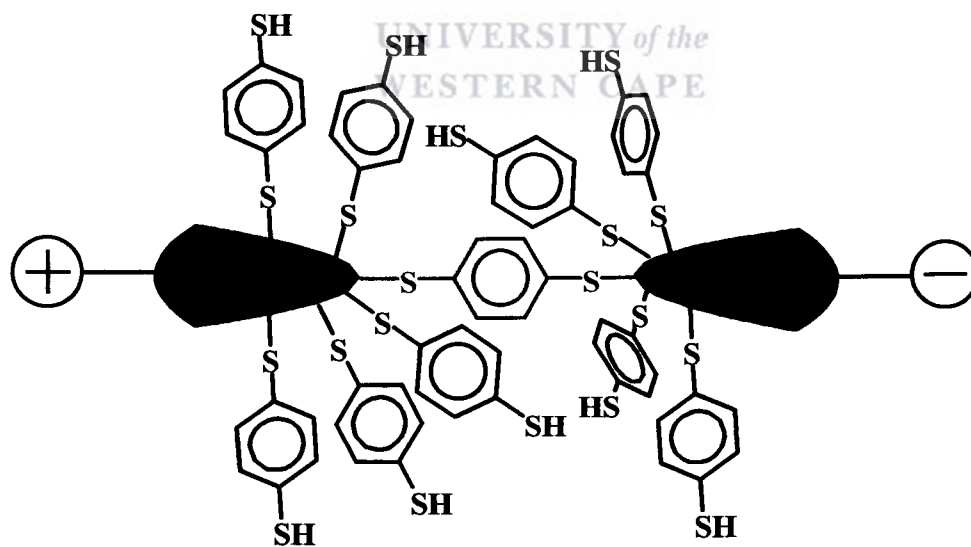


Figure 4.6: Schematic of benzene-1,4-dithiolate SAM with one molecule bridging the electronic circuit.^{32b}

solution of THF onto the two facing gold electrodes of the break junction, which were broken in solution under an argon atmosphere resulting in the formation of a SAM. The SAM was nearly perpendicular to the surface. THF was allowed to evaporate under argon

and thereafter measurements were done. The first derivative of current(voltage) ($I(V)$) showed two steps in both bias voltages with a lower step ~ 22.2 mega-ohm ($0.045 \mu\text{S}$) and the higher step ~ 13.3 mega-ohm ($0.075 \mu\text{S}$). In a control experiment with unevaporated THF alone (without the 1,4-benzenedithiol) a resistance of 1 to 2 giga-ohm was exhibited. This experiment showed that a single molecule conduct via a molecular junction. Typical current/voltage plots from the experiment are shown in Figure 4.7.

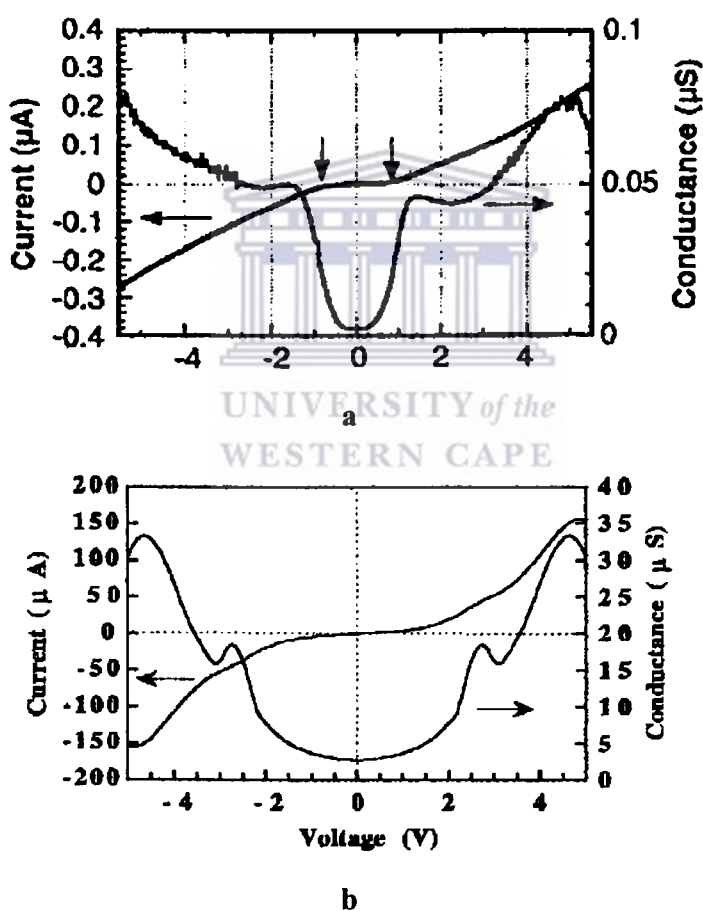


Figure 4.7 (a) Experimental I-V characteristics of the benzene-1,4-dithiolate molecule. (b) Theoretical I-V characteristics of the benzene-1,4-dithiolate molecule.^{32c}

4.4.3 The use of electrochemistry (CV) to measure conductance of molecular wires.

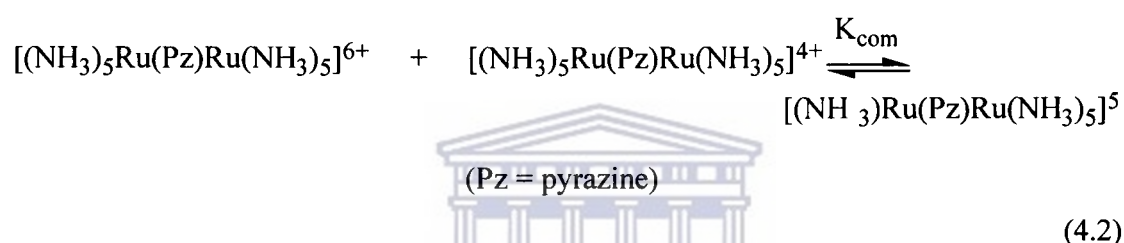
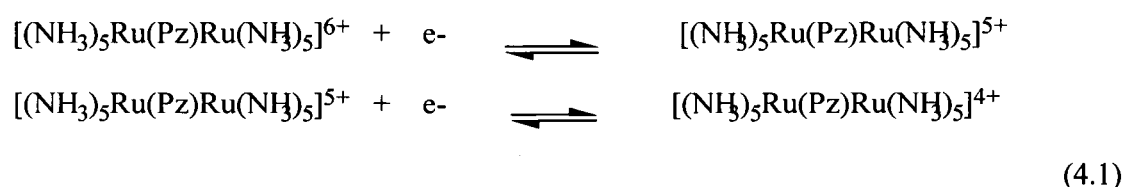
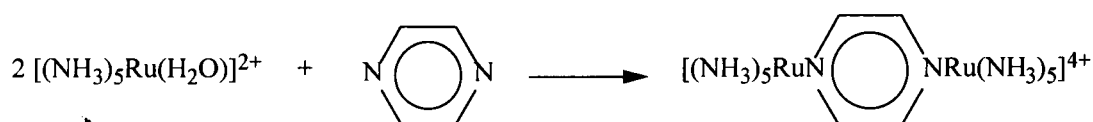
Intervalence electron transfer occurs in mixed-valence compounds, *i.e.* compounds made of two or more redox sites existing in different oxidation states.³³ Work on the study of organometallic or metal coordination compounds as molecular wires has focused on both homo- and heterometallic complexes. It has also been shown that unsaturated bridges can provide a facile pathway for electron delocalisation between metal centres.¹ Oligophenylenevinylene³⁴, oligothiophenes³⁵, alkynylene³⁶ and oligothiénylacetylide³⁷ have all been found to be useful as electronic conduits.

The present chapter is mainly limited to symmetrical mixed-valence complexes, in which a bridging ligand connects two metal atoms. In this type of complexes the metal is always an end group with the bridging ligand playing the role of a molecular wire, *i.e.* it makes possible the electron transfer between the two metal atoms, more efficiently than if they were separated by empty space.

The study of intervalence transitions offers advantages over other methods because: (i) it is based on static spectroscopic measurements, (ii) no thermodynamic factors are involved and, (iii) there is a simple basic parameter and the electronic coupling term. In physics and nanoscience, the knowledge of intramolecular electron transfer is useful in devising (bulk metal)-single molecule-(bulk metal) nanojunctions. Current research in the area is devoted to the problem of electron transport by the tunnel effect across the molecule and its dependence on distance.

Earlier works on electronic exchange between metals bridged by a ligand or spacer in homogenous solution was that of Creutz and Taube on the dimeric ruthenium with pyrazine bridge.³⁸ This has since been known as the Creutz-Taube ion.

The ion is prepared by the reaction of two equivalents of $[(\text{NH}_3)_5\text{Ru}(\text{OH}_2)]^{2+}$ and pyrazine (Eq. 4.1) The complex can be oxidised in two distinct one electron steps with reduction potentials of 0.98 V and 0.59 V (v/s N.H.E.) in aqueous solution at 25°C.



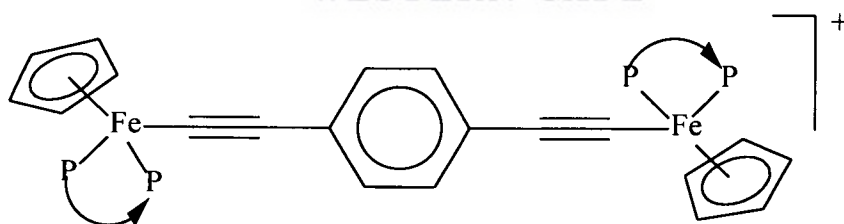
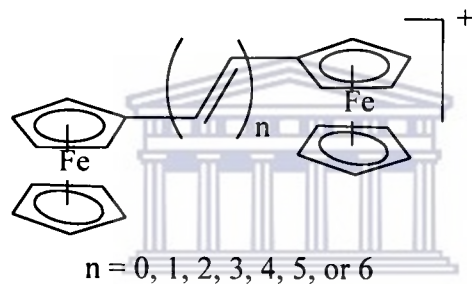
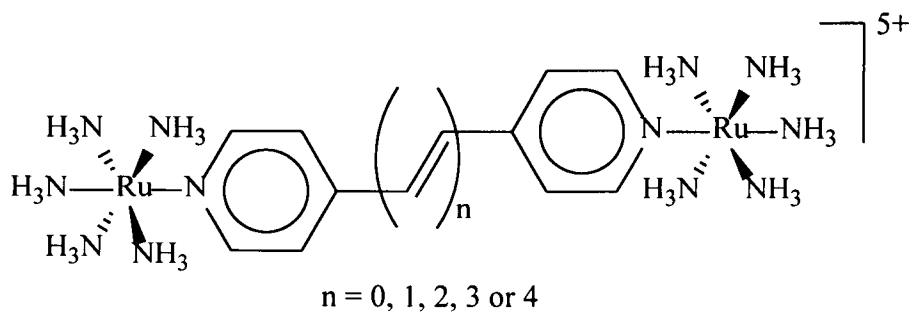
The equilibrium constant for the comproportionation, K_{com} (Eq. 4.2) of the mixed valence species is 4.0×10^6 which suggest that there is a significant interaction between the two metal centres. A weak interaction, required to obtain information on the electron transfer process from the spectroscopic parameters, would be expected to have a comproportionation equilibrium constant much closer to the statistical value of 4. The mixed valence complex $[(\text{NH}_3)_5\text{Ru}(\text{Pz})\text{Ru}(\text{NH}_3)_5]^{5+}$ possess a unique asymmetric spectroscopic feature at 1570 nm^{-1} with an extinction coefficient of $5.5 \times 10^{-3} \text{ M}^{-1}\text{cm}^{-1}$. From these near infrared studies it was shown and reasoned that the peak observed in the 1570 nm^{-1} region is due to the transition of a 2,3 state to a 3,2 state, that is an electron is transferred from one ruthenium to the other ruthenium across the pyrazine ligand or bridge. This was initially assigned as the intervalence transfer transition of a class II compound in the original paper.³⁸ This feature is absent in the spectra of the fully oxidized or fully reduced complexes. However, $\nu_{1/2}$, is much smaller than that predicted by theory, i.e. $\Delta\nu_{1/2} = (2310\nu_{\text{max}})^{1/2}$, for a class II compound and the absorption maximum of this band is solvent independent.³⁸ This suggests that the Creutz-Taube ion is best described as a class III mixed valence

compound. However related complexes show characteristics of class II mixed valence species.^{3b, 39}

Much of the literature is filled with ruthenium pentamine complexes. Ruthenium chemistry is popular because of their moderate redox potential (near 0 V vs. SCE), the great stability of its metal complexes and the ease of obtaining oxidation states II and III.^{33a} For the longer versions of the Creutz-Taube ion (with several conjugated double bonds, py-CH=CH-Py) the intervalence transitions are ill resolved.^{33a, 39a} For example, the complex $[(\text{NH}_3)_5\text{Ru}(4,4'\text{-bpy})\text{Ru}(\text{NH}_3)_5]^{5+}$, where the metal centres are further apart as compared with the Creutz-Taube ion, shows an intervalence transfer band at 1030 nm^{-1} in D_2O which is affected by the change in solvent as predicted by theory. The reduction potential of the two metal centres are 410 mV and 330 mV, much closer together than that for the Creutz-Taube ion. This indicates that communication between the metal centres is diminished. As a consequence, comproportion is much more important with $K_{\text{com}} = 23$. As the distance between the metal centres is increased, the energy of transition increases. Similar observations were made for the compound $[(\text{bpy})_2\text{ClRu}(\text{Pz})\text{RuCl}(\text{bpy})_2]^{3+}$ and related systems.⁴⁰ In these cyclometallated ruthenium complexes low or moderate electronic couplings were observed.⁴⁰ The complex show electron transfer rates, k_{et} , similar to those of pseudo exchange rates of binuclear reactions, e.g. the rate for electron transfer between $[\text{Ru}(\text{phen})_2\text{pyCl}]^{2+}$ and $[\text{Ru}(\text{bpy})_2\text{pyCl}]^+$ into $[\text{Ru}(\text{phen})_2\text{pyCl}]^+$ and $[\text{Ru}(\text{bpy})_2\text{pyCl}]^{2+}$ of $k = 4.9 \times 10^7$ compares with that of $k_{\text{et}} = 8.0 \times 10^7$ for $[(\text{bpy})_2\text{ClRu}(\text{Pz})\text{RuCl}(\text{bpy})_2]^{3+}$. However, the inclusion of furan and thiophene heterocycles in place of the double bonds improves the resolution, probably because of better co-planarity and rigidity.

A series of α,ω -diferrocenylpolyenes with $n = 1$ to 6 conjugated double bonds have been reported.^{3b, 39b 42b} Intervalence transitions gave electronic coupling terms that were dependent on the number of double bonds, with the decrease being essentially exponential. The disadvantages of the ferrocene systems are their moderate solubility and the tendency to decompose upon oxidation. Other ferrocene systems that have been

reported are bridged by 3 phenylene and 4 vinylene units.^{2b} Their intervalence band was obtained and corresponds to a coupling of 0.01 eV for a metal-metal distance of 26.5 Å.



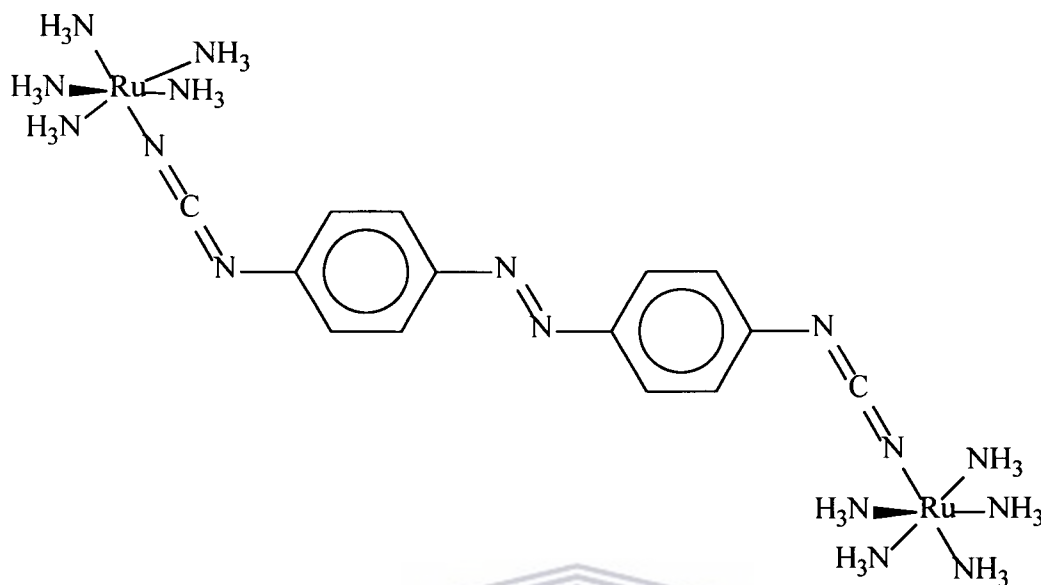


Figure 4.8: Examples of complexes that have been studied for their molecular wire properties.

Lapinte and Paul have described organometallic complexes that exhibited transitions through bridges that are made of carbon atoms. The end groups are $(\eta^5\text{-C}_5\text{Me}_5)(\text{dppe})\text{Fe}(\text{C}\equiv\text{C})\text{-}$ (dppe = diphenylphosphinoethane). The bridging groups are either 1,4-bis(ethynyl)benzene or octatetrayne and comproportionation constants (wave splitting) of 0.26 and 0.43 V were found respectively.^{2b}

4.5 Bimetallic complexes as nonlinear optical materials.

In addition to homobimetallic complexes being studied as molecular wires they are also studied as nonlinear optical materials. The large hyperpolarisabilities in these metal-organic or metal coordination complexes are attributed to the facile redox changes that are possible at the metal centre(s) and the presence of an extended π -electron framework. Traditional design rules based on conjugated organic nonlinear optical systems also apply to these materials for them to produce or promote greater second order or higher nonlinearities. Guidelines for designing organometallic complexes with enhanced nonlinearities are: (i) they must have low energy MLCT, (ii) the ligation sphere around

the metal atom must be highly polarisable and (iii) a significant difference in the amount of charge transfer between the donor and the acceptor in the ground and excited states must be achieved.⁴²

When a metal complex is a constituent of the polarisable bridge in a D- π -A structure, where D is donor group, π is conjugated system and A is an electron acceptor, two limiting cases could be identified: (i) the related uncomplexed D/A-substituted bridge already possesses second-order nonlinearity; (ii) complexation generates new NLO structures, from organic molecules with vanishing or small nonlinearity.^{42b} In these two cases the metal can play two different functions: (i) it enhances the bridge conjugation and, hence, the nonlinearity; (ii) it “switches on” or enhances the NLO response.

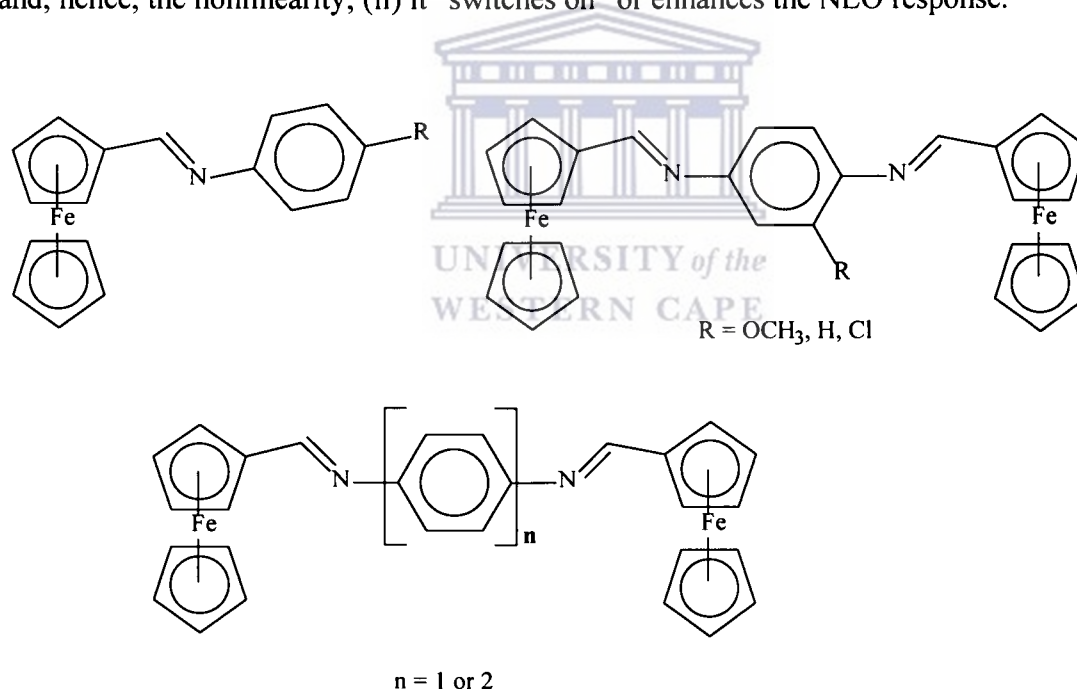


Figure 4.9: Binuclear ferrocenyl complexes with large NLO properties.

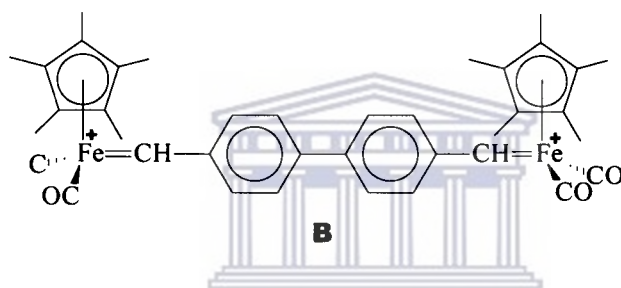
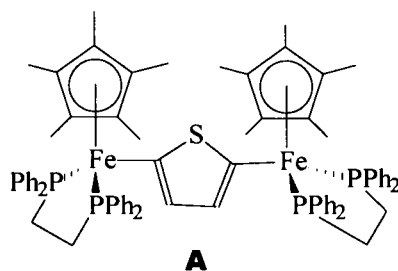
Pal *et al.* studied a series of mono- and bisferrocenyl Schiff-base complexes of the general structure shown in Figure 4.9.⁴² It was found that for the bisferrocenyl and their charge transfer salts (e.g. iodide, p-chloroanil, 2,3-dichloro-5,6-dicyano-1,4-benzoquinone, tetracyanoethylene, 7,7,8,8-tetracyanoquinodimethane) have a much higher second order nonlinearities than their analogous monoferrocenyl complexes.^{42a} In

all these complexes a strong resonant contribution to the second order nonlinear response was attributed to the MLCT transition at 532 nm. In the bisferrocenyl complex the contribution of the Schiff base ligand orbitals to the LUMO could be increased with the use of suitable substitutions on the organic spacer. The modification led to increased nonlinearities in the neutral ferrocenyl complexes. A more broad coverage of this topic does not fall under the scope of this thesis and as such this last section will suffice. It is worth noting though that a large section of NLO organometallic, binuclear complexes is dominated by heterobimetallic complexes, which is not covered in this section.

4.6 Background to the work reported in this chapter.

Compounds that have units with π -conjugation ability have been investigated for their potential use as nonlinear optical materials,⁴³ light emitting diodes,⁴³ and as molecular wires⁴⁴. Homo- and hetero-bimetallic complexes with π -conjugated bridging ligands are particularly interesting for their potential application as molecular wires.⁴⁵ Most of these bridged bimetallic complexes feature polyene bridging units, as polyenes are known to allow long range electronic coupling through π -delocalisation.^{25a, b, 46} In these polyene-bridged metal complexes, the metal-ligand interaction is usually a metal-carbon σ -bond, but the bond assumes some double bond character through electron delocalisation as one of the metal centres is oxidised. This mechanism allows electron communication in both homometallic polymers with Ni, Pd and Pt⁴⁷ and heterobimetallic (Ru/Pd, Fe/Pd and Fe/Ni)¹ oligomers with the 1,4-diethynylbenzene unit ($-\text{C}\equiv\text{C}-\text{C}_6\text{H}_4-\text{C}\equiv\text{C}-$).

A recent report by Guerchais *et al.*¹ has demonstrated that communication between two iron centres can be effected through bridging thiophene (**A**) and biphenyl (**B**) units when one of the iron centres is oxidised. Such intramolecular electron transfer should also be possible if the bridging ligand has a metal-sulfur bond. For example a number of phenylethynyl thiolate molecules inserted into alkyl thiolate matrix are known to conduct electrons when adsorbed on gold surfaces.^{30a, 48} This demonstrates that sulfur bound to a metal is capable of acting as electron conduit from a metal if there is a π -conjugated organic molecule attached to it.



Other complexes featuring metal σ -acetylides like $\text{Ni}(\text{C}\equiv\text{C}-\text{C}_6\text{H}_5)(\text{PPh}_3)(\eta^5-\text{C}_5\text{H}_5)$ have oxidisable metal centres and show nonlinear optical properties because the donor-acceptor composition is enhanced by the π -conjugation in the ligand.⁴⁹

Based on the above we envisaged that by using Schiff base ligands with two end sulfur atoms that bridge the two metal centres, we could effect the transfer of electrons *via* the bridging ligands from one metal to the other. Such dithiolato complexes should be easy to prepare since alkyldithiols are known to form bridged cyclopentadienyl complexes like $(\eta^5-\text{C}_5\text{H}_5)(\text{PBu}_3)\text{Ni}-\text{S}(\text{CH}_2)_n\text{S}-\text{Ni}(\text{PBu}_3)(\eta^5-\text{C}_5\text{H}_5)$ ($n = 2, 4, 6$).⁵⁰ This illustrates that the $\text{Ni}(\eta^5-\text{C}_5\text{H}_5)(\text{PBu}_3)$ fragment is capable of binding dithiolato ligands. The synthesis of cyclopentadienylnickel complexes with bridging dithiolato Schiff base ligands is the subject of this chapter. We have also investigated their electrochemistry to demonstrate that the π -conjugated dithiolato Schiff base ligands allow electronic communication between the two nickel atoms. Our results show that there is electronic communication between the nickel centres of these new dithiolato Schiff base complexes.

4.7. Experimental Section

4.7.1. Materials and Instrumentation

The starting material 4-aminothiophenol, 4-bromobenzaldehyde, 4-formylboronic acid, 1,4-benzenedicarboxyaldehyde, 1,3-benzenedicarboxyaldehyde and 2,5-thiophenedicarboxyaldehyde were obtained from Aldrich and were used as received. The complexes $\text{NiBr}(\text{PR}_3)(\eta^5\text{-C}_5\text{H}_5)$ ($\text{R} = \text{Bu}, \text{Ph}$)⁵⁷ and bis(diphenylphosphino)ferrocenepalladium dichloride, $\text{PdCl}_2(\text{dppf})$,⁵² were prepared by literature methods. Reagent grade hexane was distilled and stored over molecular sieves, while toluene was distilled over sodium and CH_2Cl_2 from P_2O_5 . All reactions were performed using standard Schlenk techniques under a dinitrogen atmosphere.

The ^1H and $^{31}\text{P}\{^1\text{H}\}$ NMR spectra were acquired on a Varian Gemini 2000 spectrometer at 200 MHz and 80.96 MHz respectively and referenced to residual CHCl_3 (δ 7.26) and externally to PPh_3 (δ -5.00) respectively. Elemental analysis was performed on a Carlo Erba NA 1500 in the Department of Chemistry at the University of the Western Cape. Fast Atom Bombardment mass spectra (FABMS) were run on a Finnigan MAT GCQ GC-MS, Electrospray mass spectra (ESMS) were run on a VG Platform II instrument in a positive ion mode and Matrix Assisted Laser Desorption Ionisation Time of Flight (MALDI-TOF) mass spectra were recorded on a Perseptive Biosystems-Voyager-DE STR spectrometer in a positive reflector mode at an accelerating voltage of 20kV. Electrochemical measurements were performed on a BAS 50W instrument using a standard three-electrode electroanalytical cell configuration equipped with a platinum disc working electrode (1.5mm diameter), a silver/silver chloride (Ag/AgCl) reference electrode and a platinum wire counter electrode. The supporting electrolyte used in the electrochemistry was tetrabutylammonium tetrafluoroborate (TBA-TFB)⁵³ as 0.1M solution in CH_2Cl_2 , and the concentration of the analyte was $0.03 \times 10^{-3}\text{M}$. The potential measurements were referenced internally to the ferrocene/ferrocenium redox peak at 441 mV.

4.7.2 Ligand synthesis

4.7.2.1 $\text{OHCC}_6\text{H}_4\text{C}_6\text{H}_4\text{CHO}$ (**28**)

Acetone (60 mL) was added to a mixture of 4-formylboronic acid (0.50 g, 3.3 mmol), 4-bromobenzaldehyde (0.61 g, 3.3 mmol), potassium carbonate (1.20 g, 6.6 mmol) and $\text{Pd}(\text{dppf})\text{Cl}_2$ (0.5% mole equivalent) and refluxed for 48 h. The resultant mixture was filtered and the solvent removed *in vacuo* to give an off-white residue, which was chromatographed on silica gel (60 mesh) using 1:1 CH_2Cl_2 /hexane eluent. The eluate was evaporated to dryness and the residue recrystallised from CH_2Cl_2 /hexane. Yield = 0.50 g (73%). Anal. Calcd for $\text{C}_{14}\text{H}_{10}\text{O}_2$: C, 79.98; H, 4.79. Found: C, 81.14; H, 4.30%. ^1H NMR (CDCl_3): δ 10.09 (s, 2H, CHO), 8.01 (d, 4H, $J_{\text{HH}} = 8.6$ Hz, OHCC_6H_4), 7.80 (d, 4H, $J_{\text{HH}} = 8.2$ Hz, $\text{C}_6\text{H}_4\text{C}_6\text{H}_4$). IR (cm^{-1}): $\nu(\text{C}=\text{O})$: 1710.

4.7.2.2 $\text{HSC}_6\text{H}_4\text{NC(H)-2-C}_4\text{H}_2\text{S-5-C(H)NC}_6\text{H}_4\text{SH}$ (**29**)

To a mixture of 4-aminothiophenol (1.79 g, 14.27 mmol) and 2,5-thiophenedicarboxyaldehyde (0.95 g, 7.13 mmol) was added ethanol (40 mL) and the mixture stirred overnight at room temperature. An insoluble yellow precipitate was isolated by suction filtration and washed with ethanol. Yield = 84%. Anal. Calcd for $\text{C}_{18}\text{H}_{14}\text{N}_2\text{S}_2$: C, 67.05; H, 4.38; N, 8.68. Found: C, 67.15; H, 4.43; N, 8.71%. IR (cm^{-1}): $\nu(\text{C}=\text{N})$: 1650.

Compounds **30**, **31** and **32** were synthesised in a similar manner to compound **29** using two equivalents of 4-aminothiophenol and one equivalent of the appropriate dicarboxyaldehyde. The products were all insoluble in common organic solvents but gave good elemental analyses.

4.7.2.3 $\text{HSC}_6\text{H}_4\text{NC(H)C}_6\text{H}_4\text{-3-C(H)NC}_6\text{H}_4\text{SH}$ (**30**)

A yellow solid was obtained in 87% yield. Anal. Calcd for $\text{C}_{20}\text{H}_{16}\text{N}_2\text{S}_2$: C, 68.96; H, 4.59; N, 8.04. Found C, 68.91; H, 4.66; N, 7.09%. IR (cm^{-1}): $\nu(\text{C}=\text{N})$: 1645.

4.7.2.4 $HSC_6H_4NC(H)C_6H_4-4-C(H)NC_6H_4SH$ (**31**)

A yellow solid was isolated in 84% yield. Anal. Calcd for $C_{20}H_{16}N_2S_2$: C, 68.96; H, 4.59; N, 8.04. Found C, 68.99; H, 4.73; N, 8.10%. IR (cm^{-1}): $\nu(C=N)$: 1643.

4.7.2.5 $HSC_6H_4NC(H)C_6H_4C_6H_4C(H)NC_6H_4SH$ (**32**)

A yellow precipitate was isolated in a yield of 82%. Anal. Calcd for $C_{26}H_{20}N_2S_2$: C, 73.55; H, 4.75; N, 6.60. Found: C, 73.16; H, 4.74; N, 5.97%. IR (cm^{-1}): $\nu(C=N)$: 1635.

4.7.3. Complexation of ligands with $NiBr(PR_3)(\eta^5-C_5H_5)$ (R = Bu or Ph).

All the complexes were synthesized in a similar manner to the procedure described for complex **33**. Complexes **33** – **36** were prepared using $NiBr(PBu_3)(\eta^5-C_5H_5)$ as starting material whilst $NiBr(PPh_3)(\eta^5-C_5H_5)$ was used to prepare complexes **37** – **39**.

4.7.3.1 $[Ni(\eta^5-C_5H_5)PBu_3]_2(SC_6H_4NC(H)C_4H_2S-5-C(H)NC_6H_4S)$ (**33**)

A mixture of **29** (0.24 g, 0.69 mmol) and $NiBr(PBu_3)(\eta^5-C_5H_5)$ (0.53 g, 1.38 mmol) was suspended in toluene to which Et_3N (1.5 mL) was added. The maroon colour changed to dark green after several hours of stirring at room temperature and stirring continued for 72 h. After filtration, the filtrate was evaporated to dryness and the residue recrystallised from CH_2Cl_2 /hexane to give a maroon solid in a yield of 69%. Anal. Calcd. for $C_{52}H_{76}N_2P_2S_3Ni_2$: C, 62.16; H, 7.62; N, 2.79. Found: C, 62.49; H, 7.32; N, 2.91%. 1H -NMR ($CDCl_3$): δ 8.57 (s, 2H, $N=C(H)$), 7.62 (d, 4H, $J_{HH} = 8.4$ Hz, NC_6H_4), 7.40 (s, 2H, C_4H_2S), 6.99 (d, 4H, $J_{HH} = 8.4$ Hz, SC_6H_4), 5.28 (s, 10H, C_5H_5), 1.54-1.34 (m, 36H, PBu_3), 0.92 (t, 18H, PBu_3). $^{31}P\{^1H\}$ NMR ($CDCl_3$): δ 22.40, (s, PBu_3).

4.7.3.2 $[Ni(\eta^5-C_5H_5)PBu_3]_2(SC_6H_4NC(H)C_6H_4-3-C(H)NC_6H_4S)$ (**34**)

A dark green solid was isolated in a yield of 58%. Anal. Calcd for $C_{54}H_{78}N_2P_2S_2Ni_2$: C, 64.92; H, 7.81; N, 2.80. Found: C, 64.90; H, 7.83; N, 2.80%. 1H -NMR ($CDCl_3$): δ 8.55 (s, 2H, $N=C(H)$), 8.35 (s, 1H, *iso*- C_6H_4), 7.98 (d, 2H, $J_{HH} = 8.0$ Hz, *iso*- C_6H_4); 7.64 (d, 4H, $J_{HH} = 8.4$ Hz, NC_6H_4); 7.53 (t, 1H, *iso*- C_6H_4); 6.98 (d, 4H, $J_{HH} = 8.0$ Hz, SC_6H_4); 5.28

(s, 10H, C₅H₅); 1.52-1.34 (m, 36H, PBu₃); 0.92 (t, 18H, PBu₃). ³¹P{¹H} NMR (CDCl₃): δ 22.37, (s, PBu₃).

4.7.3.3 [Ni(η⁵-C₅H₅)PBu₃]₂(SC₆H₄NC(H)C₆H₄-4-C(H)NC₆H₄S) (35)

A brown solid with a yield of 64% was isolated. Anal. Calcd for C₅₄H₇₈N₂P₂S₂Ni₂: C, 64.92; H, 7.81; N, 2.80. Found: C, 65.01; H, 7.83; N, 2.91%. ¹H-NMR (CDCl₃): δ 8.52 (s, 2H, N=C(H)), 7.95 (s, 4H, C(H)C₆H₄C(H)), 7.65 (d, 4H, J_{HH} = 8.4 Hz, NC₆H₄), 7.00 (d, 4H, J_{HH} = 8.4 Hz, SC₆H₄), 5.28 (s, 10H, C₅H₅), 1.54-1.27 (m, 36H, PBu₃), 0.92 (t, 18H, PBu₃). ³¹P{¹H} NMR (CDCl₃): δ 22.39, (s, PBu₃).

4.7.3.4 [Ni(η⁵-C₅H₅)PBu₃]₂(SC₆H₄NC(H)C₆H₄C₆H₄C(H)NC₆H₄S) (36)

A green solid was isolated in a yield of 68%. Anal. Calcd for C₆₀H₈₂N₂P₂S₂Ni₂: C, 67.06; H, 7.69; N, 2.61. Found: C, 67.14; H, 7.81; N, 2.78%. ¹H-NMR (CDCl₃): δ 8.53 (s, 2H, N=C(H)); 7.95 (d, 4H, J_{HH} = 8.4 Hz, C₆H₄C₆H₄); 7.74 (d, 4H, J_{HH} = 8.4 Hz, C₆H₄C₆H₄); 7.64 (d, 4H, J_{HH} = 8.6 Hz, NC₆H₄); 6.90 (d, 4H, J_{HH} = 8.4 Hz, SC₆H₄); 5.28 (s, 10H, C₅H₅); 1.58-1.34 (m, 36H, PBu₃); 0.93 (t, 18H, PBu₃). ³¹P{¹H} NMR (CDCl₃) δ 22.41 (PBu₃).

4.7.3.5 [Ni(η⁵-C₅H₅)PPh₃]₂(SC₆H₄NC(H)C₄H₂S-5-C(H)NC₆H₄S) (37)

A brown solid was isolated in a yield of 70%. Anal. Calcd for C₆₄H₅₂N₂S₃P₂Ni₂: C, 68.35; H, 4.66; N, 2.49. Found: C, 68.78; H, 4.59; N, 2.47%. ¹H-NMR (CDCl₃): δ 8.55 (s, 2H, N=C(H)), 7.69 (m, 12H, PPh₃), 7.35 (m, 24H, PPh₃, SC₆H₄, C₄H₂S), 6.89 (d, 4H, J_{HH} = 8.2 Hz, SC₆H₄), 5.15 (s, 10H, C₅H₅). ³¹P{¹H} NMR (CDCl₃): δ 35.33 (s, PPh₃).

4.7.3.6 [Ni(η⁵-C₅H₅)PPh₃]₂(SC₆H₄NC(H)C₆H₄-3-C(H)NC₆H₄S) (38)

A black crystalline solid was isolated in 51% yield. Anal. Calcd for C₆₆H₅₄N₂P₂S₂Ni₂: C, 70.87; H, 4.87; N, 2.50. Found: C, 70.56; H, 4.81; N, 2.21%. ¹H-NMR (CDCl₃): δ 8.54 (s, 2H, N=C(H)), 8.28 (s, 1H, C₆H₄), 8.15 (d, 2H, J_{HH} = 8.6 Hz, C₆H₄), 7.98 (d, 1H, J_{HH} = 8.4 Hz, C₆H₄), 7.71 (m, 12H, PPh₃), 7.35 (m, 22H, PPh₃, SC₆H₄), 6.89 (d, 4H, J_{HH} = 8.6 Hz, SC₆H₄), 5.16 (s, 10H, C₅H₅). ³¹P{¹H} NMR (CDCl₃): δ 35.39, (s, PPh₃).

4.7.3.7 $[Ni(\eta^5-C_5H_5)PPh_3]_2(SC_6H_4NC(H)C_6H_4-4-C(H)NC_6H_4S)$ (**39**)

A brown solid with a yield of 70% was obtained. Anal. Calcd for $C_{66}H_{54}P_2S_2N_2Ni_2$: C, 70.86; H, 4.87; N, 2.50. Found: C, 70.34; H, 4.68; N, 2.28%. 1H -NMR ($CDCl_3$): δ 8.54 (s, 2H, N=C(H)), 7.97 (s, 4H, C_6H_4), 7.65 (m, 14H, SC_6H_4 , PPh_3), 7.42 (m, 18H, PPh_3), 6.92 (d, 4H, $J_{HH} = 8.6$ Hz, SC_6H_4), 5.16 (s, 10H, C_5H_5). $^{31}P\{^1H\}$ NMR ($CDCl_3$): δ 35.35, (s, PPh_3).

4.8. Results and discussion

4.8.1 Synthesis and characterisation of ligands

The dialdehyde, $OHCC_6H_4C_6H_4CHO$, (**28**), was prepared by the Suzuki coupling reaction of 4-formylboronic acid with 4-bromobenzaldehyde catalysed by the palladium(II) complex, diphenylphosphinoferrocenepalladium dichloride. We chose this palladium catalyst for two reasons. The first is that this complex was available in our laboratory and secondly we wanted to test the effectiveness of a bidentate phosphine palladium(II) complex as a Suzuki coupling catalyst. Other palladium(II) complexes such as $Pd(OAc)_2$ and Li_2PdCl_4 have been used to effect the Suzuki coupling reaction.⁵⁴ In addition to palladium(II) catalysts, palladium(0) catalysts such as a $Pd(PPh_3)_4$ have been extensively used for the boronic acid Suzuki coupling.⁵⁵ Compound **1** was prepared in high yields (78%) and purity and only required the separation of the palladium catalyst, which was achieved by chromatography. The elemental analysis was good. The IR spectrum showed sharp peaks around 1710 cm^{-1} indicative of the carbonyl stretch. The proton NMR spectrum (Figure 4.10) confirmed the symmetric nature of the compound and the absence of any starting material. Therefore the $PdCl_2(dppf)$ used here is a very effective catalyst for the Suzuki coupling of the formylphenylboronic acid and bromophenylcarboxyaldehyde.

Dithiol Schiff base compounds (**29** - **32**) were prepared by the condensation of two equivalents of 4-aminothiophenol and one equivalent of the appropriate dialdehyde

(Scheme 4.1). Compounds **29** - **32** were isolated as yellow insoluble solids, which are stable to air and moisture. However they gradually turned reddish maroon on exposure to light over two weeks, though their elemental analysis remained the same. This colour change from yellow to reddish maroon could be due to isomerisation between *cis* and *trans* forms of the compounds about the imine bonds. A lack of solubility of these compounds in common organic solvents such as CH₂Cl₂, toluene and THF made it impossible to prove this isomerisation; though a closer examination of the ¹H-NMR spectrum of complex **33** (Figure 4.11) suggest that a similar isomerisation about the imine group might exist when the ligands form complexes with nickel. In this spectrum there are low intensity peaks at 5.21 ppm (η^5 -C₅H₅), two doublets at 5.85 and 7.70 ppm for benzene ring protons and 8.40 ppm for imine proton that are peaks associated with an isomer of complex **36**. Although another plausible explanation for the change in colour when compounds **29** - **32** were exposed to sunlight could be oxidation of the thiols to disulfides, which will also give essentially the same elemental analysis, the possibility of these compounds oxidizing to disulfides was however not investigated.

As a result of their insolubility these compounds were only characterized using elemental analysis and infrared spectroscopy. The IR spectroscopy showed typical strong peaks around 1650 to 1635 cm⁻¹ due to the imine bond (C=N) stretches. Furthermore peaks around 650 cm⁻¹ could be assigned to the C-S stretch while the small peak or hump at 3500 cm⁻¹ was assigned to SH stretch.⁵⁶ Further proof of the identity and purity of compounds **29** - **32** could also be inferred from their resultant reactions with the nickel compounds that gave pure products.

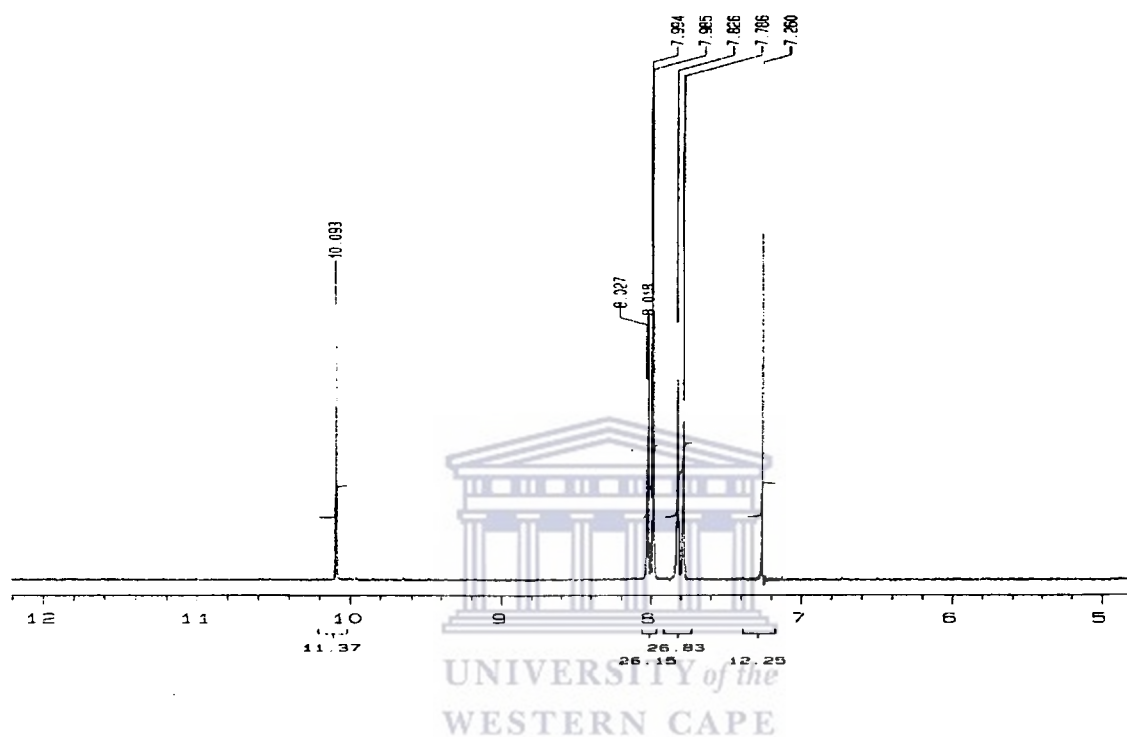
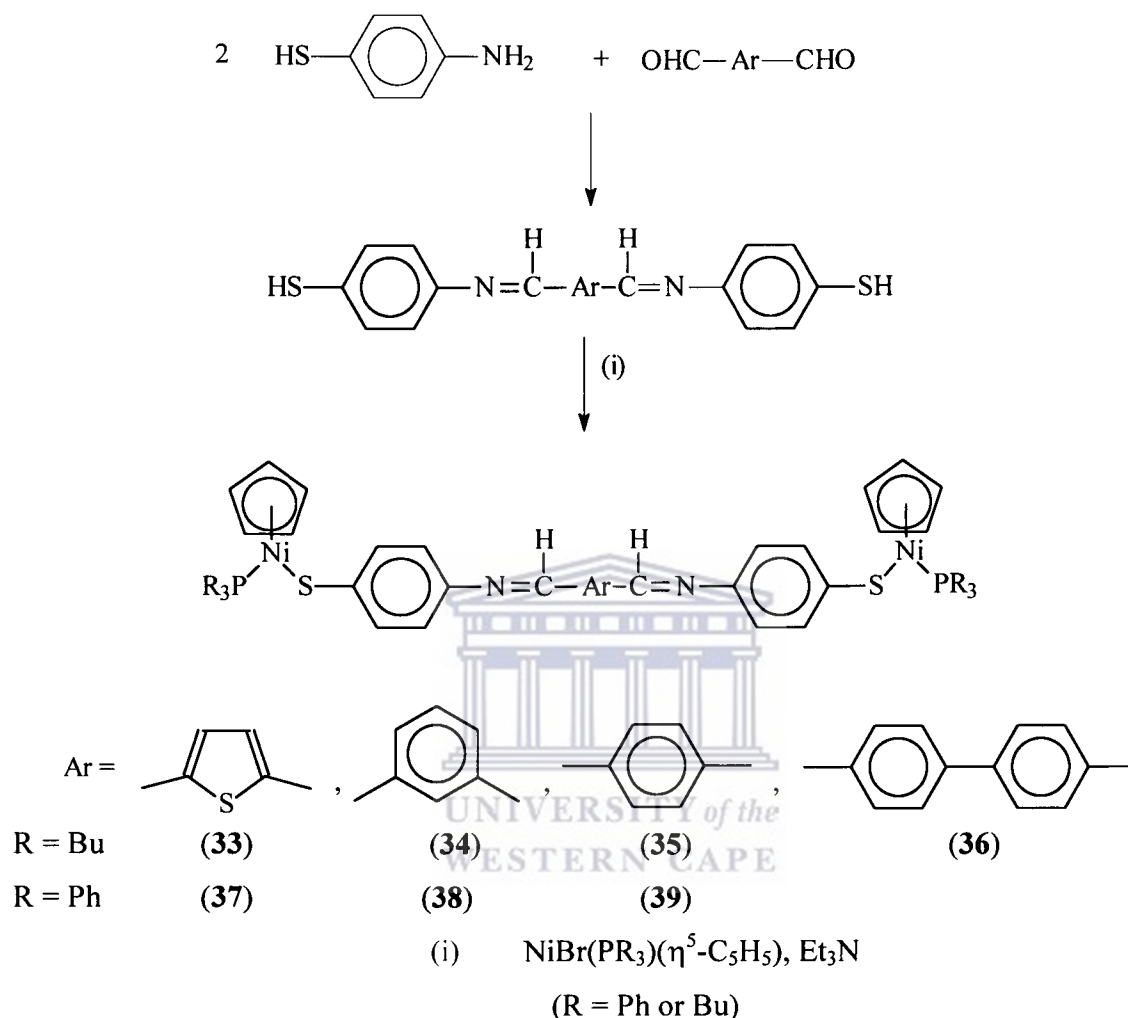


Figure 4.10: ^1H NMR of compound **28**.

4.8.2 Synthesis and characterisation of complexes

The dithiol compounds (**29** – **32**) reacted with two equivalents of $\text{NiBr}(\text{PR}_3)(\eta^5\text{-C}_5\text{H}_5)$ to form toluene soluble products when excess Et_3N was added to this mixture (Scheme 4.1).



Scheme 4.1: Synthesis of Schiff base thiol ligands and cyclopentadienylnickel(II) complexes.

The progress of the reaction could be seen by the gradual colour change from maroon to brownish-yellow or dark green. The final products in all cases were soluble in common organic solvents and thus they could be analysed using common analytical techniques. Even though the reactions were performed under inert atmosphere the final workup were done in air, indicating that the complexes are stable in solution as well as in the solid state. The complexes were analysed using a combination of NMR and IR spectroscopy, elemental analysis as well as mass spectrometry.

The IR spectra of the complexes resembled one another. The characteristic out-of-plane deformation band of the π -cyclopentadienyl ligand appears between 750 cm^{-1} and 765 cm^{-1} . These values are at slightly lower wave numbers than those of bimetallic complexes bridged by alkyl groups. In those cases the values of between 795 cm^{-1} and 785 cm^{-1} were observed.⁵⁰ The peak values of our bimetallic nickel complexes (**33** – **39**) are however comparable with those of mononickel(II) complexes of the type $\text{Ni}(\text{SC}_6\text{H}_4\text{NC}(\text{H})\text{C}_6\text{H}_4\text{X}-4)(\text{PR}_3)(\eta^5\text{-C}_5\text{H}_5)$, found in chapter 2 of this thesis and in the literature.⁵⁷ The peaks due to the imine groups have similar values to those of the free ligands.

The ^1H NMR spectra of the bimetallic nickel complexes were as expected and were typical of cyclopentadienylnickel phosphino thiolato complexes.⁵⁷ Cyclopentadienyl chemical shifts of 5.28 ppm and 5.16 ppm for the PBu_3 and PPh_3 complexes respectively were similar to 5.27 ppm and 5.13 ppm observed for the mononuclear complexes $\text{Ni}(\text{SC}_6\text{H}_4\text{X}-4)(\text{PBu}_3)(\eta^5\text{-C}_5\text{H}_5)$ and $\text{Ni}(\text{SC}_6\text{H}_4\text{X}-4)(\text{PPh}_3)(\eta^5\text{-C}_5\text{H}_5)$ ($\text{X} = \text{F}, \text{Cl}, \text{Br}$) respectively.^{57a} The signals due to the linkers were as expected. Thus the thiophene bridge gave a singlet integrating for two protons. The phenyl bridges gave a singlet integrating for four protons for the 1,4-phenyl bridge and the 1,3-phenyl bridge gave a singlet, a doublet and a triplet, integrating for one, two and one proton respectively. The biphenyl bridge gave two sets of doublets, each integrating for four protons. In all cases the protons on the ring closest to the carbon of the imine bond were invariably more downfield than those on the ring next to the nitrogen of the imine group. These assignments are based on both the shapes of the signals, the coupling constants and comparison with those of mononuclear Schiff base complexes, $\text{Ni}(\text{SC}_6\text{H}_4\text{NC}(\text{H})\text{C}_6\text{H}_4\text{X}-4)(\text{PR}_3)(\eta^5\text{-C}_5\text{H}_5)$ ^{57b} and $\text{Ni}(\text{SC}_6\text{H}_4\text{NC}(\text{H})\text{C}_6\text{H}_4\text{OC}_n\text{H}_{2n+1}-4)(\text{PR}_3)(\eta^5\text{-C}_5\text{H}_5)$ ^{57c}.

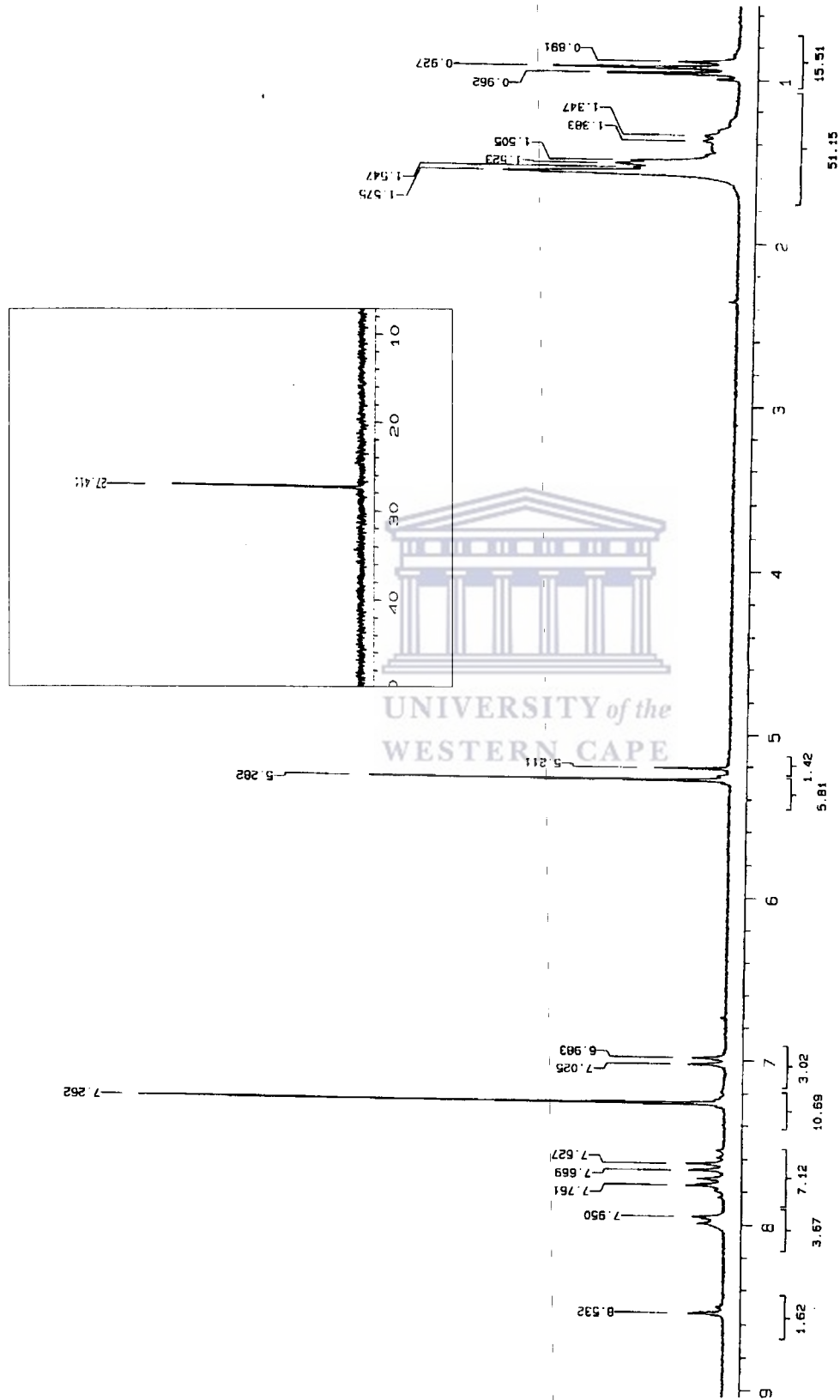


Figure 4.11: ^1H NMR spectrum of complex 36. Inset: ^{31}P NMR spectrum of complex 36.

The above assignment of bridging ligand signals is based on the tributylphosphine complexes, as these have no overlapping with resonance signals from the phosphine ligand. The triphenylphosphine complexes are expected to have similar chemical shifts for the bridging Schiff base ligands. In addition to the ^1H NMR spectra, ^{31}P NMR spectra were run for the two series. The ^{31}P NMR spectra were similar to those of the mononuclear complexes⁵⁷ and so were not unusual and thus warrant no further discussion here except to say that the shifts were dependent on the basicity of the phosphine used. These two NMR techniques showed that the complexes are symmetrical as only one set of signals was observed for particular groups, e.g. the cyclopentadienyl ring and phosphorus signal for proton and phosphorus NMR spectra respectively. Therefore the binuclear nature could be inferred from the NMR data. The similarities in the cyclopentadienyl ring and the phosphine chemical shifts, in both proton and phosphorus NMR spectra, for complexes **33** - **39** and those reported by Nevondo *et al.*^{57b} recently, point to similar electronic environment around the nickel centres in the bimetallic and the monometallic complexes. We expect this similarity in electronic environment in the bimetallic and the monometallic nickel complexes to result in similar electrochemical behaviour as will be discussed later. There was no obvious effect of the aryl or thiophene linkers on the electronic environment of the nickel centres.

In spite of the considerable solubility of the nickel complexes prepared, particularly the PBU_3 analogues, our attempts to grow crystals of complexes **33** - **39** were unsuccessful. Thus other techniques to further establish the bimetallic nature of the complexes were used. To achieve this different mass spectrometry techniques were employed and include fast atom bombardment (FAB), electrospray (ES) and matrix assisted laser desorption ionization time-of-flight (MALDI-TOF) mass spectrometry. The effect of different techniques on the stability of the ions formed will also be compared and rationalised based on the energy inherent in each ionization technique.

4.8.3 Mass spectrometric studies of the complexes.

Three mass spectrometry techniques were used to confirm the bimetallic nature of the nickel complexes. The use of three techniques was also to probe how different ionisation sources will affect the stability of the molecular ions that are formed depending on the energy difference inherent in each technique. These techniques are electrospray mass spectrometry (ESMS), fast atom bombardment mass spectrometry (FABMS) and matrix assisted laser desorption ionisation time of flight mass spectrometry (MALDI-TOFMS). Electrospray and matrix assisted laser desorption ionisation techniques are perceived to be softer ionisation techniques and hence are expected to lead to less fragmentation of the molecular ions.

4.8.3.1 Fast atom bombardment mass spectroscopic study.

The bombardment of chemical compounds dissolved in a liquid matrix, *e.g.* glycerol, by fast moving atoms followed by the mass spectroscopic analysis of the secondary ions is referred to as fast atom bombardment mass spectroscopy or FABMS for short.⁵⁸ The technique offers advantage over secondary ion mass spectrometry (SIMS), where ions are sputtered from a solid surface with a dynamic or static ion beam, because it uses a liquid matrix, which facilitates sample preparation and maintains a reservoir of undamaged molecular sample species allowing secondary molecular parent ion emission for long periods of time (several minutes) under intense particle flux. The use of beams of atoms in FABMS also avoids the technical and practical complications that might be encountered if an ion gun were used with high voltage mass spectrometers (*i.e.* the need to float the ion gun system above the accelerating voltage of the spectrometer) and reduce charge build up in the sample. Fast atom bombardment is one of the first ionisation techniques to be perceived as a soft source.⁵⁸ Thus we initially planned to use this source for the nickel thiolato complexes as it has been used for the nickel thiolate complexes in our laboratory to get molecular ion peaks.⁵⁹ Molecular ions could be observed when a FAB source was used for these nickel thiolates but no molecular ions peaks were found when electron impact ionisation (EI) source was used. Thus FAB was seen as a softer

ionisation for the metal thiolate complexes and which prompted us to use it for the present nickel thiolato complexes. The technique worked for only one complex but failed in the rest.

When FABMS of complexes **33** – **39** were run, only complex **35** produced a molecular ion peak at $m/z = 998$. The FABMS spectrum of complex **35** is shown in Fig. 4.12. An interesting observation was the excessive fragmentation that all the complexes underwent during the FABMS experiments. Two fragmentation pathways were identified from the mass spectrum of complex **35**.

The first fragmentation pathway appears to be more drastic and involves the cleavage of a C-C bond in the bridging ligand. This formed the fragmentation with $m/z = 462$ corresponding to $[\text{Ni}(\text{SC}_6\text{H}_4\text{-4-N=CH})(\text{PBU}_3)(\eta^5\text{-C}_5\text{H}_5)]^+$, which appeared in the spectrum as the parent peak. This ion resembles the simple cyclopentadienylnickel thiolates, $\text{Ni}(\text{SC}_6\text{H}_4\text{X-4})(\text{PBU}_3)(\eta^5\text{-C}_5\text{H}_5)$ ($\text{X} = \text{Cl}, \text{Br}, \text{NH}_2$)^{57a}, that have been investigated extensively by our group and could account for the apparent stability of the $m/z = 462$ ion found in the spectrum. The second involved a loss of a PBU_3 ligand to produce an ion with $m/z = 796$. This was followed by the loss of one cyclopentadienyl ligand to form an ion with $m/z = 731$. The $m/z = 731$ ion appears to be stable and did not undergo any further fragmentation.

From the peaks observed in FABMS spectrum of **35** it appears that the fragmentation of the two routes is independent of each other. In one route there is a gradual fragmentation of the complex through successive rupture of the thiol Schiff base bridging ligand. This starts by first rupturing at the imine group from a benzene unit, then the sulfur-nickel bond breaks followed by the loss of the cyclopentadienyl ring to leave a Ni- PBU_3 fragment. The other route starts by first losing the tributylphosphine group followed by the loss of a cyclopentadienyl ring. The first route seems to dominate as it invariably led to higher relative abundance of peaks, all of which were almost 100%. Complexes **33**, **34**, **36** – **39** showed no molecular ions in their FABMS; but they showed fragmentation patterns similar to that of **35**. For example, tributylphosphine complexes had $m/z = 262$

$([\text{Ni-PBu}_3]^+)$, $m/z = 327$ ($[\text{Ni}(\text{PBu}_3)(\eta^5\text{-C}_5\text{H}_5)]^+$) and $m/z = 462$ ($[\text{Ni}(\text{SC}_6\text{H}_4\text{NC}(\text{H})(\text{PBu}_3)(\eta^5\text{-C}_5\text{H}_5)]^+$). Table 4.1 shows all the common peaks found and their assignment. What is clear from the FABMS picture is a series of complexes that have their molar masses lose fragment when subjected to fast atom bombardment.

In order to lend some credibility to the fact that the molecules that did not show molecular ions in the FABMS experiments are genuinely what they have been formulated as, electrospray mass spectrometry experiments were performed. This was done in order to confirm the molecular formulae as proposed.

MASS SPECTRUM Data File: NS21A 21-MAY-99 11:37
 Sample: NS21: C54H78N2P2S2Ni2
 RT 1.44" FAB(Pos.) GC-214748300.0c BP: m/z 201.0000 Int. 91.0110 Lu 0.00
 Scan# (5)

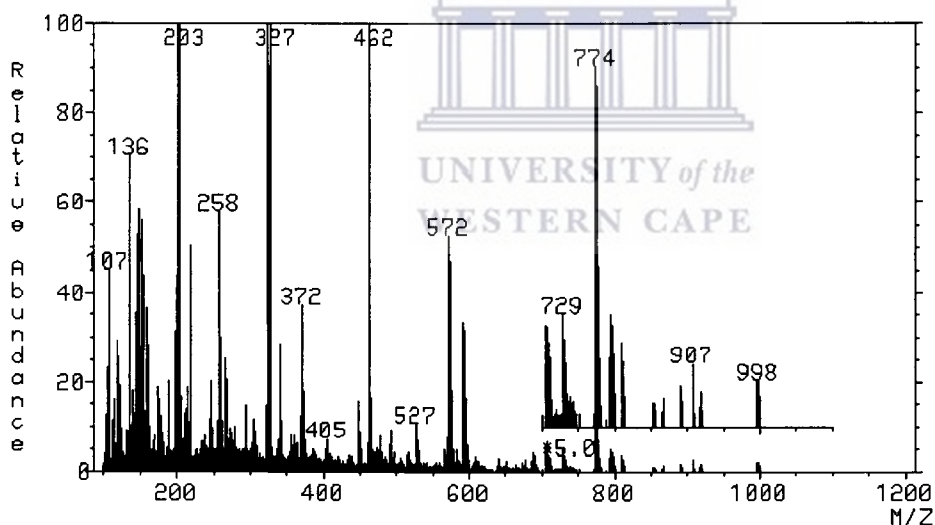
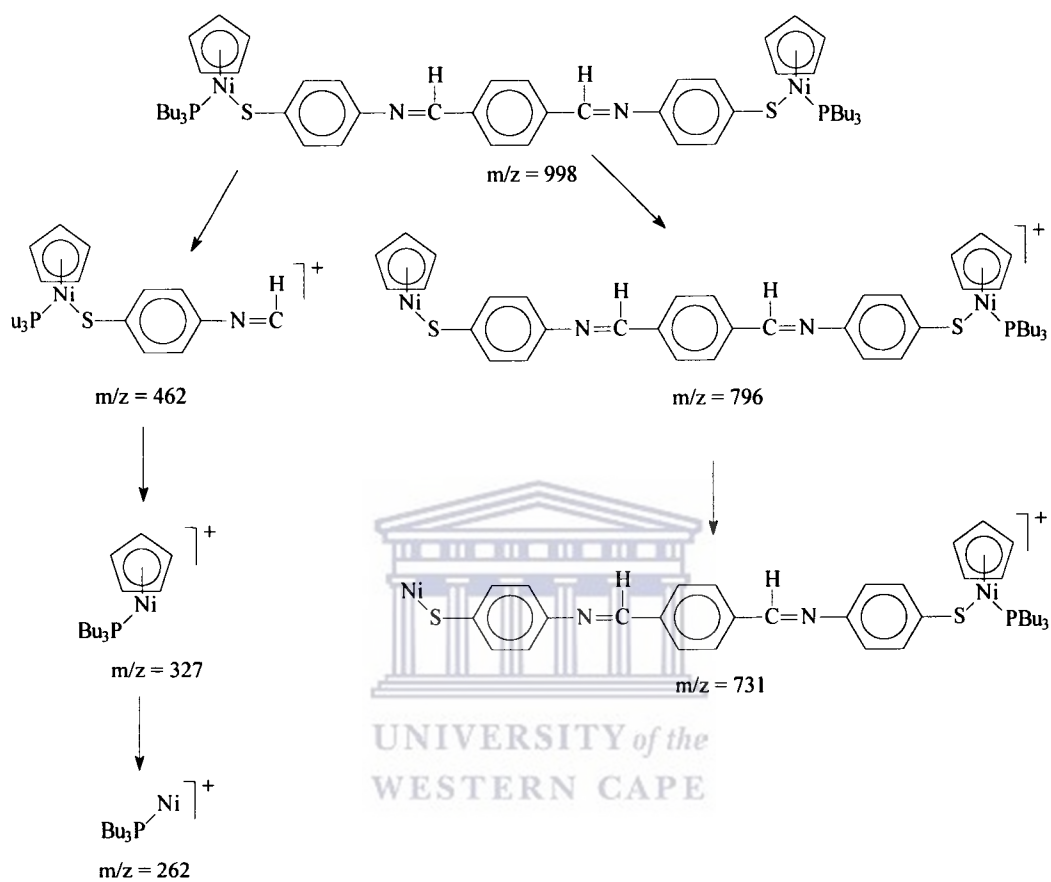


Figure 4.12: FAB mass spectrum of complex 33.

Scheme 4.2: Fragmentation pattern of complex **35** FABMS.Table 4.1: Common fragments in the PBu₃ series.

Molar mass	Fragment	33	34	35
528			✓	✓
462	$[\text{Ni}(\text{SC}_6\text{H}_4\text{NCH})(\text{PBu}_3)(\eta^5\text{-C}_5\text{H}_5)]^+$	✓	✓	✓
327	$[\text{Ni}(\text{PBu}_3)(\eta^5\text{-C}_5\text{H}_5)]^+$	✓	✓	✓
262	$[\text{Ni-PBu}_3]^+$	✓	✓	✓

4.8.3.2 The Electrospray mass spectrometry study.

Electrospray is increasingly being used as a routine technique for the studying of a diverse range of inorganic and organometallic complexes,⁶⁰ Electrospray is known to allow the transfer and subsequent detection of ions in solution to the gas phase with minimal fragmentation and decomposition.⁶¹ Henderson *et. al.* pioneered the use of ESMS to establish the structures of metal thiolate complexes.⁶² Generally this method has found use in biologically and biochemically active compounds such as silver(I) thiolates⁶³, gold(I) thiolates⁶⁴, platinum(II) thiolates⁶⁵, metal dithiolates and related complexes⁶⁶.

In applying EIMS technique to the thiolato-Schiff base complexes **33**, **35**, **36**, **37** and **39**, positive ion ESMS spectra were obtained, yielding parent ions of the type $[M + H]^+$ and $[M + NH_4]^+$ ions. These parent ions were however observed at low cone voltages with their relative abundance decreasing or disappearing altogether at increased cone voltages. Complex **37** for example gave both $[M + H]^+$ and $[M + NH_4]^+$ molecular ion peaks at a cone voltage of 5 V (Figure 4.13). When this voltage was increased from 5 V to 20 V and 40 V compound **36** gave only $[M + NH_4]^+$ molecular ion. No aggregate ions of the type $[2M + H]^+$ and $[2M + NH_4]^+$ were observed even at low cone voltage of 5 V, which give an indication of how these nickel thiolate complexes are unstable under the ESMS conditions. Aggregate ions are usually observed at low cone voltages and tend to disappear as the voltage is increased.⁶⁷ Compound **37** readily lost the PPh_3 group as evident by its absence in most of the fragments (Scheme 4.3).

The spectra of PPh_3 complexes were dominated by peaks due to the $Ni(PPh_3)_2(\eta^5-C_5H_5)^+$ and $Ni(PPh_3)(\eta^5-C_5H_5)^+$ ions, generally with relative abundance of 100% and > 50% respectively. The dominance of these fragments show that the complexes lose one $Ni(PPh_3)(\eta^5-C_5H_5)$ fragment readily, which probably rearranges to the more stable $Ni(PPh_3)_2(\eta^5-C_5H_5)^+$ ion.

The spectra of PBu_3 complexes, on the other hand, were not dominated by similar fragments, e.g. $\text{Ni}(\text{PBu}_3)_2(\eta^5\text{-C}_5\text{H}_5)^+$ and $\text{Ni}(\text{PBu}_3)(\eta^5\text{-C}_5\text{H}_5)^+$ ions. Even though the spectra of the PBu_3 complexes showed no m/z values associated with $\text{Ni}(\text{PBu}_3)_2(\eta^5\text{-C}_5\text{H}_5)^+$ and $\text{Ni}(\text{PBu}_3)(\eta^5\text{-C}_5\text{H}_5)^+$ ions, peaks assignable to fragments when these units were lost could be found in the spectra of compounds like **35**. For instance, complex **35** had a peak at $m/z = 673$ with a 75% abundance which is due to the loss of $\text{Ni}(\text{PBu}_3)(\eta^5\text{-C}_5\text{H}_5)^+$ fragment ion.

The observation of molecular ions, albeit at low abundances, show that ESMS is suited to complexes of this type. The observation that molecular ions are observed only at low cone voltage indicates that the complexes readily fragment in the ionisation chamber. In the next section, data obtained from MALDI-TOF of the same samples is presented.

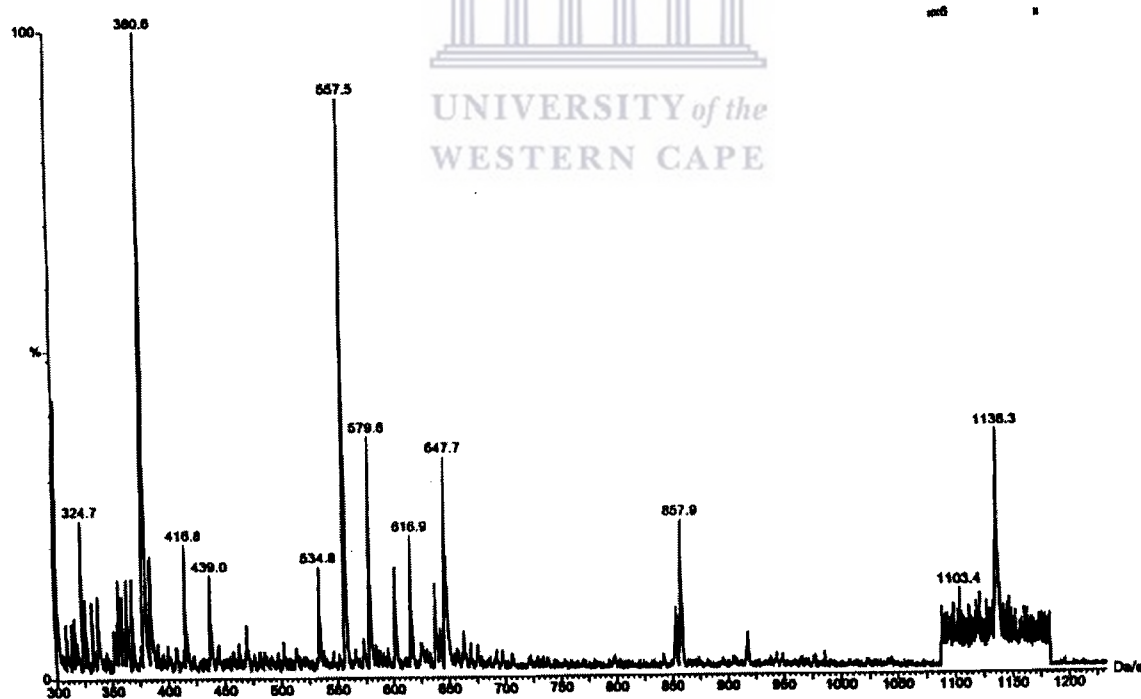
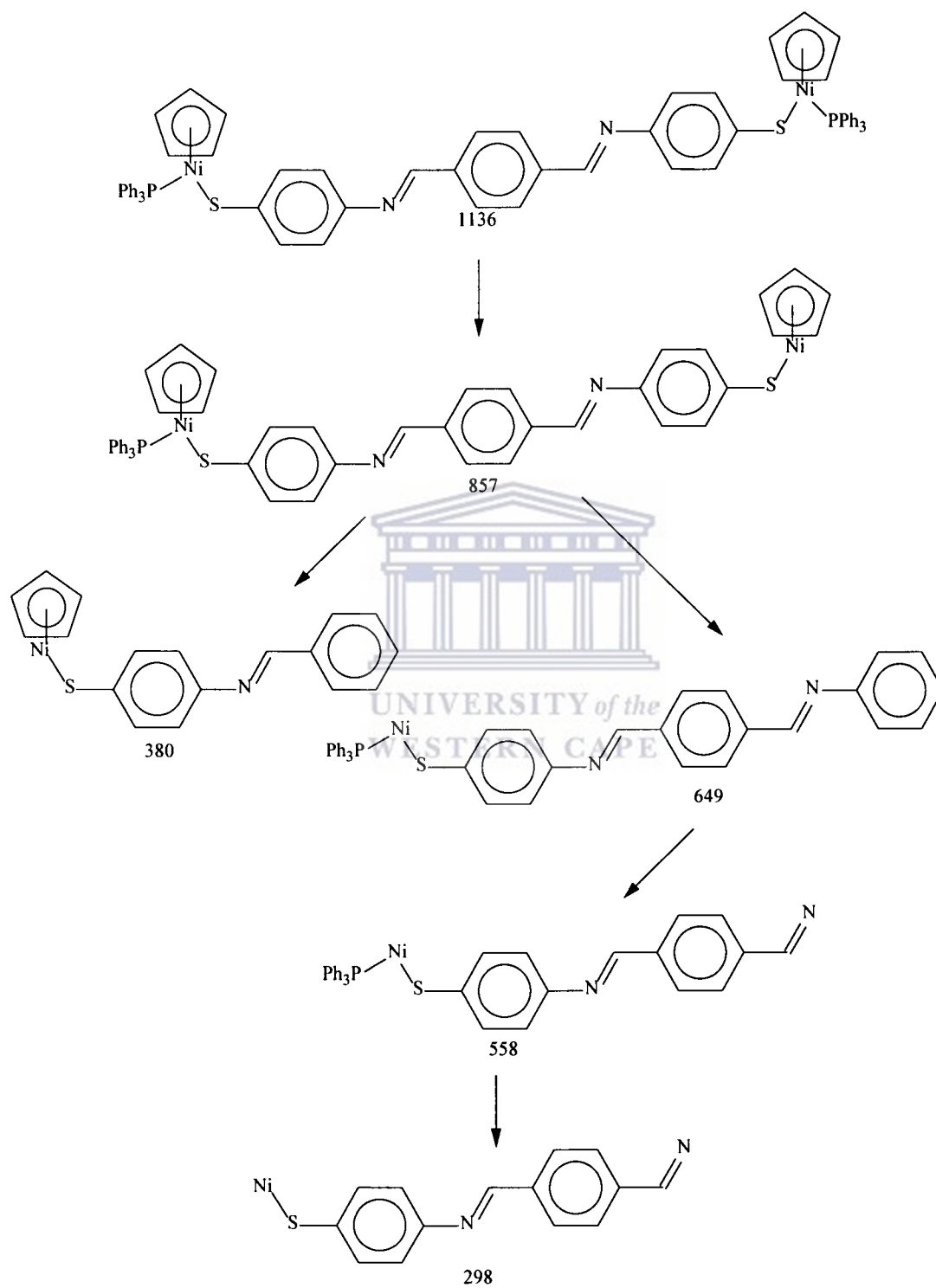


Figure 4.13: Electrospray mass spectrum of complex **36**.



Scheme 4.3: Fragmentation pattern for ESMS of the PPh₃ series.

4.8.3.3 MALDI-TOF mass spectral analysis

MALDI-TOF mass spectrometry is a technique that was developed specifically for the analysis of biological and natural products, but has been used increasingly for the analysis of organic and organometallic compounds as well as polymer samples.⁶⁸

In running the experiments three types of matrices were used as in chapter 3. These are tetrafluorophenylporphyrine (F₂₀-TPP), dithranol and dimethylhydroxycinnamic acid. In addition we used NaOH as a cationic source to assist in the ionisation process. The MALDI-TOF technique was used for complexes **33** – **36**. No molecular ion peaks were observed for the complexes under all conditions that were used in the present experiments. In all the experiments performed, fragmentation due to ionisation could only be observed at moderate to high laser intensities. At low laser intensity no ionisation occurred. At very high laser intensities, only fragments with low molecular mass (< 200) were observed.

Even though no molecular ion peaks were observed for all the complexes studied, we could observe fragment ion peaks that could be associated with parts of the molecule. In some cases we could observe molecular ion peaks of rearranged product ions (Table 4.3). This is true for complexes **34**, **35** and **36**. We observed no logical fragment ions for complex **33**, only peaks whose origins are not clear were found. Therefore MALDI-TOF mass spectrometry could not confirm the structure of compound **33**. Complexes **34** and **35** produced mass spectra with peaks of similar ion masses (Table 4.3). This is not surprising because the complexes have similar structures and the same molecular mass. Complex **36** had only one fragment ion peak in the lower region of the spectrum that could not be associated with any fragment from the molecule. Some of the fragment ion peaks showed a sodium ion in the fragment which could be traced to the NaOH in the matrix. There was no improvement in the results on changing the matrix.

Table 4.3: Some of the common fragment ions observed in the MALDI-TOF spectra.

Fragment	Molecular ion peak	33	34	35	36
Ni(PBu ₃)	261	-	-		✓
Ni(η ⁵ -C ₅ H ₅)	124	-	-		-
Ni(η ⁵ -C ₅ H ₅) ₂ ^a	188	-		✓	-
Ni(PBu ₃)(η ⁵ -C ₅ H ₅)	326	-	✓ *	✓	-
Ni ₂ S ₂ (η ⁵ -C ₅ H ₅) ₂ ^a	312	-	✓	✓	-
Ni ₂ (PBu ₃) ₂ (η ⁵ -C ₅ H ₅) ₂ ^a	698	-	✓		-
Ni ₂ (PBu ₃)(S)(η ⁵ -C ₅ H ₅) ^a	483	-	* #	✓ *	-

^a = rearranged product ion, * = with one Na⁺ ion, # = with two Na⁺ ions.

It was observed that all the spectra of the complexes run with the F₂₀-TPP matrix had a common peak with a mass of 999. The peak was initially erroneously assigned to the molecular ion peak of **34** and **35** (molecular mass of 998) until it was observed in the spectra of all complexes in which F₂₀-TPP was used. We now assign this peak to the F₂₀-TPP-Na ion that has a mass of 999. The error was also confirmed when we compared the isotopic pattern of the experimental peak with the theoretical isotopic pattern distribution (Figure 4.15).

From the above discussion it is apparent that we have not as yet found the most appropriate experimental conditions to obtain the molecular ion peaks for the Schiff base thiolato complexes studied using MALDI-TOF technique. However from the results obtained for **34** and **35**, it seems that if optimum conditions could be found, it is possible to use MALDI-TOF technique to study this type of complexes.

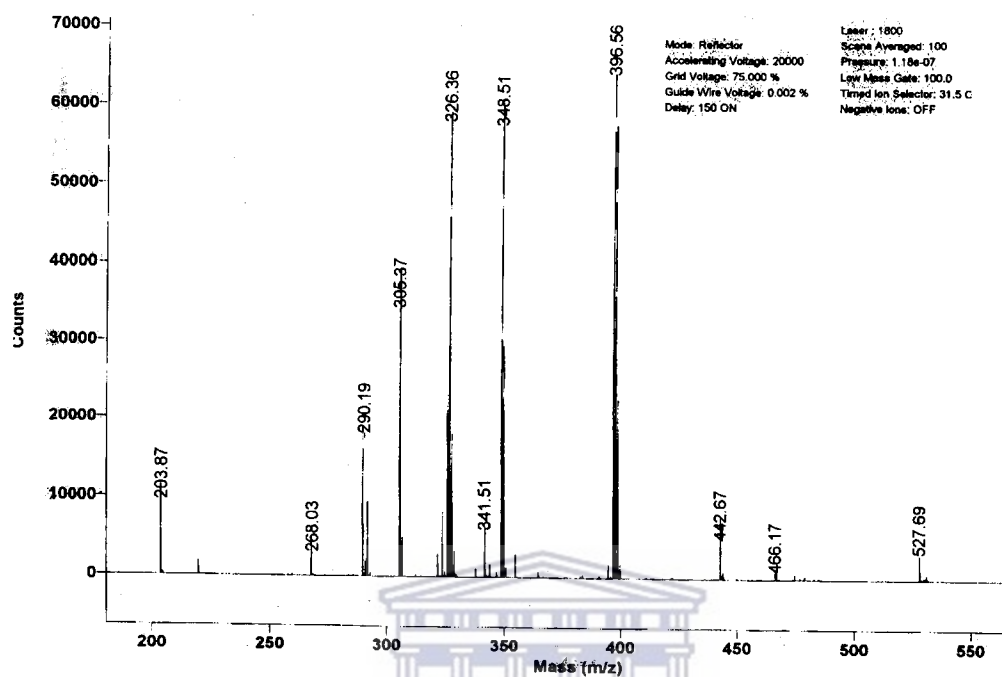


Figure 4.14: MALDI-TOF mass spectra of **35** showing fragments in Table 4.3.

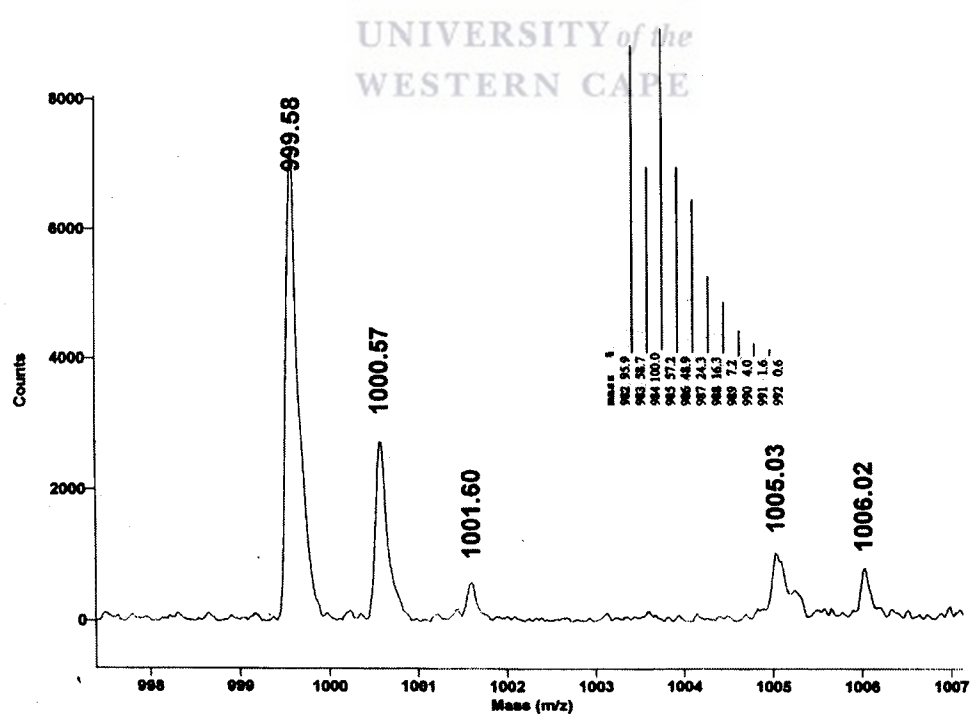


Figure 4.15: (a) Molecular ion peak observed at $m/z = 999$ and (b) the theoretical isotopic distribution of **34** and **35**.

Comparing the ionisation techniques used in this study, it is apparent that the most appropriate ionisation source for the bimetallic nickel complexes is ES source and to a lesser extent FAB source. This is based on the observation of molecular ions and logical fragmentation patterns observed in the mass spectra of all complexes.

4.8.3.4 Electrochemical studies

Historically, the study of mixed-valence molecular complexes was triggered by Taube's work on compounds such as $[(\text{H}_3\text{N})_5\text{Ru-pyz-Ru}(\text{NH}_3)_5]^{5+}$ (where pyz = pyrazine), which showed that it is possible for an electron to move between redox centres through a bridging ligand.³⁸ Thus a systematic synthesis of a great variety of molecular mixed-valence compounds was initiated in order to study electronic interactions in such systems. From this point of view we have synthesised a series of bimetallic complexes with differing bridges or linkers and probed electronic communication between the nickel centres using cyclic voltammetry.

Electrochemistry, specifically cyclic voltammetry (CV), is said to be a more convenient technique that is used to investigate the electronic interaction between the redox-active termini when complexes are chemically pure, sufficiently soluble and of a discrete nature.^{2b} Thus we have subjected the bimetallic complexes (**33**, **35**, and **36**) to cyclic voltammetric studies to probe their electronic interactions. The cyclic voltammetric experiments were done at three scan rates and also at different temperatures as well as running repetitive scans. In order to be able to compare our results with literature values, all the voltammograms were internally referenced to the ferrocene/ferrocenium couple, which will then allow comparison with those of standard calomel electrode (SCE). A major consideration for choosing complexes **33**, **35** and **36** was to see how the variation of the spacer could affect electron delocalisation, and also because the tributylphosphine fragment, $\text{NiBr}(\text{PBU}_3)(\eta^5\text{-C}_5\text{H}_5)$, analogue displays a fast reversible redox couple than the triphenylphosphine analogue.⁵⁷ In order to identify the origin of the electrochemical activity in the complexes we also ran cyclic voltammetry of the nickel starting material, $\text{NiBr}(\text{PBU}_3)(\eta^5\text{-C}_5\text{H}_5)$, and that of the ligand $\text{HSC}_6\text{H}_4\text{NC}(\text{H})\text{C}_4\text{H}_2\text{SC}(\text{H})\text{NC}_6\text{H}_4\text{SH}$.

Cyclic voltammetry of the nickel complex, $\text{NiBr}(\text{PBu}_3)(\eta^5\text{-C}_5\text{H}_5)$, had two irreversible oxidation peaks at 0.338 V and 0.996 V. None of the ligands (**29** – **32**) were sufficiently soluble in common solvents; therefore the cyclic voltammetry of **29** was run by first depositing a paste of the compound on the working electrode. The resultant voltammogram showed that the ligand had an irreversible oxidation peak at 0.699 V. When cyclic voltammetry experiment were performed on complexes **33**, **35** and **36** all showed two redox waves in the cathodic range, which were different from those of the two starting compounds, $\text{NiBr}(\text{PBu}_3)(\eta^5\text{-C}_5\text{H}_5)$ and **29**. This observation confirmed that the electrochemistry of complexes **33**, **35** and **36** were not ligand based, neither were the observations of redox activity of unreacted nickel starting material. No reduction peaks were observed when the scans were done in the opposite direction, the anodic range. Thus the couples for the complexes **33**, **35** and **36** were proved to be originating from the complexes themselves. Table 4.3 shows the redox couple values for the three complexes and also of $\text{NiBr}(\text{PBu}_3)(\eta^5\text{-C}_5\text{H}_5)$.

From Table 4.3 it is apparent that the introduction of the electron rich sulfur ligands lowers the oxidation potentials of the nickel starting material and that of the ligands. Compared with $\text{Ni}(\text{SC}_6\text{H}_4\text{X-4})(\text{PBu}_3)(\eta^5\text{-C}_5\text{H}_5)$, (X = Cl (360 mV), Br (320 mV)),^{57a} and $\text{Ni}(\text{SC}_6\text{H}_4\text{NC}_6\text{H}_4\text{X-4})(\text{PBu}_3)(\eta^5\text{-C}_5\text{H}_5)$ (X = F (350 mV), Cl (370 mV), Br (360 mV), Me (350 mV))^{57b} oxidation potentials of **33** (294 mV), **35** (298 mV) and **36** (285 mV) are also lower. The quasi-reversible redox couples found for **33**, **35** and **36** are indicative of stabilisation of the oxidised species by the presence of the electron rich thiolato ligands. This observation is in line with those of the mononickel complexes.⁵⁷ Literature reports on the electrochemical oxidation of μ -thiolato nickel complexes, $[(\eta^5\text{-C}_5\text{H}_5)\text{Ni}(\mu_2\text{-SR})]_2$, show that they form unstable radical cations if the thiolato ligand has an alkyl group.⁶⁹ However, the radical cations are stabilised by aryl thiolato ligands.⁷⁰ Hence the quasi-reversibility associated with the thiolato Schiff base complexes (**33**, **35** and **36**) must be the result of π -conjugated units that link the sulfur ends of the bridging ligands. This stabilisation has also been observed for the ruthenium complexes bridged by $\text{-C}\equiv\text{CC}_6\text{H}_4\text{C}\equiv\text{C-}$, a conjugated bridge.^{46a}

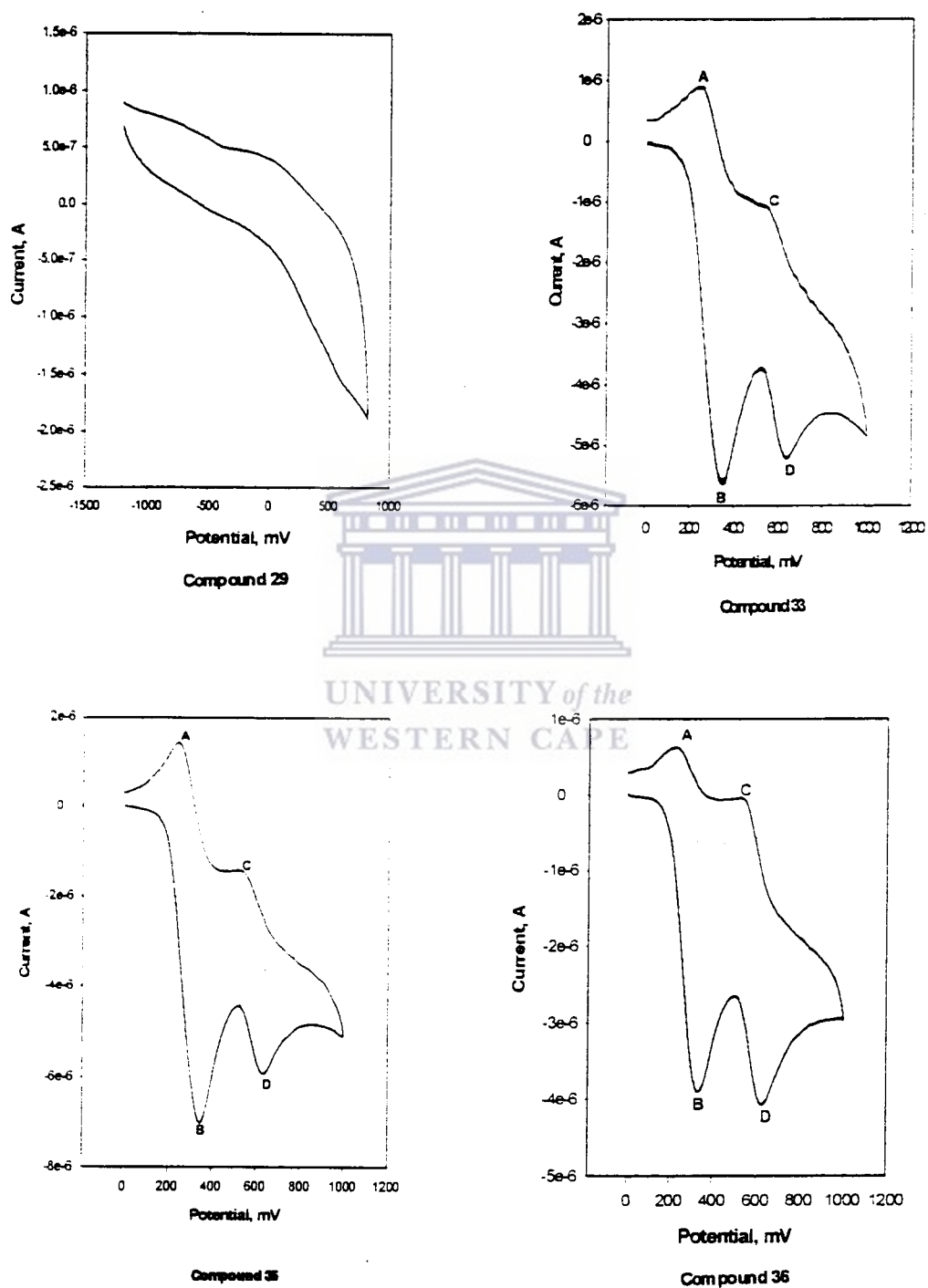


Figure 4.16: Cyclic voltammograms for 29, 33, 35 and 36.

As an example, the nature of the redox couple in complex **33** is reminiscent of the coupling of strong adsorption of products (C/D: $E_{1/2} = 590$ mV) on the electrode surface to the diffusion controlled electrochemical process (A/B: $E_{1/2} = 294$ mV).⁷¹ However, the peak separation ($\Delta E_{p,C/D}$) for the second redox process is 94 mV, a value greater than the upper limit peak separation of 65 mV for surface bound species undergoing a rapid one electron transfer.^{53b} In addition to the voltammetric peaks in the complexes **33**, **35** and **36**, the redox couple is not symmetrical as expected for those of the adsorbed species, indicating that the source of this redox couple C/D cannot be adsorbed species. The peak separation for the first redox couple ($\Delta E_{p,A/B}$) is 104 mV. Since peak separation for of both the redox couples for **33**, **35** and **36** (Table 4.3) are greater than 60 mV, the value for the peak separation of non-equilibrium one electron transfer process, the redox couples in **33**, **35** and **36** are quasi-reversible.⁷² The quasi-reversibility can be attributed to the coupling of the diffusion-controlled process to other electrode process, in this case, electron hopping along the bridging ligands in the bimetallic complexes.^{53b, 73}

Table 4.3: Cyclic voltammetry data of complexes $\text{NiBr}(\text{PBU}_3)(\eta^5\text{-C}_5\text{H}_5)$, **33**, **35** and **36**.

Complex	$E_{1/2}$ (mV)		$I_{p,a}/I_{p,c}$		ΔE_p (mV)		ΔE (mV)	K_{com}
	A/B	C/D	A/B	C/D	A/B	C/D		
SM	338	996	-	-	-	-	-	-
33	294	590	1.10	0.85	104	94	296	1.01×10^5
35	298	594	1.00	0.85	104	94	296	1.01×10^5
36	285	583	1.13	0.77	103	87	300	1.18×10^5

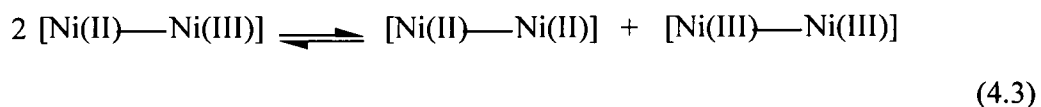
$\Delta E_p = |E_{p,ox} - E_{p,red}|$, $\Delta E = |E_{1/2,C/D} - E_{1/2,A/B}|$, $K_{com} = \exp(\Delta E.F/RT)$, SM = starting nickel complex $\text{NiBr}(\text{PBU}_3)(\eta^5\text{-C}_5\text{H}_5)$.

In order to obtain the number of electrons involved in each redox activity, Tafel analyses of each oxidation or reduction waves were done. Tafel analyses and Tafel plots are one way, and a more convenient way, of estimating the number of electrons exchanged

during any reduction or oxidation event.⁷⁴ Tafel analyses ($\ln |i| = \ln i_0 - \alpha FE/RT$) of the oxidation wave A/B and the reduction wave C/D gave a Tafel slope of about 120 mV per decade in each case, as expected for a one electron transfer process. Thus A/B and C/D redox couples in **33**, **35** and **36** represent two quasi-reversible reactions that involve the coupling of the diffusion controlled electron transfer at the electrode with the transportation of electrons along the conjugated bridges in the bimetallic complexes.^{52a, b, 53b} This is usually what is commonly observed in bimetallic or organometallic polynuclear complexes where the cyclic voltammetric peak separation is increased as a result of electron diffusion or propagation along the bridging organic conjugated groups.⁷⁵

For homonuclear bimetallic complexes, the observation of two reversible redox couples in their cyclic voltammograms usually indicates electronic interaction between the two metal centres across the organic bridging ligand.^{3b, 40, 76} On the contrary the absence of splitting of the reduction or oxidation wave indicate that the electron transfer to the metal centres occurs at the same energy pointing to the fact that no, or at best weak, electronic interaction via the bridging ligand system is occurring.³⁵ In such systems there will be an exchange of two electrons through two electron processes whose potentials are separated only by the statistical term $\Delta E = 35.6$ mV at room temperature.⁷⁷ Observation of two separate peaks indicates electronic communication even when the metal centres are identical.⁷⁸ For example, redox couple separation, ΔE , for $[(\eta^5\text{-C}_5\text{H}_5)\text{FeL}_2]_2(\mu\text{-CH=CH=CH})$ (L = CO, PMe₃, PPh₃) varies from 410 mV to 450 mV⁷⁹ whereas for $[(\eta^5\text{-C}_5\text{H}_5)\text{Fe}(\text{CO})_2]_2(\mu\text{-1,4-C}_6\text{F}_4)$ has a redox couple separation, ΔE , of 280 mV⁸⁰. For the nickel thiolato Schiff base systems it was evident from the splitting of the redox wave (see Table 4.3 for values) into two individual redox couples that there is electronic interaction between the redox centers, represented here by the nickel atoms. The ΔE values represent comproportionation constant, K_{com} , relative to the equilibrium given in equation. 4.3 and the values are given in Table 4.3. These values are greater than ΔE values for complexes that are classified as Class II mixed-valence species according to the Robin-Day classification.⁸¹ Thus the complexes can be classified as borderline cases

between Class II and Class III complexes since the values are closer to that of the Creutz-Taube ion ($K_{\text{com}} = 4 \times 10^6$) which is considered as a class III compound.⁷²



Since there are no large differences in the ΔE values for the three complexes, it is reasonable to deduce that the nature of the bridge in these complexes does not play a major role. It has been shown that the natures of the capping metal fragments influence the electronic communication more than the bridging ligand. For example, there is electronic interaction in $\text{Cl}(\eta^2\text{-dppe})_2\text{Ru-C}\equiv\text{CC}_6\text{H}_4\text{C}\equiv\text{C-RuCl}(\eta^2\text{-dppe})_2$ but not in $(\eta^5\text{-C}_5\text{H}_5)(\eta^2\text{-dppe})\text{Fe-C}\equiv\text{CC}_6\text{H}_4\text{C}\equiv\text{C-Fe}(\eta^5\text{-C}_5\text{H}_5)(\eta^2\text{-dppe})$.⁴⁶ This might be due to the mismatch in metal-ligand orbitals. The inclusion of the sulfur atom between the nickel atom and the organic bridge might dampen the differences due to the bridges by making the metal-ligand orbitals similar. This might lead to these apparent similarities in the electronic behaviour of the three complexes.

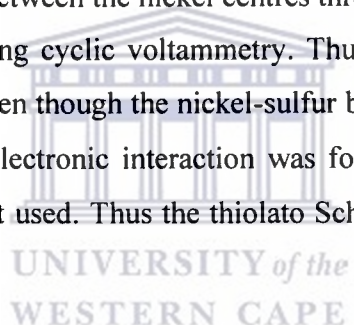
On performing multiple scans per experiment it was found that the two redox peaks changed. The first observation was that the peak amplitude decrease with each additional scan and secondly the peak potential shifted to more positive voltages. This is indicative of adsorption of the electroactive species onto the working electrode. Since the peak amplitude decreases after each scan, the implication is that the adsorbed species is nonconducting. This is similar to a polyphenol film adsorbed onto an electrode surface which is known to be insulating.⁸² If on the other hand the adsorbed species were conducting, the peak amplitude should increase with repeating scans, as is the case for electropolymerisation of aniline into polyaniline.⁸³ Performing the experiments at low temperatures did not improve the resolution of the redox couples by much, implying that there might be a competing mechanism to the electron hopping mechanism, in this case adsorption of the electroactive species.

4.9. Summary

The preparation of bimetallic nickel complexes with bridging dithiolato ligands from Schiff base thiols has been successfully undertaken. Complexes were produced in high yields and good analyses.

The bimetallic nature of the complexes synthesised was established by a combination of analytical techniques. Mass spectroscopy, mainly ESMS, gave unequivocal proof of their bimetallic nature.

The electronic communication between the nickel centres through the organic thiol Schiff base spacer was established using cyclic voltammetry. Thus electronic coupling of the two nickel centres is possible even though the nickel-sulfur bonds in these complexes are predominantly a σ -bond. The electronic interaction was found to be insensitive to the nature of the organic spacer unit used. Thus the thiolato Schiff base organic compounds behave as molecular wires.



References

1. J. Keisewetter, G. Poignant, V. Guerchais, *J. Organomet. Chem.* 2000, **595**, 81.
2. (a) M. D. Ward, *Chem. Soc. Rev.* 1995, 121; (b) F. Paul, C. Lapinte, *Coord. Chem. Rev.* 1998, **180**, 431; (c) W. Kum, A. Klein, M. Glockle, *Acc. Chem. Res.* 2000, **33**, 755; (d) R. H. Laye, S. M. Couchman, M. D. Ward, *Inorg. Chem.* 2001, **40**, 4089.
3. (a) G. Frapper, M. Kertesz, *Inorg. Chem.* 1993, **32**, 732; (b) A. C. Ribou, J.-P. Launay, K. Takahashi, T. Nihira, S. Tarutani, C. W. Spangler, *Inorg. Chem.* 1994, **33**, 1325.
4. W. E. Geiger, N. G. Connely, *Adv. Organomet. Chem.* 1992, **24**, 87.
5. J. M. Tour, L. Jones II, D. L. Pearson, J. J. S. Lamba, T. P. Burgin, G. M. Whitesides, D. L. Allara, A. N. Parith, S. V. Atre, *J. Am. Chem. Soc.* 1995, **117**, 9529.
6. J. H. K. Yip, J. Wu, K.-Y. Wong, K. P. Ho, C. S.-N. Pun, J. J. Vittal, *Organometallics*, 2002, **21**, 5292.
7. M. Sharp, M. Peterson, K. Edstron, *J. Electroanal. Chem.* 1979, **95**, 12.
8. C. M. Casado, M. Moran, J. Losada, I. Cuadrado, *Inorg. Chem.* 1995, **34**, 1668.
9. J. E. Sutton, P. M. Sutton, H. Taube, *Inorg. Chem.* 1979, **18**, 1017.
10. J. A. Page, G. Wilkinson, *J. Am. Chem. Soc.* 1952, **74**, 6149.
11. D. H. Evans, *Chem. Rev.* 1990, **90**, 739.
12. (a) V. Balzani, F. Scandola, *Supramolecular Chemistry*, Ellis Horwood, New York, 1991, (b) D. Astruc, *Acc. Chem. Res.* 1997, **30**, 383; (c) A. Gobel, G. Leibeling, M. Rudolph, W. Imhof, *Organometallics*, 2003, **22**, 759.
13. D. L. Feldheim, C. D. Keating, *Chem. Soc. Rev.* 1998, **27**, 1.
14. R. E. Martin, F. Diederich, *Angew. Chem. Int. Ed. Engl.* 1999, **38**, 1350.
15. (a). R. M. Baum, *C&EN*, 30 July 1997, 39; (b). R. Dagani, *C&EN*, 22 January 1996, 22; (c) J.-P. Launay, *L'Actualite Chimique*, July-August 1994, 37.
16. (a). M. D. Ward, *Chem. Ind.* 1996, 568; (b) J. M. Tour, *Chem. Rev.* 1996, **96**, 537.
17. (a). K. Muller, *Pure Appl. Chem.* 1993, **65**, 89; (b) D. L. Pearson, J. M. Tour, *J. Org. Chem.* 1997, **62**, 1376.

18. (a) A. Aviram (Ed.) *Molecular Electronics: Science and Technology* New York, 1992; (b) M. A. Reed, W. P. Kirk, *Nanostructure Physics and Fabrication*, Academic Press, New York, 1992; (c) J. S. Miller, *Adv. Mater.* 1990, **2**, 378.
19. J. M. Lehn, *Supramolecular Chemistry: Concepts and Perspective*, VCH, 1995.
20. (a) V. Mujita, M. Kemp, M. A. Ratner, *J. Chem. Phys.* 1994, **101**, 6856; (b) J.-P. Launay, C. Joachim, A. Gourdon, J. Bonvoisin, C. Coudret, *Sci. Chim. Lett. Dep. Sci. CNRS*, 1995, **54**, 1; (c) D. Astruc, *Electron Transfer and Radical Process in Transition Metal Chemistry*, VCH, 1995, 283; (d) C. Joachim, *New J. Chem.* 1991, **15**, 223.
21. J. M. Tour, *Trends Polym. Sci.* 1992, **2**, 332.
22. (a) N. S. Hush, *Prog. Inorg. Chem.* 1967, **8**, 891; (b) H. Kitagawa, N. Kojima, H. Sakai, *J. Chem. Soc. Dalton Trans.* 1991, 3211.
23. (a) M. B. Robin, P. Day, *Adv. Inorg. Chem. Radiochem.* 1967, **10**, 247; (b) C. Creutz, *Prog. Inorg. Chem.* 1983, **30**, 1.
24. B. J. Cooper, T. M. Vess, W. A. Kalsbeck, D. W. Wertz, *Inorg. Chem.* 1991, **30**, 2286.
25. (a) S. Woiteller, J.-P. Launay, C. W. Spangler, *Inorg. Chem.* 1989, **28**, 758; (b) J. A. Thomaas, C. J. Jones, J. A. McCleverty, D. Collins, F. E. Mabbs, C. J. Harding, M. G. Hutchings, *J. Chem. Soc. Chem. Commun.* 1992, 1796.
26. (a) C. Giuffrida, S. Campagna, *Coord. Chem. Rev.* 1994, **135-136**, 517; (b) C. E. B. Evans, M. L. Naklicki, A. R. Rezvani, C. A. White, V. V. Kodratiev, R. J. Crutchley, *J. Am. Chem. Soc.* 1998, **120**, 13096.
27. (a) A. Bolognesi, M. Catelani, S. Destri, (Sir G. Allen, J. C. Bevington (Eds.)) in *Comprehensive Polymer Science*, Pergamon Press, Oxford, 1989, **4**, 143; (b) M. Soga, T. Nakagawa, K. Ogawa, *Jpn. J. Appl. Phys., Part 1*, 1996, **35**, 1908.
28. D. Bloor, (Sir G. Allen and J. C. Bevington (Eds.)) in *Comprehensive Polymer Science*, Pergamon Press, Oxford, 1989, **4**, 687.
29. R. J. Crutchley, *Adv. Inorg. Chem.* 1994, **41**, 273.
30. (a) L. A. Bumm, J. J. Arnold, M. T. Cygan, T. D. Dunbar, T. P. Burgin, L. Jones II, D. L. Allara, J. M. Tour, P. S. Weiss, *Science*, 1996, **271**, 1705; (b) V. Mujita,

- M. Kemp, M. A. Ratner, *J. Chem. Phys.* 1994, **116**, 9759; (c) V. Mujita, M. Kemp, M. A. Ratner, *J. Chem. Phys.* 1994, **101**, 5172.
31. D. I. Gittins, D. Bethell, D. J. Schiffrin, R. J. Nichols, *Nature* 2000, **408**, 67.
32. (a) J. Chen, M. A. Reed, A. M. Rawlett, J. M. Tour, *Science* 1999, **286**, 1550; (b) M. A. Reed, C. Zhou, C. J. Muller, T. P. Burgin, J. M. Tour, *Science* 1997, **278**, 252; (c) M. di Ventra, N. D. Lang, S. T. Pantelides, *Chem. Phys.*, 2002, **281**, 189.
33. (a) J.-P. Launay, *Chem. Soc. Rev.* 2001, **30**, 386; (b) A. Ferretti, A. Lami, G. Villani, *Inorg. Chem.* 1998, **37**, 2799.
34. H. D. Sikes, J. F. Smalley, S. P. Dudek, A. R. Cook, M. D. Newton, C. E. D. Chidsey, S. W. Feldberg, *Science* 2001, **291**, 1519.
35. G. Gruner, T. Debaerdemaeker, P. Bauerle, *Chem. Commun.* 1999, 1097.
36. (a) A. El-Ghayoury, A. Harriman, A. Khatyr, R. Ziessel, *Angew. Chem. Int. Ed.* 2000, **39**, 185, (b) W. E. Meyer, A. J. Amoroso, C. R. Horn, M. Jaeger, J. A. Gladysz, *Organometallics*, 2001, **20**, 1115.
37. Y. Zhu, D. B. Millet, M. O. Wolf, S. J. Rettig, *Organometallics*, 1999, **18**, 1930.
38. C. Creutz, H. Taube, *J. Am. Chem. Soc.* 1969, **91**, 3988.
39. (a) M. Hanack, S. Deger, A. Lange, *Coord. Chem. Rev.* 1988, **83**, 115, (b) C. Creutz, *Prog. Inorg. Chem.* 1983, **39**, 1.
40. M. J. Powers, T. J. Meyer, *J. Am. Chem. Soc.* 1980, **102**, 1289.
41. A.-C. Ribou, J.-P. Launay, M. L. Sachtleben, H. Li, C. W. Spangler, *Inorg. Chem.* 1996, **33**, 3735.
42. (a) S. K. Pal, A. Krishnan, P. K. Das, A. G. Samuelson, *J. Organomet. Chem.* 2000, **604**, 248; (b) S. Di Bella, *Chem. Soc. Rev.* 2001, **30**, 355.
43. (a) J. Mata, S. Uriel, E. Peris, R. Llusar, S. Hubrechts, A. Persoons, *J. Organomet. Chem.*, 1998, **562**, 197, (b) I. R. Whittall, A. M. McDonagh, M. G. Humphrey, *Adv. Organomet. Chem.*, 1998, **42**, 291.
44. (a) F. Geiger, M. Stoldt, P. Bauerle, H. Schweizer, E. Umbach, *Adv. Mater.* 1993, **5**, 922; (b) G. Horowitz, P. Delannoy, H. Bouchriha, F. Deloffe, J.-L. Fave, F. Garnier, R. Hajlaoui, M. Heyman, F. Kouki, P. Valat, V. Wittgens, A. Yassar, *Adv. Mater.* 1994, **6**, 752; (c) K. Uchiyama, H. Akimichi, S. Hotta, H. Noge, H. Sakaki, *Synth. Met.* 1994, **63**, 57.

45. D. Touchard, P. H. Dixneuf, *Coord. Chem. Rev.* 1998, **178**, 409.
46. (a) S. R. Marder, C. B. Gorman, B. G. Tieman, L.-T. Cheng, *J. Am. Chem. Soc.* 1993, **115**, 3006, (b) O. Lavastre, J. Plass, P. Bachmann, S. Guesmi, C. Moinet, P. H. Dixneuf, *Organometallics*, 1997, **16**, 184.
47. (a) K. Sonogashira, K. Ohga, S. Takahashi, N. Hagihara, *J. Organomet. Chem.* 1980, **188**, 237; (b) S. Takahashi, K. Sonogashira, H. Morimoto, E. Murata, S. Kataoka, N. Hagihara, *J. Polym. Sci. Polym. Chem. Ed.* 1982, **20**, 565.
48. M. T. Cygan, T. D. Dunbar, J. J. Arnold, L. A. Bumm, N. F. Shedlock, T. P. Burgin, L. Jones II, D. L. Allara, J. M. Tour, P. S. Weiss, *J. Am. Chem. Soc.* 1998, **120**, 2721.
49. O. Lavastre, M. Even, P. H. Dixneuf, A. Pacreau, J. P. Vairon, *Organometallics*, 1996, **15**, 1530.
50. F. Sato, T. Yoshida, M. Sato, *J. Organomet. Chem.* 1972, **37**, 381.
51. (a) K. W. Barnett, *J. Chem. Educ.* 1974, **51**, 422; (b) J. Darkwa, *Organometallics*, 1994, **13**, 4734.
52. O. L. Caagrande jr., A. E. Gerbase, F. C. Atedile, F. O. V. da Cunha, *Polyhedron*, 1997, **16**, 171.
53. (a) A. J. Fry (P. T. Kissinger, W. R. Heinemann (eds.)) in *Laboratory Techniques in Electroanalytical Chemistry, 2nd Edition, Revised and Expanded*, Marcel Dekker, New York, p 469; (b) R. W. Murray, (A. J. Bard (ed.)), in *Electroanalytical Chemistry*, Marcel Dekker, New York, 1984, 191.
54. (a) S. Uemura, H. Takahashi, K. Ohe, *J. Organomet. Chem.* 1992, **423**, C9; (b) Y. Nishibayashi, C. S. Cho, K. Ohe, S. Uemura, *J. Organomet. Chem.* 1996, **526**, 335.
55. A. S. Matharu, C. Grover, L. Komitov, G. Anderson, *J. Mater. Chem.* 2000, **10**, 1303; b. N. Miyaura, T. Yonagi, A. Suzuki, *Synth. Commun.* 1981, **11**, 513.
56. P. Bhattacharyya, J. Parr, *J. Chem. Soc. Dalton Trans.* 1998, 3609.
57. (a) J. Darkwa, R. M. Moutloali, T. Nyokong, *J. Organomet. Chem.* 1998, **64**, 37, (b) F. A. Nevondo, A. M. Crouch, *J. Darkwa, J. Chem. Soc. Dalton Trans.* 2000, 43; (c) R. M. Moutloali, J. Bacsá, W. A. Ddamba, J. Darkwa, *J. Organomet. Chem.* 2001, **629**, 171.

58. M. M. Ross, J. R. Wyatt, R. J. Colton, J. E. Campana, *Int. J. Mass Spectrometry and Ion Processes*, 1983, **54**, 237.
59. (a) M. S. Thomas, J. Darkwa, E. T. Osei-Twum, L. A. Litorja jr. *Polyhedron*, 1999, **18**, 2803; (b) J. Darkwa, E. Y. Osei-Twum, L. A. Litorja jr., *Polyhedron* 1999, **18**, 1115.
60. (a) C. E. C. A. Hop, R. Bakhtiar, *J. Chem. Educ.* 1996, **73**, A162; R. Colton, A. D'Agostino, J. C. Traeger, *Mass Spectrom Rev.* 1995, **14**, 79.
61. (a) J. A. Alden, A. M. Bond, R. Colton, R. G. Compton, J. C. Eklund, Y. A. Mah, P. J. Mahon, V. Tedesco, *J. Electroanal. Chem.* 1998, **447**, 155; (b) A. M. Bond, R. Colton, J. C. Traeger, J. Harvey, *Inorg. Chim. Acta.* 1995, **228**, 193.
62. (a) G. A. Bowmaker, I. G. Dance, R. K. Harris, W. Henderson, I. Laban, M. L. Scudder, S. W. Oh, *J. Chem. Soc. Dalton Trans.* 1996, 2381; (b) T. Lover, G. A. Bowmaker, W. Henderson, R. P. Cooney, *Chem. Commun.* 1996, 683; (c) W. Henderson, C. O. Miles, B. K. Nicholson, J. E. Mackeay, B. Dinger, *J. Chem. Soc. Dalton Trans.* 1997, 2577.
63. K. Nomoja, Y. Kondoh, H. Nagano, M. Oda, *J. Chem. Soc. Chem. Commun.* 1995, 1679.
64. H. E. Howard-Lock, D. J. LeBlanc, C. J. L. Lock, R. W. Smith, Z. Wang, *Chem. Commun.* 1996, 1391.
65. A. Barnareggi, L. Torch, R. M. Facino, M. Carini, G. Depta, B. Casseta, N. Farrell, S. Spadacini, R. Ceserani, S. Tognella, *J. Chromatogr. B.* 1995, **669**, 247.
66. (a) A. M. Bond, R. Colton, Y. A. Mah, J. C. Traeger, *Inorg. Chem.* 1994, **33**, 2548; (b) T. J. Cardwell, *Anal. Chim. Acta* 1993, **280**, 239.
67. L. J. McCaffrey, W. Henderson, B. K. Nicholson, J. E. Mackay, M. B. Dinger, *J. Chem. Soc., Dalton Trans.*, 1997, 2577.
68. (a) E. Rivera, M. Belletête, X. X. Zhu, G. Durocher, R. Giasson, *Polymer*, 2002, **43**, 5059; (b) S. Trimpin, P. Eichhorn, H. J. Räder, K. Müllen, T. P. Knepper *J. Chromat. A*, 2001, **938**, 67; (c) T. Nakano, O. Nakagawa, T. Yade, Y. Okamoto, *Macromolecules*, 2003, **36**, 1433.
69. R. E. Dessy, R. Kornmann, C. Smith, R. Haytor, *J. Am. Chem. Soc.* 1968, **90**, 2001.

70. (a) P. D. Frisch, M. K. Lloyd, J. A. McCleverty, D. Seddon, *J. Chem. Soc. Dalton Trans.* 1973, 2268; (b). N. F. Ho, T. C. W. Mak, *J. Chem. Soc. Dalton Trans.* 1990, 359.
71. (a) R. H. Wopschall, I. Shain, *Anal. Chem.* 1967, **39**, 1515; (b) R. H. Wopschall, I. Shain, *Anal. Chem.* 1967, **39**, 1527.
72. A. G. Lappin, *Redox Mechanisms in Inorganic Chemistry*, Ellis Horwood Series in Inorganic Chemistry, 1994.
73. B. A. Gregg, A. Heller, *J. Phys. Chem.* 1991, **95**, 5976
74. C. H. Hamann, A. Hammet, W. Vielstich, *Electrochemistry*, Wiley-VCH, 1998, p 143.
75. (a) R. J. Foster, A. J. Kelly, J. G. Vos, M. E. G. Lyon, *J. Electroanal. Chem.* 1988, **270**, 365; (b) M. E. G. Lyon, H. G. Fay, J. G. Vos, A. J. Kelly, *J. Electroanal. Chem.* 1988, **250**, 207; D. M. Kelly, J. G. Vos, (M. E. G. Lyon (ed.)), in *Electroactive Polymer Electrochemistry, Part 2, Methods and Applications*, Plenum Press, New York, 1966, 173.
76. S. Guesmi, D. Touchard, P. H. Dixneuf, *J. Chem. Soc. Chem. Commun.* 1996, 2773.
77. (a) A. Tarraga, P. Molina, D. Curiel, M. D. Velasco, *Tetrahedron Lett.* 2002, **43**, 8453; (b) A. Tarraga, P. Molina, D. Curiel, M. D. Velasco, *Tetrahedron*, 2001, **57**, 6765.
78. W.-Y. Yong, H.-Y. Lam, S.-M. Lee, *J. Organomet. Chem.* 2000, **595**, 70.
79. B. A. Etzenhouser, M. D. Cavanaugh, H. N. Spurgeon, M. B. Sponsler, *J. Am. Chem. Soc.* 1994, **116**, 2221.
80. R. Chukwu, A. D. Hunter, B. D. Santarisiero, S. G. Bott, J. L. Atwood, J. Chassignac, *Organometallics*, 1992, **11**, 589.
81. C. Creutz, *Progr. Inorg. Chem.* 1983, **30**, 1.
82. M. Pravda, C. M. Jungar, E. I. Iwuoha, M. R. Smyth, K. Vytras, A. Ivaska, *Anal. Chim. Acta* 1995, **304**, 127.
83. (a) C. M. A. Brett, C. Thiemann, *J. Electroanal. Chem.* 2002, **538-539**, 215; (b) T. Lindfors, A. Ivaska, *J. Electroanal. Chem.* 2002, **535**, 65.

Chapter 5

Summary and Outlook

The work covered in this thesis is two fold. In the first instance we have prepared and characterised complexes that have (potential) liquid crystalline properties, and in the second case we have synthesised a series of organosulfur bidentate (bridging) ligands and have probed their ability to allow electronic communication between the capping nickel centres. All the organic compounds and their metal complexes are new complexes.

Organic Schiff base thiols with alkoxy chains, $\text{HSC}_6\text{H}_4\text{NC}(\text{H})\text{C}_6\text{H}_4\text{OC}_n\text{H}_{2n+1}$, $\text{HSC}_6\text{H}_4\text{NC}(\text{H})\text{C}_6\text{H}_3\text{-3,4-}(\text{OC}_{10}\text{H}_{21})_2$ and the bromo analogue $\text{BrC}_6\text{H}_4\text{NC}(\text{H})\text{C}_6\text{H}_4\text{OC}_6\text{H}_{13}$ were characterised by NMR, infrared, elemental analysis and electron impact mass spectrometry. The thiol Schiff base compounds were subsequently used to prepare nickel and palladium complexes described in chapters 2 and 3. The nickel and palladium complexes were characterised by NMR, infrared and elemental analysis. In selected cases the complexes were also characterised by single crystal X-ray diffraction and MALDI-TOF mass spectrometry.

To test liquid crystalline properties of compounds in chapters 2 and 3, thermal analyses (Differential Scanning Calorimetry and Thermal Gravimetric Analysis) were performed. The Schiff base thiols with alkoxy chains ($\text{HSC}_6\text{H}_4\text{NC}(\text{H})\text{C}_6\text{H}_4\text{OC}_n\text{H}_{2n+1}$) did not show liquid crystalline behaviour as indicated by the observation of only one endothermic event on heating. The lack of mesogenic behaviour in the compounds was attributed to hydrogen bonding between neighbouring molecules. This hypothesis was proven thiolato Schiff base thiols with two chains ($\text{HSC}_6\text{H}_4\text{NC}(\text{H})\text{C}_6\text{H}_3\text{-3,4-}(\text{OC}_{10}\text{H}_{21})_2$) and the bromo analogue of the mono alkoxy chain compounds ($\text{HSC}_6\text{H}_4\text{NC}(\text{H})\text{C}_6\text{H}_4\text{OC}_n\text{H}_{2n+1}$) showed liquid crystalline behaviour. Hydrogen bonding is weakened in the thiolato Schiff base compound with two chains due to steric crowding introduced by the second chain, while in the bromo analogue there is no possibility of forming hydrogen bonding. The optical

texture of the bromo compound was obtained and showed distinct focal conic shape, typical of smectic mesophases.

The first type of metal complexes, $\text{Ni}(\eta^5\text{-C}_5\text{H}_5)(\text{PR}_3)(\text{SC}_6\text{H}_4\text{NC}(\text{H})\text{C}_6\text{H}_4\text{OC}_n\text{H}_{2n+1})$ (R = Bu or Ph, n = 4, 6, 8, 10, 14, 16, 20), studied did not show multiple endotherms on heating and were therefore also not liquid crystalline. The lack of mesogenic behaviour is due to the bulkiness of the ancillary phosphine ligands that reduces effective packing and molecular anisotropy. This reduces intermolecular interaction needed to induce or promote liquid crystalline behaviour. From their thermal decomposition it was found that their decomposition pathways were dependent on the nature of the phosphine used. In order to induce mesomorphic behaviour, two modifications were introduced into the complexes.

The modified complexes that are reported in Chapter 3 had two design features. In the first instance the molecular length of complexes were increased and the phosphine group removed. In the second modification the complexes were made planar and lacked both the cyclopentadienyl ring and the phosphine ligands. These two types of complexes were subjected to both thermal analyses and hotstage optical microscopy. From both the DSC and optical studies it was found that the complexes are mesogenic. The textures of the complexes could however only be observed after rapid heating and annealing. This showed that in the present study, the introduction of the metal fragment leads to mesogenic behaviour even though the free ligands themselves are nonmesogenic.

From the point of view of improving the mesogenic behaviour of the complexes that have been synthesised in the study, two things are apparent. The first is that when bulky ligands are used, it is essential that the effective molecular length be increased so as to compensate for the loss of molecular anisotropy. Thus for well-behaved thermal response the molecular length of the complexes should be increased to include at least three benzene rings plus the alkoxy chain. The second is that increasing the planarity of the molecules increases molecular interaction. This tendency to increase molecular interaction leads to an increase in temperature at which the onset of liquid crystalline

behaviour occurs, which for some of the complexes, was above the temperature at which decomposition started. Thus to offset increased molecular interaction, a balance between molecular interaction and high transition temperatures for mesogenic behaviour must be found.

Chapter 4 describes the synthesis of bidentate Schiff base thiols, $\text{HSC}_6\text{H}_4\text{NC}(\text{H})(\text{C}_4\text{H}_2\text{S})\text{C}(\text{H})\text{C}_6\text{H}_4\text{SH}$, $\text{HSC}_6\text{H}_4\text{NC}(\text{H})\text{-1-(C}_6\text{H}_4\text{)-3-C}(\text{H})\text{C}_6\text{H}_4\text{SH}$, $\text{HSC}_6\text{H}_4\text{NC}(\text{H})\text{-1-(C}_6\text{H}_4\text{)-4-C}(\text{H})\text{C}_6\text{H}_4\text{SH}$ and $\text{HSC}_6\text{H}_4\text{NC}(\text{H})\text{-4-(C}_6\text{H}_4\text{C}_6\text{H}_4\text{)-4'-C}(\text{H})\text{C}_6\text{H}_4\text{SH}$ and their reactions with $\text{Ni}(\eta^5\text{-C}_5\text{H}_5)\text{PR}_3\text{X}$ ($\text{R} = \text{Bu}$ or Ph , $\text{X} = \text{Cl}$ or Br). The bidentate Schiff ligands were characterized by ^1H and ^{31}P NMR, infrared and elemental analysis. In addition to these three analytical techniques, the nickel complexes were characterised by Fast Atom Bombardment, Electro-Spray and MALDI-TOF mass spectrometry. Thus their bimetallic nature was unequivocally established.

Complexes that were studied as molecular wires were assessed using cyclic voltammetry. This simple technique showed that the Schiff base thiol bridging ligands are able to allow electronic interaction between the bridged nickel atoms. The strength of the interaction was dependent on the nature of the capping metal and not the type of the linker group that was used. The thiols Schiff base compounds were therefore found to behave as molecular wires.

To really assess the Schiff base thiols as efficient molecular wires, there is a need to change the capping metal fragments. This is in view of the fact that the cyclopentadienylnickel(II) phosphine moieties do not give fully reversible redox behaviour. This would reduce the competing modes of electron transfer, *i.e.* chemical reaction versus through-bridge electron transfer mechanisms.